INFORMATION TO USERS

This manuscript has been reproduced from the microfilm master. UMI films the text directly from the original or copy submitted. Thus, some thesis and dissertation copies are in typewriter face, while others may be from any type of computer printer.

The quality of this reproduction is dependent upon the quality of the copy submitted. Broken or indistinct print, colored or poor quality illustrations and photographs, print bleedthrough, substandard margins, and improper alignment can adversely affect reproduction.

In the unlikely event that the author did not send UMI a complete manuscript and there are missing pages, these will be noted. Also, if unauthorized copyright material had to be removed, a note will indicate the deletion.

Oversize materials (e.g., maps, drawings, charts) are reproduced by sectioning the original, beginning at the upper left-hand corner and continuing from left to right in equal sections with small overlaps.

Photographs included in the original manuscript have been reproduced xerographically in this copy. Higher quality 6" x 9" black and white photographic prints are available for any photographs or illustrations appearing in this copy for an additional charge. Contact UMI directly to order.

ProQuest Information and Learning
300 North Zeeb Road, Ann Arbor, MI 48106-1346 USA
800-521-0600



Downloaded from SHAREOK. Persistent Handle URL: https://hdl.handle.net/11244/382

UNIVERSITY OF OKLAHOMA

GRADUATE COLLEGE

Static and Dynamic Behavior of Multiphase Porous Media: Governing Equations and Finite Element Implementation

A Dissertation

SUBMITTED TO THE GRADUATE FACULTY

in partial fulfillment of the requirements for the

degree of

Doctor of Philosophy

By

Changfu Wei
Norman, Oklahoma
2001

UMI Number: 3028810



UMI Microform 3028810

Copyright 2002 by Bell & Howell Information and Learning Company.
All rights reserved. This microform edition is protected against unauthorized copying under Title 17, United States Code.

Bell & Howell Information and Learning Company
300 North Zeeb Road
P.O. Box 1346
Ann Arbor, MI 48106-1346

© Copyright by Changfu Wei 2001
All Rights Reserved.

STATIC AND DYNAMIC BEHAVIOR OF
MULTIPHASE POROUS MEDIA:
GOVERNING EQUATIONS AND FINITE ELEMENT IMPLEMENTATION

A Dissertation APPROVED FOR THE
SCHOOL OF CIVIL ENGINEERING AND ENVIRONMENTAL SCIENCE

BY

K.K. M 11/30/01

Md. Musharraf Hussain

ACKNOWLEDGMENTS

I would like to gratefully acknowledge my advisor, Dr. Kanthasamy K. Muraleetharan for his fine guidance, friendship, support and patience during the course of my studies. The devotedness from Dr. Muraleetharan toward his students' progress and pursuit of scholarly achievement is unsurpassed. The example set by Dr. Muraleetharan is one of excellence.

My gratitude goes to the members of my thesis committee: Dr. Musharraf Zaman, Dr. Randall Kolar, Dr. Tohren Kibbey, Dr. Robert Knox, and Dr. Luther White for their invaluable time, inputs and attention. Thanks also go to Dr. Gerald Miller and Dr. Mike Mooney for their kindness and encouragement in my academic efforts.

My appreciation goes to Sachin Deshpande, Prakasa Nedunuri, Karen Granger, Yunming Yang, Yong Yoew Lim, N. Ravichandran and S. Varatharaj for their friendship and help during my graduate studies.

This research was supported by a National Science Foundation (NSF) grant (Grant No. CMS-9501718) and this support is acknowledged.

Finally but not the least, I would like to thank my wife Jingong and my son Andy for their love, sacrifice and patience.

TABLE OF CONTENTS

ACKNOWLEDGMENTS

LIST OF TABLES

LIST OF FIGURES

ABSTRACT

1. INTRODUCTION 1

1.1 PRELIMINARIES 1

1.2 MICROSCOPIC CONSIDERATIONS 3

1.3 OBJECTIVES 6

1.4 CONTRIBUTIONS 7

1.5 OUTLINE OF THE DISSERTATION 8

2. CURRENT STATE OF KNOWLEDGE 10

2.1 CONTINUUM THEORIES OF POROUS MEDIA 10

2.2 STRESS-STRAIN CONSTITUTIVE MODELING 16

2.3 WAVE PROPAGATION IN POROUS MEDIA 18

2.4 FINITE ELEMENT ANALYSIS PROCEDURES 20

3. A CONTINUUM THEORY OF POROUS MEDIA

SATURATED BY TWO IMMISCIBLE FLUIDS 23

3.1 Basic Assumptions and Kinematics 23

3.2 Balance Equations 30

3.3 General Constitutive Relationships 34

3.4 Equilibrium State 40

3.5 Nonequilibrium State with Linear Dissipation 42

3.6 Rate-Independent Elastoplasticity 46

4. A NONLINEAR MODEL OF POROUS MEDIA AND ITS VARIATIONAL STRUCTURE 51

4.1 Field Equations 52

4.2 Hyperelasticity of Porous Media 57

4.3 A Theoretical Framework of Poroelastoplasticity 61

4.4 Variational Structure of the Proposed Model 65

5. A LINEARIZED MODEL AND THERMOPOROELASTICITY 77

5.1 Linearized Constitutive Relationships 77

5.2 Linearized Field Equations 81

5.3 Effective Stress in Porous Media 87

5.4 Evaluation of Material Coefficients 93

6. ACOUSTICAL WAVES IN POROUS MEDIA 103

6.1 Weak Discontinuity Waves 104

6.2 Acoustical Waves 108

6.3 Evaluation of Material Constants 112

6.4 Analysis of Numerical Results 117

6.5 Compared with Experimental Results 123

7. INITIAL AND BOUNDARY VALUE PROBLEMS (IBVP) AND FINITE ELEMENT SOLUTION PROCEDURES 129

7.1 Preliminaries 129

7.2 IBVP: Form 1 133

7.3 IBVP: Form 2 140

7.4 Nature of the Problems and Initial Conditions 146

7.5 Solution Procedures: Dynamic Analysis 149

7.6 Solution Procedures: Quasi-Static Analysis 154

7.7 Some Remarks on Implementation 155

8. NUMERICAL EXAMPLES 158

8.1 Elastic Response of a Saturated Soil Column Subjected to Loading 159

8.2 Propagation of a Step Displacement through an Unsaturated Soil Column 164

8.3 A Two-Phase Flow Problem 167

8.4 Flooding of a Centrifuge Model Embankment 174

8.5 An Embankment Subjected to Earthquake Loading 182

8.6 Consolidation of the Soils below a Foundation 191

9. CONCLUDING REMARKS AND RECOMENDATIONS 196

9.1 SUMMARY 196

9.2 CONCLUSIONS 197

9.3 RECOMMENDATIONS FOR FUTURE RESEARCH 199

REFERENCES 201

APPENDICES 212

I DISSIPATIVE FORCES AS FUNCTIONS OF FLUID MASS FLUXES 212

II COEFFICIENTS IN FIELD EQUATIONS (5.2.10)-(5.2.13) 214

III DERIVATIONS OF DYNAMIC COMPATIBILITY CONDITIONS (6.1.5)-(6.1.7) 215

IV NOMENCLATURE 218

LIST OF TABLES

4.1 SUMMARY OF THE COUPLED EQUATIONS 69

6.1 MATERIAL PARAMETERS OF MASSILON SANDSTONE SATURATED BY WATER & AIR 113

7.1 FLOW CHART OF THE SOLUTION PROCEDURE FOR DYNAMIC ANALYSIS 151

7.2 FLOW CHART OF THE SOLUTION PROCEDURE FOR QUASI-STATIC ANALYSIS 155

8.1 MATERIAL PARAMETERS OF DEL MONTE SAND 169

8.2 MATERIAL PARAMETERS OF MINCO SILT 177

8.3 HYDRAULIC AND MECHANICAL PROPERTIES OF KAOLIN USED IN THE ANALYSIS 183

8.4 MATERIAL PARAMETERS OF THE FOUNDATION SOIL 192

LIST OF FIGURES

1.1 MICROSTRUCTURE OF A THREE-PHASE POROUS MEDIA 4

3.1 A REPRESENTATIVE ELEMENTARY VOLUME (REV) 24

3.2 STATE PARAMETERS AS A FUNCTIONS OF THE SIZE OF REV 25

3.3 THE MOTION AND DISPLACEMENT OF AN INDIVIDUAL PHASE 26

3.4 LAGRANGIAN RELATIVE VELOCITY OF A FLUID PARTICLE 28

3.5 A THERMODYNAMIC SYSTEM 39

3.6 STATES OF THE SYSTEM AT EQUILIBRIUM 45

3.7 DEFINITION OF n_e^W AND n_p^W FOR POINT A 47

4.1 DEFINITION OF THE PROBLEM: A POROUS MEDIUM

EXPERIENCES A MOTION χ_t^s 69

5.1 EVALUATION OF SPECIFIC SATURATION CAPACITY 99

6.1 DISCONTINUITY SURFACE OF ACCELERATION 104

6.2 A) MOISTURE RETENTION CURVES FOR MASSILON SANDSTONE:

B) RELATION BETWEEN RELATIVE PERMEABILITY AND DEGREE

OF SATURATION. ($Kr\beta = k_r^\beta$) 115

6.3 INFLUENCE OF THE DEGREE OF SATURATION ON VELOCITIES:

A) *P1*; B) *P2*; C) *P3*; D) *S* 117

6.4 INFLUENCE OF THE DEGREE OF SATURATION ON ATTENUATION:

A) *P1*; B) *P2*; C) *P3*; D) *S* 119

6.5 INFLUENCE OF FREQUENCY ON THE PHASE VELOCITIES:

A) *P1*; B) *P2*; C) *P3*; D) *S* 121

6.6 INFLUENCE OF FREQUENCY ON THE ATTENUATION COEFFICIENTS:

A) *P1*; B) *P2*; C) *P3*; D) *S* 122

6.7 COMPARISON OF CALCULATED AND MEASURED PHASE VELOCITIES OF

P1 WAVE AND *S* WAVE (EXPERIMENTAL DATA AFTER MURPHY (1982)) 124

6.8 COMPARISONS OF CALCULATED AND MEASURED ATTENUATION OF

P1 WAVE AND *S* WAVE (EXPERIMENTAL DATA AFTER MURPHY (1982)) 125

6.9 EFFECTS OF S_{rw} ON: A) THE VELOCITY OF P1; B) THE ATTENUATION OF *P1* 127

7.1 BOUNDARY CONDITIONS 132

7.2 THE SPECIFIED ELEMENT BOUNDARIES $\partial\Omega^e \cap \Gamma_{ij}^n$ 138

8.1 A SOIL COLUMN SUBJECTED TO A LOAD 159

8.2 COMPARISONS OF NUMERICAL AND ANALYTICAL SOLUTIONS

FOR VERTICAL DISPLACEMENTS AT DEPTH 0.0 M AND 1.0 M 161

8.3 COMPARISONS OF NUMERICAL AND ANALYTICAL SOLUTIONS

FOR PORE WATER PRESSURES AT VARIOUS LOCATIONS 162

8.4 COMPARISONS OF THE NUMERICAL AND ANALYTICAL SOLUTIONS

FOR THE VERTICAL DISPLACEMENTS ALONG THE COLUMN 163

8.5 TIME HISTORY OF THE VERTICAL DISPLACEMENTS

AT DEPTH OF 0.5 CM AND 2.0 CM 165

8.6 PORE WATER AND AIR PRESSURE RESPONSES AT DEPTH 0.5 CM AND 2.0 CM. 166

8.7 SCHEMATIC OF LIAKOPOULOS' EXPERIMENT (LIAKOPOULOS, 1965) 168

8.8 COMPARISONS OF NUMERICAL PREDICTIONS AND EXPERIMENTAL

RESULTS FOR THE PORE WATER PRESSURES ALONG THE SAND COLUMN 171

8.9 COMPARISON OF NUMERICAL PREDICTIONS AND EXPERIMENTAL RESULTS

FOR THE PORE WATER PRESSURES AT HEIGHTS 0.975 M AND 0.625 M 171

8.10 EVOLUTION OF THE PORE AIR PRESSURE PROFILE BASED ON THE NUMERICAL PREDICTIONS 172

8.11 TIME HISTORY OF THE PORE AIR PRESSURES AT HEIGHTS 0.975 M AND 0.625 M BASED ON THE NUMERICAL PREDICTIONS 173

8.12 EVOLUTION OF THE DEGREE OF SATURATION PROFILE BASED ON THE NUMERICAL PREDICTIONS 173

8.13 EVOLUTION OF THE VERTICAL DISPLACEMENT PROFILE BASED ON THE NUMERICAL PREDICTIONS 174

8.14 MODEL DIMENSIONS AND INSTRUMENTATION FOR CENTRIFUGE MODEL #3 (AFTER MILLER ET AL. (2000)) 175

8.15 TIME HISTORIES OF WATER LEVEL AND CENTRIFUGE ACCELERATION 176

8.16 FINITE ELEMENT MESH OF THE CENTRIFUGE MODEL EMBANKMENT 176

8.17 COMPARISON OF THE PREDICTED HORIZONTAL DISPLACEMENT AT NODE # 22 WITH THE MEASURED RESULTS 178

8.18 COMPARISON OF PREDICTED VERTICAL DISPLACEMENTS WITH THE MEASUREMENTS 179

8.19 COMPARISONS OF THE PREDICTED PORE WATER PRESSURES WITH THE MEASUREMENTS 180

8.20 CHANGES IN THE DEGREE OF SATURATION OF ELEMENT #85, 102, AND 200. 181

8.21 FINITE ELEMENT DISCRETIZATION OF THE KAOLIN EMBANKMENT 184

8.22 INITIAL NET STRESS CONTOURS OF THE EMBANKMENT 185

8.23 TIME HISTORIES OF THE DISPLACEMENTS AT NODE #49 AND #89 186

8.24 Time Histories of the Pore Pressure in Element #10, #14, and #69 188

8.25 Time Histories of the Accelerations of Element # 82

and the Base Motion 189

8.26 Stress Contours at 15.5 Seconds 190

8.27 Definition of the Consolidation Problem 192

8.28 Pore Water Pressure Dissipation in Element #6 and #9 193

8.29 Change of the Displacement at Node #11 194

8.30 Pore Water Pressure Contours 195

ABSTRACT

The mechanical behavior of porous media such as geomaterials is largely governed by the interactions of the solid skeleton (or grains) with the fluids existing in the pores. These interactions occur through the interfaces between bulk components. Traditional analysis procedures of porous media, based on the principle of effective stress and Darcy's law, commonly fail to account for these interactions. In this dissertation, a continuum theory of multiphase porous media is developed, capable of rigorously characterizing the interactions among bulk components. Central to the theory is the implementation of the dynamic compatibility conditions that microscopically represent the constraints on the pressure jumps through interfaces. It is shown that Terzaghi's effective stress and capillary pressure can be characterized within a common framework. Within this context, a theoretical framework for poroelastoplasticity is developed, allowing the hysteresis in capillary pressure and plastic deformation of skeleton to be simulated in a hierarchical way. It is found that the mixture theory-based models of porous media can be linked with Biot's poroelasticity theory. A linear model based on the proposed theory is developed and used to analyze the propagation of acoustic waves in unsaturated soils and favorable comparisons to experimental results are obtained. A finite element procedure is developed and implemented into a computer code (called U_DYSAC2) for elastoplastic static and dynamic analyses of saturated and unsaturated porous media. Numerical examples including wave propagation, two-phase flow, consolidation, and seismic behavior of an embankment are presented. These examples show the capability of the theory for modeling a wide variety of behaviors of porous media.

Chapter 1 INTRODUCTION

1.1 Preliminaries

Study of the behavior of porous media is of great interest in a number of diverse fields, such as civil engineering, environmental science, petroleum engineering, chemical engineering, geophysics, and biomechanics. Failure of a slope after a heavy precipitation, moisture movement in the region surrounding a waste containment area, propagation of earthquake impulses in geomaterials, collapse of an earth dam, and multiphase flow in biological tissues are among the engineering problems where understanding the behavior of porous media becomes crucial.

A porous medium is an assemblage of the solid particles forming a matrix (skeleton) whose voids are filled with several fluids, e.g. water, oil, air and gas. For a porous medium consisting of certain components*, its overall behavior is by and large controlled by the interactions among various coexisting phases. Hence, the analysis of the porous media requires a rigorous procedure that can properly characterize these interactions. Such a procedure was first developed by Biot (1941, 1956a&b, 1962, 1972, 1977). Thus far, most of the procedures extensively used in the analysis of the behavior

* The word "component" and "phase" will be used interchangeably in this dissertation.

of porous media are based on the generalized formulations of Biot's theory. These models consist of two key components, i.e. the principle of effective stress owed to Terzaghi (1936) and flow equations represented by, for example, Darcy's law (Aifantis, 1980).

It has been well recognized that Darcy's law is valid for the fluid dissipation with low Reynold's number, e.g. for laminar flow, which generally is the case in the porous media. On the other hand, the Terzaghi's effective stress principle strictly holds only for the porous media constituted by an elastic and/or plastic solid component that is incompressible. If the porous medium consists of an elastically compressible solid component, this principle remains applicable, although it needs to be slightly modified (Lade and de Boer, 1997). For the porous materials such as the rock masses with occluded porosity and the swelling soils, however, the concept of Terzaghi's effective stress cannot be applied. The reason is that in those porous media the solid phase may experience irreversible compression so that the effective stresses cannot be defined in the customary sense (Coussy, 1989b; Bennethum et al., 1997; Murad and Cushman, 1997).

The restrictive character of the effective stress principle becomes even more obvious when we try to generalize this principle to account for the behavior of the porous materials with multiphase flow. In modeling unsaturated soils, for instance, the difficulties in developing a single effective stress equation have been well recognized (Aitchison and Donald, 1956; Bishop and Donald, 1961; Bishop and Blight, 1963; Blight, 1965). These difficulties lead to the introduction of the theory of mixtures in deriving the governing equations of porous media. In the models of porous media derived from the

continuum theory of mixtures, the microscopic structures of the porous media have been smeared out, and hence volume fractions or porosity is usually introduced to recover these microscopic structures. Consequently, the *closure equations* due to introducing volume fractions must be developed so that a closure description of the porous media can be achieved. Thus far, however, a procedure that can be satisfactorily used to derive the closure equations has not been developed. A rigorous theoretical framework that can be generally applied to modeling the behavior of porous media remains to be done. This motivates the research of this dissertation.

1.2 Microscopic Considerations

One of the salient features of porous media is the existence of the interfaces among various coexisting components (as schematically shown in Fig. 1.1). Basically, the interactions, such as phase change and hydraulic dragging between two bulk components, take place only through the interfaces (assuming the electro-magnetic effects are negligible). At the microscopic scale, the mechanical interactions on an interface can be categorized into two groups. One is the dragging force due to the relative motions of various components in the direction tangential to the interface; the other is due to the material impenetrability and represents some sort of force equilibrium, i.e. the *capillary equilibrium*, in the direction normal to the interface.

If the porous medium is isotropic, as usually assumed in a local averaging procedure, the first type of interactions has a macroscopic counterpart, i.e. the hydrodynamic drag, which can be taken into account by using the flow equations of

Darcy's type (Aifantis, 1980; Prevost, 1980). An example of the second type of interactions at the macroscopic scale is the moisture retention curve usually introduced in the analysis of multiphase flow. The moisture retention curve is a relationship between matric suction (i.e. the capillary pressure on the interface between two fluids) and the degree of saturation. Although this kind of relationships has been extensively investigated, its character remains poorly understood (Muccino et al., 1998). Furthermore, little is known so far about the coupling effects between the deformation and the matric suction.

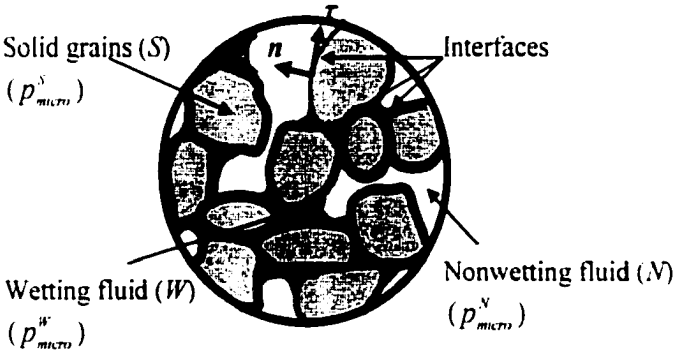

Figure 1.1 Microstructure of a three-phase porous medium

To get insights into the problem, we intuitively consider the capillary equilibrium from a microscopic point of view. Let p^{α}_{micro} be the *microscopic* pressure of α-component (see Fig. 1.1). At equilibrium, the pressure difference $(p^{\alpha}_{micro} - p^{\beta}_{micro})$ on $\alpha\beta$-interface is not arbitrary, and it is a function of surface tension, temperature, the local geometry of

voids, the local distribution of fluid content, etc.. This is the so-called dynamic compatibility conditions on the interfaces (Wilmanski, 1995). Assuming isotropy of the porous medium, these dynamic compatibility conditions can be averaged onto the macroscopic scale to yield the relationships between the capillary pressures and some macroscopic state variables Ξ (e.g. the porosity and degree of saturation). Hence, we can write $p^{\alpha} - p^{\beta} = \nu^{\alpha\beta}(\Xi)$, where p^{α} is the (averaged) pressure of α-phase and $\nu^{\alpha\beta}$ is a function of state variables Ξ. In the limit case where the porous medium is constituted by incompressible solid grains and saturated by a single fluid, the material impenetrability yields the constraint $p^{S}_{micro} = p^{W}_{micro}$ on the interface. As a consequence, $p^{S} = p^{W}$, i.e. the capillary pressure is zero. Based on the theory of porous media, it can be easily proved that the zero capillary pressure condition, i.e. $p^{S} = p^{W}$, yields the Terzaghi's effective stress equation for the saturated porous media (Prevost, 1980; Murad and Cushman, 1997). In other cases, however, $p^{\alpha} - p^{\beta}$ is generally not equal to zero.

The capillary equilibrium in porous media is achieved through local fluid flow, a *capillary relaxation* process due to the fluid exchange driven by the non-equilibrium capillary forces between the pores of different sizes. It must be noted that, although the local fluid flow may be substantially influenced by the macroscopic fluid flow driven by pressure gradient or *vice versa*, the former has nothing in common with the latter. In fact, the capillary relaxation time is generally of the same order as or even larger than the characteristic time scale of macroscopic fluid flow (Buyevich, 1995) and that of the skeleton deformation. Consequently, the Terzaghi's effective stress principle can not be applied to the porous media such as swelling soils (Bennethum et al., 1997; Murad,

1999), in which the effects of the capillary relaxation on the overall behavior of the material can no longer be neglected. Furthermore, since the capillary relaxation may induce energy loss, the change of capillary pressures with the material state is usually irreversible and accompanied by *hysteresis* phenomena.

From the above discussions, it is quite obvious that the effective stresses and the capillary pressures are closely correlated through the dynamic compatibility conditions on the interfaces. At macroscopic scale, the dynamic compatibility conditions on the interfaces can be represented by the relationships between the capillary pressures and state variables. Since these relationships are independent of any balance equations or constitutive relationships for an individual component, they can be used as the closure equations mentioned above. Therefore, in order to develop a continuum model of porous media, it becomes crucial to properly simulate the change of the capillary pressures with the state of the material.

1.3 Objectives

The objective of this dissertation is to develop a *continuum* model of porous media capable of rigorously incorporating the effects of the interactions on the interfaces discussed above. The porous media of concern are those saturated by two immiscible simple fluids. To this end, the general structure of constitutive relationships is first investigated within the frameworks of the continuum theory of porous media and the irreversible thermodynamics. A nonlinear continuum model of the porous media is then developed, which accounts for the finite deformation and elastoplasticity. A

thermoporoelastic model is derived from a formal linearization of the general theory, and employed to simulate the propagation of the body waves in the porous media. General initial/boundary value problems concerning the behavior of porous media are constructed, and the corresponding finite element solution procedures are presented. Various numerical examples are introduced to show the validity and capability of the proposed model in simulating the behavior of porous media.

1.4 Contributions

To the author's knowledge, the following aspects of this dissertation are original:

- The effective stresses and capillary pressures are found to have a common microscopic origin, that is, the dynamic compatibility conditions on the interfaces. By considering these compatibility conditions, the restrictions on the use of the effective stresses can be removed.

- A theoretical framework capable of rigorously incorporating the dynamic compatibility conditions on the interfaces is established. Within this framework, it is possible to describe the nonlinear behaviors, such as plasticity and capillary hysteresis of multiphase porous media, in a unified way.

- Establishing a connection between the Biot's theory of porous media and the models of porous media based on the continuum theory of mixtures. Through this connection, a continuum model of the porous media saturated by multiple fluids can be developed in a rather straightforward manner.

1.5 Outline of the Dissertation

The outline of the dissertation is as follows. After a review of the state of knowledge in Chapter 2, general constitutive relationships are developed within the framework of the theory of mixtures in Chapter 3. The emphasis here is on the restrictions exerted by the second law of thermodynamics on various dissipative mechanisms, particularly, the irreversibility of the capillary pressures and plastic deformation. Based on the general constitutive relationships developed in Chapter 3, a nonlinear model of the porous media is derived in Chapter 4. By investigating the variational structure of the proposed model, a connection is established between the Biot's theory of porous media and those based on the theory of mixtures. Such a connection provides a way to incorporate the dynamic compatibility conditions on the interfaces into a continuum model of porous media and allows the field equations for the porous media with multiple fluids to be easily generated.

By directly linearizing the general theory developed in Chapter 3&4, a thermoporoelastic model is presented in Chapter 5. Through these derivations, it is clearly shown that the restrictions in the application of the effective stress can be released by introducing the dynamic compatibility conditions on the interfaces. Furthermore, it is shown that many classic models used in geomechanics are derivable from the proposed theory. As an application and validation of the proposed theory, Chapter 6 investigates the propagation conditions of the body waves in porous media, where theoretical results are compared with experimental data.

Chapter 7 deals with the initial/boundary value problems on the static and dynamic behaviors of porous media. Two sets of the statements of problems are considered that are appropriate for various situations. The corresponding finite element solution procedures are developed and implemented. Finally, several numerical examples using the finite element code developed are presented in Chapter 8.

Chapter 2 CURRENT STATE OF KNOWLEDGE

2.1 Continuum Theories of Porous Media

The first continuum theory of porous media was developed by Biot (1941, 1956a&b, 1962), and was used to describe the isothermal, linear elastic behavior of the porous media saturated by a single fluid. This theory was later generalized to account for the finite elastic deformation of saturated porous media (Biot, 1972). The above generalization involves two important concepts, i.e. the pressure function $\mu(p^{w})$ and the increase of the total fluid mass in a unit volume of the porous medium (denoted by m). Function μ relates the fluid chemical potential to the fluid pressure p^{w}. Variable m equals ($Jn\rho^{w} - n_0\rho_0^{w}$), where J is the determinant of the deformation gradient $\boldsymbol{F}$, n is the porosity, and ρ^{w} is the fluid mass density; a quantity with a subscript "0" represents an initial value. Later, Biot (1977) presented a more general theory of porous media by introducing the so called "principle of virtual dissipation", a generalization of d'Alembert's principle to non-linear irreversible thermodynamics. This principle is quite heuristic, although it can be used to generate the field equations of the porous media in a very straightforward manner.

In Biot's theory, due to the use of variable m, the flow equation is put into a convective format that is particularly appropriate for the flow in the porous media with a deforming skeleton. In the convective description, the motion of the fluid is described with respect to the (material points of) solid skeleton. Since the fluid outside the domain spanned by the deforming skeleton has no influence on the behavior of the porous medium, it is more convenient to describe the fluid motion with respect to the deforming skeleton. In this setting, the convected flow equation keeps objectivity. This is desirable for the analysis of the porous media at finite deformation. Furthermore, the boundary conditions can be very easily defined in a numerical procedure based on the convective formulation.

Recently, Biot's theory had been generalized into the global context of the thermodynamics of open continua by Coussy (1989a&b, 1995). In Coussy's model, the concept of plastic porosity is introduced so that the irreversible compression of solid grains can be taken into account. Generally, the irreversible part of m may have two contributions, i.e. the plastic deformation of the skeleton and plastic porosity. If the solid grains experience irreversible compression, the plastic porosity is not derivable from the plastic deformation of the skeleton, and an independent evolution equation must be developed for it. In this case, the effective stresses are no longer appropriate for the description of the constitutive behavior of porous media. Clearly, Coussy's model is more general than the effective stress-based models that will be discussed later in this chapter. Recently, Coussy's model has been slightly modified and applied to the numerical analysis of the behavior of saturated porous media (Amero, 1999).

The generalized formulations of Biot's theory most extensively used in practice are those developed by Zienkiewicz et al. (1977, 1982) and Prevost (1980), which are all heuristic in nature. Since these models themselves place no restrictions on the constitutive relationships of the porous media, phenomenological stress-strain relationships that are based on some stress measures (e.g. the effective stresses) must be introduced. In addition, the Darcy's-type flow equations are intuitively employed to describe the fluid diffusion. Note that the above models are appropriate for many saturated geomaterials, for which the stress measure can be properly defined. In general, however, an intuitive choice of the stress measure in modeling the material behavior must be done with caution, since it may incur thermodynamic inconsistency. We will further discuss this point in the following section.

One of major difficulties in applying Biot's theory (including its generalizations) stems from the fact that these models do not consider the microscopic structures that play critical roles in the overall behaviors of the porous media, as discussed in the last chapter. The theories of mixtures can play a role in alleviating this difficulty. Comprehensive reviews on this subject can be found in Bedford and Drumheller (1983) and de Boer (1996). Within the framework of the mixture theories, some variables, e.g. the volume fractions of individual components, are employed to represent the microstructure of porous media. This induces the equation-deficiency problem. Therefore, complementary equations must be developed so that a complete set of governing equations can be obtained. These complementary equations are usually called the closure equations. One of the key steps in developing a model of porous media is to formulate the closure equations.

Traditionally, the closure equations are obtained in one of the following ways. One may introduce additional constitutive equations (Morland, 1972; Bowen, 1980; de Boer, 1996; de Boer and Bluhm, 1999). Alternatively, the introduced variables are treated as internal variables and their evolution equations are developed based on the principles of continuum mechanics (Bowen, 1982; Svendsen and Hutter, 1995). In addition, balance equations can be directly established for the introduced variables (Goodman and Cowin, 1972; Passman, 1977; Wilmanski, 1996).

Among the models mentioned above, those proposed by Bowen (1982) and de Boer et al. (de Boer, 1996; de Boer and Bluhm, 1999) are of primary interest here. In Bowen's theory, the volume fractions are introduced as internal variables so that the microstructure of the porous media can be taken into account to some extent. This theory accounts for the pore relaxation effects that are important for some applications, e.g. the subsurface oil production processes. This theory includes the Biot's poroelasticity model as a particular case and can be used in the analysis of the elastically deforming porous media with multiphase flow. Although the thermodynamic restriction on the evolution of volume fractions is given, the evolution equations have not been explicitly treated in Bowen's theory. Furthermore, Bowen's theory does not take into account the compressibility of the solid phase. It has been recognized, however, that the compressibility of the solid phase plays important roles in the overall behavior of porous media (Lade and de Boer, 1997).

Recently, de Boer and his coworkers (e.g., de Boer, 1996; de Boer and Bluhm, 1999) proposed a procedure that can be used to formulate the closure equations in the

continuum models of porous media. In this procedure, the deformation gradient (defined in Chapter 3) is decomposed into two components accounting for the deformation of real material and change of the porosity. It is noted that both of these two components contain the microscopic aspects of the porous medium. If a constitutive relationship is developed for one of these two deformation components, the other is fully determined. Consequently, an additional constitutive equation is obtained, and it can be used as the closure equation. Although this model can be used to describe the behavior of saturated porous media, its usefulness in modeling the porous media saturated by multiple fluids is uncertain. The reason for this is that the microscopic interactions on the interfaces, which have been discussed in the previous chapter, cannot be taken into account. In fact, it is unclear so far how to apply the above procedure to multiphase porous media.

In recent years, following a line quite different from those cited above, Gray and his coworkers (Hassanizadeh and Gray, 1990; Gray and Hassanizadeh, 1991) proposed a model of porous media, in which interfaces are explicitly considered as independent phases. This model gives some new insights into the constitutive structure of multiphase porous media. Remarkably, it was found for the first time that the evolution of capillary pressure is restricted under the second law of thermodynamics. This result can be used to deduce the relationship between the capillary pressure and state variables of the material. Oddly, this important result seems to have been overlooked or, at least, underutilized. In the application of the above model, although it was recognized that the effects of the capillary relaxation could be significant, the time effect had been simply omitted in interpreting the capillary phenomena (Gray and Hassanizadeh, 1991; Hassanizadeh and Gray, 1993; Muccino et al., 1998).

Based on their theory, Hassanizadeh and Gray (1993) proposed that the suction (P^c) must be a function of the degree of saturation (s^w) and the area density of the meniscus (a^{wn}) and the hysteresis can be explained as simply the projection of the hypersurface $P^c - s^w - a^{wn}$ on to the $P^c - s^w$ plane. To verify this conjecture, Celia and his coworkers have developed a functional relationship among P^c, s^w, and a^{wn} based on a pore-scale computational model (Reeves and Celia, 1996; Celia et al., 1998). They found that, although the suction is a function of s^w and a^{wn}, the explicit form of the hypersurface $P^c - s^w - a^{wn}$ still depends on the path of state, e.g. imbibition or drainage, to some extent. Clearly, this result is inconsistent with the above conjecture.

Here, it is worthwhile to emphasize that the *hysteresis* in the capillary pressure is phenomenological and it represents a kind of energy dissipation. From the standpoint of continuum mechanics, it should be possible to link the hysteresis phenomenon with some dissipative mechanism occurring in the porous media. In other words, capillary phenomena can be simulated within the framework of the continuum mechanics. This point will be an underlying theme of this dissertation. Very recently, parallel to the procedure developed by Gray and his coworkers, a thermomechanical model of porous media have been developed by Muraleetharan and Wei (1999), in which the volume fractions are introduced as state variables. One of the important results of this work is that the thermodynamic restrictions on the evolutions of all the capillary pressures have been established. In this dissertation, using the standard principles of continuum mechanics, the theoretical results of Muraleetharan and Wei's work will be further generalized, and a continuum model of porous media will be derived.

2.2 Stress-Strain Constitutive Modeling

Modeling the stress-strain constitutive behavior of porous media has been closely linked with the efforts to identify the relevant stress measures concerning the behavior of porous media. In phenomenological approaches, the stress measures used to describe the constitutive relationships of porous media include the total stresses, the effective stresses (Terzaghi, 1936), the two stress state variables (Fredulund and Morgenstern, 1977), and those based on the mixture theories. The effective stress-based constitutive models, such as the celebrated Cam Clay model (Schofield and Wroth, 1968), are thermodynamically consistent in general, when applied to the saturated porous media constituted by incompressible solid grains (see, e.g., Ehlers, 1989, 1993; Coussy, 1995: pp.84-208). In modeling the saturated porous media constituted by an elastically compressible solid phase, the effective stresses can still be employed with slight modifications (Lade and de Boer, 1997). These observations are very important, since most of the constitutive models of porous media available in literature are based on the Terzaghi's effective stresses.

Due to the success in modeling the saturated porous media based on the effective stresses, it becomes natural to generalize the effective stress concept to the multiphase porous media (see, e.g., Bolzon et al., 1996). In modeling the porous media saturated by two immiscible fluids, such as unsaturated soils, the most frequently used effective stress equation is the so-called Bishop's formulation (Bishop, 1959). Difficulty in applying this formulation was recognized by Aitchison and Donald (1956), Bishop and Donald (1961), Bishop and Blight (1963), and Matyas and Radhakrishna (1968). This led to a tentative proposition by Fredlund and Morgenstern (1977) that any pair among net stress, suction,

and the excess of total stress over pore water pressure can be used as independent stress state variables. Here, the net stress equals to the total stress minus pore air pressure and the suction is the subtraction of pore water pressure from pore air pressure.

In the early practice of unsaturated soil mechanics, the two stress state variables had been used to simulate some discrete, local aspects of the mechanical behavior of unsaturated soils. Important contributions to this topic include the works by Coleman (1962), Fredlund (1979), Lloret and Alanso (1980, 1985), Escario and Arez (1986), and Fredlund et al. (1987). Although these works cover many aspects of unsaturated soils, an integrated scheme for the constitutive behavior of porous materials was not available until Alonso et al. (1990) presented an elatsoplastic model using the concept of two stress state variables. Alonso et al. (1990) developed their model within the framework of the Cam Clay model (Schofield and Wroth, 1968) by introducing the concept of LC curve (i.e. the load-collapse curve). This model was examined based on experimental data by Cui and Delage (1996), Wheeler and Sivakumar (1995), and Wheeler (1996). It was found that for the completeness of the model specific water volume (the volume of water plus solids in a volume of soil containing a unit volume of solid) must be included.

Based on Wheeler's model (Wheeler, 1996) and the bounding surface plasticity (Dafalias and Herrmann, 1986), Muraleetharan and Nedunuri (1998) developed an elastoplastic model for the unsaturated soils. This model keeps all the main features of Wheeler's model. In addition, Muraleetharan and Nedunuri's model can handle the cyclic plasticity of the unsaturated soils. Although it is quite primitive, this model seems to be the first one that incorporates cyclic plasticity of unsaturated soils.

In recent years, the two stress state variables become more and more popular in modeling the behavior of unsaturated soils. Although the constitutive models based on these two variables may capture some features of the porous materials, the thermodynamic basis for the use of the two stress state variables has not yet been established. This may create concerns in applications, since it is difficult to imagine that one can employ a stress measure confidently without knowing its conjugated strain. In fact, difficulties in applying these models have been recognized (Li et al., 1999; Vaunat et al., 2000). In addition, it is quite obvious that the two stress state variables can be applied only for porous media saturated by two immiscible fluids and can not be generalized for porous media with multiple fluids.

The stress-strain constitutive relationships can also be established within the framework of theory of mixtures (e.g., Robin et al., 1996; Loret and Khalili, 2000). Studies in this respect are primitive, though such models are practically and theoretically appealing. Due to its thermodynamic consistency, the approach to developing constitutive relationships based on the theory of mixtures is more rigorous than the others mentioned above. In fact, the effective stress models can be viewed as particular cases of the models based on the theory of mixtures (see, e.g. Ehlers, 1993).

2.3 Wave Propagation in Porous Media

Interestingly, the early studies on the dynamic behavior of porous media concern exclusively the wave propagation in porous media (e.g., Biot, 1956a&b; Brutsaert, 1964). Thus far, the analysis procedures for the wave propagation in the poroelastic materials

saturated by a single fluid have been fairly well developed (Bourbie et al., 1987). These analysis procedures are generally based on Biot's theory or its generalized formulations. They predict the existence of two compressible waves and one rotational wave in a saturated porous material. The rotational wave and the faster compressional wave are similar to those in the single-phase continua, though the former is slightly dissipative. However, the second compressional wave, usually called Biot's wave, is highly diffusive, and hence generally elusive in the experimental observations. The Biot's wave was first observed by Plona (1980) and later confirmed by Berryman (1980). Several analytical solutions have been presented in the literature that treat the problem of wave propagation in saturated porous media under various conditions (see, for example, Garg et al., 1974; Simon et al., 1984; de Boer et al., 1993, and Gajo and Mongiovi, 1995).

By contrast, the problem of wave propagation in the porous media saturated by multiple fluids received limited attention from researchers. It seems that Brutsaert (1964) is the first one who generalized Biot's theory to account for the acoustical behavior of porous media such as unsaturated soils. He found that in general there exist three compressional waves in the porous media saturated by two immiscible fluids. The existence of the third compressional wave is due to the presence of a second fluid component in the pores. The first analytical solution of the problems concerning the body waves in unsaturated porous media is owed to Garg and Nayfeh (1986). This model is based on a generalization of Biot's theory, where additional constitutive equations (the closure equations) were assumed for the porosity and the degree of saturation.

In a different context, Tuncay and Corapcioglu (1996, 1997) developed a model to describe the body waves in the poroelastic materials saturated by two fluids. In this model, the field equations valid in microscopic scale are directly averaged to macroscopic level, and the capillary equilibrium on the meniscus between the water and air is explicitly taken into account. This model also predicts the existence of the third compressional wave. Intrinsically, this model is equivalent to a generalization of Biot's model.

Thus far, several experimental studies have been presented in the literature regarding the acoustical properties of elastic porous media. A comprehensive review on this subject was given by Bourbie et al (1987). Most of these studies are concerned with high frequency (i.e. ultrasonic) waves only. In the higher frequency range, however, the basic assumptions in a usual linear model of porous media, e.g. frequency-independent and continuum, may break down. For the purpose of comparison with the theoretical results based on the continuum models, the experimental observations on the low frequency waves are desirable. Murphy (1982, 1984) provided such an experimental study, considering the acoustical waves in the Missillon sandstone saturated by water and air.

2.4 Finite Element Analysis Procedures

Several finite element analysis procedures available in the literature are all based on the simple generalizations of the Biot's theory. In the procedures developed in the early stage, the constitutive behaviors of the porous media are described exclusive by using the

effective stresses. In these models, the effect of the degree of saturation on the behavior of the porous media are implicitly and approximately taken into account by introducing some relationships that present the fluid compressibility as a function of the degree of saturation. Here, the works by Ghaboussi and Kim (1984), Chang and Duncan (1983), and Vardoulakis and Bestos (1983, 1986) are good examples.

Fully coupled analysis procedures of the behavior of multiphase porous media are only available in recent literature, and majority of these studies is devoted to the static problem. Extensive references are given and discussed in a new book by Lewis and Schrefler (1998). The key components of these models include the formulations of Biot's type, soil-water relationship, hydraulic properties as functions of the water content, and a effective stress formulation (usually Bishop's formulation).

It seems that the first dynamic analysis procedure considering the effect of negative water pressure on the deformation of unsaturated soils was given by Zienkiewicz et al (1990b). In a strict sense, this procedure is not fully coupled, since for convenience the authors had assumed that the air pressure remains constant and equal to the ambient air pressure. On the other hand, recent research shows that the air pressure might experience significant change during the deformation process (Schrefler and Zhan, 1993). Furthermore, during a dynamic event, even stronger coupling between the air and the other phases may be expected. In recent years, a fully coupled dynamic analysis procedure, capable of simulating the multiphase flow within deformable porous media, have been developed by Li et al (1990) and Li and Zienkiewicz (1992). This procedure can be viewed as an extension of the one by Zienkiewicz et al (1990). In this procedure,

however, the gas phase is formally considered as an independent phase. This procedure was later extended to the finite deformation problems by Meroi et al (1995), and very recently it has been used in analyzing the dynamic behavior of unsaturated soils (Schrefler and Scotta, 2001).

Although there is increasing interest in using the two-stress-state variables to model the constitutive relationships of unsaturated soils, application of these constitutive models in the numerical analysis is still primitive. Several applications concerning the static behaviors of unsaturated soils can be found in the literature, for instance, Alonso et al (1998) and Thomas and He (1998). Thus far, it seems that no dynamic analysis procedures are available that explicitly incorporate the constitutive relationships using the two-stress-state variables.

Chapter 3 A CONTINUUM THEORY OF POROUS MEDIA SATURATED BY TWO IMMISCIBLE FLUIDS

The objective of this chapter is to develop a continuum theory of porous media saturated by two immiscible fluids within the framework of the theory of mixtures. We assume that the fluid is *simple*, i.e. no molecular diffusion is considered. For clarity and generality, the fluids will be denoted as the *wetting* fluid (W) or *non-wetting* fluid (N) corresponding to the relative value of their wetting potentials.

In what follows, it is assumed that any point in the domain spanned by the solid skeleton is simultaneously occupied by all the phases. This is the point of view of the continuum theory of mixtures. However, the procedure followed here differs from the other theories of mixtures in that it explicitly deals with *the dynamic compatibility conditions on the interfaces* discussed in Chapter 1.

3.1 Basic Assumptions and Kinematics

In the theory to be developed below, *macroscopic* state parameters and balance equations are obtained by integrating their *microscopic* counterparts based on a local averaging procedure (Hassanizadeh and Gray, 1979 I&II). For instance, the volume fraction of a bulk component is a macroscopic (or average) quantity obtained by dividing

the total volume of that component in the representative elementary volume* (REV) by the total volume of the REV (see Fig. 3.1).

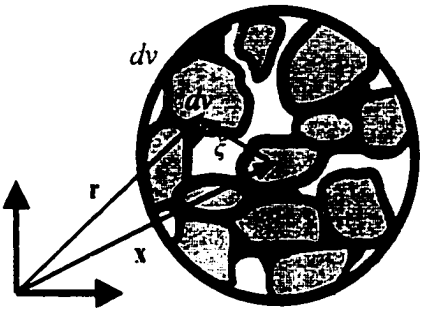

$$n^{\gamma}(x,t) = \frac{\sum dv^{\gamma}}{dv}$$

Figure 3.1 A representative elementary volume (REV)

Let D be the characteristic size of the REV used in the averaging procedure. If a state parameter is computed using the averaging volumes (REVs) that vary from a small size to a very large size, the computed quantity will fluctuate with D when D is less than a certain value ℓ (as shown in Fig. 3.2). When $\ell < D < L$, the computed parameter is not very sensitive to the size of the REV. If, however, the size of the REV is further increased so that $D > L$, gross inhomogeneities are induced that may affect the stability of the averaged parameter. To obtain meaningful average quantities, it is required that the size of the averaging volume (REV) must satisfy the inequality $\ell << D << L$ (Whitaker, 1969). Typically, $\ell = 50$ micron for sands and $\ell = 1$ micron for clays, whereas $L = 1$ cm. In this range of D, all the average quantities are independent of the size of the REV.

* A representative elementary volume (REV) is the infinitesimal averaging volume used in the averaging procedure.

In the following, we assume that an averaging volume of such a characteristic size exists for the porous media under considerations. Consequently, all the macroscopic state parameters can be defined in the domain of concern and represented by the functions of spatial coordinates and time.

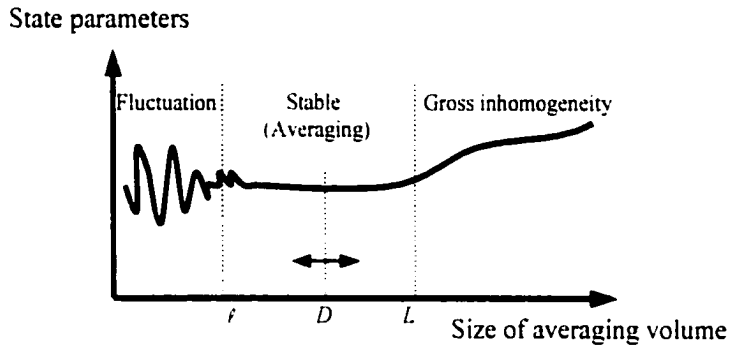

Figure 3.2 State parameters as a function of the size of REV

In what follows, α or β is used to denote an individual bulk component; $\alpha\beta$ represents an interface between α-phase and β-phase. Standard solid mechanics sign convention is used, i.e. tensile stresses are positive. Let $\mathcal{B}^\alpha \subset \mathbb{R}^3$ be a fixed but otherwise arbitrary reference configuration of α-phase. As usual in the theory of mixtures, each individual phase is assigned an independent motion defined by

$$\chi_t^\alpha : \mathcal{B}^\alpha \mapsto \mathcal{S}_t^\alpha \subset \mathbb{R}^3, \text{ i.e. } \boldsymbol{x} = \chi_t^\alpha(\boldsymbol{X}^\alpha) = \chi^\alpha(\boldsymbol{X}^\alpha, t). \qquad (3.1.1)$$

where $\alpha = S, W, N$; $\mathcal{S}_t^\alpha \subset \mathbb{R}^3$ is the current configuration, and $t \in [0, T] \subset \mathbb{R}^+$ the elapsed time; $\boldsymbol{X}^\alpha$ represents the coordinate of a particle (denoted by p^α) of α-phase in its

reference configuration; **x** is the spatial position of p^α at time t (see Fig. 3.3). Function $\chi^\alpha(\boldsymbol{X}^\alpha,t)$ is assumed to be invertible and differentiable as many times as necessary. Inverting (3.1.1) leads to

$$\boldsymbol{X}^\alpha = \chi_t^{\alpha\,-1}(\boldsymbol{x}) = \chi^{\alpha\,-1}(\boldsymbol{x},t). \tag{3.1.2}$$

The velocity and acceleration of p^α are defined, respectively, by

$$\boldsymbol{v}^\alpha(\boldsymbol{x},t) = \frac{\partial \chi^\alpha(\boldsymbol{X}^\alpha,t)}{\partial t}, \tag{3.1.3}$$

and

$$\boldsymbol{a}^\alpha(\boldsymbol{x},t) = \frac{\partial^2 \chi^\alpha(\boldsymbol{X}^\alpha,t)}{\partial^2 t} = \frac{\partial \boldsymbol{v}^\alpha(\boldsymbol{x},t)}{\partial t} + \boldsymbol{v}^\alpha \cdot \nabla \boldsymbol{v}^\alpha, \tag{3.1.4}$$

where ∇ represents the spatial gradient, and the operator $(\partial/\partial t + \boldsymbol{v}^\alpha \cdot \nabla)$ is the so-called material derivative with respect to the motion of α - phase and written as D^α/Dt.

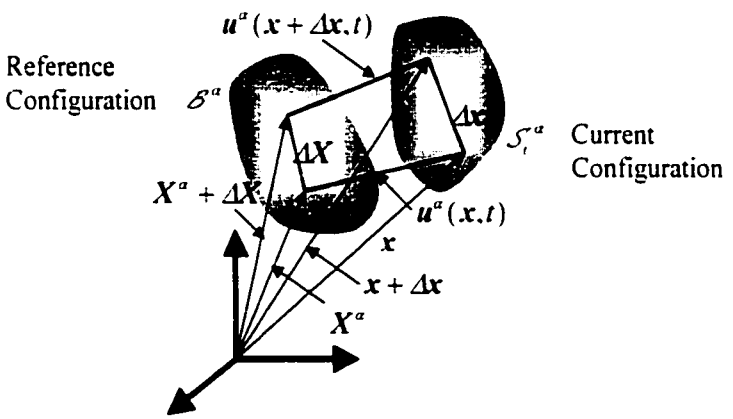

Figure 3.3 The motion and displacement of an individual phase

The displacement of the material point $\boldsymbol{X}^\alpha$ is given by (see Fig. 3.3)

$$\boldsymbol{u}^\alpha(\boldsymbol{x},t) = \chi^\alpha(\boldsymbol{X}^\alpha,t) - \boldsymbol{X}^\alpha. \tag{3.1.5}$$

where equation (3.1.2) is used. It is assumed for convenience that the reference and initial current configuration (at $t=0$) are coincident. With equation (3.1.5) and by the definitions of (3.1.3) and (3.1.4), one has

$$\boldsymbol{v}^\alpha(\boldsymbol{x},t) = \frac{\partial \boldsymbol{u}^\alpha(\boldsymbol{x},t)}{\partial t}\Big|_{\boldsymbol{x}^\alpha} = \frac{D^\alpha}{Dt}\boldsymbol{u}^\alpha(\boldsymbol{x},t). \tag{3.1.6}$$

and

$$\boldsymbol{a}^\alpha(\boldsymbol{x},t) = \frac{\partial \boldsymbol{v}^\alpha(\boldsymbol{x},t)}{\partial t}\Big|_{\boldsymbol{x}^\alpha} = \frac{D^\alpha}{Dt}\boldsymbol{v}^\alpha(\boldsymbol{x},t). \tag{3.1.7}$$

Conventionally, the reference configuration of the solid skeleton is used as the reference configuration for the motions of the fluids in the mixture. Such a convention is justified by the fact that, as far as the fluids are concerned, of interest only is the part within the domain spanned by the solid skeleton, i.e. $\mathcal{S}_t^S$. When the *reference* configuration $\mathcal{B}^S$ of the solid skeleton is used, the description of the motions is called Lagrangian (or material). Otherwise, if the *current* configuration $\mathcal{S}_t^S$ of the solid skeleton is used, the description of the motions is Eulerian (or spatial).

In either case, it is useful to define the relative displacement and relative velocity of a fluid *with respect to the deforming solid skeleton*. Let $\boldsymbol{x} \in \mathcal{S}_t^S$, the *relative* displacement of the material point of fluid α is defined as

$$\boldsymbol{u}_r^\alpha(\boldsymbol{x},t) = \boldsymbol{u}^\alpha(\boldsymbol{x},t) - \boldsymbol{u}^S(\boldsymbol{x},t). \tag{3.1.8}$$

The corresponding relative velocity of a fluid is therefore given, in the Eulerian description, by

$$w^{\alpha}(x,t)=\left.\frac{\partial u_t^{\alpha}(x,t)}{\partial t}\right|_{X^{\alpha}\&X^{S}\ fixed}=v^{\alpha}(x,t)-v^{S}(x,t),\ x\in\mathcal{S}_t^{\alpha}. \qquad (3.1.9)$$

Now, what is the *Lagrangian* counterpart of the relative velocity of a fluid particle? Due to its importance in developing the flow equations, we will derive in details the Lagrangian relative velocity of a fluid particle in the following. Let $W^{\alpha}(X^{S},t)$ $= w^{\alpha}\circ\chi^{S}(X^{S},t)$, where $f\circ g$ represents a compound function. By definition (3.1.9), it is noted that $W^{\alpha}(X^{S},t)$ does not represent the Lagrangian relative velocity of a fluid particle, since the mapping $\chi_t^{\alpha\,-1}:x\mapsto X^{\alpha}$ $(\alpha=W,N)$ changes from time to time.

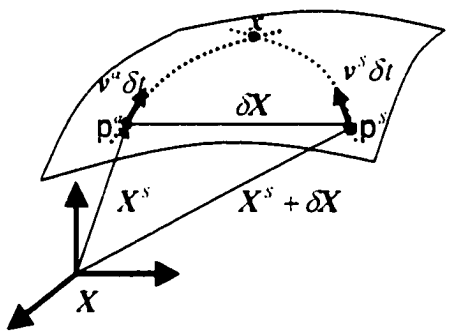

Figure 3.4 Lagrangian relative velocity of a fluid particle

Consider a fluid particle p^{α} located at $x^{1}=\chi^{S}(X^{S},t)\in\mathcal{S}_t^{1}$ (as shown in Fig. 3.4). In a neighborhood of p^{α}, there exists a solid particle p^{S} located at $x^{2}=\chi^{S}(X^{S}+\delta X,t)$ $\in\mathcal{S}_t^{S}$, which will meet p^{α} after δt seconds. We may write

$$\begin{aligned} \boldsymbol{x}^t + \boldsymbol{v}^a(\boldsymbol{x}^t, t)\delta t &= \boldsymbol{x}^s + \boldsymbol{v}^s(\boldsymbol{x}^s, t)\delta t \\ &\approx \boldsymbol{\chi}^s(\boldsymbol{X}^s, t) + \boldsymbol{F}\delta\boldsymbol{X} + \boldsymbol{v}^s(\boldsymbol{x}^t, t)\delta t. \end{aligned} \tag{3.1.10}$$

It follows from (3.1.10) that

$$\boldsymbol{F}\delta\boldsymbol{X} = (\boldsymbol{v}^a - \boldsymbol{v}^s)\delta t. \tag{3.1.11}$$

From the derivations given above, it is clear that the Lagrangian relative velocity of p^a is

$$\boldsymbol{W}_r^a(\boldsymbol{X}^s, t) = \frac{\delta\boldsymbol{X}}{\delta t} = \boldsymbol{F}^{-1}(\boldsymbol{v}^a - \boldsymbol{v}^s), \tag{3.1.12}$$

where $\boldsymbol{F}^{-1}$ is the inverse of the deformation gradient $\boldsymbol{F}$ of the solid skeleton defined by

$$\boldsymbol{F} = \frac{\partial\boldsymbol{\chi}^s}{\partial\boldsymbol{X}^s} = \boldsymbol{I} + \frac{\partial\boldsymbol{u}^s}{\partial\boldsymbol{X}^s}. \tag{3.1.13}$$

where $\boldsymbol{I}$ is the second-order unit tensor with components δ_{iI} (i or $I = 1, 2, 3$), and δ_{iI} is the Kronecker delta. In the following, it is assumed that the transformations between configurations preserve the orientation, i.e. $J = det\,\boldsymbol{F} > 0$.

In deriving equation (3.1.12), it is clear that $\boldsymbol{W}_r^a(\boldsymbol{X}^s, t)$ represents the velocity of a fluid particle at $\boldsymbol{X}^s$ approaching to (or escaping from) the solid particle p^s that will meet (or met) the fluid particle at the moment t. In fact, $\boldsymbol{W}_r^a(\boldsymbol{X}^s, t)$ is the *convective* representation of the relative velocity of a fluid, and obtained by *pulling back* the relative velocity (3.1.9) to the reference configuration.

For later use, we define the Lagrangian strain tensor (i.e. the Green-St. Venant strain tensor) as

$$\boldsymbol{E} = \frac{1}{2}(\boldsymbol{C} - \boldsymbol{I}) = \frac{1}{2}(\boldsymbol{F}^T \boldsymbol{F} - \boldsymbol{I}), \tag{3.1.14}$$

where $\boldsymbol{C} = \boldsymbol{F}^T \boldsymbol{F}$ is the right Cauchy-Green deformation tensor. Linearizing (3.1.14) yields

$$\boldsymbol{E} \cong sym(\nabla \boldsymbol{u}^s) = \frac{1}{2}\left[\left(\frac{\partial \boldsymbol{u}^s}{\partial \boldsymbol{x}}\right)^T + \frac{\partial \boldsymbol{u}^s}{\partial \boldsymbol{x}}\right] = \boldsymbol{\varepsilon}, \tag{3.1.15}$$

where *sym*() represents the symmetrical part of a tensor object and $\boldsymbol{\varepsilon}$ is the strain tensor of the solid skeleton at infinitesimal deformation.

3.2 Balance Equations

The local forms of macroscopic balance equations, developed by Hassanizadeh and Gray (1979 I & II) and Gray and Hassanizadeh (1989) based on a local averaging procedure, are introduced here. This set of balance equations differs from the others in that it includes the balance equations for the interfaces between two bulk phases. Furthermore, the exchange terms in this set of balance equations are physically very well motivated. From now onwards, it is assumed that the interfaces do not carry any averaged thermodynamical properties. This assumption is general enough for the development of a continuum model, since the macroscopic properties of the interfaces are in general much smaller than their bulk-phase counterparts.

For a bulk phase, the mass balance is

$$\frac{D^\alpha(n^\alpha \rho^\alpha)}{Dt} + n^\alpha \rho^\alpha \nabla \cdot \boldsymbol{v}^\alpha = \sum_{\beta \neq \alpha} \hat{c}^\alpha_{\alpha\beta}, \tag{3.2.1}$$

and for an interface

$$0 = -\hat{e}^{\alpha}_{\alpha\beta} - \hat{e}^{\beta}_{\alpha\beta}, \tag{3.2.2}$$

where $\hat{e}^{\alpha}_{\alpha\beta}$ accounts for the rate of mass transfer through $\alpha\beta$-interface to α-bulk phase; n^{α} and ρ^{α} are the volume fraction and *true* mass density, respectively. All the terms with a carat represents exchange terms. (3.2.2) states that $\alpha\beta$-interface does not store any excessive mass. For later discussions, it is useful to introduce the total mass density of the mixture, which is defined by

$$\rho = \sum_{\alpha=S,W,N} n^{\alpha}\rho^{\alpha}. \tag{3.2.3}$$

The equations of linear momentum balance for a bulk phase is represented by

$$n^{\alpha}\rho^{\alpha}\frac{D^{\alpha}\boldsymbol{v}^{\alpha}}{Dt} - \nabla\cdot\left(n^{\alpha}\boldsymbol{t}^{\alpha}\right) - n^{\alpha}\rho^{\alpha}\boldsymbol{b}^{\alpha} = \sum_{\beta\neq\alpha}\hat{\boldsymbol{T}}^{\alpha}_{\alpha\beta}, \tag{3.2.4}$$

and for an interface

$$0 = -\left(\hat{\boldsymbol{T}}^{\alpha}_{\alpha\beta} + \hat{e}^{\alpha}_{\alpha\beta}\boldsymbol{v}^{\alpha}\right) - \left(\hat{\boldsymbol{T}}^{\beta}_{\alpha\beta} + \hat{e}^{\beta}_{\alpha\beta}\boldsymbol{v}^{\beta}\right), \tag{3.2.5}$$

where $\boldsymbol{t}^{\alpha}$ is the macroscopic *true* Cauchy stress tensor of a bulk phase; $\hat{\boldsymbol{T}}^{\alpha}_{\alpha\beta}$ represents the rate of linear momentum transferring to α-phase due to its mechanical interactions with β phase. The total linear momentum transfer has two contributions: one is due to the mass change and the other is due to the mechanical interactions. Therefore, (3.2.5) states that the total linear momentum transfer from α to β is always equal to that from β to α. In the following, it is assumed for simplicity that the external body supplies of linear momentum for all the phases are equal, i.e. $\boldsymbol{b}^{\alpha} = \boldsymbol{b}$ ($\alpha = S, W, N$). The total (Cauchy) stress tensor $\boldsymbol{\sigma}$ of the mixture is defined by

$$\boldsymbol{\sigma} = \sum_{\alpha} n^{\alpha} \boldsymbol{t}^{\alpha} . \tag{3.2.6}$$

Assuming that the moment of momentum is conservative for all the individual phases (i.e. microscopically, they are non-polar materials), one may obtain

$$\boldsymbol{t}^{\alpha} = \left(\boldsymbol{t}^{\alpha}\right)^{T} . \tag{3.2.7}$$

Hence, by definition (3.2.6), the total Cauchy stress $\boldsymbol{\sigma}$ is also symmetrical, i.e.

$$\boldsymbol{\sigma} = \boldsymbol{\sigma}^{T} . \tag{3.2.8}$$

The equations of energy balance for a bulk phase is

$$n^{\alpha}\rho^{\alpha}\frac{D^{\alpha}E^{\alpha}}{Dt} - n^{\alpha}\boldsymbol{t}^{\alpha} : \boldsymbol{d}^{\alpha} - \nabla\cdot\left(n^{\alpha}\boldsymbol{q}^{\alpha}\right) - n^{\alpha}\rho^{\alpha}h^{\alpha} = \sum_{\beta\neq\alpha}\hat{Q}^{\alpha}_{\alpha\beta} , \tag{3.2.9}$$

and for an interface

$$0 = -\sum_{\gamma=\alpha,\beta}\left[\hat{Q}^{\gamma}_{\alpha\beta} + \hat{\boldsymbol{T}}^{\gamma}_{\alpha\beta}\cdot\boldsymbol{v}^{\gamma} + \hat{e}^{\gamma}_{\alpha\beta}\left(E^{\gamma} + \frac{1}{2}\boldsymbol{v}^{\gamma}\cdot\boldsymbol{v}^{\gamma}\right)\right] \tag{3.2.10}$$

where $\boldsymbol{t}^{\alpha} : \boldsymbol{d}^{\alpha}$ represents, in indicial notation, $t^{\alpha}_{ij}d^{\alpha}_{ij}$, and $\boldsymbol{v}^{\alpha}\cdot\boldsymbol{v}^{\alpha} = v^{\alpha}_{i}v^{\alpha}_{i}$; $\boldsymbol{d}^{\alpha}$ is the symmetrical part of the velocity gradient, i.e. $\boldsymbol{d}^{\alpha} = 1/2[(\nabla\boldsymbol{v}^{\alpha})^{T} + \nabla\boldsymbol{v}^{\alpha}]$; h^{α} the external supply of energy; $\boldsymbol{q}^{\alpha}$ the heat flux; $\hat{Q}^{\alpha}_{\alpha\beta}$ the rate of energy transferring to α-phase through $\alpha\beta$-interface. (3.2.10) shows that the energy exchange through an interface has three contributions associated with heat exchange, mechanical interaction, and mass exchange.

The entropy balance for a bulk phase is

$$n^\alpha \rho^\alpha \frac{D^\alpha \eta^\alpha}{Dt} - \nabla \cdot \left(n^\alpha \varphi^\alpha\right) - n^\alpha \rho^\alpha \omega^\alpha = \sum_{\beta \neq \alpha} \hat{\Phi}^\alpha_{\alpha\beta} + \Lambda^\alpha . \qquad (3.2.11)$$

and for an interface

$$0 = -\left(\hat{\Phi}^\alpha_{\alpha\beta} + \hat{e}^\alpha_{\alpha\beta}\eta^\alpha\right) - \left(\hat{\Phi}^\beta_{\alpha\beta} + \hat{e}^\beta_{\alpha\beta}\eta^\beta\right), \qquad (3.2.12)$$

where η^α is the entropy density; φ^α the surface flux term of entropy and it is assumed that $\varphi^\alpha = \boldsymbol{q}^\alpha / \theta$; ω^α the external supply of entropy with $\omega^\alpha = h^\alpha / \theta$; Λ^α the net production of entropy in α-phase. From now onwards, all the phases are assumed to have the same temperature θ at a local point. (3.2.12) implies that the interfaces can not store or generate entropy. The total entropy density of the mixture η is defined by

$$\rho\eta = \sum_{\alpha = S,W,N} n^\alpha \rho^\alpha \eta^\alpha . \qquad (3.2.13)$$

Finally, the second law of thermodynamics requires that

$$\Lambda = \sum_{\alpha = S,W,N} \Lambda^\alpha \geq 0 , \qquad (3.2.14)$$

where Λ is the total net production of the entropy of the mixture. For later use, we introduce the Helmholtz free energy A^α defined by the Legendre transformation.

$$A^\alpha = E^\alpha - \theta\eta^\alpha , \qquad (3.2.15)$$

and the total free energy density of the mixture ψ given by

$$\rho\psi = \sum_{\alpha = S,W,N} n^\alpha \rho^\alpha A^\alpha . \qquad (3.2.16)$$

3.3 General Constitutive Relationships

In order to determine the state of the porous medium by using the balance equations presented above, the following independent fields must be evaluated:

In mass balance: $n^\alpha \rho^\alpha$, or alternatively, n^α & ρ^α

In linear momentum balance: $\boldsymbol{v}^\alpha$, or alternatively, $\boldsymbol{u}^\alpha$

In energy balance: θ

where $\alpha = S, W, N$; $\boldsymbol{u}^\alpha$ is the displacement defined by (3.1.5). To this end, it is necessary to establish the constitutive relationships for the following state parameters:

$$E^\alpha \text{ (or } A^\alpha), \eta^\alpha, \boldsymbol{q}^\alpha, \boldsymbol{t}^\alpha, \dot{\boldsymbol{e}}^\alpha_{\alpha\beta}, \hat{\boldsymbol{T}}^\alpha_{\alpha\beta}$$

It is noted that since at any point of the domain all the phases share the same temperature an independent constitutive equation is not needed for $\hat{Q}^\alpha_{\alpha\beta}$.

For simplicity, we consider the porous media with an elastic solid skeleton saturated by two *inviscid* fluids (the elastoplasticity of the porous media will be discussed later). By introducing the principle of local action* (Odgen, 1984: pp.172-174), the set of constitutive variables proves to be

$$\Xi = \{\theta, \nabla\theta, n^\beta, \nabla n^\beta, \rho^\alpha, \nabla\rho^\alpha, \boldsymbol{F}, \boldsymbol{w}^\beta\}, \qquad (3.3.1)$$

---

* Let $\mathcal{N}(\boldsymbol{X}^*)$ be a neighborhood of the point $\boldsymbol{X}^*$. The principle of local action states that the material response at $\boldsymbol{X}^*$ is dependent on the history of the motion inside $\mathcal{N}(\boldsymbol{X}^*)$ only and unaffected by the motion outside $\mathcal{N}(\boldsymbol{X}^*)$. The constitutive law based on this principle is *local*.

where $\alpha = S, W, N$; $\beta = W, N$. Note that the volume fractions of fluids are included as constitutive variables. The reason for this is that the volume fractions can be used to represent the local structure of the porous medium and therefore the interactions between two bulk components through the interfaces. In the proposed model, no internal constraints are introduced. That is, all the bulk phases are assumed compressible (ρ^{α} is a variable). As shown in Chapter 6, any model of porous media with internal constraint excludes at least one mode of acoustic waves. This of course is not a desirable feature for a general model as developed here.

As a starting point, we postulate the following constitutive equations for the free energies:

$$A^{S} = A^{S}\left(\theta, \rho^{S}, \boldsymbol{E}\right), \tag{3.3.2}$$

$$A^{W} = A^{W}\left(\theta, \rho^{W}, n^{W}\right), \tag{3.3.3}$$

and

$$A^{N} = A^{N}\left(\theta, \rho^{N}, n^{N}\right). \tag{3.3.4}$$

In postulating these constitutive equations, it has been assumed that the free energy density of an individual phase is solely determined by the state variables of this individual phase. The inclusion of the volume fractions in (3.3.2)-(3.3.4) is one of the distinguishing features of the theory presented hereafter. Since the volume fraction of solid can be determined by integrating the mass balance equation of the solid phase with $\boldsymbol{u}^{S}$ and ρ^{S} given, n^{S} is not explicitly included in (3.3.2). Due to the requirement of the material objectivity*, $\boldsymbol{E}$ is used in (3.3.2) instead of $\boldsymbol{F}$. In addition, because the influence

* This is a basic assumption in continuum mechanics stating that two observers in relative motion make no (mathematical and physical) difference in deducing the macroscopic properties of a material under test. In other words, material properties are unaffected by a superposed rigid body motion and a constitutive relationship has the same form for all the observers.

of deformation on a fluid can be implicitly accounted for by using the volume fraction. $\boldsymbol{E}$ is excluded in (3.3.3) and (3.3.4).

With the assumption that the interfaces do not carry averaged thermodynamic properties, it can be shown that the sufficient and necessary conditions for (3.3.2)-(3.3.4) to satisfy the entropy inequality (3.2.14) are (Muraleetharan and Wei, 1999)

$$\eta^{\alpha} = -\frac{\partial A^{\alpha}}{\partial \theta}, \ \eta = -\frac{\partial \psi}{\partial \theta}, \tag{3.3.5}$$

$$\boldsymbol{t}^{W} = -p^{W}\boldsymbol{I}, \tag{3.3.6}$$

$$\boldsymbol{t}^{N} = -p^{N}\boldsymbol{I}, \tag{3.3.7}$$

$$\boldsymbol{t}^{S} = \boldsymbol{t}^{e} - p^{S}\boldsymbol{I}, \tag{3.3.8}$$

where $\alpha = S, W, N$, and

$$\theta\Lambda = \sum_{\beta=W,N} \dot{n}^{\beta}\Pi^{\beta} - \sum_{\beta=W,N} \boldsymbol{w}^{\beta}\cdot\boldsymbol{r}^{\beta} + \sum_{\alpha\beta=SW,WN,NS} \hat{e}^{\alpha}_{\alpha\beta}\left(G^{\alpha} - G^{\beta}\right) + \nabla\theta\cdot\frac{\boldsymbol{q}}{\theta} \geq 0, \tag{3.3.9}$$

where ρ is the total mass density defined by (3.2.3); η the total entropy defined by (3.2.13); ψ the total free energy density defined by (3.2.16);

$$p^{\alpha} = \left(\rho^{\alpha}\right)^{2}\frac{\partial A^{\alpha}}{\partial \rho^{\alpha}}, \ \alpha = S, W, N \tag{3.3.10}$$

and

$$\boldsymbol{t}^{e} = \rho^{S}\boldsymbol{F}\frac{\partial A^{S}}{\partial \boldsymbol{E}}\boldsymbol{F}^{T}. \tag{3.3.11}$$

p^{α} is the *thermodynamic pressure* of α-phase; (3.3.6) and (3.3.7) show that p^{W} and p^{N} equal to the real material pressure.

In the entropy inequality (3.3.9),

$$\Pi^{\beta} = p^{\beta} - p^{S} - n^{\beta}\rho^{\beta}\frac{\partial A^{\beta}}{\partial n^{\beta}}, \tag{3.3.12}$$

$$\boldsymbol{r}^{\beta} = -\sum_{\gamma \neq \beta}\hat{\boldsymbol{T}}^{\beta}_{\beta\gamma} + \left(p^{\beta} - n^{\beta}\rho^{\beta}\frac{\partial A^{\beta}}{\partial n^{\beta}}\right)\nabla n^{\beta} - n^{\beta}\rho^{\beta}\frac{\partial A^{\beta}}{\theta}\nabla\theta, \tag{3.3.13}$$

$$\boldsymbol{q} = \sum_{\alpha=S,W,N} n^{\alpha}\boldsymbol{q}^{\alpha}, \tag{3.3.14}$$

and

$$G^{\alpha} = A^{\alpha} + \frac{p^{\alpha}}{\rho^{\alpha}}. \tag{3.3.15}$$

G^{α} is the chemical potential of α phase, which is usually called the Gibbs free energy. The physical significance of G^{α} will be explained later.

To get insights into the structure of the constitutive relationships presented above, we define a new energy density function for the porous medium as follows,

$$W\left(\theta, \boldsymbol{E}, n^{W}, n^{S}, m_{t}^{\alpha}\right) = \rho_{R}\psi\left(\theta, \boldsymbol{E}, n^{W}, n^{S}, \rho^{\alpha}\right), \tag{3.3.16}$$

where $\alpha = S, W, N$; $\rho_{R} = J\rho = (\det \boldsymbol{F})\rho$; ψ is given by (3.2.16); m_{t}^{α} is the *partial* mass density of α phase with respect to the reference configuration, i.e.

$$m_{t}^{\alpha} = Jn^{\alpha}\rho^{\alpha}. \tag{3.3.17}$$

Clearly, W represents the total free energy stored in a volume of the porous medium that is unit before deformation.

Employing (3.2.6), (3.3.5)-(3.3.8), (3.3.10), (3.3.11), (3.3.15)-(3.3.17), and (3.3.2)-(3.3.4), one may easily prove that

$$\rho\eta = -J^{-1}\frac{\partial W}{\partial \theta}. \tag{3.3.18}$$

$$\boldsymbol{\sigma} = J^{-1}\boldsymbol{F}\frac{\partial W}{\partial \boldsymbol{E}}\boldsymbol{F}^{T}. \tag{3.3.19}$$

$$G^{\alpha} = \frac{\partial W}{\partial m_t^{\alpha}}. \tag{3.3.20}$$

and

$$\Pi^{\beta} = -J^{-1}\frac{\partial W}{\partial n^{\beta}}. \tag{3.3.21}$$

where $\alpha = S, W, N$; $\beta = W, N$. It is now instructive to compare the continuum model described by (3.3.16)-(3.3.21) with Bowen's model (Bowen, 1982). It is noted that the present model differs from the latter in the following aspects: firstly, the partial mass density of solid skeleton, i.e. m_t^S, is included as a constitutive variable in the present model; secondly, Π^{β} in (3.3.21) clearly has physical meaning as explained in the next section. The direct consequence of including m_t^S in the model is that the compressibility of the solid phase can be considered in the present model.

The physical significance of G^{β} is now interpreted as follows. If the exchange of mass between two components is neglected, dm_t^{β} represents the total mass change of β fluid in a volume of the porous medium that is unit before deformation. Consider two large reservoirs of fluids with constant pressure p_a^W and p_a^N, respectively. Let these two reservoirs connect, respectively, with the wetting and nonwetting fluids in a unit volume of the porous medium (see Fig.3.5). The two reservoirs and the unit volume of porous medium now constitute a single thermodynamic system. G^{β} equals to the work done *reversibly and isothermally* on the system in the following process: firstly, to extract a unit mass of β fluid from the reservoir with constant p_a^{β}; then, to increase the pressure

of this unit mass of fluid up to p^{β}, which is the equilibrium pressure of the fluid in the sample; finally, to inject it into the sample of the porous medium at p^{β}. Consequently, we have

$$G^{\beta} = -\frac{p_0^{\beta}}{\rho_0^{\beta}} - \int_{p_1^{\beta}}^{p^{\beta}} \zeta \, d\left[\frac{1}{\rho^{\beta}(\zeta)}\right] + \frac{p^{\beta}}{\rho^{\beta}} = \int_{p_0^{\beta}}^{p^{\beta}} \frac{d\zeta}{\rho^{\beta}(\zeta)}. \qquad (3.3.22)$$

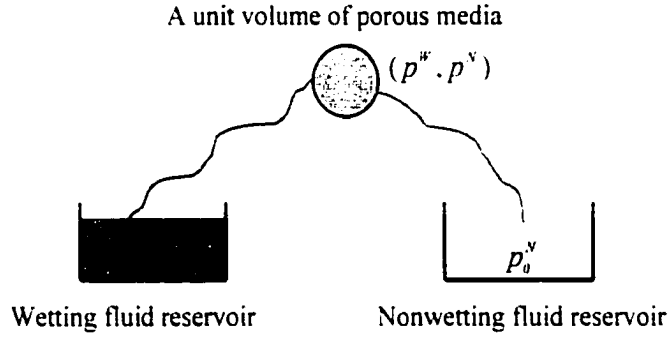

Figure 3.5 A thermodynamic system

The physical explanation of G^{β} described above was first presented by Biot (1972), who dealt with the porous media saturated by a single fluid. Biot called G^{β} the "pressure function". It should be noted that (3.3.22) is based on the assumption that ρ^{β} is solely determined by p^{β}, i.e. the fluid is assumed to be ideal. It must be pointed out that this assumption generally is inconsistent with the theory of porous media (Bowen, 1982). For many applications, however, such an assumption is appropriate. We will discuss this point further in Chapter 5.

3.4 Equilibrium State

At equilibrium, the corresponding constitutive variables in (3.3.1) read

$$\Xi_{eq} = \{\theta, \mathbf{0}, n^{\beta}, \mathbf{0}, \rho^{\alpha}, \mathbf{0}, \mathbf{F}, \mathbf{0}\}, \tag{3.4.1}$$

where $\alpha = S, W, N$; $\beta = W, N$; $(\,)_{eq}$ denotes the set of state variables at equilibrium. (3.4.1) implies that the gradient of state variables are zero. In addition, all the other rate-type quantities, e.g. $\dot{n}^{\beta}$ and $e^{\alpha}_{\alpha\beta}$, are also zero. Since the entropy attains its minimum (zero) at equilibrium, it follows that

$$\left.\frac{\partial \mathcal{O}}{\partial z_c}\right|_{\Xi_{eq}} = 0, \tag{3.4.2}$$

where $\mathcal{O} = \theta\Lambda$, and z_c's ($c = 1, 2, \cdots, 11$) are given by

$$Z = \left\{ z_i \big|_{i=1,2,3,\cdots,11} \right\} = \left\{ \dot{n}^{\beta}, \mathbf{w}^{\beta}, \hat{e}^{\alpha}_{\alpha\beta}, \nabla\theta \right\}, \tag{3.4.3}$$

$\beta = W, N$; $\alpha\beta = SW, WN, NS$. Conditions given by (3.4.2) yields

$$\Pi^{\beta}_{eq} = 0, \tag{3.4.4}$$

$$\mathbf{r}^{\beta}_{eq} = \mathbf{0}, \tag{3.4.5}$$

$$\left(G^{\alpha} - G^{\beta}\right)_{eq} = 0, \tag{3.4.6}$$

and

$$\mathbf{q}_{eq} = \mathbf{0}. \tag{3.4.7}$$

(3.4.6) states that at equilibrium the chemical potential function G^{α} continues through the interface between two phases. This is the classical Maxwell condition for a phase equilibrium line. Combined with (3.4.4), (3.3.12) yields

$$\left(p^{\beta}-p^{S}\right)_{eq}=\left(n^{\beta}\rho^{\beta}\frac{\partial A^{\beta}}{\partial n^{\beta}}\right)_{eq},\ \beta=W,N. \tag{3.4.8}$$

Equation (3.4.8) shows that at equilibrium some kinds of constraints are imposed on the pressure difference between a fluid and the solid (i.e. the capillary pressure). Equivalently, the matrix suction $p^{N}-p^{W}$ can be represented by

$$\left(p^{N}-p^{W}\right)_{eq}=\left(n^{N}\rho^{N}\frac{\partial A^{N}}{\partial n^{N}}-n^{W}\rho^{W}\frac{\partial A^{W}}{\partial n^{W}}\right)_{eq}. \tag{3.4.9}$$

In general, the right-hand sides of (3.4.8) and (3.4.9) do not vanish due to the dependence of free energies on the volume fractions. It is quite obvious that (3.4.8) and (3.4.9) represent the macroscopic counterparts of the dynamic compatibility conditions on the interfaces, which have been discussed in Chapter 1. Since (3.4.8) and (3.4.9) comes out naturally due to the inclusion of the volume fractions as constitutive variables, they can be used as the closure equations. It is also noted that for the porous media saturated by two fluids only two closure equations are independent.

In what follows, Π^{β} ($\beta=W,N$) will be termed as the *capillary potentials* with respect to the solid phase. This terminology is relevant, since Π^{α} is a relative quantity and may vanish at equilibrium, which is consistent with the fact that at equilibrium the chemical potentials of all the phases are equal. For later use, it is useful to define the capillary potential of the nonwetting fluid with respect to the wetting fluid as

$$\Pi^{m}=\Pi^{N}-\Pi^{W}. \tag{3.4.10}$$

Unlike the capillary potentials Π^m and Π^α ($\alpha = W, N$), at equilibrium the capillary pressure between α and β phases (i.e. $p^\alpha - p^\beta$) is generally not equal to zero.

3.5 Nonequilibrium State with Linear Dissipation

For many applications such as those with flow or heat conduction in the porous media, the assumption of thermodynamic equilibrium is too restrictive. In this section, our attentions will be turned to the nonequilibrium states that *slightly* deviate from equilibrium. As noted in Section 3.1, the kinematics of the fluids is defined solely within the domain of the current configuration of the solid $\chi^S(\mathcal{B}, t)$. That is, the fluids outside this domain are of no concerns. Naturally, the motions of the fluids should be described with respect to the motion of the solid. This approach at least has two advantages over the others (e.g. Prevost, 1980; Bowen, 1982): 1) all the fields can be defined in the same domain; 2) objectivity can be achieved automatically.

Now, we first cast the *residual dissipation* inequality of (3.3.9) into the form with respect to the reference configuration as

$$\mathcal{D}_{res} = \sum_{\beta=W,N} \dot{n}^\beta \hat{H}^\beta - \sum_{\beta=W,N} \boldsymbol{W}_C^\beta \cdot \hat{\boldsymbol{R}}^\beta + \sum_{\alpha\beta=SW,WN,NS} J\hat{e}^\alpha_{\alpha\beta}\left(G^\alpha - G^\beta\right) + GRAD\theta \cdot \hat{\boldsymbol{Q}} \geq 0, \quad (3.5.1)$$

where $\mathcal{D}_{res} = J\theta\Lambda$,

$$\hat{H}^\beta = J\hat{\Pi}^\beta, \quad (3.5.2)$$

$$\hat{\boldsymbol{R}}^\beta = J\boldsymbol{F}^T\hat{\boldsymbol{r}}^\beta, \quad (3.5.3)$$

and

$$\hat{\boldsymbol{Q}} = J\hat{\boldsymbol{q}}\boldsymbol{F}^{-T}. \quad (3.5.4)$$

while $\hat{\Pi}^{\beta}$, $\hat{\boldsymbol{r}}^{\beta}$, and $\hat{\boldsymbol{q}}$ are the dissipative parts of Π^{β}, $\boldsymbol{r}^{\beta}$, and $\boldsymbol{q}/\theta$, respectively; $GRAD$ is the gradient operator with respect to $\boldsymbol{X}^{s}$. The terms in the right-hand side of the equality in (3.5.1) represent the energies dissipated by the capillary relaxation, fluid diffusion, mass exchange, and heat conduction, respectively.

The functional forms of the dissipative forces can be assumed as

$$\hat{H}^{\gamma} = \hat{H}^{\gamma}\left(Z_{eq}, \dot{n}^{\beta}, \boldsymbol{W}_{(r)}^{\beta}, GRAD\theta\right), \tag{3.5.5}$$

$$\hat{\boldsymbol{R}}^{\gamma} = \hat{\boldsymbol{R}}^{\gamma}\left(Z_{eq}, \dot{n}^{\beta}, \boldsymbol{W}_{(r)}^{\beta}, GRAD\theta\right), \tag{3.5.6}$$

and

$$\hat{\boldsymbol{Q}} = \hat{\boldsymbol{Q}}\left(Z_{eq}, \dot{n}^{\beta}, \boldsymbol{W}_{(r)}^{\beta}, GRAD\,\theta\right), \tag{3.5.7}$$

where $\beta = W, N$; Z_{eq} is the set of the state variables at equilibrium given by

$$Z_{eq} = \left\{\theta, n_{*}^{\beta}, \rho_{*}^{\alpha}, \boldsymbol{E}\right\}. \tag{3.5.8}$$

$\boldsymbol{W}_{(r)}^{\beta}$ is the *Lagrangian* (or *convective*) relative velocities of a fluid particle defined by (3.1.12). It can be easily seen that the dissipation functions assumed above are objective. For simplicity and without loss of much generality, we assume that the solid has at least a center of symmetry, i.e. $\boldsymbol{Q} = -\boldsymbol{I}$ belongs to the symmetry group of the solid. With this assumption and following Bowen (1982), it can be proved that for linear dissipation,

$$\frac{\partial \hat{H}^{\gamma}}{\partial \boldsymbol{W}_{(r)}^{\beta}} = \frac{\partial \hat{H}^{\gamma}}{\partial (GRAD\theta)} = \boldsymbol{0}, \tag{3.5.9}$$

and

$$\frac{\partial \hat{\boldsymbol{R}}^{\gamma}}{\partial \dot{n}^{\beta}} = \frac{\partial \hat{\boldsymbol{Q}}}{\partial \dot{n}^{\beta}} = \boldsymbol{0}. \tag{3.5.10}$$

Therefore, (3.5.5)-(3.5.7) can be linearized as follows,

$$\hat{H}^{\gamma} = \sum_{\beta=W,N} \zeta_{\beta}^{\gamma} \dot{n}^{\beta}, \tag{3.5.11}$$

$$\hat{\boldsymbol{R}}^{\gamma} = -\sum_{\beta=W,N} \boldsymbol{\mu}_{\beta}^{\gamma} \cdot \boldsymbol{W}_{c}^{\beta} - \boldsymbol{\mu}_{\theta}^{\gamma} \cdot GRAD\,\theta, \tag{3.5.12}$$

and

$$\hat{\boldsymbol{Q}} = -\sum_{\beta=W,N} \boldsymbol{\omega}_{\beta}^{\theta} \cdot \boldsymbol{W}_{c}^{\beta} - \boldsymbol{\omega}^{\theta} \cdot GRAD\,\theta, \tag{3.5.13}$$

Finally, the rates of mass exchanges is assumed as

$$J\hat{e}_{\alpha\beta}^{\alpha} = \zeta_{\alpha\beta}\left(G^{\beta} - G^{\alpha}\right), \tag{3.5.14}$$

In (3.5.11)-(3.5.14), the coefficients are the functions of θ, n^{β}, ρ^{β}, and $\boldsymbol{E}$. The spatial forms of (3.5.12) and (3.5.13) can be derived by using (3.5.3) and (3.5.4), and it follows that

$$\hat{\boldsymbol{r}}^{\gamma} = -\sum_{\beta=w,n} \hat{\boldsymbol{\mu}}_{\beta}^{\gamma} \cdot \boldsymbol{w}^{\beta} - \hat{\boldsymbol{\mu}}_{\theta}^{\gamma} \cdot \nabla\theta, \tag{3.5.15}$$

and

$$\hat{\boldsymbol{q}} = -\sum_{\beta=w,n} \hat{\boldsymbol{\omega}}_{\beta}^{\theta} \cdot \boldsymbol{w}^{\beta} - \hat{\boldsymbol{\omega}}^{\theta} \cdot \nabla\theta, \tag{3.5.16}$$

where

$$\hat{\boldsymbol{\mu}}_{\beta}^{\gamma} = J^{-1}\boldsymbol{F}^{-T}(\boldsymbol{\mu}_{\beta}^{\gamma})\boldsymbol{F}^{-1}, \quad \hat{\boldsymbol{\mu}}_{\theta}^{\gamma} = J^{-1}\boldsymbol{F}^{-T}(\boldsymbol{\mu}_{\theta}^{\gamma})\boldsymbol{F}^{T}. \tag{3.5.17}$$

$$\hat{\boldsymbol{\omega}}_{\beta}^{\theta} = J^{-1}\boldsymbol{F}(\boldsymbol{\omega}_{\beta}^{\theta})\boldsymbol{F}^{-1}, \quad \hat{\boldsymbol{\omega}}^{\theta} = J^{-1}\boldsymbol{F}(\boldsymbol{\omega}^{\theta})\boldsymbol{F}^{T}. \tag{3.5.18}$$

It needs to be pointed out noted that unlike (3.5.12) and (3.5.13) $\hat{\boldsymbol{R}}^{\gamma}$ and $\hat{\boldsymbol{Q}}$ can also be put as the functions of fluid mass fluxes (see Appendix I).

Assuming the mixture at equilibrium is thermodynamically stable, the dissipative energy function given in the left hand side of (3.5.1) attains its minimum at equilibrium (as schematically shown in Fig. 3.6). Hence, the coefficients in (3.5.11)-(3.5.14) are restricted by

$$\det\left(\frac{\partial^2 \mathcal{D}_{res}}{\partial z_i \partial z_j}\right) > 0, \tag{3.5.19}$$

where $z_i (i = 1,2,\cdots,11)$ are the components of $\{\dot{n}^\beta, \boldsymbol{W}_i^\beta, \hat{e}_{\alpha\beta}^\alpha, GRAD\,\theta\}$, $\beta = W, N$.

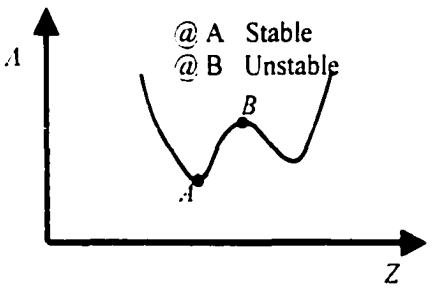

Figure 3.6 States of the system at equilibrium

Inserting (3.5.15) into (3.3.13) and noting that $\boldsymbol{r}^\beta = \boldsymbol{r}_{eq}^\beta + \hat{\boldsymbol{r}}^\beta = \hat{\boldsymbol{r}}^\beta$, one obtains an expression for $\sum_{\beta \neq \alpha} \hat{\boldsymbol{T}}_{\alpha\beta}^\alpha$ $(\alpha = W, N)$, which can be deleted from (3.2.4). By using (3.3.10), (3.3.3), (3.3.4), and (3.3.15), it can be proved that

$$n^\beta \rho^\beta \frac{D^\beta \boldsymbol{v}^\beta}{Dt} - n^\beta \rho^\beta \boldsymbol{b} + n^\beta \rho^\beta \nabla G^\beta = \hat{\boldsymbol{r}}^\beta, \quad \beta = W, N \tag{3.5.20}$$

where $\hat{\boldsymbol{r}}^\beta$ is the drag (dissipative) force given by (3.5.15). This is the spatial form of the flow equation of a fluid. It is remarkable that, instead of the pressure gradient, a more

general chemical potential, i.e. G^{α}, becomes the driving force for the multiphase flow. This result is expected, since the motions of various components are coupled in a multiphase porous medium.

For many applications, the chemical potential of a fluid may be approximately evaluated by using (3.3.22). It follows immediately that

$$n^{\beta}\rho^{\beta}\frac{D^{\beta}\boldsymbol{v}^{\beta}}{Dt} - n^{\beta}\rho^{\beta}\boldsymbol{b} + n^{\beta}\nabla p^{\beta} = \hat{\boldsymbol{r}}^{\beta}. \tag{3.5.21}$$

Usually, it is more convenient to use (3.5.21) than (3.5.20) in a numerical analysis, since p^{α} can be directly measured.

3.6 Rate-Independent Elastoplasticity

The theory developed above applies only to the porous media with an elastic solid skeleton. In many applications, however, plastic deformation may become dominant. In this section, the above theory is generalized to account for the elastoplastic deformation of the skeleton. Deformation is assumed to be rate-independent, i.e. any relaxation effects are neglected. To avoid dealing with too much kinematics, which remains controversial for finite (plastic) deformation, we assume that the deformation is infinitesimal and the strain tensor can be additively decomposed into an elastic part and a plastic part, i.e.

$$\boldsymbol{E} = \boldsymbol{E}_{e} + \boldsymbol{E}_{p}. \tag{3.6.1}$$

In addition, it is also assumed that the volume fractions can be additively decomposed into two components as

$$n^{\beta} = n_e^{\beta} + n_p^{\beta},\ \beta = W, N \tag{3.6.2}$$

where n_e^{β} is the recoverable part and n_p^{β} the irreversible part (see Figure 3.7).

Since the porosity n equals to the summation of n^W and n^N, one obtains

$$n_e = n_e^W + n_e^N,\ n_p = n_p^W + n_p^N \tag{3.6.3}$$

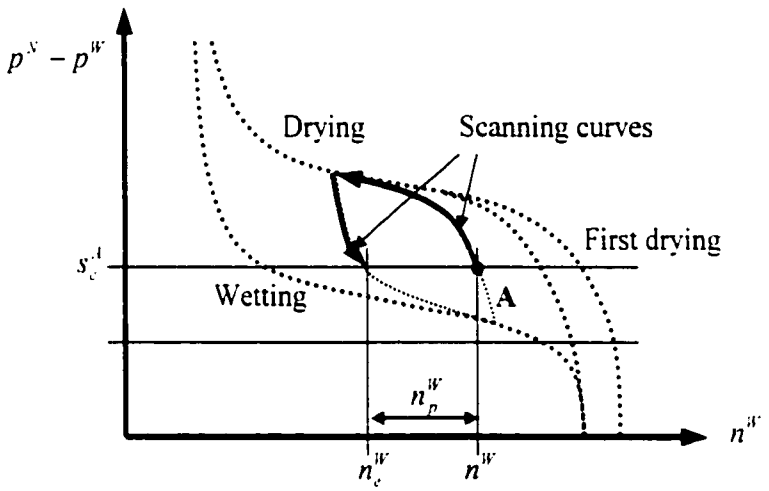

Figure 3.7 Definition of n_e^W and n_p^W for point **A**

Consequently, the free energy functions can be assumed as

$$A^S = \hat{A}^S(\theta, \rho^S, \boldsymbol{E}_e, \chi), \tag{3.6.4}$$

$$A^W = \hat{A}^W(\theta, \rho^W, n_e^W, v^W), \tag{3.6.5}$$

and

$$A^N = \hat{A}^N(\theta, \rho^N, n_e^N, v^N). \tag{3.6.6}$$

where χ, ν^W, and ν^N are the internal variables which characterize the hardening states of deformation and volume fraction. With (3.6.1) and (3.6.2), equations (3.6.4)-(3.6.6) can be expressed equivalently as

$$A^S = A^S(\theta, \rho^S, \boldsymbol{E}, \boldsymbol{E}_p, \chi), \tag{3.6.7}$$

$$A^W = A^W(\theta, \rho^W, n^W, n_p^W, \nu^W), \tag{3.6.8}$$

and

$$A^N = A^N(\theta, \rho^N, n^N, n_p^N, \nu^N). \tag{3.6.9}$$

Similar to the procedure followed by Muraleetharan and Wei (1999), one can prove that with (3.6.7)-(3.6.9) equations (3.3.5)-(3.3.8) and (3.3.10)-(3.3.14) remain valid. In addition, since the capillary relaxation effects are neglected, we obtain

$$\Pi^\beta = p^\beta - p^S - n^\beta \rho^\beta \frac{\partial A^\beta}{\partial n^\beta} = 0, \tag{3.6.10}$$

or

$$p^\beta - p^S = n^\beta \rho^\beta \frac{\partial A^\beta}{\partial n^\beta} \tag{3.6.11}$$

The residual dissipation inequality becomes

$$\mathcal{D}_p + \mathcal{D}_{diff} \geq 0, \tag{3.6.12}$$

where $\mathcal{D}_p$ is the dissipated energy due to the plastic deformation and $\mathcal{D}_{diff}$ is due to the diffusion and heat conduction. They are given, respectively, by

$$\mathcal{D}_p = \boldsymbol{\pi} : \dot{\boldsymbol{E}}_p + \zeta \cdot \dot{\chi} + \sum_{\beta=W,N} s^\beta \dot{n}_p^\beta + \sum_{\beta=W,N} \iota^\beta \dot{\nu}^\beta, \tag{3.6.13}$$

and

$$\mathcal{D}_{diff} = -\sum_{\beta=W,N} \boldsymbol{w}^\beta \cdot \hat{\boldsymbol{\tau}}^\beta + \nabla\theta \cdot \hat{\boldsymbol{q}} \tag{3.6.14}$$

Variables $\boldsymbol{\pi}$, ι^W, and ι^N are the thermodynamic forces given by

$$\boldsymbol{\pi} = -n^S \rho^S \frac{\partial A^S}{\partial \boldsymbol{E}_p}, \quad \boldsymbol{\zeta} = -n^S \rho^S \frac{\partial A^S}{\partial \boldsymbol{\chi}}, \quad s^\beta = -n^\beta \rho^\beta \frac{\partial A^\beta}{\partial n_p^\beta}, \quad \iota^\beta = -n^\beta \rho^\beta \frac{\partial A^\beta}{\partial \nu^\beta} \tag{3.6.15}$$

Noting that

$$\hat{A}^S(\theta, \rho^S, \boldsymbol{E}_e, \boldsymbol{\chi}) = \hat{A}^S(\theta, \rho^S, \boldsymbol{E} - \boldsymbol{E}_p, \boldsymbol{\chi}) = A^S(\theta, \rho^S, \boldsymbol{E}, \boldsymbol{E}_p, \boldsymbol{\chi}). \tag{3.6.16}$$

and

$$\hat{A}^\beta(\theta, \rho^S, n_e^\beta, \nu^\beta) = \hat{A}^\beta(\theta, \rho^S, n^\beta - n_p^\beta, \nu^\beta) = A^\beta(\theta, \rho^S, n^\beta, n_p^\beta, \nu^\beta), \tag{3.6.17}$$

one can easily prove that

$$\boldsymbol{\pi} = n^S \boldsymbol{t}^e, \tag{3.6.18}$$

and

$$s^\beta = p^\beta - p^S, \quad \beta = W, N. \tag{3.6.19}$$

Since $\mathcal{D}_p$ and $\mathcal{D}_{diff}$ stem from totally different internal dissipation mechanisms, they can be uncoupled. It follows that

$$(n^S \boldsymbol{t}^e) : \dot{\boldsymbol{E}}_p + \boldsymbol{\zeta} \cdot \dot{\boldsymbol{\chi}} + \sum_{\beta = W, N} (p^\beta - p^S) \dot{n}_p^\beta + \sum_{\beta = W, N} \iota^\beta \dot{\nu}^\beta \geq 0, \tag{3.6.20}$$

and

$$-\sum_{\beta = W, N} \boldsymbol{w}^\beta \cdot \hat{\boldsymbol{\tau}}^\beta + \nabla\theta \cdot \hat{\boldsymbol{q}} \geq 0 \tag{3.6.21}$$

Fluid diffusion and heat conduction are restricted by (3.6.21), which have been discussed in the last section. Equation (3.6.20) is the plastic dissipation inequality and will be used to develop a potential theory of plasticity for the porous media in the coming chapter.

It is now instructive to note that, for the saturated porous media constituted by incompressible solid grains, $s^W = p^W - p^S = 0$, and $n^S \boldsymbol{t}^e$ is just the Terzaghi's effective

stresses (Prevost, 1980). In this case, $(n^s \boldsymbol{t}^s) : \dot{\boldsymbol{E}}_p + \zeta \cdot \dot{\chi} \geq 0$, representing the energy dissipation due to the plastic deformation of the solid skeleton. Clearly, the effective stresses are the thermodynamic forces conjugated to the plastic strains. This justifies use of effective stresses in modeling the stress-strain constitutive relationships of saturated porous media. If the solid skeleton does not experience irreversible deformations and $n_p = n_p^w + n_p^s = 0$, the free energy functions have the following forms.

$$A^s = A^s(\theta, \rho^s, \boldsymbol{E}), \tag{3.6.22}$$

$$A^w = A^w(\theta, \rho^w, n^w, n_p^w, v), \tag{3.6.23}$$

and

$$A^s = A^s(\theta, \rho^s, n^s, n_p^s, v). \tag{3.6.24}$$

It is noted that n_p^w and n_p^s are not independent. Hence, A^w and A^s include the same hardening variable. The plastic dissipation inequality now reads

$$-(p^s - p^w)\dot{n}_p^w + \iota \dot{v} \geq 0, \tag{3.6.25}$$

where v is the internal variable representing the *moisture content hardening* and ι is the conjugated thermodynamic force given by

$$\iota = -\frac{\partial}{\partial v}(n^w \rho^w A^w + n^s \rho^s A^s) \tag{3.6.26}$$

(3.6.25) implies that the hysteresis in the suction can be simulated as the irreversibile change of the moisture content within the framework of the classic elastoplastic theory.

Chapter 4 A NONLINEAR MODEL OF POROUS MEDIA AND ITS VARIATIONAL STRUCTURE

In the theory developed in the previous chapter, some state variables, such as the *true* mass density of a bulk component (ρ^{α}) and the *true* Cauchy stress tensor of the solid component ($\boldsymbol{t}^{s}$), cannot be directly accessed through experiment. Hence, it is awkward to apply the above theory in practice. By using the general results previously obtained, this chapter intends to develop a continuum model describing porous materials based on the state variables that are experimentally accessible.

In the following, continuum field equations are first presented. All the formulations are given exclusively in the Lagrangian setting that is more appropriate for porous media as discussed before. Then a hyperelastic model of porous media is developed, explicitly accounting for the dynamic compatibility conditions on interfaces. A theoretical framework of poroelastoplasticity is developed, and it can be used to describe the nonlinear behaviors of porous media, such as plasticity and hysteresis, in a hierarchical way. Finally, the proposed model is mapped into a general framework, which can be directly inferred from the *principle of virtual dissipation* attributed to Biot (1977). Within this framework, a connection between Biot's theory and the mixture theory-based models of porous media is established.

4.1 Field Equations

For simplicity, our attentions will be focused on the porous media without phase change, i.e. all the terms with mass exchange will be simply dropped. Multiplying (3.2.1) by $J(=\det \boldsymbol{F})$, and noting that $\dot{J} = J\nabla\cdot\boldsymbol{v}^S = Jdiv(\boldsymbol{v}^S)$ *, we obtain the following Lagrangian form of the mass balance equations for the bulk components.

$$\dot{m}_t^S = 0, \tag{4.1.1}$$

and

$$\dot{m}_t^\beta + DIV\left(m_t^\beta \boldsymbol{W}_t^\beta\right) = 0,\ \beta = W, N, \tag{4.1.2}$$

where $m_t^\beta = Jn^\alpha\rho^\alpha$, the mass of α-phase in a volume of the porous medium which is unit before the deformation; $\boldsymbol{W}_t^\beta$ is the convective relative velocity of a fluid defined by (3.1.12), and DIV the *material* divergence operator (i.e. with respect to the reference configuration). Equation (4.1.1) implies that m_t^S is constant, which is obvious for the porous media without phase change. Integrating (4.1.2) over the time period $[t_0, t]$ yields

$$m^\beta + DIV\boldsymbol{M}^\beta = 0,\ \beta = W, N, \tag{4.1.3}$$

where m^β is the change in the mass of β-fluid in a volume of the porous medium, which is a unit volume before the deformation, i.e. $m^\beta = m_t^\beta - m_0^\beta$, m_0^β represents the initial total mass of β-fluid in a unit volume of undeformed porous medium. The initial total mass of the porous medium per unit undeformed volume is given by $m_0 = m_0^S + m_0^W + m_0^N$; $\boldsymbol{M}^\beta$ is represented by

---

* In the following, the over dot represents the material derivative with respect to the motion of the skeleton, e.g. $\dot{a} = D^s a/Dt$.

$$\boldsymbol{M}^{\beta} = \int_{t_0}^{t} m_t^{\beta} \boldsymbol{W}_t^{\beta} dt \,. \tag{4.1.4}$$

$(\boldsymbol{M}^{\beta})_I$ can be viewed as the total mass of β-fluid that flowed across a material surface which, before the deformation, is a unit area with the unit normal in direction I (= 1, 2, 3).

Without mass exchange, the equation of linear momentum balance for an interface, i.e. (3.2.5), becomes

$$\hat{\boldsymbol{T}}_{\alpha\beta}^{\alpha} + \hat{\boldsymbol{T}}_{\alpha\beta}^{\beta} = 0\,,\ \alpha\beta = SW, WN, NS\,, \tag{4.1.5}$$

and therefore

$$\sum_{\alpha\beta = SW, WN, NS} \left(\hat{\boldsymbol{T}}_{\alpha\beta}^{\alpha} + \hat{\boldsymbol{T}}_{\alpha\beta}^{\beta}\right) = 0\,. \tag{4.1.6}$$

The equation of total linear momentum balance for the porous medium is obtained by summing up (3.2.4) for all the bulk phases, i.e.

$$\rho \dot{\boldsymbol{v}}^{S} + \sum_{\beta = W, N} n^{\beta} \rho^{\beta} \dot{\boldsymbol{w}}^{\beta} + \sum_{\beta = W, N} n^{\beta} \rho^{\beta} \boldsymbol{w}^{\beta} \cdot \nabla \boldsymbol{v}^{S} = div\boldsymbol{\sigma} + \rho \boldsymbol{b}. \tag{4.1.7}$$

where $\boldsymbol{w}^{\beta}$ is the relative velocity defined by (3.1.9), *div* the *spatial* divergence operator, ρ the total mass density of the mixture given by (3.2.3), and $\boldsymbol{\sigma}$ the total *Cauchy* stress tensor defined by (3.2.6). Multiplying (4.1.7) by J, we deduce the Lagrangen form of the total linear momentum balance as

$$\rho_R \dot{\boldsymbol{V}}^{S} + \sum_{\beta = W, N} m_t^{\beta} \left[\dot{\boldsymbol{W}}^{\beta} + \boldsymbol{W}_t^{\beta} \cdot GRAD\boldsymbol{V}^{S}\right] = DIV\boldsymbol{P} + \rho_R \boldsymbol{B} \tag{4.1.8}$$

where

$$\boldsymbol{V}^{S}(\boldsymbol{X}^{S}, t) = \boldsymbol{v}^{S} \circ \chi_t^{S}(\boldsymbol{X}^{S}, t)\,, \tag{4.1.9}$$

$$\boldsymbol{B}(\boldsymbol{X}^{S}, t) = \boldsymbol{b} \circ \chi^{S}(\boldsymbol{X}^{S}, t) \tag{4.1.10}$$

$$\rho_R = J\rho = \sum_{\alpha=S,W,N} m_t^\alpha = m_0 + \sum_{\beta=W,N} m^\beta . \tag{4.1.11}$$

and

$$\boldsymbol{P}^T = J\boldsymbol{F}^{-T}\boldsymbol{\sigma} = \frac{\partial W}{\partial \boldsymbol{F}} . \tag{4.1.12}$$

where (3.3.19) has been used. $\boldsymbol{P}^T$ is usually called the first *Piola-Kichhoff stress* tensor. With (4.1.2) and (4.1.4), the left-hand side of (4.1.8) can be cast into

$$\rho_R \dot{\boldsymbol{V}}^s + \sum_{\beta=W,N} \left[\boldsymbol{F}\ddot{\boldsymbol{M}}^\beta + 2\left(\dot{\boldsymbol{M}}^\beta \cdot GRAD\right)\boldsymbol{V}^s + \boldsymbol{W}^\beta DIV\, \dot{\boldsymbol{M}}^\beta \right] \tag{4.1.13}$$

The last two terms in the bracket of (4.1.13), which represent the linear momentum contributions due to the convection, are high-order small quantities. For convenience, these two terms are omitted in the following derivations. Therefore, (4.1.8) becomes

$$\rho_R \dot{\boldsymbol{V}}^s + \sum_{\beta=W,N} \boldsymbol{F}\ddot{\boldsymbol{M}}^\beta = DIV\, \boldsymbol{P} + \rho_R \boldsymbol{B} \tag{4.1.14}$$

The Eulerian form of the flow equation of a fluid is given by (3.5.20). Pre-multiplying (3.5.20) by $J\mathbf{F}^T$, and using (3.5.3), we obtain the following convective representation of the flow equation of a fluid,

$$m_t^\beta \boldsymbol{F}^T \dot{\boldsymbol{V}}^S + \boldsymbol{C}\ddot{\boldsymbol{M}}^\beta = m_t^\beta \boldsymbol{B}_c - m_t^\beta GRADG^\beta + \hat{\boldsymbol{R}}^\beta . \tag{4.1.15}$$

where the linear momentum contributions due to convection have been dropped; $\boldsymbol{B}_c = \boldsymbol{F}^T\boldsymbol{B} = \boldsymbol{F}^T\boldsymbol{b} \circ \chi_t^\alpha(\boldsymbol{X}^S, t)$; $\boldsymbol{C}$ is the right Cauchy-Green deformation tensor, i.e. $\boldsymbol{C} = \boldsymbol{F}^T\boldsymbol{F}$; $\hat{\boldsymbol{R}}^\beta$ are the friction-like drag forces given by (3.5.12). For some applications, e.g. the deformation of an earth dam subjected to earthquake loading, the relative acceleration of a fluid is negligible*. Then, (4.1.15) becomes

* We will discuss this point further in Chapter 6.

$$m_t^\beta \boldsymbol{F}^r \dot{\boldsymbol{V}}^S = m_t^\beta \boldsymbol{B}_t - m_t^\beta GRAD\, G^\beta + \hat{\boldsymbol{R}}^\beta \tag{4.1.16}$$

Substituting the pressure function given by (3.3.22) into (4.1.16), it follows that

$$m_t^\beta \boldsymbol{F}^r \dot{\boldsymbol{V}}^S = m_t^\beta \boldsymbol{B}_t - n^\beta GRAD\, P^\beta + \hat{\boldsymbol{R}}^\beta . \tag{4.1.17}$$

where P^α is the *Kirchhoff* pressure of β-fluid defined by $P^\alpha(\boldsymbol{X}^S, t) = Jp^\alpha \circ \chi^S(\boldsymbol{X}^S, t)$

As assumed before, at any point in the domain of concern all the coexisting components have the same temperature. Hence, there is only one equation for the energy balance, i.e. the total energy balance of the porous medium as a whole. Applying (4.1.5) to (3.2.10), we get

$$\hat{Q}_{\alpha\beta}^\alpha + \hat{Q}_{\alpha\beta}^\beta + \hat{\boldsymbol{T}}_{\alpha\beta}^\alpha \cdot \boldsymbol{w}^\alpha + \hat{\boldsymbol{T}}_{\alpha\beta}^\beta \cdot \boldsymbol{w}^\beta = 0 , \tag{4.1.18}$$

where $\alpha\beta = SW, WN, NS$. Summing (4.1.18) over all the interfaces, it follows after some manipulations that

$$\sum_{\alpha=S,W,N} \sum_{\beta\neq\alpha} \hat{Q}_{\alpha\beta}^\alpha = -\sum_{\alpha=W,N} \left(\sum_{\beta\neq\alpha} \hat{\boldsymbol{T}}_{\alpha\beta}^\alpha \right) \cdot \boldsymbol{w}^\alpha . \tag{4.1.19}$$

Define the total energy density of the porous medium as

$$E_R = \rho_R E = \sum_{\alpha=S,W,N} m^\alpha E^\alpha . \tag{4.1.20}$$

By summing up (3.2.15), we obtain

$$E_R = \rho_R \psi + \rho_R \eta\theta . \tag{4.1.21}$$

When (3.2.9) is multiplied by J and summed up for the three bulk phases, we obtain

$$\dot{E}_R - \boldsymbol{S} : \dot{\boldsymbol{E}} - DIV\,\boldsymbol{Q} - h_R = -\sum_{\beta=W,N} DIV\left(\dot{\boldsymbol{M}}^{\beta} E^{\beta}\right) - \sum_{\beta=W,N}\left(J\boldsymbol{F}^{T}\sum_{\gamma\neq\beta}\hat{\boldsymbol{T}}^{\beta}_{\beta\gamma}\right)\cdot \boldsymbol{W}_{t}^{\beta}, \quad (4.1.22)$$

where $\boldsymbol{S}$ is the second *Piola-Kirchhoff* stress tensor given by

$$\boldsymbol{S} = \boldsymbol{F}^{-1}\boldsymbol{P} = \frac{\partial W}{\partial \boldsymbol{E}}. \quad (4.1.23)$$

The external supply of energy h_R is

$$h_R = \rho_R h = \sum_{\alpha=S,W,N} m_t^{\alpha} h^{\alpha}. \quad (4.1.24)$$

and the heat flux $\boldsymbol{Q}$ is related to $\boldsymbol{q}$ by the Piola identity, i.e.

$$\boldsymbol{Q} = J\boldsymbol{q}\boldsymbol{F}^{-T}. \quad (4.1.25)$$

It is noted that the first term in the right-hand side of (4.1.22) accounts for the rate of energy loss due to the fluid flowing outside the domain and the second term represents the rate of the energy loss due to the hydrodynamic drag. The existence of these two terms in the energy balance equation is one of the main features of the diffusive-like materials such as the porous media of concern here.

By using (3.2.15), (4.1.21), (3.3.13), (3.3.15), (3.3.16), (3.3.18)-(3.3.21), (4.1.1), and (4.1.2), E_R and E^{β} can be eliminated from (4.1.22), and it follows that

$$\theta\dot{\eta}_R - DIV\left[\boldsymbol{Q} - \sum_{\beta=W,N}(\theta\eta^{\beta}\dot{\boldsymbol{M}}^{\beta})\right] - h_R = \sum_{\beta=W,N}\hat{H}^{\beta}\dot{n}^{\beta} - \sum_{\beta=W,N}\boldsymbol{W}_{t}^{\beta}\cdot\hat{\boldsymbol{R}}^{\beta}. \quad (4.1.26)$$

where $\boldsymbol{Q}$ is given by (3.5.13); $\hat{H}^{\beta}$ and $\hat{\boldsymbol{R}}^{\beta}$ denote the dissipative forces given by (3.5.11) and (3.5.12), respectively; $\eta_R = \rho_R\eta = J\rho_0\eta$; η and η^{β} are the entropy density

functions defined by (3.3.18) and (3.3.5), respectively. It is noted that the right-hand side of (4.1.26) represents two important internal dissipative mechanisms in the porous media with multiple fluids, i.e. the capillary relaxation and fluid diffusion.

The dissipative force $\hat{H}^\beta$ is evaluated by (3.5.11). Introducing (3.3.21) and (3.5.2), we obtain the closure equations as

$$H^\beta = J\Pi^\beta = -\frac{\partial W}{\partial n^\beta} = \hat{H}^\beta, \ \beta = W, N \tag{4.1.27}$$

Thus far, a closed set of governing equations for the porous media saturated by two immiscible fluids has been established. This set of equations includes the mass balance equation (4.1.3), equation of motion (4.1.14), flow equation (4.1.15), energy balance equation (4.1.26), and closure equation (4.1.27), as well as the energy function W defined by (3.3.16) together with (3.2.16) and (3.3.2)-(3.3.4). The independent state variables of the porous medium include $\boldsymbol{V}^S$ (or $\boldsymbol{u}^S$), $\boldsymbol{M}^\beta$ (or m^β,), n^β, and θ. It needs to be pointed out that the explicit constitutive functions, i.e. (3.3.2)-(3.3.4), are material-dependent and must be specified in application.

4.2 Hyperelasticity of Porous Media

In the terminology of continuum mechanics, hyperelasticity states that there exists an energy function such that the stress equals the derivative of the energy function with respect to its conjugated strain (e.g., Desai and Siriwardane (1984)). In recent years, hyperelastic models have found many successful applications in modeling the behavior of porous media, see, for example, Vermeer (1978), Loret (1985), Lade and Nelson (1987),

Molenkamp (1988), and Borja et al. (1997), among others. In contrast to the hypoelasticity-based models, which may entail nonvanishing dissipation in a closed cycle of deformation (Zytynski et al., 1978), the hyperelastic models are founded on fundamental thermodynamic laws.

From the field equations presented above, it is noted that a set of independent state variables can be chosen as $(\theta, \boldsymbol{E}, m_t^W, m_t^N, n^W, n^N)$, where $m_t^S \left(= m_0^S\right)$ has been excluded. Compared to the other variables, n^W and n^N are *hidden* (i.e. internal), and they exist only in the capillary relaxing processes (some sort of internal dissipative mechanisms) as shown in the right-hand side of (4.1.26). In other words, n^W and n^N can be determined *only* by relating them to some internal dissipative mechanisms. The thermodynamic aspects of these mechanisms have been discussed in the previous chapter, where we show that the evolution of n^W and n^N is driven by the capillary pressures. The conjugated problem now can be presented as

$$\left(\eta_R, \boldsymbol{S}, G^W, G^N\right) \Leftrightarrow \left(\theta, \boldsymbol{E}, m_t^W, m_t^N\right), \tag{4.2.1}$$

where

$$\eta_R = \frac{\partial W}{\partial \theta}\left(\theta, \boldsymbol{E}, m^W, m^N, n^W, n^N\right) \tag{4.2.2}$$

$$\boldsymbol{S} = \frac{\partial W}{\partial \boldsymbol{E}}\left(\theta, \boldsymbol{E}, m^W, m^N, n^W, n^N\right) \tag{4.2.3}$$

and

$$G^\beta = \frac{\partial W}{\partial m^\beta}\left(\theta, \boldsymbol{E}, m^W, m^N, n^W, n^N\right), \ \beta = W, N \tag{4.2.4}$$

where n^W and n^N are obtained by using (4.1.27) in a viscoelastic model or by using a elastoplastic model discussed in the coming section.

In some applications, the capillary equilibrium can be achieved immediately and the hysteresis in the capillary pressure is trivial. In such cases, the viscosity due to the capillary relaxation is negligible, and (4.1.27) becomes

$$H^{\beta} = \frac{\partial W}{\partial n^{\beta}} = 0\,,\ \beta = W, N \tag{4.2.5}$$

It is remarkable that when the effects of the capillary relaxation are not considered equation (4.2.5) represent the constraints on the hyperelastic model (4.2.2)-(4.2.4). As discussed before, these constraints stem from the *dynamic compatibility conditions on the interfaces*.

The energy function in (4.2.2)-(4.2.5) is defined as a mass-weighted average of the Helmholtz free energies of the solid and the fluids, i.e.

$$W\left(\theta, \boldsymbol{E}, m_0^S, m_t^{\beta}, n^{\beta}\right) = m_0^S A^S\left(\theta, \boldsymbol{E}, \rho^S\right) + \sum_{\gamma = W,N} m_t^{\gamma} A^{\gamma}\left(\theta, n^{\gamma}, \rho^{\gamma}\right), \tag{4.2.6}$$

where β is repeated over W and N; in the right-hand side, $\rho^{\beta} = m_t^{\beta}/(Jn^{\beta})$, and $J = det\,\boldsymbol{F}$. It must be noted that an explicit inclusion of m_0^S in the LHS of (4.2.6) is unnecessary since m_0^S is a constant. However, inclusion of m_0^S helps make clear that the true mass density of the solid component, i.e. ρ^S, is changeable through $\rho^S = m_0^S/[J(1-n^W-n^N)]$. The compressibility of the solid phase is therefore explicitly included in the presented model. It can be proven that if ρ^S is excluded, the capillary pressures may vanish at equilibrium (Bowen, 1982). However, vanishing capillary pressures have never been observed in the multiphase porous media.

Because the chemical potential G^{β} can not be measured directly in laboratories, it is inconvenient to use directly the model represented by (4.2.2)-(4.2.6). Hence, it is desirable to establish relationships between G^{β} and some measurable variables such as p^{β}. As discussed in Chapter 3, in isothermal conditions G^{β} can be represented by

$$G^{\beta} = \int_{p_0^{\beta}}^{p^{\beta}} \frac{d\zeta}{\rho^{\beta}(\zeta)} \tag{4.2.7}$$

where ρ^{β} is assumed as a function of p^{β} only. This assumption is acceptable for many applications, since n^{β} generally has little influence on ρ^{β}. It is noted that to be consistent with (4.2.7) the fluid pressure in a porous media is thermodynamically defined as the pressure of an outside fluid in local contact with the solid skeleton and in thermodynamic equilibrium with it (Biot, 1977). Such a pressure simply is what we measure in an experiment! In nonisothermal conditions, (4.2.7) must be modified, and a detailed account can be found in Biot (1977).

By introducing (4.2.7), it can be proven that θ, $\boldsymbol{E}$, and m^{β} are the functions of η_R, $\boldsymbol{S}$, p^{w}, and p^{N}. Define a new energy function by the Legendre's transformation as,

$$\hat{W}(\theta, \boldsymbol{S}, G^{w}, G^{N}, n^{w}, n^{N}) = W - \boldsymbol{S} : \boldsymbol{E} - G^{w} m^{w} - G^{N} m^{N} + \eta_R \theta \tag{4.2.8}$$

where $\boldsymbol{S}$ is the second Piola-Kirchhoff stress tensor defined by (4.1.23). With the introduction of (4.2.8), it is easily seen that

$$\theta = \frac{\partial \hat{W}}{\partial \eta_R}(\eta_R, \boldsymbol{S}, G^{w}, G^{N}, n^{w}, n^{N}), \tag{4.2.9}$$

$$\boldsymbol{E} = -\frac{\partial \hat{W}}{\partial \boldsymbol{S}}\left(\eta_R, \boldsymbol{S}, G^W, G^N, n^W, n^N\right), \tag{4.2.10}$$

$$m^\beta = -\frac{\partial \hat{W}}{\partial G^\beta}\left(\eta_R, \boldsymbol{S}, G^W, G^N, n^W, n^N\right), \ \beta = W, N \tag{4.2.11}$$

and

$$H^\beta = -\frac{\partial \hat{W}}{\partial n^\beta}\left(\eta_R, \boldsymbol{S}, G^W, G^N, n^W, n^N\right), \ \beta = W, N \tag{4.2.12}$$

Since n^β can be evaluated by using the evolution equations as discussed before and G^β is a function of p^β ($\beta = W, N$), all the variables in (θ, $\boldsymbol{E}$, m^β) are the functions of η_R, $\boldsymbol{S}$, p^W, and p^N. Therefore, η_R, $\boldsymbol{S}$, p^W, and p^N can be used as independent state variables in modeling the behavior of the porous media saturated by two immiscible fluids. This result is useful in developing stress-strain constitutive relationships as will be discussed in the following.

4.3 A Theoretical Framework of Poroelastoplasticity

The energy dissipation associated with plastic infinitesimal deformation in the porous media saturated by two fluids is restricted by inequality (3.6.20). In the following, it is assumed that the compressibility of the solid component is very small so that $\rho_S \approx const$. This assumption is reasonable for many porous media such as unsaturated soils. Noting that $m_I^S = (\det \boldsymbol{F}) n^S \rho^S = const$, we take the time derivative of this equation and obtain

$$\dot{n}^S = -\dot{n} = -n^S div \boldsymbol{v}^S = -n^S \boldsymbol{I} : \dot{\boldsymbol{E}}, \tag{4.3.1}$$

where n is the porosity of the porous medium. It follows from (4.3.1) that

$$\dot{n}_p = \dot{n}_p^W + \dot{n}_p^N = n^S \boldsymbol{I} : \dot{\boldsymbol{E}}_p \tag{4.3.2}$$

Hence, the plastic porosity is derivable from the plastic deformation. By introducing (4.3.2), $\dot{n}_p^N$ can be eliminated from the left-hand side of (3.6.20). This yields

$$\mathcal{D}_p = n^S(\boldsymbol{t}^S + p^N \boldsymbol{I}) : \dot{\boldsymbol{E}}_p - (p^N - p^W)\dot{n}_p^W + \boldsymbol{\zeta} \cdot \dot{\boldsymbol{\chi}} + \iota \dot{\nu} \geq 0. \tag{4.3.3}$$

where ν is the parameter accounting for the *moisture content hardening*; $\boldsymbol{\chi}$ accounts for the hardening of solid matrix. It is noted that since $\dot{n}_p^N$ can be determined using $\dot{n}_p^W$ and $\dot{\boldsymbol{E}}_p$ through (4.3.2), the hardening parameter ν^N in (3.6.9) must be replaced by ν and $\boldsymbol{\chi}$.

Let

$$\boldsymbol{\sigma}^{eff} = n^S(\boldsymbol{t}^S + p^N \boldsymbol{I}). \tag{4.3.4}$$

and

$$S_{wt} = p^N - p^W \tag{4.3.5}$$

$\boldsymbol{\sigma}^{eff}$ can be viewed as the Cauchy effective stress tensor and S_{wt} is usually called the matric suction. Equation (4.3.3) shows that the thermodynamic forces associated with $\dot{\boldsymbol{E}}_p$ and $\dot{n}_p^W$ are, respectively, $\boldsymbol{\sigma}^{eff}$ and S_{wt}. In a fully saturated condition, $S_{wt} = 0$, i.e. $p^N = p^W$: (4.3.4) yields

$$\boldsymbol{\sigma}^{eff} = n^S(\boldsymbol{t}^S + p^W \boldsymbol{I}) = (n^S \boldsymbol{t}^S - n p^W \boldsymbol{I}) + p^W \boldsymbol{I} = \boldsymbol{\sigma} + p^W \boldsymbol{I} \tag{4.3.6}$$

Clearly, in this case, $\boldsymbol{\sigma}^{eff}$ becomes the Terzaghi's effective stress tensor. That is, the effective stresses can be considered as a particular case of $\boldsymbol{\sigma}^{eff}$ and S_{wt} as stress

measures. This feature is desirable when σ^{eff} and S_M are used as stress measures in constitutive modeling as discussed in the following.

Cast (4.3.3) into

$$\mathcal{D}_p = \sigma^{eff} : \dot{E}_p - S_M \dot{n}_p^W + \zeta \cdot \dot{\chi} + \iota \dot{\nu} = Y \cdot \dot{X} = D(\dot{X}) \geq 0 , \qquad (4.3.7)$$

where $Y = (\sigma^{eff}, S_M, \zeta, \iota)$ and $X = (E_p, -n_p^W, \chi, \nu)$. We will describe the constitutive model within the generalized stress **Y**-space. Suppose that there exists a convex surface $f(Y)$ containing the origin in **Y**-space such that plastic dissipation occurs only when the surface is reached. $f(Y)$ is called the yield surface, which can be determined through experiments. Hence, the plastic dissipation problem can be stated as,

$$D(\dot{X}) = \sup_{Y^* \in f} (Y^* \cdot \dot{X}) \geq 0 \qquad (4.3.8)$$

Rate-independence requires that $D(\dot{X})$ be a positively homogeneous function of degree one only, i.e. $D(c\dot{X}) = cD(\dot{X})$ for any $c > 0$.

(4.3.8) can be viewed as a representation of the principle of maximal plastic dissipation (Lubliner, 1990: pp.117-120), which is equivalent to the following normality law,

$$\dot{X} \in N_f(Y) , \qquad (4.3.9)$$

where $N_f(Y)$ is the cone of outward normals to $f(Y)$ in Y-space. This gives the evolution equations of E_p, n_p^W, and the internal variables. Explicitly, we obtain

$$\dot{\boldsymbol{E}}_p = \dot{\lambda}\frac{\partial f}{\partial \boldsymbol{\sigma}^{eff}},\ -\dot{n}_p^w = \dot{\lambda}\frac{\partial f}{\partial S_M},\ \dot{\boldsymbol{\chi}} = \dot{\lambda}\frac{\partial f}{\partial \boldsymbol{\zeta}},\ \dot{\nu} = \dot{\lambda}\frac{\partial f}{\partial \iota} \tag{4.3.10}$$

while it requires that

$$\dot{\lambda} \geq 0,\ f(\boldsymbol{\sigma}^{eff}, S_M, \boldsymbol{\zeta}, \iota) \leq 0, \text{ and } \dot{\lambda} f(\boldsymbol{\sigma}^{eff}, S_M, \boldsymbol{\zeta}, \iota) = 0 \tag{4.3.11}$$

(4.3.11) is the general loading/unloading criterion for the elastoplastic problem expressed in the standard Kuhn-Tucker form (Luenberger, 1984). Equation (4.3.10) represents the flow rule *associated* with the yield surface. For many naturally deposited geomaterials, however, the normality is not satisfied. Therefore, a *nonassociated* flow rule must be introduced. In such cases, the yield surface function $f(\boldsymbol{Y})$ in (4.3.10) must be replaced by a potential function $g(\boldsymbol{Y})$.

To evaluate multiplier $\dot{\lambda}$, it is noted that $f(\boldsymbol{\sigma}^{eff}, S_M, \boldsymbol{\zeta}, \iota) = 0$ when $\dot{\lambda} > 0$. Assuming $\boldsymbol{\zeta} = \boldsymbol{\zeta}(\boldsymbol{\chi})$ and $\iota = \iota(\nu)$, it follows that

$$0 = \dot{f} = \frac{\partial f}{\partial \boldsymbol{\sigma}^{eff}} : \dot{\boldsymbol{\sigma}}^{eff} + \frac{\partial f}{\partial S_M}\dot{S}_M + \frac{\partial f}{\partial \boldsymbol{\zeta}} \cdot \frac{\partial \boldsymbol{\zeta}}{\partial \boldsymbol{\chi}} \cdot \dot{\boldsymbol{\chi}} + \frac{\partial f}{\partial \iota}\frac{\partial \iota}{\partial \nu}\dot{\nu} \tag{4.3.12}$$

Inserting (4.3.10) into (4.3.12), we obtain $\dot{\lambda}$ after some manipulations as

$$\dot{\lambda} = -f_\sigma / H_p, \tag{4.3.13}$$

where

$$f_\sigma = \frac{\partial f}{\partial \boldsymbol{\sigma}^{eff}} : \dot{\boldsymbol{\sigma}}^{eff} + \frac{\partial f}{\partial S_M}\dot{S}_M, \tag{4.3.14}$$

and

$$H_p = \frac{\partial f}{\partial \boldsymbol{\zeta}} \cdot \frac{\partial \boldsymbol{\zeta}}{\partial \boldsymbol{\chi}} \cdot \frac{\partial f}{\partial \boldsymbol{\zeta}} + \frac{\partial f}{\partial \iota}\frac{\partial \iota}{\partial \nu}\frac{\partial f}{\partial \iota} \tag{4.3.15}$$

Thus far, all the evolution formulations of plastic deformation and internal variables have been presented. Explicit elastic stress-strain relationships will be derived in the coming chapter. If $f(\boldsymbol{Y})$ and (or) potential function $g(\boldsymbol{Y})$, as well as hardening laws $\zeta = \zeta(\chi)$ and $\iota = \iota(\nu)$, are specified, the stress-strain behavior of the porous media can be fully determined. Note that the above theoretical framework has a hierarchical structure. If the porous medium is fully saturated by a single fluid, we set $f(\boldsymbol{Y}) = f(\boldsymbol{\sigma} + p^{w}\boldsymbol{I}, \zeta)$, and the above model is just the general case of the effective stress-based elastoplastic models. If the solid skeleton does not experience irreversible deformation, $f(\boldsymbol{Y}) = f(S_{w}, \iota)$ and $\dot{\boldsymbol{E}}_{p} = 0$; the above model describes the irreversible behavior (i.e. hysteresis) in the suction. Another interesting case is that, when the hysteresis in the suction is negligible, we have $f(\boldsymbol{Y}) = f(\boldsymbol{\sigma}^{eff}, \zeta)$. In this case, the effects of the suction on the material hardening can be taken into account by assuming the hardening law as $\zeta = \zeta(S_{w}, \chi)$. The last model is very useful in modeling the elastoplastic behavior of unsaturated soils, since by properly constructing the hardening law $\zeta = \zeta(S_{w}, \chi)$ the elastoplastic models based on the effective stresses can be easily generalized to unsaturated soils within this framework.

4.4 Variational Structure of the Proposed Model

In this section, the theory presented above will be employed to deduce an important principle, i.e. the *principle of virtual dissipation*, which is owed to Biot (1977). Through these derivations, a connection will be established between the Biot's theory and those

based on the theory of mixtures, providing the way to take into account the dynamic compatibility conditions on the interfaces in a continuum model of porous media.

In the model presented above, temperature θ is used as an independent state variable. In fact, since θ and the entropy density η_R are thermodynamically conjugated to each other, either θ or η_R can be used as an independent state variable. If, however, phase change occurs in the porous media, η_R may vary with the proportion of each bulk phase, while the temperature θ remains constant. Therefore, use of η_R as a state variable can generally provide a better description of the porous media. Both sides of (4.1.26) is divided by θ, and it follows, after some manipulations, that

$$\dot{\eta}_R = h_R/\theta + \dot{s} + \dot{s}^*, \tag{4.4.1}$$

where

$$\dot{s} = DIV\,[\dot{\boldsymbol{Q}} - \sum_{\beta=W,N}(\eta^\beta \dot{\boldsymbol{M}}^\beta)], \tag{4.4.2}$$

and

$$\theta\dot{s}^* = \sum_{\beta=W,N}\hat{H}^\beta \dot{n}^\beta - \sum_{\beta=W,N}\dot{\boldsymbol{M}}^\beta \cdot \hat{\hat{\boldsymbol{R}}}^\beta - \left(-\dot{\boldsymbol{Q}} + \sum_{\beta=W,N}\eta^\beta \dot{\boldsymbol{M}}^\beta\right)\cdot GRAD\theta \tag{4.4.3}$$

In (4.4.3), $\hat{\hat{\boldsymbol{R}}}^\beta = \hat{\boldsymbol{R}}^\beta / m_r^\beta$; $\dot{\boldsymbol{Q}} = \boldsymbol{Q}/\theta$ is the entropy production solely due to the heat conduction. Equation (4.4.1) implies that entropy density η_R has three contributions: 1) h_R/θ due to the external supply of heat, which is known; 2) s due to the heat and fluid fluxes; and 3) s^* due to the internal dissipation. Integrating (4.4.2) over $[t_0, t]$ yields

$$s = -DIV\boldsymbol{\Phi}, \tag{4.4.4}$$

where it is assumed that at initial state $s=0$; $\boldsymbol{\Phi}$ can be viewed as the total entropy flowing across a surface, which, before the deformation, is a unit area and

$$\boldsymbol{\Phi} = \int_{s_0} [-\hat{\boldsymbol{Q}} + \sum_{\beta=W,N} (\eta^{\beta} \dot{\boldsymbol{M}}^{\beta})] dt \tag{4.4.5}$$

If s and s^* are known, η_R is obtained by integrating (4.4.1). On the other hand, if $\boldsymbol{\Phi}$ is given, s can be calculated through (4.4.4), and s^* is evaluated by using (4.4.3). Therefore, the independent state variables can be chosen as $\boldsymbol{u}^s$, m^{β} (or $\boldsymbol{M}^{\beta}$), n^{β}, and s (or $\boldsymbol{\Phi}$). The corresponding dependent variables now include $\boldsymbol{S}$ (or $\boldsymbol{P}$ or $\boldsymbol{\sigma}$), G^{β}, and θ. In constitutive assumptions for the dissipative forces, i.e. (3.5.5)-(3.5.7), θ is used as a constitutive variable. If $\boldsymbol{\Phi}$ is used instead of θ, we may assume that

$$\hat{H}^{\gamma} = \hat{H}^{\gamma}\left(Z_{eq}, \dot{n}^{\beta}, \dot{\boldsymbol{M}}^{\beta}, \dot{\boldsymbol{\Phi}}\right), \tag{4.4.6}$$

$$\hat{\boldsymbol{R}}^{\gamma} = \hat{\boldsymbol{R}}^{\gamma} / m_{\gamma} = \hat{\boldsymbol{R}}^{\gamma}\left(Z_{eq}, \dot{n}^{\beta}, \dot{\boldsymbol{M}}^{\beta}, \dot{\boldsymbol{\Phi}}\right), \tag{4.4.7}$$

and

$$GRAD\,\theta = \hat{\boldsymbol{Q}}\left(Z_{eq}, \dot{n}^{\beta}, \dot{\boldsymbol{M}}^{\beta}, \dot{\boldsymbol{\Phi}}\right). \tag{4.4.8}$$

It can be shown that the set of equations (3.5.5)-(3.5.7) is equivalent to the set of (4.4.6)-(4.4.8) in the sense that either one can be derived from the other.

Assuming the system deviates slightly from equilibrium, it follows from (4.4.3) that

$$\theta \dot{s}^* = \sum_{i=1,\ldots,5} X_i \dot{q}_i \quad \text{or} \quad \theta \delta s^* = \sum_{i=1,\ldots,5} X_i \delta q_i . \tag{4.4.9}$$

where q_i and X_i are scalar or tensor objects given in the following sets, i.e.

$$\{q_k, k = 1,2,....5\} = \{\boldsymbol{M}^{\alpha}, \boldsymbol{M}^{s}, n^{\alpha}, n^{s}, \boldsymbol{\Phi}\}, \tag{4.4.10}$$

and

$$\{X_k, k = 1,2,....5\} = \{-\hat{\boldsymbol{R}}^{\alpha}, \hat{\boldsymbol{R}}^{s}, \hat{H}^{\alpha}, \hat{H}^{s}, -GRAD\theta\} \tag{4.4.11}$$

For linear dissipation, we apply Onsager's principle (de Groot, 1952) and obtain

$$X_i = \frac{\partial \hat{D}}{\partial \dot{q}_i}, \tag{4.4.12}$$

where $\hat{D}$ is a intrinsic dissipation function represented by the following quadratic form,

$$\hat{D} = \frac{1}{2} \sum_{i,j=1,..,5} B_{ij} \dot{q}_i \dot{q}_j \tag{4.4.13}$$

while $B_{ij} = B_{ji}$ and $\det(B_{ij}) \geq 0$. By applying the assumption of material symmetry (see section 3.5), further restriction is obtained over B_{ij}. It turns out that $B_{13} = B_{31} = B_{14} = B_{41} = 0$, $i = 1, 2, \& 5$. Finally, by introducing (4.4.9), (4.4.12) and (4.4.13), we derive

$$\theta \hat{s}^{\cdot} = \sum_{i=1,..,5} \frac{\partial \hat{D}}{\partial \dot{q}_i} \dot{q}_i = 2\hat{D} \tag{4.4.14}$$

Now, the governing equations can be categorized into six coupled field equations and summarized in Table 4.1. The corresponding independent fields are chosen as $\boldsymbol{u}^{s}$, $\boldsymbol{M}^{\beta}$, n^{β}, and $\boldsymbol{\Phi}$. Consider a subdomain of the material body. The initial configuration of this subdomain is denoted by Ω, which has a boundary Γ with the unit normal $\boldsymbol{N}$ (see Fig. 4.1). Without losing generality, it is assumed that, at initial state, $\boldsymbol{u}^{s} = \boldsymbol{M}^{\beta} = \boldsymbol{\Phi} = \boldsymbol{0}$, $\dot{\boldsymbol{u}}^{s} = \dot{\boldsymbol{M}}^{\beta} = \dot{\boldsymbol{\Phi}} = \boldsymbol{0}$, $\dot{n}^{\beta} = 0$, $n^{\beta} = n_0^{\beta}$, $\theta = \theta_0$, $\rho_{\alpha} = m_{\alpha}$ and $m^{\beta} = m_0^{\beta}$. For the time being,

it is not necessary to specify the boundary conditions. Suppose that, during a thermo-mechanical process, Ω arrives at a new state represented by ($\boldsymbol{u}^s$, $\boldsymbol{M}^\beta$, n^β, $\boldsymbol{\Phi}$). To obtain the variational description of the problem, let the virtual displacement of the state be represented by ($\delta\boldsymbol{u}^s$, $\delta\boldsymbol{M}^\beta$, δn^β, $\delta\boldsymbol{\Phi}$).

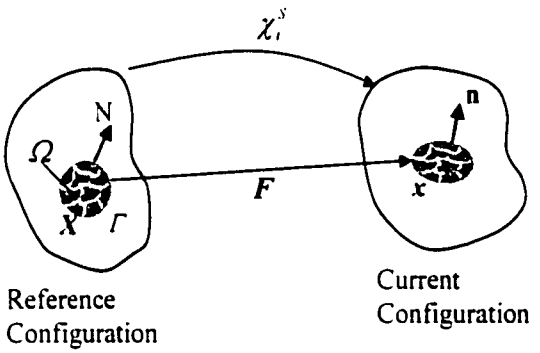

Figure 4.1 Definition of the problem: a porous medium experiences a motion χ_t^s

Table 4.1 Summary of the coupled equations

Fields (State variables)	Coupled field equations		
	Field	Constitutive	Supplementary
$\boldsymbol{u}^s$	(4.1.14)	(4.2.10)	(3.1.13), (3.1.14), (4.1.3)
$\boldsymbol{M}^\beta$	(4.1.15)	(4.2.11)	(4.1.3), (4.4.7)
n^β	(4.1.27)	(4.4.6)	(4.4.6)
$\boldsymbol{\Phi}$	(4.4.8)	(4.2.9)	(4.4.1), (4.4.3), (4.4.4)

Note: $\beta = W, N$

To begin with, it is assumed that the body force field $\boldsymbol{b}$ per unit mass can be derived from a potential $U(\boldsymbol{x})$, i.e.

$$\boldsymbol{b}(\boldsymbol{x},t) = -\nabla U(\boldsymbol{x},t) \tag{4.4.15}$$

and

$$\boldsymbol{B}_t(\boldsymbol{X},t) = -\boldsymbol{F}^T \nabla U(\boldsymbol{x},t) = -GRAD[U \circ \chi^S(\boldsymbol{X},t)] \tag{4.4.16}$$

By introducing Gauss's theorem and integration by part, the weak form of (4.1.14) can be expresses as

$$\begin{aligned} 0 &= \int_\Omega (\rho_R \ddot{\boldsymbol{u}}^S + \sum_{\beta=W,N} \boldsymbol{F}\ddot{\boldsymbol{M}}^\beta - DIV\,\boldsymbol{P} - \rho_R \boldsymbol{B})\delta \boldsymbol{u}^S dV \\ &= \delta E^S_{Kin} + \int_\Omega [\boldsymbol{P} : \delta \boldsymbol{F} + \rho_R (\nabla U)\delta \boldsymbol{u}^S] dV - \int_\Gamma \boldsymbol{f}\delta \boldsymbol{u}^S dA, \end{aligned} \tag{4.4.17}$$

where $\boldsymbol{f}$ is the mechanical force per unit initial (undeformed) area on the boundary Γ, i.e. $f_i = P_{ij}N_j$, and N_j is the component of $\boldsymbol{N}$; δE^S_{Kin} is the kinetic energy of the solid component and given by

$$\delta E^S_{Kin} = \int_\Omega (\rho_R \ddot{\boldsymbol{u}}^S + \sum_{\beta=W,N} \boldsymbol{F}\ddot{\boldsymbol{M}}^\beta)\delta \boldsymbol{u}^S dV \tag{4.4.18}$$

Divide both sides of (4.1.15) by m_t^β and insert (4.4.16) into the resulting equation. It follows that

$$\boldsymbol{F}^T \ddot{\boldsymbol{u}}^S + (m_t^\beta)^{-1} \boldsymbol{C}\ddot{\boldsymbol{M}}^\beta = -GRAD(G^\beta + U) + \hat{\ddot{\boldsymbol{R}}}^\beta, \tag{4.4.19}$$

where $\hat{\ddot{\boldsymbol{R}}}^\beta$ is given by (4.4.7) or (4.4.12).

Similarly, with introduction of Gauss's theorem and (4.1.3), the weak form of (4.4.19) can be presented as

$$
\begin{aligned}
0 &= \int_\Omega [\boldsymbol{F}^T \ddot{\boldsymbol{u}}^S + (m_t^\beta)^{-1} \boldsymbol{C}\ddot{\boldsymbol{M}}^\beta + GRAD(G^\beta + U) - \hat{\dot{\boldsymbol{R}}}^\beta]\delta \boldsymbol{M}^\beta dV \\
&= \delta E_{Kin}^\beta + \int_\Omega [(G^\beta + U)\delta m^\beta - \hat{\dot{\boldsymbol{R}}}^\beta \delta \boldsymbol{M}^\beta] dV + \int_\Gamma (G^\beta + U)\boldsymbol{N}\delta \boldsymbol{M}^\beta dA,
\end{aligned}
\tag{4.4.20}
$$

where $\beta = W$ & N, and

$$
\delta E_{Kin}^\beta = \int_\Omega [\boldsymbol{F}^T \ddot{\boldsymbol{u}}^S + (m_t^\beta)^{-1} \boldsymbol{C}\ddot{\boldsymbol{M}}^\beta]\delta \boldsymbol{M}^\beta dV \tag{4.4.21}
$$

The weak form of the closure equation (4.1.27) is

$$
0 = \int_\Omega (-H^\beta + \hat{H}^\beta)\delta n^\beta dV \tag{4.4.22}
$$

Finally, The weak form of the heat conduction equation (4.4.8) is written as

$$
\begin{aligned}
0 &= \int_\Omega (GRAD\theta - \hat{\dot{\boldsymbol{Q}}})\delta \boldsymbol{\Phi} dV \\
&= \int_\Omega (\theta \delta s - \hat{\dot{\boldsymbol{Q}}}\delta \boldsymbol{\Phi}) dV + \int_\Gamma \theta \boldsymbol{N}\delta \boldsymbol{\Phi} dA
\end{aligned}
\tag{4.4.23}
$$

where use of (4.4.4) has been made.

Summing up (4.4.17), (4.4.20), (4.4.22), and (4.2.23) yields the variational equation of the problem, i.e.

$$
\begin{aligned}
&\int_\Omega \{(\rho_R \ddot{\boldsymbol{u}}^S + \sum_{\beta=W,N} \boldsymbol{F}\ddot{\boldsymbol{M}}^\beta)\delta \boldsymbol{u}^S + \sum_{\beta=W,N} [\boldsymbol{F}^T \ddot{\boldsymbol{u}}^S + (m_t^\beta)^{-1} \boldsymbol{C}\ddot{\boldsymbol{M}}^\beta]\delta \boldsymbol{M}^S\}] dV \\
&+ \int_\Omega [\boldsymbol{P} : \delta \boldsymbol{F} + \sum_{\beta=W,N} (G^\beta \delta m^\beta) - \sum_{\beta=W,N} H^\beta \delta n^\beta + \theta \delta s] dV \\
&+ \int_\Omega [(m_0 + \sum_{\beta=W,N} m^\beta)(\nabla U)\delta \boldsymbol{u}^S + \sum_{\beta=W,N} (U\delta m^\beta)] dV \\
&+ \int_\Omega [-\sum_{\beta=W,N} (\hat{\dot{\boldsymbol{R}}}^\beta \delta \boldsymbol{M}^\beta) + \sum_{\beta=W,N} (\hat{H}^\beta \delta n^\beta) - \hat{\dot{\boldsymbol{Q}}}\delta \boldsymbol{\Phi}] dV \\
&+ \int_\Gamma \{-\boldsymbol{f}\delta \boldsymbol{u}^S + \sum_{\beta=W,N} [(G^\beta + U)\boldsymbol{N}\delta \boldsymbol{M}^\beta] + \theta \boldsymbol{N}\delta \boldsymbol{\Phi}\} dA \\
&= 0.
\end{aligned}
\tag{4.4.24}
$$

To simplify (4.4.24), we define a new energy function by using Legendre's transformation as follows.

$$\hat{V}(\eta_R, \boldsymbol{E}, m^\beta, n^\beta) = W(\theta, \boldsymbol{E}, m^\beta, n^\beta) + \eta_R\theta \tag{4.4.25}$$

where $\beta = W$ and N. It follows that

$$\theta = \frac{\partial \hat{V}}{\partial \eta_R} \tag{4.4.26}$$

Furthermore, it follows from (4.2.3), (4.2.4), and (4.1.26) that

$$\boldsymbol{S} = \frac{\partial \hat{V}}{\partial \boldsymbol{E}}, \tag{4.4.27}$$

$$G^\beta = \frac{\partial \hat{V}}{\partial m^\beta}, \tag{4.4.28}$$

and

$$H^\beta = -\frac{\partial \hat{V}}{\partial n^\beta} \tag{4.4.29}$$

With introducing (4.4.26)-(4.4.29), (4.4.9) and (4.4.12), the variational equation (4.4.25) can be cast into

$$\delta E_{Kin} + \delta_R E_{in} + \delta \mathcal{G} + \int_\Omega \theta \delta s^* dV = \delta \mathcal{F}. \tag{4.4.30}$$

where

$$\delta_R E_{in} = \int_\Omega [\boldsymbol{P} : \delta \boldsymbol{F} + \sum_{\beta=W,N} (G^\beta \delta m^\beta) - \sum_{\beta=W,N} H^\beta \delta n^\beta + \theta \delta s] dV = \int_\Omega \delta_R \hat{V} dV ; \tag{4.4.31}$$

the term $\delta_R \hat{V}$ represents the restricted variation of $\hat{V}$ with $\delta s^* = 0$ and $\delta h_R = 0$; $\mathcal{F}$ is the work done by the generalized external force acting on the boundary Γ and

$$\delta \mathcal{F} = \int_\Gamma \{\boldsymbol{f} \delta \boldsymbol{u}^S - \sum_{\beta=W,N} [(G^\beta + U) N \delta \boldsymbol{M}^\beta] - \theta N \delta \boldsymbol{\Phi}\} dA ; \tag{4.4.32}$$

$\mathcal{G}$ is the potential of the body force and given by

$$\mathcal{G} = \int_{\Omega} (m_0 + \sum_{\beta=W,N} m^{\beta}) U dV ; \tag{4.4.33}$$

E_{Kin} is the total kinetic energy of the porous media and its virtual variation is given by

$$\delta E_{Kin} = \int_{\Omega} \{ (\rho_R \ddot{\boldsymbol{u}}^S + \sum_{\beta=W,N} \boldsymbol{F}\ddot{\boldsymbol{M}}^{\beta}) \delta \boldsymbol{u}^S + \sum_{\beta=W,N} [\boldsymbol{F}^T \ddot{\boldsymbol{u}}^S + (m_t^{\beta})^{-1} \boldsymbol{C}\ddot{\boldsymbol{M}}^{\beta}] \delta \boldsymbol{M}^{\beta} \} dV \tag{4.4.34}$$

Thus far, we have recovered Biot's *principle of virtual dissipation* (Biot, 1977), which states that given h_R a true solution ($\boldsymbol{u}^S$, $\boldsymbol{M}^{\beta}$, n^{β}, $\boldsymbol{\Phi}$) must satisfy (4.4.30) with constraints (4.1.3), (4.4.3), and (4.4.4). This principle can be viewed as a generalization of d'Alembert's principle to nonlinear irreversible thermodynamics. As pointed out by Biot (1977), the principle of virtual dissipation is very general. In fact, it can be applied to the porous media saturated by k ($k > 2$) immiscible fluids. In such cases, $\beta = W, N$ is simply replaced by $\beta = 1,2,\ldots,k$, and all the equations presented above are applicable. However, it must be emphasized that in order to take into account the dynamic compatibility conditions on the interfaces the energy function W can be assumed as

$$W(\theta, \boldsymbol{E}, m_0^S, m^{\alpha}, n^{\alpha}) = m_0^S A^S(\theta, \boldsymbol{E}, \rho^S) + \sum_{\beta=1,2,\ldots,k} m_t^{\beta} A^{\beta}(\theta, n^{\beta}, \rho^{\beta}), \tag{4.4.35}$$

where $\alpha = 1,2,\ldots,k$; A^i ($i = s,1,2,\ldots,k$) depends on m^i only through $\rho^i = m_t^i / Jn^i$ ($J = \det \boldsymbol{F}$), and $m_t^S = m_0^S = const$.

It is instructive to make some remarks on the constitutive assumption in (4.4.35). Here, the free energy of an individual component is assumed to be a function of the state

variables of this component only. Since a bulk component interacts with the others in the porous medium only through the interfaces surrounding it (neglecting the electro-magnetic effects), the volume fraction and true mass density need to be introduced as state variables. For example, the deformation of the skeleton can influence the free energy of α fluid, and yet such effects can be represented directly by the change in n^α and ρ^α. Therefore, it is unnecessary to include $\boldsymbol{E}$ as an argument in A^α. Similarly, the content of α fluid may also influence the free energy of the solid skeleton, but this effect occurs solely through the boundary of the solid grains, which are assumed to be isotropically distributed. Hence, this effect can be directly reflected by the change in the pressure of the solid grains, and correspondingly, ρ^S but n^α is included as an argument of A^S.

Another important point regarding (4.4.35) is that the energy function W depends on ρ^S through $m_\eta^S = J(1 - \sum_{\beta=1,2,\ldots,k} n^\beta)\rho^S$. This is one of the distinguishing features of the presented model. It is worthy to note that the celebrated model of porous media by Bowen (1982), which was developed within the framework of the theory of mixtures, can be derived solely by using the principle of virtual dissipation and by assuming that

$$W(\theta, \boldsymbol{E}, m^\alpha, n^\alpha) = \sum_{i=S,1,2,\ldots,k} m_i^i A^i(\theta, \boldsymbol{E}, n^\alpha, \rho_\alpha) \qquad (4.4.36)$$

where ρ_α is the partial mass density, i.e. $\rho_\alpha = n^\alpha \rho^\alpha$; α is repeated from 1 to k. Comparing (4.4.35) to (4.4.36), it can be easily seen that if ρ^S is excluded in (4.4.35) the presented model is just a particular case of Bowen's model. In the Bowen's model,

however, the exclusion of ρ^s as a state variable leads to an unacceptable result stating that the pressure differences on the interfaces (i.e. suction) will vanish at thermodynamic equilibrium. This result is inconsistent with experimental observations. Furthermore, it is well-recognized (Lade and de Boer, 1997) that the compressibility of the solid phase, which is represented by using ρ^s, has significant influence on the behavior of the porous medium. Therefore, it is important to include ρ^s as a state variable in a general model.

With introduction of the principle of virtual dissipation, it is quite straightforward to derive the field equations presented in Section 4.1. This is achieved by simply following a procedure inverse to that used in this section. To recover all the constitutive equations, however, it is useful to introduce the Euler-Lagrange's equations, which are also derivable from the principle of virtual dissipation with the incorporation of the generalized coordinates. A detailed account of this development was given by Biot (1972, 1977), and will not be repeated here.

From the above derivations, it is shown that the constitutive assumptions made in the theories of mixtures are generally more restrictive than those in Biot's theory. This point can be seen from an inspection of (4.4.35) or (4.4.36). In Biot's theory, the total free energy function W is assumed directly as a function of some macroscopic state variables, such as the left-hand side of (4.4.35) or (4.4.36) (also see, e.g., Coussy, 1995: Ch.10). The choice of the constitutive variables is quite intuitive, since in general it is difficult to identify appropriate constitutive variables (not to mention an explicit constitutive function form). This provides great challenges in applying Biot's theory. In the theory of mixtures, however, any component existing in the porous media is viewed

as an independent phase, and the energy function W is assumed as a mass weighted average of the free energies of all individual components, such as the right-hand side of (4.4.35) or (4.4.36). Since each individual component is considered as a continuum, its free energy function can be more easily obtained. Hence, one of the greatest challenges in the theory of mixture is to identify the parameters representing the interactions among various components. In spite of these differences, Biot's theory can be closely linked with the models of porous media based on the theories of mixtures, as discussed above.

Chapter 5 A LINEARIZED MODEL AND THERMOPORO-ELASTICITY

The objectives of this chapter are two-fold: first, to obtain a set of governing equations for thermoporoelasticity by linearizing the general theory presented in the previous chapters; second, to show how the restrictions in applying the effective stresses can be released by considering the dynamic compatibility conditions on the interfaces. Although discussions are limited to the linear range, insights into the nonlinear model of porous media may be gained through linearizing the general theory.

The outline of this chapter is as follows: Section 1 concerns the linearization of the general constitutive relationships; the linear field equations are derived in Section 2; in Section 3, the effective stress, an important concept in the conventional soil mechanics, is formulated based on the results previously presented. In Section 4, a general account of the physical significance and the evaluation of elastic coefficients are presented.

5.1 Linearized Constitutive Relationships

In the general model developed in Chapters 3&4, three free energy functions need to be specified, i.e.

$$A^s = \hat{A}^s(\theta, \rho^s, \boldsymbol{E}), \tag{5.1.1}$$

and

$$A^{\beta} = \hat{A}^{\beta}\left(\theta, \rho^{\beta}, n^{\beta}\right),\ \beta = W, N \tag{5.1.2}$$

Assume that the porous medium is initially at an equilibrium state represented by

$$\Xi_{eq} = \left\{\theta_0, n_0^{\beta}, \rho_0^{\alpha}, \boldsymbol{E}_0, \boldsymbol{w}_0^{\beta}\right\} = \left\{\theta_0, n_0^{\beta}, \rho_0^{\alpha}, \boldsymbol{0}, \boldsymbol{0}\right\}, \tag{5.1.3}$$

where $\alpha = S, W, N$ and $\beta = W, N$. Under a small external disturbance, the porous medium arrives at a new state with

$$\Xi = \left\{\theta_0 + \theta, n_0^{\beta} + n^{\beta}, \rho_0^{\alpha} + \rho^{\alpha}, \boldsymbol{E}, \boldsymbol{w}^{\beta}\right\}. \tag{5.1.4}$$

From now onwards in this chapter, θ, n^{β}, ρ^{α}, $\boldsymbol{E}$, and $\boldsymbol{w}^{\beta}$ are all viewed as incremental variables. By using Taylor's series, (5.1.1) and (5.1.2) are expanded about Ξ_{eq} to yield, respectively,

$$\begin{aligned} n_0^S \rho_0^S A^S = {} & \frac{1}{2} n_0^S \boldsymbol{E} : \boldsymbol{D} : \boldsymbol{E} - \frac{1}{2} n_0^S c_S \theta^2 + \frac{1}{2} n_0^S K_S \left(\frac{\rho^S}{\rho_0^S}\right)^2 \\ & - n_0^S \lambda_{vol}^S \theta \frac{\rho^S}{\rho_0^S} - n_0^S \theta \boldsymbol{J}_{the}^S : \boldsymbol{E} + n_0^S \frac{\rho^S}{\rho_0^S} \boldsymbol{J}_{pie}^S : \boldsymbol{E} + O\left(\varepsilon^3\right), \end{aligned} \tag{5.1.5}$$

and

$$\begin{aligned} n_0^{\beta} \rho_0^{\beta} A^{\beta} = {} & -\frac{1}{2} n_0^{\beta} c_{\beta} \theta_0^2 + \frac{1}{2} n_0^{\beta} K_{\beta} \left(\frac{\rho^{\beta}}{\rho_0^{\beta}}\right)^2 + \frac{1}{2} n_0^{\beta} \Theta_n^{\beta} \left(n^{\beta}\right)^2 \\ & - n_0^{\beta} \lambda_{vol}^{\beta} \theta \frac{\rho^{\beta}}{\rho_0^{\beta}} + n_0^{\beta} \lambda_{vol}^{\beta} n^{\beta} \frac{\rho^{\beta}}{\rho_0^{\beta}} - n_0^{\beta} \lambda_{the}^{\beta} \theta n^{\beta} + O\left(\varepsilon^3\right), \end{aligned} \tag{5.1.6}$$

where $O(\varepsilon^3)$ represents the higher-order (>2nd) terms; $A^{\alpha}\left(\alpha = S, W, N\right)$ is the corresponding *incremental* free energy function of α-phase. For a linear model, the proposed quadratic forms of free energy functions, i.e. (5.1.5) and (5.1.6), are sufficient for the discussions. It is noted that the first order terms are all dropped in the above

linearized equations. As will be clear later, this is simply due to the fact that we are dealing with an incremental model. The coefficients in (5.1.5) and (5.1.6) generally are the functions of Ξ_{eq}, and their physical significance will be discussed later.

With (5.1.5) and (5.1.6), (3.3.10) and (3.3.11) can be linearized as follows,

$$p^S = K_S \frac{\rho^S}{\rho_0^S} + \boldsymbol{J}^S_{\rho e} : \boldsymbol{E} - \lambda^S_{\rho\theta}\theta\,. \tag{5.1.7}$$

$$p^\beta = K_\beta \frac{\rho^\beta}{\rho_0^\beta} + \lambda^\beta_{\rho n} n^\beta - \lambda^\beta_{\rho\theta}\theta\,,\ \beta = W, N \tag{5.1.8}$$

and

$$\boldsymbol{t}^e = \boldsymbol{D} : \boldsymbol{E} + \boldsymbol{J}^S_{\rho e} : \boldsymbol{I}_4 \frac{\rho^S}{\rho_0^S} - \boldsymbol{J}^S_{\theta e} : \boldsymbol{I}_4\theta\,. \tag{5.1.9}$$

where p^α ($\alpha = S, W, N$) and $\boldsymbol{t}^e$ represent the incremental values; $\boldsymbol{I}_4$ is an isotropic fourth-order tensor with components $(\boldsymbol{I}_4)_{ijkl} = 1/2\left(\delta_{ik}\delta_{jl} + \delta_{il}\delta_{jk}\right)$. In (5.1.7)-(5.1.9) and from now onward, the higher order terms are dropped for clarity, and the porous media are assumed to be statistically isotropic. Hence, it follows that

$$\boldsymbol{J}^S_{\rho e} = \lambda^S_{\rho e}\boldsymbol{I}\,. \tag{5.1.10}$$

$$\boldsymbol{J}^S_{\theta e} = \lambda^S_{\theta e}\boldsymbol{I}\,. \tag{5.1.11}$$

and

$$\boldsymbol{D} : \boldsymbol{E} = \lambda_S(\boldsymbol{I} : \boldsymbol{E})\boldsymbol{I} + 2\mu_S\boldsymbol{E}\,. \tag{5.1.12}$$

where λ_S and μ_S are the Lamé's constants of the solid skeleton. Obviously, by its very definition, K_α ($\alpha = S, W, N$) is the *isothermal* bulk modulus of α phase. The total Cauchy stress, i.e. (3.2.6), now reads

$$\sigma = n_0^S\left(\lambda_S - \lambda_{\rho e}^S\right)(\boldsymbol{I}:\boldsymbol{E})\boldsymbol{I} + 2n_0^S\mu_S\boldsymbol{E} + n_0^S\lambda_{\rho e}^S\frac{\rho^S}{\rho_0^S}\boldsymbol{I} - \sum_{\alpha=S,W,N} n_0^\alpha K_\alpha\frac{\rho^\alpha}{\rho_0^\alpha}\boldsymbol{I}$$
$$- \sum_{\beta=W,N} n_0^\beta\lambda_{\rho n}^\beta n^\beta\boldsymbol{I} + \left(-n_0^S\lambda_{\eta e}^S + \sum_{\alpha=S,W,N} n_0^\alpha\lambda_{\rho\theta}^\alpha\right)\theta\boldsymbol{I} \tag{5.1.13}$$

The specific entropy of a bulk phase is obtained by linearizing (3.3.5), i.e.

$$\rho_0^S\eta^S = c_S\theta + \lambda_{\rho\theta}^S\frac{\rho^S}{\rho_0^S} + \boldsymbol{J}_{\eta e}^S:\boldsymbol{E}, \tag{5.1.14}$$

and

$$\rho_0^\beta\eta^\beta = c_\beta\theta + \lambda_{\rho\theta}^\beta\frac{\rho^\beta}{\rho_0^\beta} + \lambda_{\eta n}^\beta n^\beta, \tag{5.1.15}$$

where $\beta = W, N$. By definition, the specific heat capacity of an individual phase is $c_v^\alpha = \theta_0 c_\alpha$ ($\alpha = S, W, N$). The total specific entropy of the mixture is now given by

$$\rho_0\eta = \sum_{\alpha=S,W,N}\left(n_0^\alpha c_\alpha\right)\theta + \sum_{\alpha=S,W,N} n_0^\alpha\lambda_{\rho\theta}^\alpha\frac{\rho^\alpha}{\rho_0^\alpha} + n_0^S\boldsymbol{J}_{\eta e}^S:\boldsymbol{E} + \sum_{\beta=W,N} n_0^\beta\lambda_{\eta n}^\beta n^\beta \tag{5.1.16}$$

Neglecting the viscosity due to capillary relaxation, the closure equations (3.4.8), which are the macroscopic counterparts of the dynamic compatibility conditions on the interfaces, can be linearized to yield

$$p^\beta - p^S = n_0^\beta\Theta_n^\beta n^\beta + n_0^\beta\lambda_{\rho n}^\beta\frac{\rho^\beta}{\rho_0^\beta} - n_0^\beta\lambda_{\eta n}^\beta\theta,\ \beta = W, N \tag{5.1.17}$$

Finally, the incremental chemical potentials are

$$\rho_0^\beta G^\beta = K_\beta\frac{\rho^\beta}{\rho_0^\beta} + \lambda_{\rho n}^\beta n^\beta - \lambda_{\rho\theta}^\beta\theta,\ \beta = W, N \tag{5.1.18}$$

The constitutive relationships described above include the following coefficients: λ_s, μ_s, $\lambda^s_{\rho e}$, $K_\alpha(\alpha = S, W, N)$, $\lambda^\beta_{\rho n}(\beta = W, N)$, $\Theta^\beta_n(\beta = W, N)$, $c_\alpha(\alpha = S, W, N)$, $\lambda^s_{\theta e}$, $\lambda^\beta_{\theta n}$, $(\beta = W, N)$ and $\lambda^\alpha_{\rho\theta}(\alpha = S, W, N)$. It must be noted that, for a model to be physically possible, certain restrictions must be imposed on the listed material coefficients. For the linear model presented above, the free energies represented by (5.1.5) and (5.1.6) must always have nonnegative values. For free energy A^s to be nonnegative, it is necessary that

$$3\lambda_s + 2\mu_s > 0. \tag{5.1.19}$$

$$\mu_s > 0. \tag{5.1.20}$$

$$K_s > 0. \tag{5.1.21}$$

and

$$\left(\lambda_s + \frac{2}{3}\mu_s\right)K_s \geq \left(\lambda^s_{\rho e}\right)^2. \tag{5.1.22}$$

For nonnegative $A^\beta(\beta = W, N)$, it is required that

$$K_\beta > 0. \tag{5.1.23}$$

$$\Theta^\beta_n \geq 0. \tag{5.1.24}$$

and

$$K_\beta \Theta^\beta_n \geq \left(\lambda^\beta_{\rho n}\right)^2. \tag{5.1.25}$$

5.2 Linearized Field Equations

In the following, it is assumed that the effects of the mass exchange terms can be neglected. The mass balance equation, i.e. (3.2.1), now can be cast into the following linear forms

$$\frac{n_0^S}{\rho_0^S}\frac{\partial \rho^S}{\partial t}+\frac{\partial n^S}{\partial t}+n_0^S\nabla\cdot\boldsymbol{v}^S=0, \tag{5.2.1}$$

and

$$\frac{n_0^\beta}{\rho_0^\beta}\frac{\partial \rho^\beta}{\partial t}+\frac{\partial n^\beta}{\partial t}+n_0^\beta\nabla\cdot\mathbf{v}^\beta=0,\ \beta=W,N \tag{5.2.2}$$

The equation of motion for the porous medium is obtained by summing up the linear momentum balance equations, i.e. (3.2.4), over all the phases. By introducing (5.1.13), the linear counterpart of this equation is expressed as,

$$\begin{aligned}\sum_{\alpha=S,W,N} n_0^\alpha\rho_0^\alpha\frac{\partial^2\boldsymbol{u}^\alpha}{\partial t^2}&=n_0^S\left(\lambda_S+\mu_S-\lambda_{\rho e}^S\right)\nabla\nabla\cdot\boldsymbol{u}^S+n_0^S\mu_S\nabla\cdot\nabla\boldsymbol{u}^S+n_0^S\lambda_{\rho w}^S\nabla\left(\frac{\rho^S}{\rho_0^S}\right)\\&-\sum_{\alpha=S,W,N} n_0^\alpha K_\alpha\nabla\left(\frac{\rho^\alpha}{\rho_0^\alpha}\right)-\sum_{\beta=W,N} n_0^\beta\lambda_{\rho n}^\beta\nabla n^\beta+\left(-n_0^S\lambda_{\theta e}^S+\sum_{\alpha=S,W,N} n_0^S\lambda_{\rho w}^S\right)\nabla\theta\end{aligned} \tag{5.2.3}$$

Inserting (3.5.15) and (5.1.18) into the linearized form of flow equation (3.5.20), one obtains

$$n_0^\beta\rho_0^\beta\frac{\partial^2\boldsymbol{u}^\beta}{\partial t^2}=-n_0^\beta\lambda_{\rho n}^\beta\nabla n^\beta-n_0^\beta K_\beta\nabla\left(\frac{\rho^\beta}{\rho_0^\beta}\right)-\hat{\mu}^\beta\boldsymbol{w}^\beta+n_0^\beta\lambda_{\rho\theta}^\beta\nabla\theta, \tag{5.2.4}$$

where $\beta=W,N$; in using (3.5.15), the cross effects have been omitted, i.e. $\hat{\boldsymbol{r}}^\beta$ depends on $\boldsymbol{w}^\beta$ only. Subtraction of (5.2.4) from (5.2.3) repeatedly for both fluids yields the linear form of the linear momentum balance equation of the solid skeleton, i.e.

$$\begin{aligned}n_0^S\rho_0^S\frac{\partial^2\boldsymbol{u}^S}{\partial t^2}&=n_0^S\left(\lambda_S+\mu_S-\lambda_{\rho e}^S\right)\nabla\nabla\cdot\boldsymbol{u}^S+n_0^S\mu_S\nabla\cdot\nabla\boldsymbol{u}^S\\&-n_0^S\left(K_S-\lambda_{\rho e}^S\right)\nabla\left(\frac{\rho^S}{\rho_0^S}\right)+\sum_{\beta=W,N}\hat{\mu}^\beta\boldsymbol{w}^\beta+\left(n_0^S\lambda_{\rho\theta}^S-n_0^S\lambda_{\theta e}^S\right)\nabla\theta\end{aligned} \tag{5.2.5}$$

The total energy balance of the porous medium is given by (4.1.26), and its linear form can be expressed as follows,

$$\theta_0 \rho_0 \frac{\partial \eta}{\partial t} + div\, \boldsymbol{q} = 0 \tag{5.2.6}$$

Inserting (3.5.16) and (5.1.16) into (5.2.6) yields

$$\theta_0 \left[\sum_{\alpha=S,W,N} \left(n_0^\alpha c_\alpha\right) \frac{\partial \theta}{\partial t} + \sum_{\alpha=S,W,N} \frac{n_0^\alpha \lambda_{\rho\theta}^\alpha}{\rho_0^\alpha} \frac{\partial \rho^\alpha}{\partial t} + \sum_{\beta=W,N} n_0^\beta \lambda_{\theta n}^\beta \frac{\partial n^\beta}{\partial t} + n_0^S \lambda_{\theta e}^S \nabla \cdot \frac{\partial \boldsymbol{u}^S}{\partial t} \right] \tag{5.2.7}$$
$$- \sum_{\beta=W,N} \hat{\omega}_\beta^\theta \nabla \cdot \boldsymbol{w}^\beta - \hat{\omega}^\theta (\nabla \cdot \nabla \theta) = 0$$

Thus far, all the field equations governing the linear thermoelasticity of the porous media saturated by two immiscible fluids have been presented. The closed set of field equations includes: the mass balance equations (5.2.1) and (5.2.2), the linear momentum balance equations (5.2.4) and (5.2.5), and the energy balance equation (5.2.7), as well as the closure equation (5.1.17) with constitutive equations (5.1.7) and (5.1.8). The total number of the *independent* field equations is 9, which equals to the number of the unknowns, i.e. $\{\theta, \boldsymbol{u}^\alpha, \rho^\alpha, n^\beta\}$, $\alpha = S, W, N$ and $\beta = W, N$.

The field equations presented above can be further cast into a more compact form by deleting n^β and ρ^α ($\alpha = S, W, N$ and $\beta = W, N$). Integrating (5.2.1) and (5.2.2) with respect to time yields, respectively,

$$n_0^S \frac{\rho^S}{\rho_0^S} + n^S + n_0^S \nabla \cdot \boldsymbol{u}^S = 0, \tag{5.2.8}$$

and

$$n_0^\beta \frac{\rho^\beta}{\rho_0^\beta} + n^\beta + n_0^\beta \nabla \cdot \boldsymbol{u}^\beta = 0, \tag{5.2.9}$$

where $\beta = W, N$; $n^S = -n^W - n^N$. With incorporation of (5.2.8), (5.2.9), (5.1.17), (5.1.7), and (5.1.8), ρ^α and n^α are deleted from (5.2.4), (5.2.5), and (5.2.7). It follows that

$$\begin{aligned} n_0^S \rho_0^S \frac{\partial^2 \boldsymbol{u}^S}{\partial t^2} = {} & \left(M_{SS} + n_0^S \mu_S\right) \nabla\nabla \cdot \boldsymbol{u}^S + n_0^S \mu_S \nabla \cdot \nabla \boldsymbol{u}^S + M_{SW} \nabla\nabla \cdot \boldsymbol{u}^W \\ & + M_{SN} \nabla\nabla \cdot \boldsymbol{u}^N + \sum_{\beta = W,N} \hat{\mu}^\beta \left(\frac{\partial \boldsymbol{u}^\beta}{\partial t} - \frac{\partial \boldsymbol{u}^\beta}{\partial t} \right) + H_{S\theta} \nabla\theta . \end{aligned} \tag{5.2.10}$$

$$\begin{aligned} n_0^W \rho_0^W \frac{\partial^2 \boldsymbol{u}^W}{\partial t^2} = {} & M_{SW} \nabla\nabla \cdot \boldsymbol{u}^S + M_{WW} \nabla\nabla \cdot \boldsymbol{u}^W + M_{WN} \nabla\nabla \cdot \boldsymbol{u}^N \\ & - \hat{\mu}^W \left(\frac{\partial \boldsymbol{u}^W}{\partial t} - \frac{\partial \boldsymbol{u}^S}{\partial t} \right) + H_{W\theta} \nabla\theta . \end{aligned} \tag{5.2.11}$$

$$\begin{aligned} n_0^N \rho_0^N \frac{\partial^2 \boldsymbol{u}^N}{\partial t^2} = {} & M_{SN} \nabla\nabla \cdot \boldsymbol{u}^S + M_{WN} \nabla\nabla \cdot \boldsymbol{u}^W + M_{SN} \nabla\nabla \cdot \boldsymbol{u}^N \\ & - \hat{\mu}^N \left(\frac{\partial \boldsymbol{u}^n}{\partial t} - \frac{\partial \boldsymbol{u}^s}{\partial t} \right) + H_{N\theta} \nabla\theta , \end{aligned} \tag{5.2.12}$$

and

$$c \frac{\partial \theta}{\partial t} + \sum_{\beta = W,N} \left(Q_\beta - \hat{\omega}_\beta^\theta \right) \nabla \cdot \frac{\partial \boldsymbol{u}^\beta}{\partial t} + \left(Q_S + \sum_{\beta = W,N} \hat{\omega}_\beta^\theta \right) \nabla \cdot \frac{\partial \boldsymbol{u}^S}{\partial t} - \hat{\omega}^\theta \nabla \cdot \nabla\theta = 0, \tag{5.2.13}$$

where the coefficients $M_{\alpha\beta}$, and $H_{\alpha\theta}$ are given in Appendix II. c , Q_S , Q_W , and Q_N are given, respectively, by

$$c = \theta_0 \left[\sum_{\alpha = S,W,N} \left(n_0^\alpha c_\alpha \right) - \sum_{\beta = W,N} \frac{\left(\lambda_{\rho\theta}^\beta - n_0^\beta \lambda_{\theta m}^\beta \right) \left(H_{\beta\theta} - n_0^\beta \lambda_{\rho\theta}^\beta \right)}{K_\beta - n_0^\beta \lambda_{\rho m}^\beta} \right], \tag{5.2.14}$$

$$Q_\beta = -\frac{\theta_0\left(\lambda^\beta_{\rho\theta} - n_0^\beta \lambda^\beta_{\theta n}\right)\left(M_{\beta\beta} - n_0^\beta K_\beta\right)}{K_\beta - n_0^\beta \lambda^\beta_{\rho n}}, \quad \beta = W, N \tag{5.2.15}$$

and

$$Q_S = \theta_0\left[n_0^S \lambda^S_{\theta\kappa} - \frac{\lambda^S_{\rho\theta}\left(M_{SS} - n_0^S \lambda_S - n_0^S \lambda^S_{\rho\kappa}\right)}{K_S - \lambda^S_{\rho\kappa}}\right] \tag{5.2.16}$$

The final set of governing equations includes (5.2.10)-(5.2.13), which govern the linear, isotropic, thermoelasticity of the porous media saturated by two immiscible, compressible fluids. Note that the model represented by the above governing equations has a symmetrical structure.

Without the thermal effects, Equations (5.2.10)-(5.2.13) are similar to the generalized formulations of Biot's theory used in the analyses of the wave propagation in porous media, see, for instance, Brutsaert (1964), Bowen (1982), Garg and Nayfeh (1986), Santos et al. (1990), and Tuncay and Corapcioglu (1997), among others. However, the proposed model differs from those cited above in that it is capable of rigorously considering the dynamic compatibility conditions on interfaces discussed in Section 1.2. It is noted that, in the generalized Biot's models, the relationship between the capillary pressure and moisture content, which is a macroscopic counterpart of the dynamic compatibility conditions on interfaces, was introduced intuitively; moreover, this relationship was used in these models only to obtain some material constants. In the model presented here, however, the relationships between capillary pressures and state variables (including moisture content) are considered as the original components of the model (see Eq. (5.1.17)). This treatment is thermodynamically consistent, as discussed in the previous chapter.

The field equations represented by (5.2.10)-(5.2.13) are only applicable to the porous materials where each fluid phase is interconnected. In reality, however, the content of a fluid may change from time to time. When n_0^N decreases to a small value, i.e. when $n_0^W > \theta_r$ (θ_r is a positive value close to *but less than* the porosity n), the nonwetting fluid will be disconnected and trapped in the wetting one. In such a case, both fluids will macroscopically move together. For simplicity, the thermal effects will be omitted in the following discussions. Once $n_0^W > \theta_r$, one may set $n_0^N = 0$. (5.2.10)-(5.2.12) yields Biot's model for the saturated porous media (Biot, 1956a), i.e.

$$n_0^S \rho_0^S \frac{\partial^2 \boldsymbol{u}^S}{\partial t^2} = \nabla\left[(A+N)\nabla\cdot\boldsymbol{u}^S + Q\nabla\cdot\boldsymbol{u}^W\right] + N\nabla\cdot\nabla\boldsymbol{u}^S + \hat{\mu}\boldsymbol{w}^W, \quad (5.2.17)$$

and

$$n_0\rho_0^W \frac{\partial^2 \boldsymbol{u}^W}{\partial t^2} = \nabla\left(Q\nabla\cdot\boldsymbol{u}^S + R\nabla\cdot\boldsymbol{u}^W\right) - \hat{\mu}\boldsymbol{w}^W. \quad (5.2.18)$$

where

$$A = n_0^S\left(\lambda_S + K_S - 2\lambda_{pe}^S\right) - \frac{n_0 n_0^S (K_S - \lambda_{pe}^S)^2}{n_0 K_S + n_0^S K_W + n_0 n_0^S (n_0\Theta_n^W - 2\lambda_{pn}^W)}, \quad (5.2.19)$$

$$N = n_0^S \mu_S, \quad (5.2.20)$$

$$Q = \frac{n_0 n_0^S (\lambda_{pe}^S - K_S)(n_0\lambda_{pn}^W - K_W)}{n_0 K_S + n_0^S K_W + n_0 n_0^S (n_0\Theta_n^W - 2\lambda_{pn}^W)}, \quad (5.2.21)$$

and

$$R = \frac{n_0^2[K_S K_W - n_0^2(\lambda_{pn}^W)^2 + n_0 K_W \Theta_n^W)]}{n_0 K_S + n_0^S K_W + n_0 n_0^S (n_0\Theta_n^W - 2\lambda_{pn}^W)}. \quad (5.2.22)$$

It must be pointed out that, in the Biot's model, there exists a term called the coupling mass, i.e. ρ_{12}. This term arises quite intuitively as a result of local nonuniformities in the flow when the constituents of the mixture move relative to one another (Biot, 1956 I; Coussy, 1995: pp.31-34). Although the coupling mass may be important in dynamics of

the fluids containing particles or bubbles (Soo, 1967), its effects on the porous media, such as those considered here, remain unclear. However, it has been recognized (Bowen, 1976) that the coupling mass term does not follow the principle of material indifference (objectivity) and it is difficult to motivate base on the continuum theory of mixtures.

5.3 Effective Stress in Porous Media

The principle of effective stresses, usually attributed to Terzaghi (1936), plays a crucial role in modeling the behavior of geomaterials. In fact, majority of the stress-strain constitutive relationships of geomaterials used in practice is based on the effective stresses. According to Terzaghi (1936), the effective stress principle may be stated as: all measurable effects of a change of stress, such as compression, distortion, and a change of shear strength of a soil are exclusively due to change in effective stress. For saturated soils, Terzaghi proposed that the effective stress equals to the excess of the total applied stress over the pore pressure. In the past decades, many efforts have been made to develop the effective stress formulations for the porous media with multiple fluids. However, it turns out that generalization of the Terzaghi effective stress concept to a mutiphase system is not straightforward.

In the following, the effective stress formulations will be developed based on the Terzaghi principle of effective stress. For convenience, we only consider the isothermal conditions. Assume that $n_0^w \neq 0$ and $n_0^s \neq 0$. With introducing (5.1.7)-(5.1.9), (5.1.17), and (5.2.8), the mass densities ρ^α and volume fractions n^α is eliminated from (5.1.13). This yields

$$\sigma + (\chi_W p^W + \chi_N p^N) I = n_0^S \left[\lambda_S - \frac{(\lambda_{pe}^S)^2}{K_S} + \left(\frac{\lambda_{pe}^S}{K_S} - 1 \right) \frac{a_e}{a_S} \right] (I : E) I + 2 n_0^S \mu_S E . \quad (5.3.1)$$

where

$$\chi_W = n_0^W + n_0^S \left(\frac{\lambda_{pe}^S}{K_S} - 1 \right) \frac{a_W}{a_S} . \quad (5.3.2)$$

$$\chi_N = n_0^N + n_0^S \left(\frac{\lambda_{pe}^S}{K_S} - 1 \right) \frac{a_N}{a_S} . \quad (5.3.3)$$

$$a_e = n_0^S \left(\frac{\lambda_{pe}^S}{K_S} - 1 \right) . \quad (5.3.4)$$

$$a_S = \frac{n_0^S}{K_S} + \frac{K_W}{n_0^W [\Theta_n^W K_W - (\lambda_{sm}^W)^2]} + \frac{K_N}{n_0^N [\Theta_n^N K_N - (\lambda_{sm}^N)^2]} . \quad (5.3.5)$$

$$a_W = \frac{n_0^W \lambda_{sm}^W - K_W}{n_0^W [\Theta_n^W K_W - (\lambda_{sm}^W)^2]} . \quad (5.3.6)$$

and

$$a_N = \frac{n_0^N \lambda_{sm}^N - K_N}{n_0^N [\Theta_n^N K_N - (\lambda_{sm}^N)^2]} . \quad (5.3.7)$$

By Terzaghi's definition, the effective stress formulation for a linear model of the porous media saturated by two immiscible fluids can be represented by

$$\sigma' = \sigma + (\chi_W p^W + \chi_N p^N) I \quad (5.3.8)$$

Thus far, all the individual components are assumed to be arbitrarily compressible. This assumption is too general for practical use. In (5.1.7)-(5.1.9), coefficients λ_{se}^S and $\lambda_{sm}^\beta (\beta = W, N)$ account for the coupling effects in the porous media. For some porous materials, these coupling coefficients may be small. For instance, in the unsaturated soils, the coupling between the volume fraction and the mass density of an individual component is negligible. In such cases, it is reasonable to assume that

$$\left|\lambda_{sn}^{\beta}\right| << K_{\beta},\ \left|\lambda_{\rho c}^{S}\right| << K_{S}. \tag{5.3.9}$$

In addition, since the microscopic pressure difference on the interface mainly depends on the surface tension and the curvature of the interface, its macroscopic counterpart, i.e. the capillary pressures, must be influenced dominantly by the fluid content and not by the mass density of the fluids. Therefore, from (5.1.17), it is reasonable to expect that

$$\lambda_{sn}^{\beta} << \Theta_{n}^{\beta} << K_{S} \tag{5.3.10}$$

The second inequality of (5.3.10) is quite obvious, since Θ_{n}^{β} generally is not more than 10^{4} kPa *by its definition* and K_{S} larger than 10^{6} kPa (say, for geomaterials).

With (5.3.9) and (5.3.10), (5.3.2) and (5.3.3) lead to

$$\chi_{W} = \frac{n_{0}^{N} n_{0}^{S} \Theta_{n}^{N}}{n_{0}^{N}\Theta_{n}^{N} + n_{0}^{W}\Theta_{n}^{W}} + n_{0}^{W} = 1 - \chi_{N}. \tag{5.3.11}$$

With $\Theta_{n}^{\beta} \geq 0$ $(\beta = W, N)$, it can be deduced from (5.3.11) that $0 \leq \chi_{W} \leq 1$ and $0 \leq \chi_{N} \leq 1$. Now, (5.3.8) becomes

$$\boldsymbol{\sigma}' = \boldsymbol{\sigma} + [\chi_{W} p^{W} + (1 - \chi_{W}) p^{N}]\boldsymbol{I} \tag{5.3.12}$$

This is the so-called Bishop effective stress formulation for unsaturated soils (Bishop, 1959). The stress-strain relationship, i.e. (5.3.1), can be written as

$$\boldsymbol{\sigma}' = n_{0}^{S}\left[\lambda_{S} - \frac{\left(\lambda_{\rho c}^{S}\right)^{2}}{K_{S}} + \frac{n_{0}^{W} n_{0}^{N} \Theta_{n}^{W} \Theta_{n}^{N}}{n_{0}^{N}\Theta_{n}^{N} + n_{0}^{W}\Theta_{n}^{W}}\right](\boldsymbol{I} : \boldsymbol{E})\boldsymbol{I} + 2n_{0}^{S}\mu_{S}\boldsymbol{E}. \tag{5.3.13}$$

where σ' is the effective stress defined by (5.3.12). It is noted that whether or not the assumptions made in (5.3.9) and (5.3.10) are generally applicable to the porous media needs experimental justifications. As discussed in Section 5.4, however, the consequences of these assumptions are consistent with the experimental observations in unsaturated soil mechanics (Fredlund and Rahardjo, 1993).

The above stress-strain relationships are applicable only to the porous materials with interconnecting fluid phases. As discussed in the last section, when $n_0^W > \theta_r$, the porous media will become saturated, and the nonwetting fluid will be trapped in the wetting phase. In such a case, one may set $n^W = n$, $n^S = -n$, and $n_0^S = 1 - n_0$, where n is the change in the porosity of the material.

Following a procedure similar to that used in deriving (5.3.13), one may develop the effective stress formulation for the saturated porous media. In the following, it is instructive to consider the following three particular cases usually met in practice.

a) Both components are *nearly* incompressible. In this case, $K_s \to +\infty$ and $K_w \to +\infty$. Due to the impenetrability on the interface between the fluid and the solid, the microscopic pressure of the fluid must be equal to that of the solid, i.e. $p_{micro}^W = p_{micro}^S$. Therefore, for the statistically isotropic porous media, $p^S = p^W$. Since $\rho^W / \rho_0^W \to 0$ and $\theta = 0$, (5.1.17) implies that $\Theta_n^W \to 0$. This is expected, since in this case the free energy of the fluid is independent of the porosity, i.e. the volume fraction of the fluid. Inserting (5.1.9) into (3.2.6) with $n_0^N = 0$, one can prove that

$$\boldsymbol{\sigma} + p^W \boldsymbol{I} = n_0^S \lambda_S (\boldsymbol{I} : \boldsymbol{E}) \boldsymbol{I} + 2 n_0^S \mu_S \boldsymbol{E} . \qquad (5.3.14)$$

This is a representation of Terzaghi's effective stress principle for the linear, isotropic elastic saturated porous media, and it is suitable for some saturated granular soils (e.g. sands). For a linear model, (5.3.14) implies that the effective stress tensor is

$$\boldsymbol{\sigma}' = \boldsymbol{\sigma} + p^W \boldsymbol{I} = \left[n_0^S \boldsymbol{t}^S - n_0 p^W \boldsymbol{I} \right] + p^W \boldsymbol{I} = n^S \boldsymbol{t}^e . \qquad (5.3.15)$$

where $\boldsymbol{t}^e$ is defined by (3.3.11). The first equation of (5.3.15) is the classic effective stress formulation (Terzaghi, 1936).

b) The fluid is nearly incompressible and the (individual) solid component compressible. This model is useful in dealing with porous media such as rock and concrete. In this case, $K_W \to +\infty$:

$$p^S = \left(\frac{K_S}{n_0 n_0^S \Theta_n^W + K_S} \right) p^W + \frac{n_0 n_0^S \Theta_n^W \left(\lambda_{ve}^S - K_S \right)}{n_0 n_0^S \Theta_n^W + K_S} \boldsymbol{I} : \boldsymbol{E} , \qquad (5.3.16)$$

and the stress-strain relationship is expressed by

$$\boldsymbol{\sigma} + \alpha_B p^W \boldsymbol{I} = n_0^S \left[\lambda_S + \nu \right] (\boldsymbol{I} : \boldsymbol{E}) \boldsymbol{I} + 2 n_0^S \mu_S \boldsymbol{E} , \qquad (5.3.17)$$

where

$$\alpha_B = 1 - \frac{n_0^S \left(n_0 n_0^S \Theta_n^W + \lambda_{ve}^S \right)}{n_0 n_0^S \Theta_n^W + K_S} , \qquad (5.3.18)$$

and

$$\nu = \frac{n_0 n_0^S \Theta_n^W - \left(\lambda_{ve}^S + 2 n_0 n_0^S \Theta_n^W \right) \lambda_{ve}^S}{n_0 n_0^S \Theta_n^W + K_S} . \qquad (5.3.19)$$

Similarly, (5.3.17) implies that the effective stress formulation now becomes

$$\sigma' = \sigma + \alpha_B p^W \boldsymbol{I}, \tag{5.3.20}$$

where α_B is usually called the Biot coefficient. $n_0 < \alpha_B \leq 1$, since $+\infty > K_S > \lambda^S_{\rho e}$. It is noted that the effective stress formulation represented by (5.3.20) is usually employed in modeling the rock-like porous materials (Lade and de Boer, 1997).

c) Both components are compressible. Similarly, in such a case, the linear elastic stress-strain relationship reads

$$\sigma + \alpha_B p^W \boldsymbol{I} = n_0^S (\lambda_S + \nu)(\boldsymbol{I} : \boldsymbol{E})\boldsymbol{I} + 2n_0^S \mu_S \boldsymbol{E}, \tag{5.3.21}$$

where α_B is now given by

$$\alpha_B = 1 - \frac{n_0^S \{n_0 \lambda^W_{sm}(K_S - \lambda^S_{\rho e}) + \lambda^S_{\rho e} K_W + n_0 n_0^S [\Theta_n^W K_W - (\lambda^W_{sm})^2]\}}{n_0 n_0^S [\Theta_n^W K_W - (\lambda^W_{sm})^2] + K_W K_S}. \tag{5.3.22}$$

and ν is

$$\nu = -\frac{(\lambda^S_{\rho e})^2}{K_S} + \frac{n_0 (n_0^S)^2 [\Theta_n^W K_W - (\lambda^W_{sm})^2](\lambda^S_{\rho e} - K_S)^2}{K_S \{n_0 n_0^S [\Theta_n^W K_W - (\lambda^W_{sm})^2] + K_W K_S\}}. \tag{5.3.23}$$

With inequality (5.1.25) and noting that $\lambda^S_{\rho e} < K_S < +\infty$ and $\lambda^W_{sm} < K_W < +\infty$, one can easily prove that $n_0 < \alpha_B < 1$. Remarkably, if the coupling coefficient λ^W_{sm} is negligible, (5.3.21) and (5.3.22) become equivalent to (5.3.18) and (5.3.19), respectively. Hence, λ^W_{sm} can be confidently neglected when the fluid has low compressibility.

From the above discussions, it is clear that an explicit expression for the effective stress is primarily determined by the compressibility of individual phases coexisting in the porous media. For the porous media saturated by a single fluid, if both the solid and

the fluid have low compressibility, the Terzaghi effective stress is applicable; otherwise, model b) or c) must be introduced. It is also noted that for the problems of infinitesimal deformation coefficients α_β may be considered as constants, since ρ^S, ρ^W, n and $\boldsymbol{E}$ change slightly, and all the coefficients existing in the model are practically constant. This feature has great practical and theoretical significance in modeling the behavior of porous media. As for multiphase systems, however, it seems very awkward (though possible) to employ an explicit effective stress formulation in modeling the stress-strain behavior, since χ_w and χ_n are generally the functions of the state variables.

5.4 Evaluation of Material Coefficients

Suppose that the initial porosity n_0 and the degree of saturation of the wetting fluid, i.e. S_r, are known. In the linear model presented above, there exist 24 coefficients yet to determine, which can be categorized into the following three groups:

Group 1 (mechanical effects): λ_S, μ_S, $\lambda_{\nu\varepsilon}^S$, K_α ($\alpha = S, W, N$), $\lambda_{\nu m}^\beta$, and Θ_n^β ($\beta = W, N$).

Group 2 (thermal effects): c_α, $\lambda_{n\varepsilon}^S$, $\lambda_{\theta m}^\beta$, and $\lambda_{\nu\theta}^\alpha$ ($\alpha = S, W, N$; $\beta = W, N$).

Group 3 (conductivity): $\hat{\mu}^\beta$, $\hat{\omega}_\beta^\theta$, and $\hat{\omega}^\theta$ ($\beta = W, N$).

It is noted that these coefficients are generally the functions of θ_0, n_0^W, n_0^N, and/or $\rho_0^\alpha (\alpha = S, W, N)$. In Group 3, $\hat{\omega}^\theta$ is the thermal conductivity of the mixture, and $\hat{\mu}^\beta$ may be related to the permeability of the fluid flow. Both coefficients can be measured in laboratories (Bear, 1972). $\hat{\omega}_\beta^\theta$ represent the coupling between the temperature and fluid

diffusion. For many applications, the coupling effects between heat conduction and fluid diffusion are negligible, and these parameters are usually dropped.

In what follows, our attentions will be focused on the evaluation of the material coefficients in Group 1 & 2. According to their characteristics, the coefficients in each group can be further distinguished among deformation properties, coupling properties, and intrinsic properties. The intrinsic constants, which represent the properties of an individual component, include bulk moduli K_α, specific heat capacity $c_v^\alpha (= \theta_0 c_\alpha)$, and $\lambda_{ij\theta}^\alpha$. The last coefficient can be expressed as

$$\lambda_{ij\theta}^\alpha = 3K_\alpha \alpha_\theta^\alpha . \tag{5.4.1}$$

From (5.1.7) and (5.1.8), it is clear that α_θ^α is just the thermal dilatational coefficient of α-component. The compressibility of an individual phase is defined by

$$C_\alpha = (K_\alpha)^{-1} . \tag{5.4.2}$$

It is noted that all the intrinsic properties of materials are accessible in routine experiments or can even be obtained in the standard handbooks, see, for instance, Clark (1966). Unlike the intrinsic properties, all the other material coefficients generally are not transparent and must be determined by correlating them to the phenomenological parameters of porous media. These coefficients include the coupling properties λ_{ije}^S, λ_{ijm}^β, $\lambda_{\theta e}^S$, and $\lambda_{\theta m}^\beta$, the Lamé coefficients λ_S and μ_S, and the suction coefficient Θ_n^β.

The phenomenological parameters used to evaluate the material constants of the proposed model can be experimentally determined. To begin with, it is useful to

introduce some important concepts associated with the experiments such as constant-suction, drained, and undrained. During a constant-suction experiment, the matric suction (i.e. the difference between p^{N} and p^{W}) remains constant. In a completely drained test, no change in the pressure of a fluid is allowed, i.e. pressure increments p^{N} and p^{W} must be zero. In a fully undrained test, however, it requires that no local diffusion be permitted and no fluids escape out of the domain spanned by the skeleton. Concisely, the fully undrained condition is defined by

$$\boldsymbol{u}^{S} = \boldsymbol{u}^{W} = \boldsymbol{u}^{N}. \tag{5.4.3}$$

With (5.4.3), balance equations (5.2.8) and (5.2.9) may be added together to yield

$$\varepsilon_{v} = -\boldsymbol{I} : \boldsymbol{E} = \sum_{\alpha\, S,W,N} n_{0}^{\alpha} \frac{\rho^{\alpha}}{\rho_{0}^{\alpha}}, \tag{5.4.4}$$

where ε_{v} is the volumetric strain of the matrix, which is positive in compression. (5.4.4) gives another representation of the undrained condition.

If the compressibility of the solid grain is excluded and the content of the wetting fluid vanishes (i.e. the dry porous media), the stress-strain relationship (5.3.1) become

$$\boldsymbol{\sigma} = n_{0}^{S}\lambda_{S}(\boldsymbol{I} : \boldsymbol{E})\boldsymbol{I} + 2n_{0}^{S}\mu_{S}\boldsymbol{E}. \tag{5.4.5}$$

This is the linear, isotropic, elastic model of the dry porous media. Clearly, $\lambda(=n_{0}^{S}\lambda_{S})$ and $\mu(=n_{0}^{S}\mu_{S})$ are the Lamé coefficients that account for the isotropic linear elastic deformation of the solid matrix solely due to the rearrangement of solid grains. It seems that λ and μ can be determined through a direct test on the "dry" sample. In reality,

however, such a point of view is incorrect. For instance, it is well recognized that inclusion of small amount of moisture may drastically change the mechanical behavior of the granular materials (Hornbaker et al., 1997). Therefore, in the experiments to determine the phenomenological properties, the samples of very low moisture content should be excluded. Comparing (5.3.1), (5.3.13), (5.3.14), (5.3.17), and (5.3.21), one may notice that, irrespective of fluid content and drained conditions, the shear modulus of the porous media can always be represented by

$$G = \mu = n_0^S \mu_S , \tag{5.4.6}$$

which can be directly measured in a laboratory test.

By their definitions, $\lambda_{\rho e}^S$ and λ_S are independent of the fluid contents. Hence, these two coefficients can be obtained by testing the fully saturated samples. For the fully saturated porous media under isothermal conditions, given K_S, K_W, and μ_S as well as the initial volume fractions of individual phases, one still has $\lambda_{\rho e}^S$, λ_S, $\lambda_{\rho m}^W$, and Θ_0^W to determine. The last four coefficients may be obtained by correlating them to the phenomenological parameters such as the drained bulk modulus K_D, the undrained bulk modulus K_U, and the Skempton coefficient B. References on the interpretation and evaluation of the phenomenological parameters of the saturated porous media are abundant in the literature, see, for instance, Biot & Willis (1957), and Kümpel (1991), among others. In the following, it will be assumed that the coupling between the mass density ρ^W and the volume fraction n^W can be neglected. Hence, $\lambda_{\rho n}^W = 0$. We will skip

experimental details and only concern with the correlation between the material constants of the proposed model and the phenomenological parameters.

Taking the trace of both sides of (5.3.21), one obtain

$$\frac{1}{3}(\boldsymbol{I}:\boldsymbol{\sigma})+\alpha_B p^w = n_0^s\left(\lambda_s+\frac{2}{3}\mu_s+\nu\right)\boldsymbol{I}:\boldsymbol{E}. \tag{5.4.7}$$

where α_B and ν are given by (5.3.18) and (5.3.19), respectively. In a fully drained compression test, the fluid pressure in a saturated sample is constant, i.e. $p^w = 0$. Therefore, by definition, K_D can be represented as

$$K_D = n_0^s\left(\lambda_s+\frac{2}{3}\mu_s+\nu\right) \tag{5.4.8}$$

For a fully undrained compression of a saturated sample, using (5.1.7), (5.1.8), (5.1.17), (5.2.8), (5.2.9), and (5.4.3), one can prove that

$$p^w = -\pi(\boldsymbol{I}:\boldsymbol{E}), \tag{5.4.9}$$

where

$$\pi = \frac{\left(K_s + n_0^f n_0^s \Theta_n^w - n_0^s \lambda_{pe}^s\right)K_w}{n_0^f K_w + n_0 K_s + n_0^f n_0^s \Theta_n^w} \tag{5.4.10}$$

By using (5.4.9), p^w is eliminated from (5.4.7). It follows that

$$\frac{1}{3}(\boldsymbol{I}:\boldsymbol{\sigma}) = (K_D + \pi\alpha_B)(\boldsymbol{I}:\boldsymbol{E}) \tag{5.4.11}$$

where (5.4.8) has been used. By definition, the undrained bulk modulus of the saturated porous material is now represented by

$$K_u = K_D + \pi\alpha_B \tag{5.4.12}$$

The Skempton coefficient B can be derived through establishing the relationship between the mean stress and the pore water pressure. Using (5.4.9) and (5.4.11), one obtain

$$-\frac{1}{3}(\boldsymbol{I}:\boldsymbol{\sigma})=\left(\alpha_B+\frac{K_D}{\pi}\right)p^W \tag{5.4.13}$$

Therefore, the pore pressure coefficient is

$$B=\left(\alpha_B+\frac{K_D}{\pi}\right)^{-1}=\frac{\pi}{K_T} \tag{5.4.14}$$

or

$$\pi = BK_T \tag{5.4.15}$$

Inserting (5.4.15) into (5.4.12), we obtain an expression for Biot's coefficient as

$$\alpha_B=\frac{1}{B}\left(1-\frac{K_D}{K_T}\right) \tag{5.4.16}$$

Given K_D, K_T, and B, parameters π and α_B are obtained by using (5.4.15) and (5.4.16), respectively. Now, (5.3.18), (5.3.19), (5.4.8) and (5.4.10) can be solved simultaneously to obtain $\lambda^S_{\rho e}$, λ_S, and Θ^W_n. It must be pointed out that, unlike $\lambda^S_{\rho e}$ and λ_S, coefficients Θ^W_n are generally dependent on the fluid contents for the multiphase porous media. Therefore, $\lambda^W_{\rho n}$ and Θ^W_n together with $\lambda^N_{\rho n}$ and Θ^N_n must be determined through the phenomenological properties obtained by the tests of the samples with the specified degree of saturation. In the following, it is assumed that $\lambda^W_{\rho n}=0$ and $\lambda^N_{\rho n}=0$.

The first phenomenological parameter to consider is the *specific saturation capacity* Γ_T (as shown in Fig. 5.1), which is the inverse of the slope of the relationship between

the matric suction ($p^{N} - p^{W}$) and the specific moisture content (n^{ϕ}). In the experiments to determine such a relationship, the volume of the sample is usually kept constant. It follows from (5.1.17) that

$$p^{N} - p^{W} = n_0^{N} \Theta_n^{N} n^{N} - n_0^{W} \Theta_n^{W} n^{W}, \tag{5.4.17}$$

where use has been made of $\lambda_{pn}^{\beta} = 0$ and $\theta = 0$. Since the volume of the specimen is constant, $n^{W} + n^{N} = n \approx 0$. Consequently, (5.4.17) becomes

$$p^{N} - p^{W} = -\left(n_0^{N} \Theta_n^{N} + n_0^{W} \Theta_n^{W}\right) n^{W} \tag{5.4.18}$$

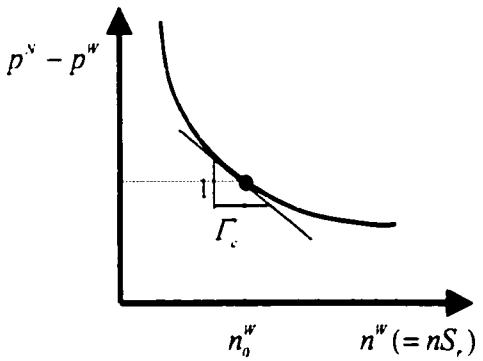

Figure 5.1 Evaluation of specific saturation capacity

By definition, the specific saturation capacity Γ_c is

$$\Gamma_c = -\left(n_0^{N} \Theta_n^{N} + n_0^{W} \Theta_n^{W}\right)^{-1} \tag{5.4.19}$$

Similar to those used for the saturated porous media, the other empirical parameters used to determine the material constants of the unsaturated porous media include various bulk moduli obtained under various controlled drained conditions. These bulk moduli are

the drained and undrained bulk moduli as well as the bulk moduli obtained by the tests under mixed drained conditions. In a test with mixed drained conditions, the pressure of one fluid is kept constant (fully drained) and the drainage of the other fluid is completely prevented. It must be pointed out that the fluid diffusion in a multiphase system is generally much slower than the deformation of the solid skeleton. It is therefore difficult, though possible, to perform the experiments as mentioned above in laboratories. In practice, some justifiable assumptions, which depend on the problems of concerns, may be introduced to simplify the theoretical and experimental procedures.

In the following, it is assumed that the assumptions made in (5.3.9) and (5.3.10) are valid. Taking the trace of both sides of (5.3.13) and using (5.3.12), we get

$$p_{net} - \chi_W S_M = n_0^S \left[\lambda_S + \frac{2}{3}\mu_S - \frac{\left(\lambda_{\rho\varepsilon}^S\right)^2}{K_S} + \frac{n_0^W n_0^N \Theta_n^W \Theta_n^N}{n_0^N \Theta_n^N + n_0^W \Theta_n^W} \right] (\boldsymbol{I} : \boldsymbol{E}), \qquad (5.4.20)$$

where p_{net} and S_M are the mean net stress and the matric suction, respectively, and defined by

$$p_{net} = \frac{1}{3}\boldsymbol{I} : \boldsymbol{\sigma} + p^N, \qquad (5.4.21)$$

and

$$S_M = p^N - p^W \qquad (5.4.22)$$

(5.4.20) can be cast into

$$-\boldsymbol{I} : \boldsymbol{E} = \frac{-p_{net}}{K_M} + \frac{S_M}{H}, \qquad (5.4.23)$$

where K_M is the constant-suction bulk modulus, and H is the bulk modulus associated matric suction. Both K_M and H can be experimentally determined. In fact, experiments

show that (5.4.23) can be used to evaluate the elastic volumetric strain for unsaturated soils (Fredulund and Rahardjo, 1993: Ch. 12). Comparing (5.4.23) with (5.4.20), one obtains

$$K_{sf} = n_0^S \left[\lambda_S + \frac{2}{3}\mu_S - \frac{\left(\lambda_{\rho e}^S\right)^2}{K_S} + \frac{n_0^W n_0^N \Theta_n^W \Theta_n^N}{n_0^N \Theta_n^N + n_0^W \Theta_n^W} \right], \tag{5.4.24}$$

and

$$\chi_W = H^{-1} K_{sf} \tag{5.4.25}$$

(5.4.25) can be used to experimentally determine the effective stress parameter χ_W. With K_{sf} and H given, (5.4.19) and (5.3.11) now can be solved for Θ_n^W and Θ_n^N.

It is worthy to note that (5.4.24) also gives a relationship between the material constants and phenomenological parameters. However, the last term in the bracket of (5.4.24) is generally much smaller than the sum of the first three terms so that the value of K_{sf} may not be explicitly dependent on Θ_n^W and Θ_n^N in some cases. Hence, use of (5.4.24) in determining Θ_n^W and Θ_n^N should be avoided.

Thus far, the coefficients yet to be evaluated are the thermal parameters $\lambda_{\theta e}^S$ and $\lambda_{\theta n}^\beta$ ($\beta = W, N$). Coefficient $\lambda_{\theta e}^S$ represents the coupling between temperature and the deformation of the solid skeleton, and $\lambda_{\theta n}^\beta$ accounts for the coupling effects between temperature and the volume fractions of fluids. In the following, it is assumed that $\lambda_{\theta n}^\beta = 0$. Note that (5.4.20) is derived for the isothermal conditions. Under nonisothermal conditions, (5.4.20) will become

$$p_{net} - \chi_w S_{sl} = K_{sl}(\boldsymbol{I} : \boldsymbol{E}) + n_0^s \left(\frac{\lambda_{\rho e}^s}{K_s} \lambda_{\rho\theta}^s - \lambda_{\theta e}^s \right) \theta \,. \qquad (5.4.26)$$

The coefficient of the last term in the RHS of (5.4.26) can be decomposed into

$$n_0^s \left(\frac{\lambda_{\rho e}^s}{K_s} \lambda_{\rho\theta}^s - \lambda_{\theta e}^s \right) = 3K_{sl}\alpha_{sl}^{\theta} \qquad (5.4.27)$$

It is clear that α_{sl}^{θ} is the thermal dilatation coefficient that can be measured by exposing the material sample to varying temperature while keeping constant suction and zero net mean stress. Solving (5.4.27), one obtain

$$\lambda_{\theta e}^s = \frac{\lambda_{\rho e}^s}{K_s} \lambda_{\rho\theta}^s - \frac{K_{sl}\alpha_{sl}^{\theta}}{n_0^s} \qquad (5.4.28)$$

In this section, sufficient information is provided to determine the material coefficients of the proposed model. Note that the procedure used to evaluate material constants is not unique. In practice, a few justifiable assumptions may drastically simplify the experimental procedure. For instance, as far as unsaturated soils are concerned, only shear modulus G, specific saturation capacity Γ_s, and bulk moduli H and K_{sl} (see (5.4.23)) need to be determined in the laboratory. Given these phenomenological parameters, all the elastic parameters in the proposed model can be obtained by using the relationships developed above. As a particular example, the material constants of the Massilon sandstone will be evaluated in the next chapter.

Chapter 6 ACOUSTICAL WAVES IN POROUS MEDIA

As an application and validation of the linear model previously developed, this chapter is devoted to analyzing the propagation conditions and characteristics of acoustical waves in the porous media saturated by two immiscible fluids. Simulation of acoustical waves in porous media is of great interest in geophysics, petroleum engineering, chemical engineering, and geotechnical engineering. For example, acoustic waves can be used to improve oil recovery processes (Beresnev and Johnson, 1994); a detailed analysis of acoustic waves in porous media also finds its application in interpreting dynamic soil tests (Gajo and Mongiovi, 1994).

In the following, our discussions will be confined mainly to the relatively low frequency range ($< 10^4$ Hz). In a model of porous media, two sets of relationships are frequency-dependent, i.e. the flow equations and closure equations. It must be noted that in the linear model developed in the previous chapter, the flow diffusion is assumed to be linear or, equivalently, the model only considers laminar flow. Biot (1956a&b) had shown that the laminar flow assumption breaks down if the frequency exceeds a certain limit. In the closure equation (5.1.17), the viscous terms associated with the capillary relaxation are omitted. Such an assumption applies only in the low frequency range.

6.1 Weak Discontinuity Waves

Weak discontinuity is defined such that, through a material surface within the domain of concern, the acceleration field is subjected to a jump, but the displacement and velocity fields are continuous over the whole *open* domain. As will be shown later, such a discontinuity surface may propagate through the porous media in the form of purely elastic waves without attenuation.

Suppose that a field φ is subjected to a jump at some points in the domain of concerns Ω, and these points form a continuous, differentiable surface $\varsigma_n(t)$ (i.e. an orientable 2-dimensional differentiable manifold), represented by $\psi(\boldsymbol{x},t)=0,\ \boldsymbol{x}\in\Omega$ (Fig. 6.1). Taking the material derivative of $\psi(\boldsymbol{x},t)$ with respect to the motion of the solid skeleton yields

$$\frac{D^s}{Dt}\psi(\boldsymbol{x},t)=\frac{\partial}{\partial t}\psi(\boldsymbol{x},t)+\boldsymbol{v}^s\cdot\nabla\psi(\boldsymbol{x},t)=0. \qquad (6.1.1)$$

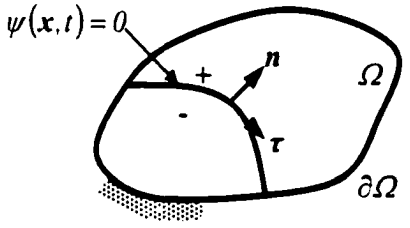

Figure 6.1 Discontinuity surface of acceleration

Let $\boldsymbol{n}$ be the unit vector normal to $\psi(\boldsymbol{x},t)$ and $\boldsymbol{\tau}$ be a unit tangent vector. Then,

$$\boldsymbol{n} = \nabla\psi \Big/ |\nabla\psi|, \quad \boldsymbol{n}\cdot\boldsymbol{\tau} = 0. \tag{6.1.2}$$

If the gliding on the discontinuity surface in $\boldsymbol{\tau}$ direction is excluded, it follows from (6.1.1) and (6.1.2) that

$$U = \boldsymbol{v}^{s}\cdot\boldsymbol{n} = \frac{\partial\psi}{\partial t}\Big/|\nabla\psi|. \tag{6.1.3}$$

where U is the only nontrial component of the propagation velocity of $\varsigma_0(t)$.

From the definition of weak discontinuity, it follows that

$$[\![\boldsymbol{u}^{\alpha}]\!] = \boldsymbol{0}, \quad [\![\boldsymbol{v}^{\alpha}]\!] = \boldsymbol{0}. \tag{6.1.4}$$

where $\alpha = S, W, N$; $[\![\varphi]\!] = \varphi^{+} - \varphi^{-}$, φ^{+} and φ^{-} denote the values of φ on the positive and negative side of the wave front $\varsigma_0(t)$. Using (6.1.4), one obtains the following kinematical compatibility conditions (a detailed proof is presented in Appendix III).

$$\left[\!\left[\frac{\partial\boldsymbol{v}^{\alpha}}{\partial t}\right]\!\right] = -\boldsymbol{a}^{\alpha}U, \tag{6.1.5}$$

$$[\![\nabla\boldsymbol{v}^{\alpha}]\!] = \boldsymbol{a}^{\alpha}\otimes\boldsymbol{n}, \tag{6.1.6}$$

and

$$[\![\nabla\nabla\boldsymbol{u}^{\alpha}]\!] = -U^{-1}\boldsymbol{a}^{\alpha}\otimes\boldsymbol{n}\otimes\boldsymbol{n}, \tag{6.1.7}$$

where $\boldsymbol{a}^{\alpha}$ represents the normal jump of the spatial gradient of the velocity $\boldsymbol{v}^{\alpha}$ through $\varsigma_0(t)$; $\otimes$ denotes the tensor product, e.g., $(\boldsymbol{m}\otimes\boldsymbol{n})_{ij} = m_i n_j$.

In the following, our attention is limited to the isothermal condition and all the temperature terms will be dropped. Applying (6.1.4)-(6.1.7) to (5.2.10)-(5.2.12), it immediately follows that

$$n_0^S \rho_0^S U^2 \boldsymbol{a}^S = M_{SS}\boldsymbol{a}^S \cdot \boldsymbol{nn} + 2n_0^S \mu_S \boldsymbol{a}^S + M_{SW}\boldsymbol{a}^W \cdot \boldsymbol{nn} + M_{SN}\boldsymbol{a}^N \cdot \boldsymbol{nn}, \qquad (6.1.8)$$

$$n_0^W \rho_0^W U^2 \boldsymbol{a}^W = M_{SW}\boldsymbol{a}^S \cdot \boldsymbol{nn} + M_{WW}\boldsymbol{a}^W \cdot \boldsymbol{nn} + M_{WN}\boldsymbol{a}^N \cdot \boldsymbol{nn}, \qquad (6.1.9)$$

and

$$n_0^N \rho_0^N U^2 \boldsymbol{a}^N = M_{SN}\boldsymbol{a}^S \cdot \boldsymbol{nn} + M_{WN}\boldsymbol{a}^W \cdot \boldsymbol{nn} + M_{NN}\boldsymbol{a}^N \cdot \boldsymbol{nn}, \qquad (6.1.10)$$

Since $\boldsymbol{\tau} \cdot \boldsymbol{n} = 0$, it follows from (6.1.9) and (6.1.10) that $\boldsymbol{a}^W \cdot \boldsymbol{\tau} = 0$ and $\boldsymbol{a}^N \cdot \boldsymbol{\tau} = 0$. That is, $\boldsymbol{a}^\beta$ ($\beta = W, N$) have only one component, which is parallel to the unit normal vector $\boldsymbol{n}$. This result is expected, since the inviscid fluids cannot resist any shear displacement. Let $\boldsymbol{a}^S = a_n^S \boldsymbol{n} + a_\tau^S \boldsymbol{\tau}$ and $\boldsymbol{a}^\beta = a^\beta \boldsymbol{n}$ ($\beta = W, N$). Inserting these two equation into (6.1.8)-(6.1.10) yields

$$n_0^S \rho_0^S U^2 a_\tau^S = n_0^S \mu_S a_\tau^S, \qquad (6.1.11)$$

$$n_0^S \rho_0^S U^2 a_n^S = (M_{SS} + 2n_0^S \mu_S) a_n^S + M_{SW} a^W + M_{SN} a^N, \qquad (6.1.12)$$

$$n_0^W \rho_0^W U^2 a^W = M_{SW} a_n^S + M_{WW} a^W + M_{WN} a^N, \qquad (6.1.13)$$

and

$$n_0^N \rho_0^N U^2 a^N = M_{SN} a_n^S + M_{WN} a^W + M_{NN} a^N. \qquad (6.1.14)$$

Equation (6.1.11) immediately yields the speed of the only rotational wave (i.e. shear wave) in the porous media as

$$U_S^2 = \mu_S / \rho_0^S, \qquad (6.1.15)$$

and (6.1.12)-(6.1.14) now constitute an eigenvalue problem, and the corresponding characteristic equation is given by

$$\det\left(z - U^{-2}\kappa\right) = 0, \tag{6.1.16}$$

where

$$\kappa = \begin{bmatrix} M_{SS} + 2n_0^S\mu_S & M_{SW} & M_{SN} \\ M_{SW} & M_{WW} & M_{WN} \\ M_{SN} & M_{WN} & M_{SN} \end{bmatrix}, \tag{6.1.17}$$

and

$$z = diag(n_0^S\rho^S, n_0^W\rho^W, n_0^N\rho^N). \tag{6.1.18}$$

Since κ and z are positive-definite, (6.1.16) has three positive solutions for U^{-2}, implying that there exist three compressional (also called *longitudinal* or *dilatational*) waves propagating in the porous media saturated by two immiscible fluids.

It is now instructive to discuss the effect of the internal constraints on the wave propagation in porous media. Such kinds of constraints are associated with the compressibility of the individual components. Assume that a bulk phase (say, the solid phase) is incompressible, i.e. $\rho^S = 0$ (ρ^S is an incremental quantity). Using (5.1.17), (5.1.7), (5.1.8), (5.2.8), (5.2.9), and (6.1.7), we can prove that there is a constraint among $\boldsymbol{a}^\alpha$ ($\alpha = S, W, N$) independent of (6.1.12)-(6.1.14), i.e. only two of $\boldsymbol{a}^\alpha$ are independent. Therefore, as pointed out in Chapter 3, applying any internal constraint to the model at least excludes one mode of the waves.

In a finite element analysis of deformation, it is sometimes assumed for convenience that the relative acceleration of a fluid can be neglected (Zienkiewicz and

Shiomi, 1984; Li and Zienkiewicz, 1990). Under this assumption, one has $\partial \boldsymbol{v}^S/\partial t = \partial \boldsymbol{v}^W/\partial t = \partial \boldsymbol{v}^N/\partial t$, and correspondingly, $\boldsymbol{a}^S = \boldsymbol{a}^W = \boldsymbol{a}^N$. Hence, the set of field equations, i.e. (5.2.10)-(5.2.12), delivers only two body waves: a rotational wave and a compressional wave. Generally, in many slow phenomena, e.g. an earth dam under earthquake loading, the compressible waves due to the existence of the fluids, i.e. the second and third compressional waves, have little influence on the deformation of the solid skeleton. Therefore, the assumption made above usually applies in such cases.

6.2 Acoustical Waves

Existence of three compressional waves in the porous media saturated by two immiscible fluids has been shown in the last section. In reality, all these waves are not the pure waves and not carried independently by any individual component. In addition, due to the relative motion of the components, all these waves are dispersive and attenuated.

The body waves in a continuum can be categorized into two kinds, which corresponds to shear and compression, respectively. To obtain the equations of wave propagation, the shear waves are first uncoupled from the compressional waves. Let

$$\nabla \cdot \boldsymbol{u}^\alpha = \varepsilon_\alpha \quad (\alpha = S, W, N), \tag{6.2.1}$$

and

$$\nabla \times \boldsymbol{u}^\alpha = \boldsymbol{\Omega}_\alpha \quad (\alpha = S, W, N). \tag{6.2.2}$$

Applying the *divergence* operator, i.e. $\nabla \cdot ( )$, to both sides of (5.2.10)-(5.2.12) and dropping all the temperature terms, one obtains the equations of propagation for the compressional waves as follows,

$$z\ddot{\varepsilon} = \kappa\nabla^2\varepsilon + \hat{d}\dot{\varepsilon}. \tag{6.2.3}$$

where κ and z are given by (6.1.17) and (6.1.18), respectively; $\varepsilon^T = (\varepsilon_s, \varepsilon_w, \varepsilon_N)$, and

$$\hat{d} = \begin{bmatrix} \hat{\mu}^W + \hat{\mu}^N & -\hat{\mu}^W & -\hat{\mu}^N \\ -\hat{\mu}^W & \hat{\mu}^S & 0 \\ -\hat{\mu}^N & 0 & \hat{\mu}^N \end{bmatrix} \tag{6.2.4}$$

Similarly, applying the *curl* operator, i.e. $\nabla\times(\ )$, to both sides of (5.2.10)-(5.2.12), one obtains the equations of propagation for the shear waves, i.e.

$$z\ddot{\Omega} = h\nabla^2\Omega + \hat{d}\dot{\Omega}. \tag{6.2.5}$$

where $\Omega^T = (\Omega_s, \Omega_w, \Omega_N)$, and

$$h = \begin{bmatrix} n_0^s\mu_s & 0 & 0 \\ 0 & 0 & 0 \\ 0 & 0 & 0 \end{bmatrix} \tag{6.2.6}$$

Consider a harmonic pertubation wave traveling through the porous medium in the direction n. The solutions of (6.2.3) and (6.2.5) now can be represented by

$$\varepsilon = A\exp[i(\zeta n\cdot x - \omega t)], \tag{6.2.7}$$

and

$$\Omega = B\exp[i(\zeta n\cdot x - \omega t)], \tag{6.2.8}$$

where $A^T = (A_s, A_w, A_N)$; $B^T = (B_s, B_w, B_N)$; ζ is the wave number; ω is the angular frequency; $i = \sqrt{-1}$. In general, ζ is a complex number, i.e. $\zeta = \zeta_r + i\zeta_i$, where ζ_r and

ζ_r are the real and imaginary parts of ζ, respectively. ζ_i is usually called the attenuation coefficient. The phase velocity is defined as $v = \omega/\zeta_r$.

Inserting (6.2.7) into (6.2.3), one obtains after some rearrangements that

$$\left(-\omega^2 z + \zeta^2 \kappa - i\omega \hat{d}\right) A = 0 \tag{6.2.9}$$

For (6.2.9) to have nonzero solutions, it is required that

$$\det\left(-\omega^2 z + \zeta^2 \kappa - i\omega \hat{d}\right) = 0 \tag{6.2.10}$$

This equation is sometimes called the dispersion relation of the compressional waves. Given angular frequency ω, (6.2.10) can be numerically solved for ζ, and therefore the phase velocity and the attenuation coefficient can be evaluated. In general, for a given angular frequency ω, the polynomial expanded from (6.2.10) has three complex roots for $(\omega/\zeta)^2$ and the wave number ζ has six roots. However, only three of these roots physically make sense, since the amplitude of the waves must decrease with time and the imaginary part of ζ (i.e. ζ_i) is always nonnegative. Therefore, there exist three compressional waves in general, which are denoted by *P1*, *P2*, and *P3*, respectively, such that $v_{P1} > v_{P2} > v_{P3}$.

Before solving (6.2.10), however, it is instructive to examine first its character in the zero and infinite frequency limits. As $\omega \to 0$ so that $\zeta \to 0$ and ω/ζ becomes finite, it can be shown from the expansion of (6.2.10) that

$$\left(\omega/\zeta\right)^2\left[1-v_{c0}^2\left(\zeta/\omega\right)^2\right]=0. \tag{6.2.11}$$

where

$$v_{c0}^2=\frac{M_{SS}+2n_0^S\mu_S+M_{WW}+M_{SN}+2\left(M_{SW}+M_{WN}+M_{SN}\right)}{n_0^S\rho^S+n_0^W\rho^W+n_0^N\rho^N}. \tag{6.2.12}$$

(6.2.11) implies that, in this particular case, the three phase velocities become v_{c0}, 0, and 0, respectively. Physically, this situation corresponds to those wherein all the three components move together, i.e. $\hat{\mu}^W\to+\infty$ and $\hat{\mu}^N\to+\infty$. Alternatively, as $\omega\to+\infty$ such that $\zeta\to+\infty$ and ω/ζ remains finite, (6.2.10) degenerate to (6.1.16) with $U^2=(\omega/\zeta)^2$. Therefore, the infinite frequency limit is equivalent to the case with no viscous coupling, that is, $\hat{\mu}^W\to 0$ and $\hat{\mu}^N\to 0$. The corresponding waves are usually called the purely elastic waves (Biot, 1956a).

Similarly, inserting (6.2.8) into (6.2.5) yields

$$\left(-\omega^2\boldsymbol{z}+\zeta^2\boldsymbol{h}-i\omega\hat{\boldsymbol{d}}\right)\boldsymbol{B}=\boldsymbol{0}. \tag{6.2.13}$$

and the corresponding dispersion relation of the shear waves is

$$\det\left(-\omega^2\boldsymbol{z}+\zeta^2\boldsymbol{h}-i\omega\hat{\boldsymbol{d}}\right)=0. \tag{6.2.14}$$

For a given frequency ω, (6.2.14) has only one nonvanishing solution for $(\omega/\zeta)^2$, i.e. there is only one shear wave (called the *S*-wave). As $\omega\to 0$ and ω/ζ becomes finite,

$$v_s^2=v_{s0}^2=\frac{n_0^S\mu_S}{n_0^S\rho^S+n_0^W\rho^W+n_0^N\rho^N}. \tag{6.2.15}$$

v_{s0} given by (6.2.15) is the velocity of the shear wave when all the three components move together. As $\omega \to +\infty$ and ω/ζ remains finite, equation (6.2.14) degenerate to $n_0^s \rho^s (\omega/\zeta)^2 = n_0^s \mu_s$. Clearly, this case corresponds to those wherein viscous coupling vanishes. The velocity of the shear wave is now given by (6.1.15).

From the discussions given above, it is clear that in a low-frequency range there are only one compressional wave and the shear wave traveling through the porous medium, and the strong viscous coupling leads the three compressional waves to coalesce into a single front. As mentioned in the end of the last section, in many finite element analyses of geotechnical structures subjected to dynamic loading in the lower frequency range, it is generally acceptable to drop the relative acceleration terms of the fluids. The only consequence of dropping the relative velocity of the fluids is the exclusion of the effect of the second and the third compressional waves on the deformation.

6.3 Evaluation of Material Constants

This section further concerns the material constants of the linear model presented in Chapter 5. To this end, Massilon sandstone will be introduced as an example. The material and acoustical properties of Massilon sandstone are well documented in the literature (see, Murphy, 1982; Murphy, 1984; Bourbié et al. 1987: Ch. 5), and the material parameters are summarized in Table 6.1. In the following, it is assumed that the coupling between the mass density and the volume fraction of a fluid is negligible. This assumption is reasonable for geomaterials as discussed in Chapter 5. Therefore, one has

$\lambda_{pm}^{W} = \lambda_{pm}^{N} = 0.0$. Under the isothermal condition, the following parameters remain to specify: λ_S, μ_S, λ_{pc}^{S}, Θ_n^W, Θ_n^N, $\hat{\mu}^W$, and $\hat{\mu}^N$.

Table 6.1 Material Parameters of Massillon Sandstone Saturated by Water and Air

Material Parameters	Symbol	Value	Unit
Porosity	n	0.23	-
Density of solid grain	ρ^S	2650.0	kg/m^3
Density of water	ρ^W	997.0	kg/m^3
Density of gas	ρ^N	1.10	kg/m^3
Bulk modulus of solid grain	K_S	3.5×10^{7}	kPa
Bulk modulus of water	K_W	2.25×10^{6}	kPa
Bulk modulus of air	K_N	0.11×10^{3}	kPa
Viscosity of water	η_W	1.0×10^{-3}	$Pa\,s$
Viscosity of air	η_N	1.8×10^{-5}	$Pa\,s$
Intrinsic permeability	k	2.5×10^{-12}	m^2
Bulk modulus of the matrix	K	1.02×10^{6}	kPa
Shear modulus of the matrix	G	1.44×10^{6}	kPa

The last four parameters are generally dependent on the degree of saturation. Θ_n^W and Θ_n^N can be obtained using (5.4.19), (5.4.25), and (5.3.11). For Massilon sandstone, however, the explicit relationship between modulus H and the degree of saturation S_r is not available. An alternative equation must be introduced. Experiments show that

although there is some discrepancy χ_W is always located in the vicinity of S_r for many types of porous materials (Donald, 1961; Blight, 1961). Therefore, in the following it is assumed as a first approximation that $\chi_W = S_r$. With (5.4.19), and (5.3.11), one obtains

$$n_0^S \Theta_n^N = \frac{S_r - n_0^W}{n_0^S \Gamma_c}. \tag{6.3.1}$$

and

$$n_0^W \Theta_n^W = \Gamma_c^{-1} - n_0^N \Theta_n^N. \tag{6.3.2}$$

The specific saturation capacity Γ_c is calculated through the moisture retention curve, i.e. the relationship between the matric suction (S_{ψ}) and the degree of saturation. Here, Brooks and Corey (1964) expressions are employed, i.e.

$$S_{\psi}(S_r) = p_d S_e^{-1/\lambda}. \tag{6.3.3}$$

where p_d is the air-entry value pressure, λ a positive constant to be specified, and S_e the effective degree of saturation given by

$$S_e = \begin{cases} 0.0 & S_r \le S_{rW} \\ \dfrac{S_r - S_{rW}}{S_{rN} - S_{rW}} & S_{rW} < S_r < S_{rN} \\ 1.0 & S_r \ge S_{rN} \end{cases}$$

where S_{rW} and S_{rN} are the residual and air-entry degree of saturation, respectively.

Coefficients $\hat{\mu}^{\beta}$ $(\beta = W, N)$ can be related to the permeability by

$$\hat{\mu}^{\beta} = \frac{(n^{\beta})\eta_{\beta}}{k k_r^{\beta}(n^W)}. \tag{6.3.4}$$

where k is the intrinsic permeability of the porous medium; η_β and k_r^β represent the shear viscosity and relative permeability of β-fluid, respectively. According to Brooks and Corey (1964), the relative permeabilities for the liquid and the air are given by

$$k_r^W = S_e^{(2+3\lambda)/\lambda}, \tag{6.3.5}$$

and

$$k_r^N = (1 - S_e)^2 \left(1 - S_e^{(2+\lambda)/\lambda}\right), \tag{6.3.6}$$

respectively. Since no data for the moisture retention and the permeability of Massilon sandstone are available, the following values of parameters are chosen in the analysis: $p_d = 50$ kPa, $\lambda = 1.5$, $S_{rW} = 0.1$, $S_{rN} = 0.85 \sim 1.0$. The moisture retention curve of the sandstone and the relative permeability curves of the liquid and air are shown in Fig. 6.2a and b, respectively.

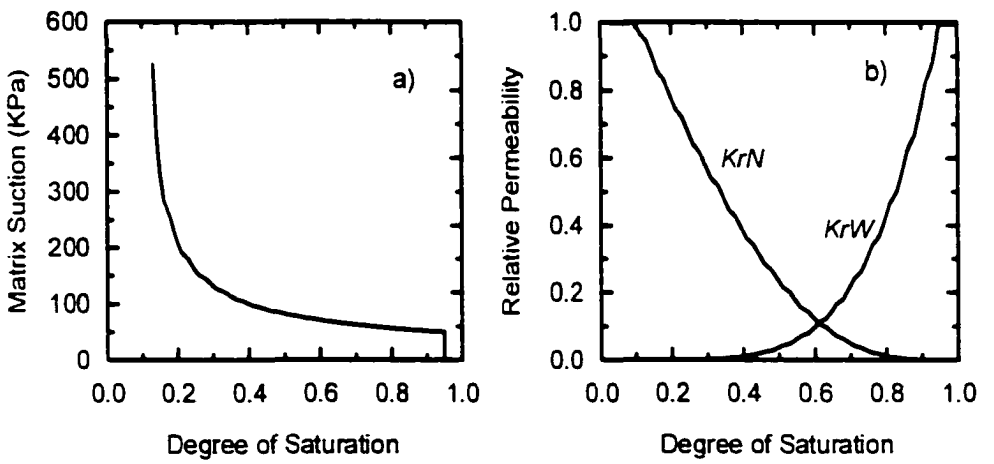

Figure 6.2 a) Moisture retention curves for Massilon sandstone; b) Relation between relative permeability and degree of saturation. ($Kr\beta = k_r^\beta$)

To evaluate the elastic constants of the solid matrix, (5.4.24) can be employed. Since the last term in (5.4.24) is $O(max(\Theta_n^w, \Theta_n^s))$, which is several orders less than the bulk modulus of the matrix for geomaterials. It is therefore reasonable to set

$$K = K_M = n_0^S \left[\lambda_S + \frac{2}{3}\mu_S - \frac{(\lambda_{pe}^S)^2}{K_S} \right]. \qquad (6.3.7)$$

where K is given in Table 6.1, and μ_s directly obtained through (5.4.6) as 1.87×10^6 kPa. If λ_{pe}^S is known, λ_S can be computed through (6.3.7). To evaluate λ_{pe}^S, however, it is necessary to introduce other phenomenological parameters, such as the pore pressure coefficient B and the drained bulk modulus of the matrix K_D, which are unfortunately lacking for Massilon sandstone. On the other hand, parametric study shows that *for wave propagation problems* no significant change in the results can be observed with λ_{pe}^S varying from $0 \sim 1 \times 10^7$ kPa provided that λ_S is calculated through (6.3.7). This can be easily understood from the fact that all the elements in the matrix κ of (6.2.10) are influenced very slightly by the choice of λ_{pe}^S, for instance, $M_{SS} \equiv K + 4/3\, n_0^S \mu_S$, which is only influenced by K and μ_S. Correspondingly, from (5.3.18), the Biot coefficient α_B may be varied from *1.0* down to *0.56* with varying λ_{pe}^S. Such a range of α_B covers those values that most kinds of geomaterials may have. Hence, we simply choose $\lambda_{pe}^S = 1.0 \times 10^7$ kPa or correspondingly $\alpha_B = 0.78$, and from (6.3.7) $\lambda_S = 2.935 \times 10^6$ kPa. Thus far, all the material parameters are evaluated, and polynomial equation (6.2.10) and (6.2.14) can therefore be solved numerically.

6.4 Analysis of Numerical Results

In the following, based on the solutions to (6.2.10) and (6.2.14), the behavior of the acoustical waves in the sandstone saturated by water and air are discussed in details. From these discussions, some general acoustical behavior of the porous media saturated by two immiscible fluids will be deduced. In the examples presented in this section, S_w is chosen as *95%*.

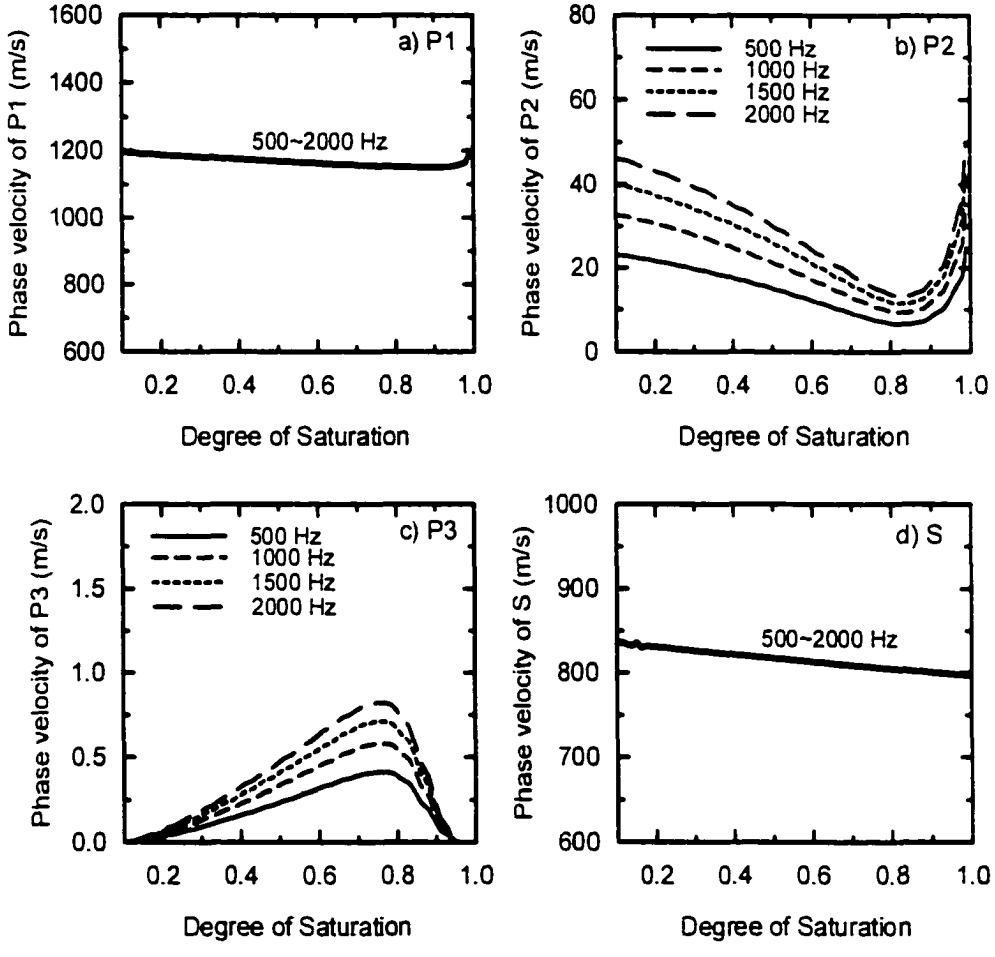

Figure 6.3 Influence of the degree of saturation on the velocities: a) *P1*; b) *P2*; c) *P3*; d) *S*

Figure 6.3 illustrates the influence of the degree of saturation on the velocities of the various types of waves for four different frequencies, i.e. *500*, *1000*, *1500*, and *2000* Hz. In Fig. 6.3a, it is shown that as the degree of saturation increases the velocity of the first compressional wave *P1* decrease slightly. When $S_r > 95\%$, v_{p1} rapidly increases with S_r. Two mechanisms may be used to explain this observation: on the one hand, v_{p1} decreases with increase in the density of the mixture; on the other hand, v_{p1} increases with decrease in the compressibility of the mixture. Since the air is much lighter and more compressible than the water, in low saturation range, the decrease in v_{p1} due to the water replacing the air in the pores cannot be compensated by the increase in v_{p1} due to the decrease in the compressibility when S_r increases. In higher saturation range, however, the increase in v_{p1} due to the decrease in compressibility much overweighs the decrease in v_{p1} due to the increase of the density of the matrix. Fig. 6.3a also shows that for all the four frequencies no significant differences in the corresponding velocity curves can be observed.

Fig. 6.3b shows that similar to v_{p1} the velocity of the second compressional wave v_{p2} decreases with the degree of saturation increasing up to *85%* and then it increase rapidly when the porous material approaches the fully saturated condition. It is also seen that within the frequency range *500~2000* Hz the *P2* of higher frequency has higher velocity. As shown in Fig. 6.3c, unlike v_{p1} and v_{p2}, the velocity of *P3* increases with S_r increasing up to about *75%* and then decreases. When $S_r < S_{rw}$ or $S_r > S_{rw}$, v_{p3} vanishes

and *P3* disappears. This implies that the third compressional wave coexists with the capillary pressures, and whenever the matric suction vanishes *P3* disappears. Similar to v_{p2}, the *P3* of higher frequency also has higher velocity. Fig. 6.3d shows that the velocity of the shear wave slightly decreases with S_r increasing. The reason for this is that the decrease in v_S due to the increase of the density of the matrix is always dominant with the water replacing the air in the pore space. It can also be seen from Fig. 6.3d that within the frequency range *500~2000* Hz, the effect of frequency on the shear wave is trivial.

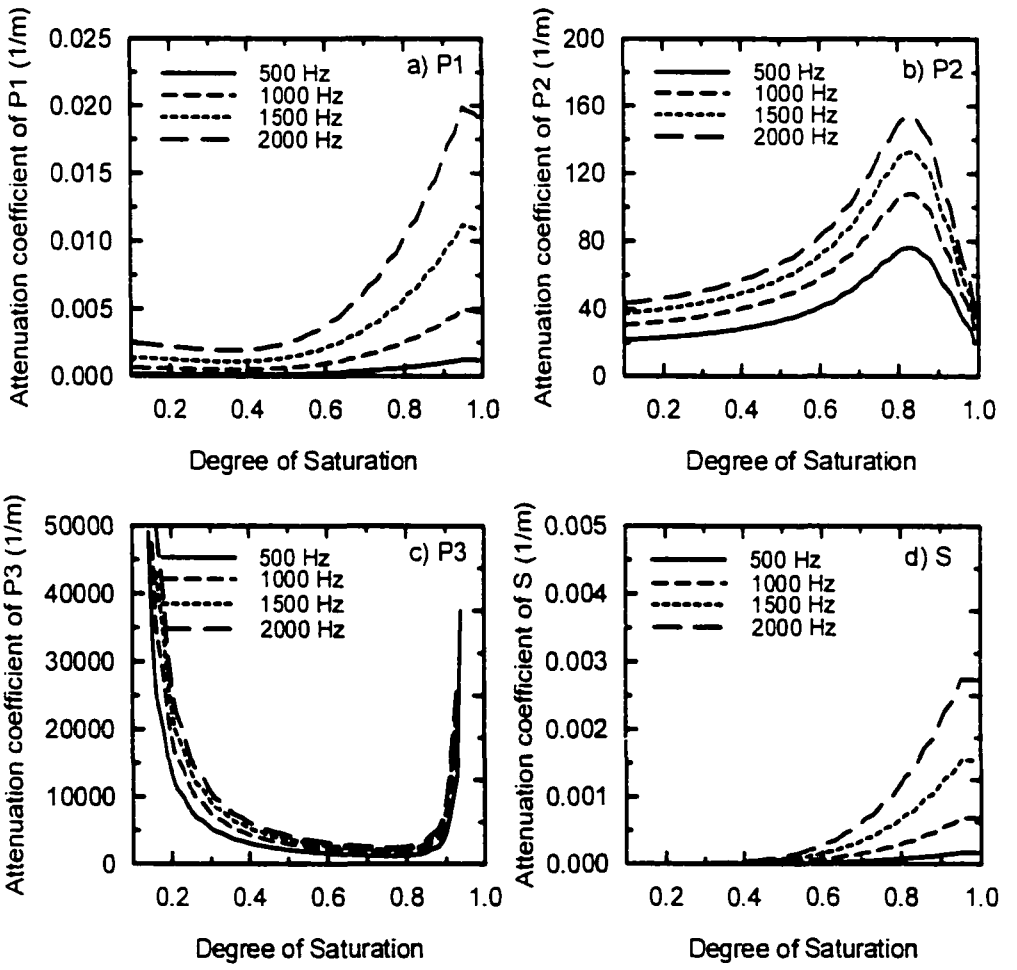

Figure 6.4 Influence of the degree of saturation on attenuation: a) *P1*; b) *P2*; c) *P3*; d) *S*

Fig. 6.4 illustrates the effects of the degree of saturation and the frequency on the attenuation coefficient (i.e. ζ_i) for the four different waves. As expected, in all the cases, the waves of higher frequency always attenuate more rapidly. When $S_r < 50\%$, slight attenuation is observed for the *P1* of frequency more than *1000* Hz (Fig. 6.4a). For the *S* wave (Fig. 6.4d) and *P1* wave of frequency lower than *500* Hz, the attenuation is trivial. When $S_r > 50\%$, *S* and *P1* are attenuated rapidly with the increase in saturation and the attenuation reaches a peak value at around $S_r = S_{rN}$, where the air phase is trapped in the water. Existence of peak values in the attenuation curves of P1 and S waves was also observed by Tuncay and Corapcioglu (1996), whose analysis was based on a linear model developed by using a averaging procedure (Tuncay and Corapcioglu, 1997). In Tuncay and Corapcioglu's work, moisture retention curve is represented by Van Genuchten's relationship (Van Genuchten, 1980), which is smooth for $S_{rw} < S_r \leq S_{rN}$.

It is noted from Fig. 6.2b that the relative permeability of the water become significant only when $S_r > 50\ \%$. Therefore, it is quite clear that the attenuation of *P1* or *S* is dominated by the (local) fluid diffusion. The same conclusion has been drawn by Yin et al (1992) in interpreting experimental data. Fig. 6.4b shows that at $S_r \cong 82\%$ the attenuation of *P2* reaches its peak and whenever one of the fluid phases disconnects it is minimal. In contrast, as shown in Fig. 6.4c, *P3* attenuates strongly when one of the fluid phases tends to disconnect and the attenuation of *P3* has smaller values in between S_{rw} and S_{rN}. This again implies that there exists an affinity between *P3* and the capillary phenomenon.

The effects of frequency on the waves have been briefly discussed above for the frequency range from *500~2000* Hz. Figures 6.5 and 6.6 illustrate these effects in a much wider frequency spectrum. It is worthy to be noted that because of the frequency-dependent behavior of acoustical waves the cases of frequency more than 10^5 Hz are more mathematical than physical in nature. Furthermore, in the higher frequency range where wavelength may be less than the size of pores, the continuum assumption breaks down. Hence, the following discussion is limited to the frequency range less than 10^5 Hz.

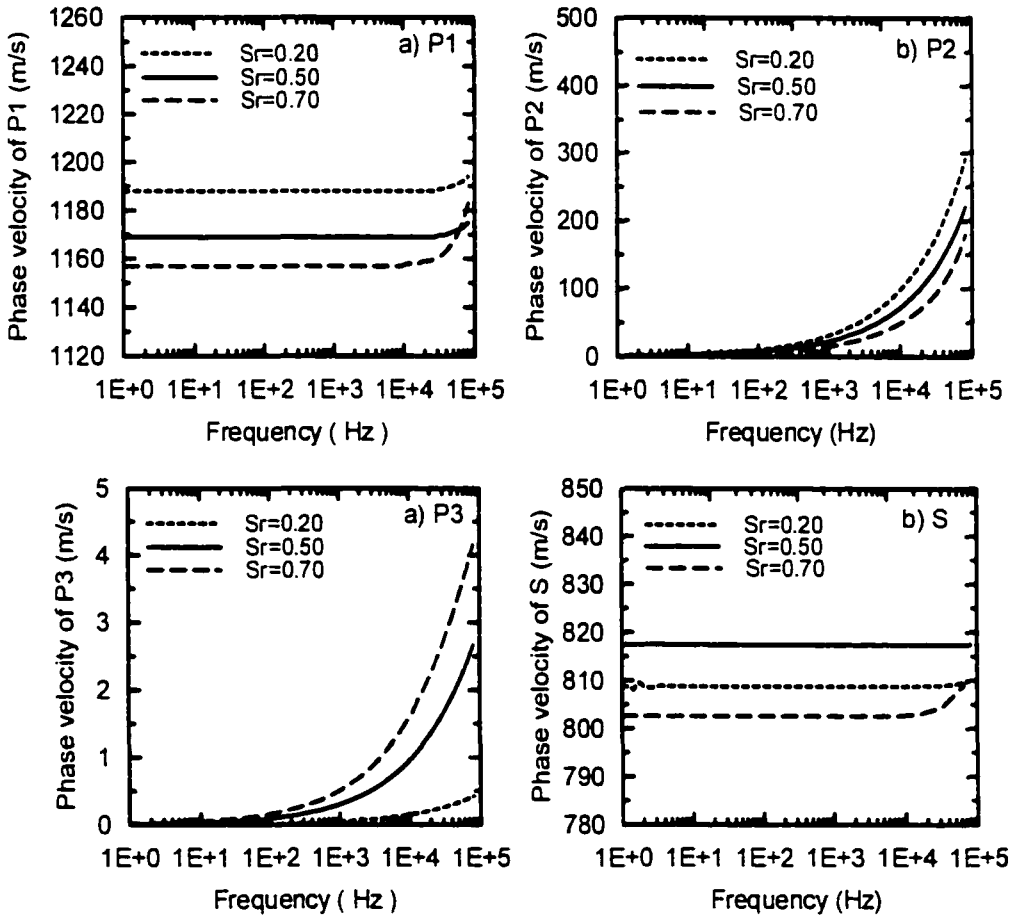

Figure 6.5 Influence of frequency on the phase velocities: a) *P1*; b) *P2*; c) *P3*; d) *S*

In the acoustical range ($< 10^4$ Hz.), the current example shows that the effects of frequency on the phase velocities of *P1* and *S* are small. In ultrasonic range ($> 10^4$ Hz.), however, this may not be the case. As shown in Fig. 6.5a, the velocity of *P1* can be greatly influenced by the frequency in ultrasonic range. Unlike *P1* and *S*, the effects of frequency on the second and the third compressional waves are significant, as shown in Fig. 6.5b&c. For these two waves, the phase velocity increases with the frequency increasing in the range of $0 \sim 10^5$ Hz. As expected, for all the waves, the attenuation increases with the increase in the frequency.

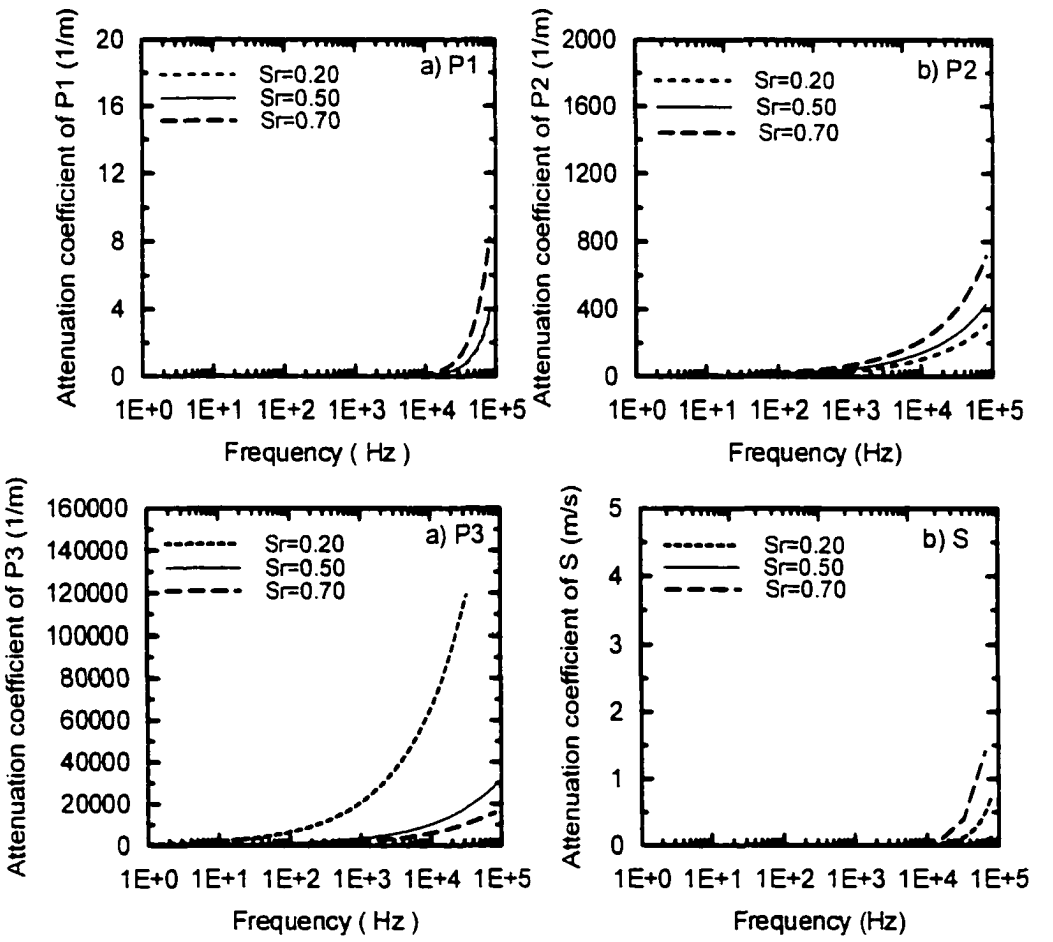

Figure 6.6 Influence of frequency on the attenuation coefficients: a) *P1*; b) *P2*; c) *P3*; d) *S*

From the above discussions, it is clear that unlike *P1* wave and *S* wave *P2* and *P3* are very sensitive to the frequency and they attenuate rapidly. Therefore, *P2* and *P3* waves are not true waves and they are associated with some kind of dissipation. Among all the waves, the shear wave has lowest attenuation. The first compressional wave *P1* is the fastest and attenuates more slowly; the second compressional wave *P2* is slower than *P1* but faster than *P3*. *P2* is sometimes called Biot's wave and it has a higher attenuation coefficient than *P1*. The slowest wave is the third compressional wave *P3*, and furthermore *P3* is most strongly attenuated. In reality, it could be extremely difficult, if not impossible, to observe *P3*. Even the second compressional wave *P2* can not be routinely observed in the laboratory. In fact, the first formal observation of *P2* was not reported until 1980 (Plona, 1980; Berryman, 1980), almost 25 years after Biot presented his theory (Biot, 1956a). It is noted that the elusive nature of *P2* and *P3* does not mean that they are not important. Since *P2* and *P3* may consume significant energy during numerous reflections and transmissions on the interfaces (Geertsma and Smit, 1961), it is important to understand the characters of these two waves so that the acoustical behavior of porous media can be properly described.

6.5 Comparison to Experimental Results

In this section, the numerical results presented above will be compared to the experimental data on the acoustical waves in the Massilon sandstone saturated by water and air (Murphy, 1982 & 1984). The material properties are the same as those given in Table 6.1 and discussed in Section 3, except that S_{wr} is chosen as 0.85. As will be seen

later, for $S_{rN} = 0.85 \sim 1.0$, the effects of S_{rN} on the phase velocities of S and P1 waves are trivial. However, the choice of S_{rN} will significantly influence the attenuation.

The calculated and measured velocities of the first compressional wave *P1* and the shear wave *S* are shown in Fig.6.7, from which it can be seen that the agreements between the theoretical and experimental results are favorable. As the model predicted, the velocities of *P1* and *S* slightly decrease with the degree of saturation increasing. For *P1*, the experiment shows that close to the fully saturated conditions the phase velocity increases rapidly. This feature is properly captured in the predicted results.

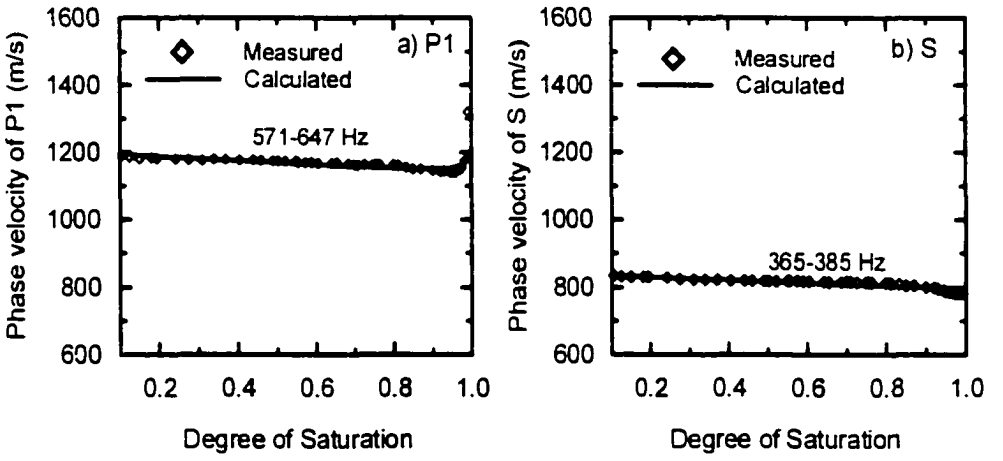

Figure 6.7 Comparison of calculated and measured phase velocities of P1 wave and S wave (Experimental data after Murphy (1982))

The calculated and measured results for the attenuation of waves are presented in Fig. 6.8. The attenuation is now represented by a dimensionless quantity Q^{-1}, i.e. specific attenuation, defined by

$$1/Q = 2\pi|\zeta_i|/|\zeta_r|. \qquad (6.5.1)$$

where ζ_r and ζ_i are the real and imaginary parts, respectively, of the wave number. Physically, the specific attenuation represents the energy loss per cycle. Although the dissipative mechanism of waves remains unclear, many factors are believed to have contributions to the energy loss. Such factors include intergranular friction, breakage of chemical bondage, capillary force, fluid/solid inertial coupling, various relaxation processes, local fluid diffusion, and so on. On the other hand, the theoretical model used in the analysis is a linear elastic model so that it can only account for the attenuation due to the local diffusion. Therefore, it seemingly does not make sense to compare the theoretical results directly with the measured data.

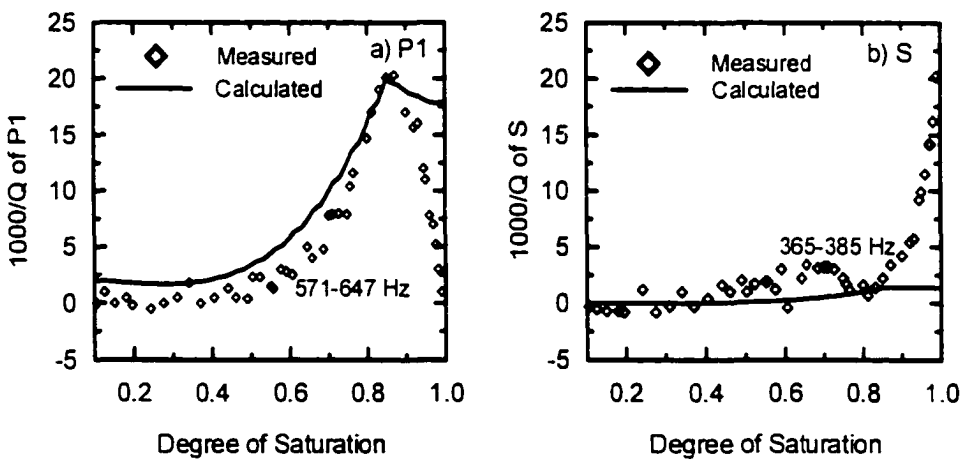

Figure 6.8 Comparisons of calculated and measured attenuation of P1 wave and S wave (Experimental data after Murphy (1982))

By extensively analyzing the experimental data, Yin et al. (1992) proposed that the measured attenuation of waves may be viewed as the superposition of three portions: the effects of open pore boundary Q_{open}^{-1}, the local fluid diffusion Q_{local}^{-1}, and the viscoelastic frame deformation Q_{frame}^{-1}. The last one is independent of the degree of saturation. Therefore, under a certain experimental condition, the attenuation due to diffusion may be obtained as $Q_{local}^{-1} \equiv Q^{-1} - Q_{frame}^{-1}$. Using this method, we redrew Murphy (1982)'s data in Fig. 6.8. It can be seen that the theoretical predictions are reasonably good when $S_r < S_{r,N}$. As S_r exceeds $S_{r,N}$ and approaches 100%, however, the theoretical results significantly deviate from the experimental data for both *P1* and *S*.

Both experimental and theoretical results show that the calculated phase velocity of *P1* has a peak value. From the theoretical results, it is noted that v_{P1} reaches its peak when S_r is about $S_{r,N}$, i.e. when air phase is disconnected and trapped in the water. To ascertain this observation, Fig.6.9 further presents the calculated velocity and attenuation of *P1* corresponding to different $S_{r,N}$ values. It is shown that although the velocity of *P1* is not significantly influenced by $S_{r,N}$, the attenuation of *P1* has a peak value when $S_r \approx S_{r,N}$ for all different $S_{r,N}$.

Experimental studies may be needed to confirm the correlation between the peak value of the attenuation of *P1* and $S_{r,N}$. On the other hand, sufficient experimental data shows that the attenuation of *P1* reaches a peak at the saturation ranging from 85%~95% (Murphy, 1982&1984; Yin et al., 1992). Yin et al. (1992) provided an explanation for

this phenomenon. They noticed that when the degree of saturation is about S_{rN} the air phase exists in the water only as separate pockets. As a P wave travels through the porous material containing separate air pockets, the large compressibility contrast between the water and the air generates local liquid flow around the air pocket, which consumes energy from the P wave. A quantitative analysis of this mechanism is provided by Yin (1992), where he showed that the peak of the attenuation of P1 is reached approximately at $S_r \approx S_{rN}$. Clearly, the theoretical result presented above supports Yin et al.'s conclusions.

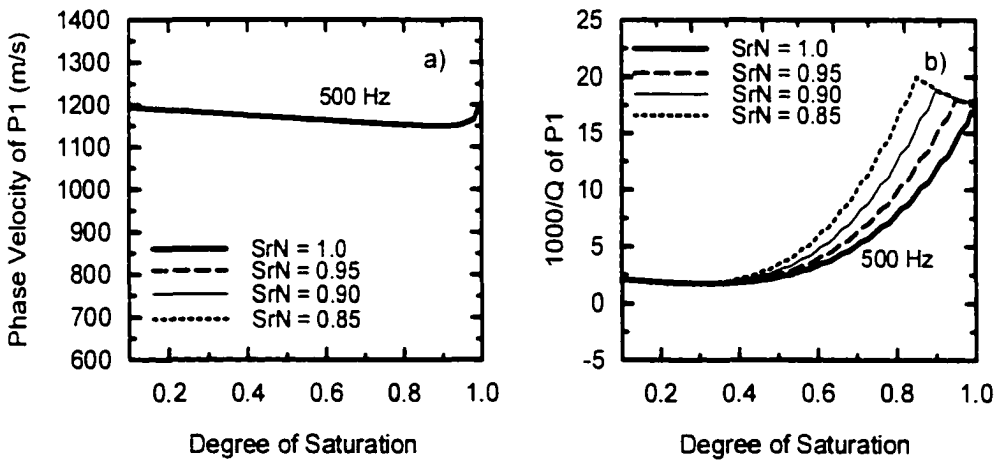

Figure 6.9 Effects of S_{rN} on: a) the velocity of P1; b) the attenuation of P1

As mentioned above, the attenuation is overestimated for $P1$ and underestimated for S when the degree of saturation exceeds S_{rN}. The discrepancy may be explained as follows. In compression, the interstitial liquid offers resistance due to its low

compressibility. For higher saturation, the gradient of local liquid pressure is lower in the pores. Therefore, based on the local fluid flow mechanism by Yin et al. (1992), when $S_r > S_{rN}$, the higher saturation leads to a more uniform pressure distribution and hence the lower energy dissipation. In shear, however, the gradient of local liquid pressure may be higher due to the higher saturation. Hence, greater attenuation is expected when the saturation increases. In the present simple model, the effect of local fluid flow around the air pockets has not been properly considered. Hence, great discrepancy in the high saturation range is expected.

Although the wave attenuation has great potential use in practice (e.g. in monitoring oil recovery processes), it remains poorly understood and underutilized. It must be pointed out that in higher saturation the effect of local diffusion will become dominant in attenuation and a simple linear elastic model may be not sufficient to account for such complex phenomena.

Chapter 7 INITIAL AND BOUNDARY VALUE PROBLEMS (IBVP) AND FINITE ELEMENT SOLUTION PROCEDURES

7.1 Preliminaries

In this chapter, the initial/boundary value problems (IBVP) of porous media and their solution procedures are presented. The governing equations presented in Chapter 4 are very general in the sense that they account for thermal effects and finite deformation. In what follows, however, our attention will be focused solely on the mechanical aspects of the porous media, and it is assumed that

1. the material is in the isothermal condition, i.e. $\theta = \theta_0$;
2. deformation of the solid skeleton is infinitesimal. In this case, the current configuration is approximately coincident with the reference configuration. $\boldsymbol{F} \approx \boldsymbol{I} + \boldsymbol{\varepsilon}$, $\boldsymbol{\varepsilon} = sym(\nabla \boldsymbol{u}^s)$, and $J = \det \boldsymbol{F} \approx 1 + \boldsymbol{I} : \boldsymbol{\varepsilon}$.
3. body force is due to the gravity, i.e. $U = -\boldsymbol{b}\boldsymbol{x}$. $\boldsymbol{b}$ is the gravitational acceleration, which may also include those induced in centrifuge testing.

In addition, the effects of capillary relaxation will be neglected. This is equivalent to the assumption that the capillary equilibrium can be achieved immediately. It is also assumed for convenience that the hysteresis in the capillary pressures is negligible. The cross

effects (i.e. Knudsen effect) of the relative velocities of fluids on drag force $\hat{\boldsymbol{R}}^{\beta}$ in (4.4.19) will be dropped in the following derivations. Therefore, it follows from (4.4.12), (4.4.13), and (4.4.7) that

$$\hat{\hat{\boldsymbol{R}}}^{\beta} = \hat{\boldsymbol{R}}^{\beta}/m_{\iota}^{\beta} = -\boldsymbol{J}^{\beta}\dot{\boldsymbol{M}}^{\beta},\ \beta = W, N \tag{7.1.1}$$

where coefficient $\boldsymbol{J}^{\beta}$ is a second-order tensor and can be related to the permeability coefficient of Darcy's flow equation as discussed later.

To derive the weak statements of the IBVP, we first define the space of configuration and the space of variation. Let L^2 denote the Hilbert space of all the *generalized* displacements $\varphi: \mathcal{B}\times[0,\infty) \to \mathbb{R}^{\dim}$ that are square integrable, i.e.

$$\|\varphi\|_{L^2}^2 = \int_{\mathcal{B}} \|\varphi\|^2 dV < \infty, \tag{7.1.2}$$

where φ can be a scalar object or a vector object; *dim* is *3* for vector fields and *1* for scalar fields. Let H^1 be the Hilbert space of $\varphi: \mathcal{B}\times[0,\infty) \to \mathbb{R}^{\dim}$ such that φ and the gradient $\nabla\varphi$ belong to L^2. For our purpose, it is sufficient to define the spaces of configuration and variation as follows,

$$\mathcal{C}_{\varphi} = \{\varphi : \mathcal{B}\times[0,\infty) \to \mathbb{R}^{\dim} \mid \varphi \in H^1,\ \varphi = \bar{\varphi} \text{ on } \Gamma_{\varphi}\} \quad \text{(Space of configuration)}$$

and

$$\mathcal{V}_{\varphi} = \{\eta : \mathcal{B} \to \mathbb{R}^{\dim} \mid \eta \in H^1,\ \eta = 0 \text{ on } \Gamma_{\varphi}\} \quad \text{(Space of variation)}$$

where Γ_{φ} represents the boundary with φ being specified as $\bar{\varphi}$. It is noted that η is a function of spatial coordinate only and independent of time.

In general, the choice of the generalized displacements in describing the problem is not unique. In what follows, two sets of generalized displacements will be introduced to represent the IBVP. The first one has been used in Chpater 4 to derive variational equations and includes $\{\boldsymbol{u}^S, \boldsymbol{M}^W, \boldsymbol{M}^N\}$*. For an IBVP, the boundary conditions corresponding to this set of displacements are specified as

- *Essential boundary conditions*

$$\boldsymbol{u}^S = \bar{\boldsymbol{u}} \qquad \text{on } \Gamma_u, \tag{EB1-1}$$

$$\boldsymbol{M}^W = \bar{\boldsymbol{M}}^W \qquad \text{on } \Gamma_{M^W}, \tag{EB1-2}$$

$$\boldsymbol{M}^N = \bar{\boldsymbol{M}}^N \qquad \text{on } \Gamma_{M^N}, \tag{EB1-3}$$

where $(\bar{M}^\beta)_i$ represents the total mass of β-fluid that has flowed through unit area of Γ_{M^W} (i.e. the relative mass displacement of the fluid) in i^{th} direction.

- *Natural boundary conditions*

$$\boldsymbol{\sigma} \cdot \boldsymbol{n} = \boldsymbol{f} \qquad \text{on } \Gamma_\sigma, \tag{NB1-1}$$

$$G^W = \bar{G}^W \qquad \text{on } \Gamma_{G^W}, \tag{NB1-2}$$

$$G^N = \bar{G}^N \qquad \text{on } \Gamma_{G^N}, \tag{NB1-3}$$

where $\bar{G}^\beta$ can be related to the specified pressure $\bar{p}^\beta$ through (4.2.7). For convenience and without losing much generality, it is assumed that the boundary of the domain can be additively decomposed into various sets of two disjointed parts and

$$\partial\mathcal{B} = \Gamma_\sigma \cup \Gamma_u = \Gamma_{G^W} \cup \Gamma_{M^W} = \Gamma_{G^N} \cup \Gamma_{M^N} \tag{7.1.3}$$

---

* n^W and n^N are not used as generalized displacements here, since they can be viewed as the internal variables associated with the capillary equilibrium and relaxation. In a finite element procedure, internal variables are usually eliminated at the Gaussian (i.e. quadrature) point level.

and

$$\Gamma_{\sigma} \cap \Gamma_{u} = \Gamma_{G^{W}} \cap \Gamma_{M^{W}} = \Gamma_{G^{N}} \cap \Gamma_{M^{N}} = \Phi \tag{7.1.4}$$

where Φ denotes the zero set. The meaning of (7.1.3) and (7.1.4) is schematically shown Fig.7.1.

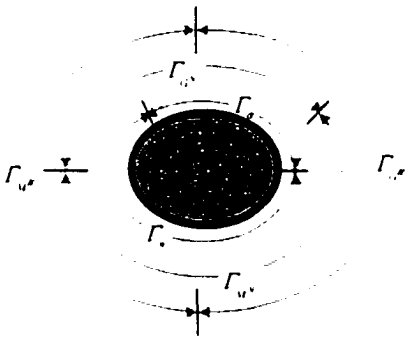

Figure 7.1 Boundary conditions

As discussed in Chapter 6, if the higher frequency modes of the problem is not of main concern, for instance, when a structure is subjected to earthquake loading, wave loading or static loading, the effects of the relative accelerations of fluids on the behavior of the porous medium are negligible*. In such cases, $\{\boldsymbol{u}^{S}, G^{W}, G^{N}\}$ can be introduced as the fundamental unknowns in describing the IBVP. Since G^{β} is related to p^{β} through (4.2.7), $\{\boldsymbol{u}^{S}, p^{W}, p^{N}\}$ can also be equivalently used as a set of generalized displacements. The corresponding boundary conditions remains to specify are

- *Essential boundary conditions*

$$\boldsymbol{u}^{S} = \bar{\boldsymbol{u}} \qquad \text{on } \Gamma_{u}. \tag{EB2-1}$$

* This assumption is not too stringent in applications, since the high frequency modes of a loading may be damped out when stress waves propagating through the porous media.

$$p^W = \bar{p}^W \qquad \text{on } \Gamma_{p^W}. \tag{EB2-2}$$

$$p^N = \bar{p}^N \qquad \text{on } \Gamma_{p^N}. \tag{EB2-3}$$

- *Natural boundary conditions*

$$\boldsymbol{\sigma} \cdot \boldsymbol{n} = \boldsymbol{f} \qquad \text{on } \Gamma_{\sigma}. \tag{NB2-1}$$

$$\dot{\boldsymbol{M}}^W \cdot \boldsymbol{n} = n^W \rho^W \bar{w}_n^W \qquad \text{on } \Gamma_{w^W}. \tag{NB2-2}$$

$$\dot{\boldsymbol{M}}^N \cdot \boldsymbol{n} = n^N \rho^N \bar{w}_n^N \qquad \text{on } \Gamma_{w^N}. \tag{NB2-3}$$

where $\bar{w}_n^{\beta}$ represents the component of the relative velocity of β-fluid in the direction normal to the boundary. Similarly, it is assumed that the boundary of the domain can be additively decomposed into various sets of two disjointed parts ($\Gamma_{\sigma}, \Gamma_{u}$) and ($\Gamma_{w^{\beta}}, \Gamma_{p^{\beta}}$).

7.2 IBVP: Form 1

Let $\{\boldsymbol{u}^S, \boldsymbol{M}^W, \boldsymbol{M}^N\}$ be the set of the generalized displacements and $\{\boldsymbol{\phi}, \boldsymbol{q}^W, \boldsymbol{q}^N\}$ be the corresponding variations. With the assumptions and boundary conditions introduced above, the statement of the initial and boundary value problem (IBVP) can be obtained by a simple specification of variational equation (4.4.24) and the principle of virtual dissipation presented in Chapter 4. That is,

Weak form 1: Given $\boldsymbol{b}$, $\bar{\boldsymbol{u}}$, $\bar{\boldsymbol{M}}^{\beta}$, f, and $\bar{G}^{\beta}$ ($\beta = W, N$) as well as proper initial conditions, find solution $\{\boldsymbol{u}^S, \boldsymbol{M}^W, \boldsymbol{M}^N\} \in \mathcal{C}_u \times \mathcal{C}_{M^W} \times \mathcal{C}_{M^N}$ such that, for any $\{\boldsymbol{\phi}, \boldsymbol{q}^W, \boldsymbol{q}^N\} \in \mathcal{V}_u \times \mathcal{V}_{M^W} \times \mathcal{V}_{M^N}$,

$$\int_{\Omega}[\boldsymbol{\phi}\cdot(\rho\ddot{\boldsymbol{u}}^{S}-\rho\boldsymbol{b}+\sum_{\beta=W,N}\ddot{\boldsymbol{M}}^{\beta})+\sum_{\beta=W,N}\boldsymbol{q}^{\beta}\cdot(\ddot{\boldsymbol{u}}^{S}-\boldsymbol{b}+\ddot{\boldsymbol{M}}^{\beta}/m_{t}^{\beta})]dV$$
$$+\int_{\Omega}[sym(\nabla\boldsymbol{\phi}):\boldsymbol{\sigma}+\sum_{\beta=W,N}(G^{\beta}\nabla\cdot\boldsymbol{q}^{\beta})]dV+\int_{\Omega}\sum_{\beta=W,N}\boldsymbol{q}^{\beta}\cdot(\boldsymbol{J}^{\beta}\dot{\boldsymbol{M}}^{\beta})dV \qquad \text{(W-1)}$$
$$-\int_{\Gamma_{\sigma}}\boldsymbol{\phi}\cdot\boldsymbol{f}dV+\sum_{\beta=W,N}\int_{\Gamma_{c,\beta}}(\bar{G}^{\beta}\boldsymbol{q}^{\beta}\cdot\boldsymbol{n})dA=0,$$

In deriving (W-1), the higher order small quantities have been omitted; ρ is the total mass density of the porous medium, i.e. $\rho=m_{0}+m^{W}+m^{N}$. The initial conditions of the problem is specified as

$$\boldsymbol{u}^{S}(\boldsymbol{x},t_{0})=\boldsymbol{u}_{0}(\boldsymbol{x}),\ \dot{\boldsymbol{u}}^{S}(\boldsymbol{x},t_{0})=\boldsymbol{v}_{0}(\boldsymbol{x}). \qquad \text{(IC1-1)}$$

$$\boldsymbol{M}^{W}(\boldsymbol{x},t_{0})=\boldsymbol{M}_{0}^{W}(\boldsymbol{x}),\ \dot{\boldsymbol{M}}^{W}(\boldsymbol{x},t_{0})=\dot{\boldsymbol{M}}_{0}^{W}(\boldsymbol{x}). \qquad \text{(IC1-2)}$$

and

$$\boldsymbol{M}^{N}(\boldsymbol{x},t_{0})=\boldsymbol{M}_{0}^{N}(\boldsymbol{x}),\ \dot{\boldsymbol{M}}^{N}(\boldsymbol{x},t_{0})=\dot{\boldsymbol{M}}_{0}^{N}(\boldsymbol{x}). \qquad \text{(IC1-3)}$$

Eliminating $\dot{\boldsymbol{R}}^{\beta}$ from (4.1.17) by using (7.1.1) and (4.4.7), we can see that in fact $\boldsymbol{J}^{\beta}$ can be related to the permeability tensor as

$$(\boldsymbol{J}^{\beta})^{-1}=(\rho^{\beta})^{2}\frac{k_{r}^{\beta}\boldsymbol{k}}{\eta^{\beta}} \qquad (7.2.1)$$

where $\boldsymbol{k}$ is the intrinsic permeability tensor [m^{2}] and generally a function of porosity and deformation; k_{r}^{β} is the relative permeability of β-fluid and it can be represented as a function of n^{W}; η^{β} is the viscosity of β-fluid [$Pa\,s$].

In general, stress tensor $\boldsymbol{\sigma}$ and chemical potential G^{β} ($\beta=W,N$) can be expressed as functions of $\{\boldsymbol{\varepsilon},m^{W},m^{N}\}$ and internal variables $\{\boldsymbol{\varepsilon}_{p},n^{W},n^{N},q_{k}\}$ through stress-strain constitutive relationships, i.e.

$$\sigma = \hat{\sigma}(\varepsilon, m^{W}, m^{N}, \varepsilon_p, n^{W}, n^{N}, q_k), \tag{7.2.2}$$

and

$$G^{\beta} = \hat{G}^{\beta}(\varepsilon, m^{W}, m^{N}, \varepsilon_p, n^{W}, n^{N}, q_k), \tag{7.2.3}$$

where the generalized strains $\{\varepsilon, m^{W}, m^{N}\}$ are related to the generalized displacements $\{\boldsymbol{u}^{S}, \boldsymbol{M}^{W}, \boldsymbol{M}^{N}\}$ through (3.1.15) and (4.1.3); ε_p is the plastic strain tensor; q_k represents other internal variables accounting for hardening, damage, and other internal dissipative mechanisms. It is noted that in a continuum model, all the internal variables can be viewed as the functions of $\{\varepsilon, m^{W}, m^{N}\}$. Therefore, we can write the incremental forms of (7.2.2) and (7.2.3) as

$$d\sigma = \boldsymbol{C} : d\varepsilon + \boldsymbol{c}^{W} dm^{W} + \boldsymbol{c}^{N} dm^{N}, \tag{7.2.4}$$

and

$$dG^{\beta} = \boldsymbol{e}^{\beta} : d\varepsilon + \zeta^{W} dm^{W} + \zeta^{N} dm^{N}, \tag{7.2.5}$$

respectively, where the coefficients are called the tangent moduli; $\boldsymbol{C}$ is a fourth-order tensor; $\boldsymbol{c}^{\beta}$ and $\boldsymbol{e}^{\beta}$ are symmetric second-order tensors. For hyperelasticity-based models, it can be easily proved that $\boldsymbol{c}^{\beta} = \boldsymbol{e}^{\beta}$ and $\boldsymbol{C}$ has major symmetry, i.e. $C_{ijkl} = C_{klij}$.

It is noted that (7.2.2) and (7.2.3) are not conventionally used in modeling the behavior of porous media due to the involvement of m^{β}. Biot (1972, 1977) is the first to use m^{β} ($m^{\beta} = m$ for saturated porous materials) as a constitutive variable. Variable m has been used subsequently by Rice (1975) and Coussy (1989, 1995). Recently, it is introduced by Amero (1999) into a numerical model of the porous media at finite strain, where m is additively decomposed into an elastic part and an irreversible part. The

irreversibility of m^β is well motivated by experimental observations. In fact, for the porous media saturated with multiple fluids there are at least two components contributing to the irreversible part of m^β, i.e. ε_p and n_p^β. The latter has been defined in Chapter 3 as the plastic part of the volume fraction. With introduction of (4.2.7), (7.2.5) can be equivalently written as

$$dp^\beta = \boldsymbol{B}^\beta : d\boldsymbol{\varepsilon} + Z^W dm^W + Z^N dm^N \tag{7.2.6}$$

where $\boldsymbol{B}^\beta$, Z^W, and Z^N are the tangent moduli represented as functions of state variables. Equation (7.2.6) has been derived and discussed in details by Coussy (1995: pp.385-441). All the moduli in (7.2.4)-(7.2.6) can be evaluated if the stress-strain constitutive relationship and the closure equations are explicitly given.

To obtain the finite element formulations of (W-1), let the domain of concerns be additively decomposed into *nel* disjointed elements, that is,

$$\mathcal{B} = \sum_{e=1}^{nel} \Omega^e \tag{7.2.7}$$

where Ω^e ($e = 1,2,....,nel$) represent the elements connecting with each other through *nod* nodal points. Let $\overline{u}_{Ai}$, $\overline{M}_{Ai}^W$, and $\overline{M}_{Ai}^N$ be the ith components of the solution $\{\boldsymbol{u}^S, \boldsymbol{M}^W, \boldsymbol{M}^N\}$ at node A of element e. Following the standard finite element procedure (e.g. Hughes, 1987), we write the discretized forms of variables $\{\boldsymbol{u}^S(\boldsymbol{x},t), \boldsymbol{M}^W(\boldsymbol{x},t), \boldsymbol{M}^N(\boldsymbol{x},t)\}$ for $\boldsymbol{x} \in \Omega^e$ and $t \in [0,T]$ as

$$\boldsymbol{u}^{Sh}(\boldsymbol{x},t) = N_A^1(\boldsymbol{x})\overline{\boldsymbol{u}}_A(t), \text{ or } u_i^{Sh} = N_A^1 \overline{u}_{Ai}, \tag{7.2.8}$$

$$\boldsymbol{M}^{Wh}(\boldsymbol{x},t) = N_A^2(\boldsymbol{x})\overline{\boldsymbol{M}}_A^W(t), \text{ or } M_i^{Wh} = N_A^2 \overline{M}_{Ai}^W, \tag{7.2.9}$$

and

$$\boldsymbol{M}^{Nh}(\boldsymbol{x},t) = N_A^I(\boldsymbol{x})\overline{\boldsymbol{M}}_A^N(t), \text{ or } M_i^{Nh} = N_A^I \overline{M}_{Ai}^N, \tag{7.2.10}$$

where superscript h denotes the discrete counterpart of a continuous variable; capital letters A (or B) used as a subscript represents the *element* node number, and letters i (or j, k, l) as a subscript represents the spatial direction. Summation convention is used here, e.g. the repetition of A implies that the summation is repeated from 1 to n_p^{elm}, where n_p^{elm} is the total number of nodes in an element. $N_A^\alpha(\boldsymbol{x})$ ($\alpha = 1,2,3$) is the shape function of node A associated with S, W, and N, respectively, and it satisfies $N_A^\alpha(\boldsymbol{x}_B) = \delta_{AB}$, where $\boldsymbol{x}_B$ is the spatial coordinate of node B and δ_{AB} is the Kronecker delta.

Let $\mathcal{C}_\varphi^h$ and $\mathcal{V}_\varphi^h$ be finite-dimensional approximations to $\mathcal{C}_\varphi$ and $\mathcal{V}_\varphi$, respectively. Then, $\mathcal{C}_\varphi^h$ can be considered approximately as a subset of $\mathcal{C}_\varphi$, while $\mathcal{V}_\varphi^h$ is a subset of $\mathcal{V}_\varphi$. For instance, if $\boldsymbol{u}^{Sh} \in \mathcal{C}_u^h$, then $\boldsymbol{u}^{Sh} \in \mathcal{C}_u$. Let $\{\boldsymbol{\phi}^h, \boldsymbol{q}^{Wh}, \boldsymbol{q}^{Nh}\}$ be the discrete counterpart of the variations, which have the forms similar to (7.2.8)-(7.2.10), respectively. The Galerkin formulation of the problem therefore follows directly from the weak form (W-1) by replacing $\{\boldsymbol{u}^S, \boldsymbol{M}^W, \boldsymbol{M}^N\}$ and $\{\boldsymbol{\phi}, \boldsymbol{q}^W, \boldsymbol{q}^N\}$ for $\{\boldsymbol{u}^{Sh}, \boldsymbol{M}^{Wh}, \boldsymbol{M}^{Nh}\}$ and $\{\boldsymbol{\phi}^h, \boldsymbol{q}^{Wh}, \boldsymbol{q}^{Nh}\}$, respectively. This yields the coupled finite element equations as follows,

$$\sum_e \int_{\Omega^e} N_{A,j}^I \sigma_{ij} dV + \sum_e ({}^e z_{ijAB}^{11} \ddot{\overline{u}}_{Bj}) + \sum_e ({}^e z_{ijAB}^{12} \ddot{\overline{M}}_{Bj}^W) + \sum_e ({}^e z_{ijAB}^{13} \ddot{\overline{M}}_{Bj}^N) = \sum_e {}^e F_{Ai}^I. \quad \text{(FE1-1)}$$

$$\sum_e \int_{\Omega^e} N_{A,j}^I G^W dV + \sum_e ({}^e c_{ijAB}^{22} \dot{\overline{M}}_{Bj}^W) + \sum_e ({}^e z_{ijAB}^{21} \ddot{\overline{u}}_{Bj}) + \sum_e ({}^e z_{ijAB}^{22} \ddot{\overline{M}}_{Bj}^W) = \sum_e {}^e F_{Ai}^I. \quad \text{(FE1-2)}$$

and

$$\sum_e \int_{\Omega^e} N_{A,j}^I G^N dV + \sum_e ({}^e c_{ijAB}^{33} \dot{\overline{M}}_{Bj}^N) + \sum_e ({}^e z_{ijAB}^{31} \ddot{\overline{u}}_{Bj}) + \sum_e ({}^e z_{ijAB}^{33} \ddot{\overline{M}}_{Bj}^N) = \sum_e {}^e F_{Ai}^I. \quad \text{(FE1-3)}$$

where

$$ {}^{e}z^{11}_{\eta AB} = \delta_{\eta} \int_{\Omega^e} \rho N^1_A N^1_B dV , \tag{FE1-4} $$

$$ {}^{e}z^{22}_{\eta AB} = \delta_{\eta} \int_{\Omega^e} (m^W_t)^{-1} N^2_A N^2_B dV , \tag{FE1-5} $$

$$ {}^{e}z^{33}_{\eta AB} = \delta_{\eta} \int_{\Omega^e} (m^N_t)^{-1} N^3_A N^3_B dV , \tag{FE1-6} $$

$$ {}^{e}z^{21}_{\eta AB} = \delta_{\eta} \int_{\Omega^e} N^2_A N^1_B dV = {}^{e}z^{12}_{\eta BA} , \tag{FE1-7} $$

$$ {}^{e}z^{31}_{\eta AB} = \delta_{\eta} \int_{\Omega^e} N^3_A N^1_B dV = {}^{e}z^{13}_{\eta BA} , \tag{FE1-8} $$

$$ {}^{e}c^{22}_{\eta AB} = \int_{\Omega^e} J^W_{\eta} N^2_A N^2_B dV , \tag{FE1-9} $$

$$ {}^{e}c^{33}_{\eta AB} = \int_{\Omega^e} J^N_{\eta} N^3_A N^3_B dV , \tag{FE1-10} $$

$$ {}^{e}F^1_{A\eta} = \int_{\Omega^e} \rho N^1_A b_\eta dV + \int_{\partial\Omega^e \cap \Gamma^h_{\sigma\beta}} N^1_A f_\eta dA , \tag{FE1-11} $$

$$ {}^{e}F^2_{A\eta} = \int_{\Omega^e} N^2_A b_\eta dV - \int_{\partial\Omega^e \cap \Gamma^h_{\sigma\beta}} N^2_A \overline{G}^W n_\eta dA , \tag{FE1-12} $$

and

$$ {}^{e}F^3_{A\eta} = \int_{\Omega^e} N^3_A b_\eta dV - \int_{\partial\Omega^e \cap \Gamma^h_{\sigma\beta}} N^3_A \overline{G}^N n_\eta dA . \tag{FE1-13} $$

where J^{β}_{η} denotes the component of $\boldsymbol{J}^{\beta}$; $\partial\Omega^e \cap \Gamma^h_{\sigma\beta}$ represents the part of the element boundary coincident with the domain boundary where G^{β} (or equivalently, p^{β}) has been specified (see Fig.7.2).

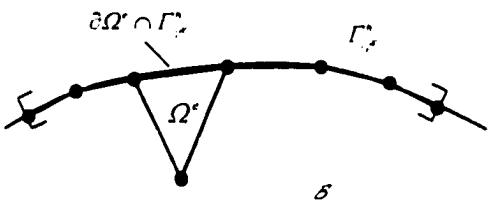

Figure 7.2 The specified element boundaries $\partial\Omega^e \cap \Gamma^h_{\sigma\beta}$

(FE1-1)-(FE1-3) can be assembled into a more compact matrix form as

$$\boldsymbol{F}^{\text{int}} + \boldsymbol{c}\dot{\boldsymbol{d}} + \boldsymbol{z}\ddot{\boldsymbol{d}} = \boldsymbol{F}^{\text{ext}} \tag{7.2.11}$$

where the components of displacements $\boldsymbol{d}$ are given as follows,

$$\{\overline{u}_{ai}, \overline{M}^{W}_{ai}, \overline{M}^{N}_{ai}\}, \tag{7.2.12}$$

a is the *global* node number; the elements in the bracket are read in order as follows: index a is repeated from 1 to *nod*, which is the total number of the nodal points, and for every a, index i is continuously repeated from 1 to I_{dim} (I_{dim} is the spatial dimension of the problem). It is noted that if a certain variable is specified on the boundary it must be excluded from (7.2.12).

$\boldsymbol{F}^{\text{int}}$ is obtained by assembling the element internal force ${}^{e}\boldsymbol{F}^{\text{int}}$ with the following components,

$$\{\int_{\Omega^e} N^I_{A,j}\sigma_{ij}dV,\ \int_{\Omega^e} N^I_{A,i}G^W dV,\ \int_{\Omega^e} N^I_{A,i}G^N dV\}. \tag{7.2.13}$$

Hence, we write

$$\boldsymbol{F}^{\text{int}} = \mathop{\mathbf{A}}_{e=1}^{nel}({}^{e}\boldsymbol{F}^{\text{int}}). \tag{7.2.14}$$

where $\mathop{\mathbf{A}}_{e=1}^{nel}$ is an operator representing the assembling procedure of the global matrices (a detailed account of implementation can be found in Hughes (1987: Ch.2 & Ch.3). Similarly, the global external force $\boldsymbol{F}^{\text{ext}}$, the global matrices $\boldsymbol{c}$, and $\boldsymbol{z}$ can be obtained by assembling their element counterparts, i.e.

$$\boldsymbol{c} = \mathop{\mathbf{A}}_{e=1}^{nel}({}^{e}\boldsymbol{c}). \tag{7.2.15}$$

$$\boldsymbol{m} = \mathop{\mathbf{A}}_{e=1}^{nel} ({}^{e}\boldsymbol{z}), \tag{7.2.16}$$

$$\boldsymbol{F}^{ext} = \mathop{\mathbf{A}}_{e=1}^{nel} ({}^{e}\boldsymbol{F}^{ext}), \tag{7.2.17}$$

where

$${}^{e}\boldsymbol{c} = \begin{bmatrix} \boldsymbol{0}, & \boldsymbol{0}, & \boldsymbol{0} \\ \boldsymbol{0}, & {}^{e}c^{22}, & \boldsymbol{0} \\ \boldsymbol{0}, & \boldsymbol{0}, & {}^{e}c^{33} \end{bmatrix}, \tag{7.2.18}$$

$${}^{e}\boldsymbol{z} = \begin{bmatrix} {}^{e}z^{11}, & {}^{e}z^{12}, & {}^{e}z^{13} \\ {}^{e}z^{21}, & {}^{e}z^{22}, & \boldsymbol{0} \\ {}^{e}z^{31}, & \boldsymbol{0}, & {}^{e}z^{33} \end{bmatrix} \tag{7.2.19}$$

and ${}^{e}\boldsymbol{F}^{ext}$ is the element external force vector with components as follows,

$$\{{}^{e}F_{0}^{1}, {}^{e}F_{0}^{2}, {}^{e}F_{0}^{3}\} \tag{7.2.20}$$

It is noted that ${}^{e}\boldsymbol{c}$ and ${}^{e}\boldsymbol{z}$ are symmetrical and hence $\boldsymbol{c}$ and $\boldsymbol{z}$ are symmetrical. This feature is desirable in a numerical procedure.

7.3 IBVP: Form 2

Here, displacement of the skeleton ($\boldsymbol{u}^{S}$), pore water pressure (p^{W}), and pore air pressure (p^{N}) are used as generalized displacements. Let their variations be $\boldsymbol{\phi}$, π^{W}, and π^{N}, respectively. (4.1.8) and (4.1.3) can be chosen as the coupled field equations, which are associated with $\boldsymbol{u}^{S}$ and p^{β} ($\beta = W$ and N), respectively. With the assumptions and natural boundary conditions introduced in Section 7.1, the weak form of (4.1.8) can be expressed as

$$\int_\tau \phi_i(\rho\ddot{u}_i^S - \sigma_{ij,j} - \rho b_i)dV = \int_\tau [\phi_i\rho(\ddot{u}_i^S - b_i) - \phi_{i,j}\sigma_{ij}]dV - \int_{\Gamma_\sigma} \phi_i f_i dA = 0 \qquad (7.3.1)$$

As will be seen later, it is more convenient to use the rate forms of mass conservation equations than the original form (4.1.3). Take the time derivative of (4.1.3) and divide both sides by ρ^β. The weak formulations of the mass balance can be put as

$$\begin{aligned} 0 &= \int_\tau \pi^\beta(\dot{m}^\beta + \dot{M}_{i,i}^\beta)/\rho^\beta\, dV \\ &= \int_\tau (\pi^\beta \dot{m}^\beta/\rho^\beta - \pi_{,i}^\beta \dot{M}_i^\beta/\rho^\beta)dV + \int_{\Gamma_{\sigma^\beta}} \pi^\beta \dot{\bar{M}}_n^\beta/\rho^\beta dA. \end{aligned} \qquad (7.3.2)$$

where $\dot{\bar{M}}_n^\beta = n^\beta\rho^\beta\dot{\bar{w}}_n^\beta$; $\beta = W, N$. Since the relative acceleration of a fluid is omitted, $\dot{\bar{M}}_i^\beta$ can be eliminated from (7.3.2) by introducing the flow equation (4.4.19). Inserting (7.1.1) and (4.2.7) into (4.4.19), it follows after some manipulations that

$$\dot{\boldsymbol{M}}^\beta = \boldsymbol{J}^{\beta-1}\left(-\frac{\nabla p^\beta}{\rho^\beta} + \boldsymbol{b} - \ddot{\boldsymbol{u}}^S\right) \qquad (7.3.3)$$

or

$$\dot{M}_i^\beta = (\boldsymbol{J}^{\beta-1})_{ij}\left(-\frac{p_{,j}^\beta}{\rho^\beta} + b_j - \ddot{u}_j^S\right) \qquad (7.3.4)$$

Now, eliminating $\dot{\bar{M}}_i^\beta$ from (7.3.2) by inserting (7.3.4) yields

$$\begin{aligned} &\int_\tau [\pi^\beta \frac{\dot{m}^\beta}{\rho^\beta} + \pi_{,i}^\beta \frac{k_r^\beta k_{ij}}{\eta^\beta}(p_{,j}^\beta + \rho^\beta \ddot{u}_j^S)]dV \\ &= \int_\tau \pi_{,i}^\beta \frac{k_r^\beta k_{ij}}{\eta^\beta}\rho^\beta b_j dV - \int_{\Gamma_{\sigma^\beta}} \pi^\beta n^\beta \dot{\bar{w}}_n^\beta dA \end{aligned} \qquad (7.3.5)$$

where $\beta = W, N$. It is noted that (7.2.1) has been used in (7.3.5). Finally, we obtain the weak statement of the initial/boundary value problem (IBVP) as follows.

Weak form 2: Given $\boldsymbol{b}$, $\bar{\boldsymbol{u}}$, $\bar{p}^{\beta}$, f, and $\bar{w}_n^{\beta}$ ($\beta = W, N$) as well as the initial conditions (IC2): $\boldsymbol{u}^S(\boldsymbol{x}, t_0) = \boldsymbol{u}_0(\boldsymbol{x})$, $\dot{\boldsymbol{u}}^S(\boldsymbol{x}, t_0) = \boldsymbol{v}_0(\boldsymbol{x})$, and $p^{\beta}(\boldsymbol{x}, t_0) = p_0^{\beta}(\boldsymbol{x})$, find solution $\{\boldsymbol{u}^S, p^W, p^N\} \in \mathcal{C}_u \times \mathcal{C}_{p^W} \times \mathcal{C}_{p^N}$ such that, for any $\{\boldsymbol{\phi}, \pi^W, \pi^N\} \in \mathcal{V}_u \times \mathcal{V}_{p^W} \times \mathcal{V}_{p^N}$, (7.3.1) and (7.3.5) must be satisfied.

Similar to the procedure followed in last section, in order to derive the finite element formulations of the IBVP, we first cast $\{\boldsymbol{u}^S, p^W, p^N\}$ and $\{\boldsymbol{\phi}, \pi^W, \pi^N\}$ into the finite-dimensional forms associated with the spatial discretization, that is,

$$u_i^{Sh} = N_A^I \bar{u}_{Ai}, \quad \phi_i = N_A^I \bar{\phi}_{Ai} \tag{7.3.6}$$

$$p^{Wh} = N_A^I \bar{p}_A^W, \quad \pi^{Wh} = N_A^I \bar{\pi}_A^W \tag{7.3.7}$$

and

$$p^{Nh} = N_A^I \bar{p}_A^N, \quad \pi^{Nh} = N_A^I \bar{\pi}_A^N \tag{7.3.8}$$

where $\{\boldsymbol{u}^{Sh}, p^{Wh}, p^{Nh}\} \in \mathcal{C}_u^h \times \mathcal{C}_{p^W}^h \times \mathcal{C}_{p^N}^h$ and $\{\boldsymbol{\phi}^{Sh}, \pi^{Wh}, \pi^{Nh}\} \in \mathcal{V}_u^h \times \mathcal{V}_{p^W}^h \times \mathcal{V}_{p^N}^h$ are the finite-dimensional counterparts of the generalized displacement and its variation, respectively. Since $\mathcal{C}_{\phi}^h$ is a subset of $\mathcal{C}_{\phi}$ and $\mathcal{V}_{\phi}^h$ a subset of $\mathcal{V}_{\phi}$, (7.2.6)-(7.2.8) must satisfy the discrete forms of (7.3.1) and (7.3.5). Noting the $\bar{\phi}_{Ai}^{Sh}$, $\bar{\pi}_A^{Wh}$, and $\bar{\pi}_A^{Nh}$ are the arbitrarily chosen small quantities, we deduce that

$$\sum_e \int_{\Omega^e} N_{A,J}^I \sigma_{ij} dV + \sum_e ({}^e z_{ijAB}^{II} \ddot{\bar{u}}_{Bj}) = \sum_e {}^e F_{Ai}^I, \tag{FE2-1}$$

$$\sum_e ({}^e \kappa_{AB}^{22} \bar{p}_B^W) + \sum_e \int_{\Omega^e} N_A^I \dot{m}^W dV + \sum_e ({}^e z_{iAB}^{2I} \ddot{\bar{u}}_{Bi}) = \sum_e {}^e F_A^2, \tag{FE2-2}$$

and

$$\sum_e ({}^e\kappa^{33}_{AB}\bar{p}^N_B) + \sum_e \int_{\Omega^e} N^3_A \dot{m}^N dV + \sum_e ({}^e z^{31}_{iAB}\ddot{\bar{u}}_{Bi}) = \sum_e {}^e F^3_A . \qquad \text{(FE2-3)}$$

where ${}^e z^{31}_{iAB}$ and ${}^e F^I_{Ai}$ are given by (FE1-4) and (FE1-11), respectively:

$${}^e\kappa^{33}_{AB} = \int_{\Omega^e} N^3_{A,i}(k^W_r k_{ij}/\eta^W) N^3_{B,j} dV , \qquad \text{(FE2-4)}$$

$${}^e\kappa^{33}_{AB} = \int_{\Omega^e} N^3_{A,i}(k^N_r k_{ij}/\eta^N) N^3_{B,j} dV , \qquad \text{(FE2-5)}$$

$${}^e z^{31}_{iAB} = \int_{\Omega^e} N^3_{A,i}(\rho^W k^W_r k_{ij}/\eta^W) N^I_B dV , \qquad \text{(FE2-6)}$$

$${}^e z^{31}_{iAB} = \int_{\Omega^e} N^3_{A,i}(\rho^N k^N_r k_{ij}/\eta^N) N^I_B dV , \qquad \text{(FE2-7)}$$

$${}^e F^3_A = \int_{\Omega^e} N^3_{A,i}(\rho^W k^W_r k_{ij}/\eta^W) b_j dV - \int_{\partial\Omega^e \cap \Gamma^h_{q^W}} N^3_A n^W \bar{w}^W_n dA , \qquad \text{(FE2-8)}$$

and

$${}^e F^3_A = \int_{\Omega^e} N^3_{A,i}(\rho^N k^N_r k_{ij}/\eta^N) b_j dV - \int_{\partial\Omega^e \cap \Gamma^h_{q^N}} N^3_A n^N \bar{w}^N_n dA , \qquad \text{(FE2-9)}$$

where $\partial\Omega^e \cap \Gamma^h_{q^\beta}$ represents the part of the element boundary coincident with the domain boundary where the fluid relative velocity $\boldsymbol{w}^\beta$ has been specified.

Taking the time derivative of

$$m^\beta = m^\beta_t - m^\beta_0 = Jn^\beta \rho^\beta - n^\beta_0 \rho^\beta_0 , \ \beta = W, N \qquad (7.3.9)$$

one obtain

$$\frac{\dot{m}^\beta}{\rho^\beta} = n^\beta \dot{u}^s_{i,i} + \dot{n}^\beta + n^\beta \frac{\dot{\rho}^\beta}{\rho^\beta} . \qquad (7.3.10)$$

where n^β can be evaluated by using the closure equations discussed in Chapter 4, and if the viscosity due to the capillary relaxation are neglected, we may simply assume that $n^\beta = n^\beta(\varepsilon_v, p^W, p^N)$. In addition, to be consistent with the assumption made in (4.2.7), ρ^β is assumed as a function of p^β only, i.e. $\rho^\beta = \rho^\beta(p^\beta)$. Therefore, (7.3.10) can be cast into

$$\frac{\dot{m}^{\beta}}{\rho^{\beta}} = \vartheta_1^{\beta}\dot{u}_{i,i}^{S} + \vartheta_2^{\beta}\dot{p}^{W} + \vartheta_3^{\beta}\dot{p}^{N} \tag{7.3.11}$$

The finite dimensional counterpart of (7.3.11) is

$$(\dot{m}^{\beta}/\rho^{\beta})^{n} = \vartheta_1^{\beta}\dot{u}_{i,i}^{Sn} + \vartheta_2^{\beta}\dot{p}^{Wn} + \vartheta_3^{\beta}\dot{p}^{Nn} \tag{7.3.12}$$

where

$$\vartheta_1^{\beta} = n^{\beta} + \frac{\partial n^{\beta}}{\partial \varepsilon_v}, \tag{7.3.13}$$

$$\vartheta_2^{\beta} = \frac{n^{\beta}\delta_{\beta W}}{K_{\beta}} + \frac{\partial n^{\beta}}{\partial p^{W}}, \tag{7.3.14}$$

and

$$\vartheta_3^{\beta} = \frac{n^{\beta}\delta_{\beta N}}{K_{\beta}} + \frac{\partial n^{\beta}}{\partial p^{N}}. \tag{7.3.15}$$

Here, $\delta_{\alpha\beta}$ has the same meaning as the Kronecker delta, i.e. $\delta_{\alpha\beta} = 1$ when $\alpha = \beta$ and $\delta_{\alpha\beta} = 0$ for otherwise; K_{β} is the bulk modulus of β component and defined by

$$K_{\beta} = \frac{1}{\rho^{\beta}}\frac{\partial \rho^{\beta}}{\partial p^{\beta}} \tag{7.3.16}$$

It is noted that in general ϑ_1^{β}, ϑ_2^{β}, and ϑ_3^{β} are changeable. Inserting (7.3.12) into (FE2-2) and (FE2-3) yields, respectively,

$$\sum_e ({}^e\kappa_{AB}^{22}\bar{p}_B^{W}) + \sum_e ({}^e c_{jAB}^{21}\dot{\bar{u}}_{Bj} + {}^e c_{AB}^{22}\dot{\bar{p}}_B^{W} + {}^e c_{AB}^{23}\dot{\bar{p}}_B^{N}) + \sum_e ({}^e z_{jAB}^{21}\ddot{\bar{u}}_{Bj}) = \sum_e {}^e F_A^2. \quad \text{(FE2-2)'}$$

and

$$\sum_e ({}^e\kappa_{AB}^{33}\bar{p}_B^{N}) + \sum_e ({}^e c_{jAB}^{31}\dot{\bar{u}}_{Bj} + {}^e c_{AB}^{32}\dot{\bar{p}}_B^{W} + {}^e c_{AB}^{33}\dot{\bar{p}}_B^{N}) + \sum_e ({}^e z_{jAB}^{31}\ddot{\bar{u}}_{Bj}) = \sum_e {}^e F_A^3. \quad \text{(FE2-3)'}$$

where

$${}^e c_{jAB}^{\alpha 1} = \int_{\Omega^e} N_A^{\alpha}\vartheta_1^{\alpha}N_{B,j}^{1}\,dV, \ \alpha = 2, 3 \tag{FE2-10}$$

and

$$ {}^{e}c_{AB}^{\alpha\beta} = \int_{\Omega^e} N_A^{\alpha} \vartheta_{\beta}^{\alpha} N_B^{\beta} dV \,, \quad \alpha, \beta = 2 \text{ or } 3 \qquad \text{(FE2-11)} $$

It is noted that, in (FE2-10) and (FE2-11), $\vartheta_{\beta}^{i} = \vartheta_{\beta}^{W}$ and $\vartheta_{\beta}^{I} = \vartheta_{\beta}^{N}$; Here, the summation convention does not apply to the repeated indexes. Semi-discrete formulations (FE2-1), (FE2-2)', and (FE2-3)' can be assembled into a more compact form as

$$ \boldsymbol{F}^{\text{int}} + \boldsymbol{c}\dot{\boldsymbol{d}} + \boldsymbol{z}\ddot{\boldsymbol{d}} = \boldsymbol{F}^{\text{ext}} \qquad (7.3.17) $$

where the global unknown vector $\boldsymbol{d}$ is represented by

$$ \{\overline{u}_a, \overline{p}_a^W, \overline{p}_a^N\}, \qquad \text{for 1-D} $$

$$ \{\overline{u}_{a1}, \overline{u}_{a2}, \overline{p}_a^W, \overline{p}_a^N\}, \qquad \text{for 2-D} $$

$$ \{\overline{u}_{a1}, \overline{u}_{a2}, \overline{u}_{a3}, \overline{p}_a^W, \overline{p}_a^N\}, \qquad \text{for 3-D} $$

a is the *global* node number, and repeated from 1 to the total number of the nodal points, i.e. n_p. The components of the element internal force ${}^{e}\boldsymbol{F}^{\text{int}}$ is represented by

$$ \{\int_{\Omega^e} N_{A,j}^{I} \sigma_{ij} dV, \; {}^{e}\kappa_{AB}^{ij} \overline{p}_B^W, \; {}^{e}\kappa_{AB}^{ij} \overline{p}_B^N\} \,, \qquad (7.3.18) $$

Matrices $\boldsymbol{c}$, $\boldsymbol{z}$, $\boldsymbol{F}^{\text{int}}$, and $\boldsymbol{F}^{\text{ext}}$ are obtained by assembling the corresponding element matrices, i.e.

$$ \boldsymbol{c} = \mathop{\mathbf{A}}_{e=1}^{nel} ({}^{e}\boldsymbol{c}), \qquad (7.3.19) $$

$$ \boldsymbol{m} = \mathop{\mathbf{A}}_{e=1}^{nel} ({}^{e}\boldsymbol{z}), \qquad (7.3.20) $$

$$ \boldsymbol{F}^{ext} = \mathop{\mathbf{A}}_{e=1}^{nel} ({}^{e}\boldsymbol{F}^{ext}), \qquad (7.3.21) $$

where

$$
{}^{e}c = \begin{bmatrix} 0, & 0, & 0 \\ {}^{e}c^{21}, & {}^{e}c^{22}, & {}^{e}c^{23} \\ {}^{e}c^{31}, & {}^{e}c^{32}, & {}^{e}c^{33} \end{bmatrix}, \tag{7.3.22}
$$

$$
{}^{e}z = \begin{bmatrix} {}^{e}z^{11}, & 0, & 0 \\ {}^{e}z^{21}, & 0, & 0 \\ {}^{e}z^{31}, & 0, & 0 \end{bmatrix}, \tag{7.3.23}
$$

and

$$
({}^{e}F^{ext})_{g} = \{{}^{e}F^{1}_{A_i}, {}^{e}F^{2}_{A}, {}^{e}F^{3}_{A}\} \tag{7.3.24}
$$

7.4 Nature of the Problems and Initial Conditions

The semi-discrete finite element formulations presented above are represented by an ordinary differential equation (ODE), i.e. (7.2.11) or (7.3.17). In application, choice of a particular set of formulations depends on the nature of the problem and computational efficiency. For example, if we are dealing with the problems of the wave propagation in the porous media, the first form of the IBVP, i.e. (7.2.11), must be used. The reason is that the effects of the relative accelerations of fluids cannot be neglected on the propagation behaviors of the waves in the porous medium. The ODE (7.2.11) has a symmetrical structure, which is a desirable feature from the numerical point of view.

If deformation and flow are of main concern and the high frequency modes of loading can be neglected, the second form of the IBVP, i.e. (7.3.17), can be used. Generally, the matrices in (7.3.17) are not symmetrical. In large-scale computations, however, this drawback is offset by a smaller set of unknowns in (7.3.17). For example, if (7.2.11) is employed, there will be totally 9 degrees of freedom (DOF) per nodal point in a 3-D problem, and if (7.3.17) is used there are only 5 DOFs in a node.

Before solving (7.2.11) or (7.3.17), it is important to assure that its solution exists and is unique. However, a proof of the existence and uniqueness of the problem goes beyond the scope of this dissertation. The interested readers may be referred to Fichera (1972) and Knops and Payne (1971) for a general account of the existence and uniqueness of elastic problems. A proof of the existence and uniqueness theorems for elastic waves propagating through fluid-saturated porous media was presented by Santos (1986 I&II). In the following, we shall go directly to the solution procedure, assuming that the problem has a unique solution.

To solve (7.2.11) or (7.3.17), the initial conditions must be specified. In general, the initial state of the porous medium can be determined by the following parameters,

Initial porosity: $n_0(\boldsymbol{x})$

Initial degree of saturation: $S_{r0}(\boldsymbol{x})$

Initial displacement: $u_i^0(\boldsymbol{x})$

Initial stress: $\sigma_{ij}^0(\boldsymbol{x})$

Initial pressure of wetting fluid: $p_0^w(\boldsymbol{x})$

Initial pressure of nonwetting fluid: $p_0^N(\boldsymbol{x})$

Initial body force: b_i^0

In addition, the initial velocity of the solid skeleton must be specified. If (7.2.11) is used, the initial values of $\dot{\boldsymbol{M}}_0^w(\boldsymbol{x})$ and $\dot{\boldsymbol{M}}_0^N(\boldsymbol{x})$ also need to be specified.

The initial state of the porous medium was formed either in a geological or in an artificial installation process. In a numerical analysis, these processes should be simulated

in order that the initial conditions can be obtained. However, such kinds of numerical simulations are not always possible. For example, if (7.3.17) is used to evaluate the initial conditions of a naturally deposited soil body, it is impossible to specify the history of the relative velocity, i.e. $\overline{w}_n^{\beta}$, of a fluid on the boundary. In this case, the initial conditions can be evaluated by the following procedure:

1. set $\overline{w}_n^{W} = \overline{w}_n^{N} = 0$,
2. input some small initial stresses $\sigma_{ij}^{0}(\boldsymbol{x})$, and compute $p_0^{W}(\boldsymbol{x})$ and $p_0^{N}(\boldsymbol{x})$ by using the relationship between the suction and degree of saturation,
3. solve the steady state equation $\boldsymbol{F}^{\mathrm{int}}(\boldsymbol{d}) = \boldsymbol{F}^{\mathrm{ext}}(t_0)$ with constraints $p^{W} = p_0^{W}$ and $p^{N} = p_0^{N}$.

It is noted that $p_0^{W}(\boldsymbol{x})$ and $p_0^{N}(\boldsymbol{x})$ are the initial *total* fluid pressures in excess of the atmospheric pressure. The reason for applying the constraints to the steady state equation in Step 3 is that $p^{W}(\boldsymbol{x})$ and $p^{N}(\boldsymbol{x})$ are the specified unknowns in the equation.

The process to solve the steady state equation will be called the *static analysis* in the following. After the static analysis, the initial state of porous medium represented by $\sigma_{ij}^{0}(\boldsymbol{x})$, $u_i^{0}(\boldsymbol{x})$, $p_0^{W}(\boldsymbol{x})$, and $p_0^{N}(\boldsymbol{x})$ will be known, and we can move to the next step of the solution. To that end, the arrays of $\dot{\boldsymbol{d}}$ and $\ddot{\boldsymbol{d}}$ are cleared, and the time history of the forces applied at $t = t_0$, e.g. the base motion, are activated.

7.5 Solution Procedures: Dynamic Analysis

For the hyperbolic problem given by (7.2.11) or (7.3.17), many solution procedures are available in the literature. A comprehensive survey and detailed analysis of various algorithms can be found in Hughes (1987: Ch.9). In the following, the Hilber-Hughes-Taylor α-method will be employed that has been commonly applied to the dynamic analysis of structures (Hilber et al., 1977). Use of the α-method in analyzing the dynamic behavior of saturated porous media was first made by Muraleetharan et al. (1994) and later by Arduino (1996). This algorithm has many desirable features as addressed later.

Basically, the α-method* can be viewed as a generalization of the Newmark method. Let the time period of solution $[t_0, t_N]$ be separated into N steps. Provided that the solution is advanced to nth time step, we try to find the solution at $t = t_{n-1}$ ($n = 1,2,....,N$). In the α-method, the time-discrete equation of (7.2.11) or (7.3.17) is written as

$$\mathbf{z}\ddot{\boldsymbol{d}}_{n-1} + (\alpha + 1)\mathbf{c}\dot{\boldsymbol{d}}_{n-1} - \alpha\mathbf{c}\dot{\boldsymbol{d}}_{n} + \boldsymbol{F}^{\text{int}}(\boldsymbol{d}_{n-1-\alpha}) = \boldsymbol{F}^{\text{ext}}(t_{n-1-\alpha}). \tag{7.5.1}$$

where $t_{n-1-\alpha} = (1+\alpha)t_{n-1} - \alpha t_n$; $\boldsymbol{d}_n \approx \boldsymbol{d}(t_n)$; $\boldsymbol{d}_{n-1-\alpha} = (1+\alpha)\boldsymbol{d}_{n-1} - \alpha\boldsymbol{d}_n$.

The Newmark recurrence formulations are retained in the α-method and they are given by

$$\boldsymbol{d}_{n-1} = \boldsymbol{d}_n + \dot{\boldsymbol{d}}_n \Delta t + [\beta\ddot{\boldsymbol{d}}_{n-1} + (\frac{1}{2} - \beta)\ddot{\boldsymbol{d}}_n](\Delta t)^2. \tag{7.5.2}$$

---

* Here, α, β, and γ are the parameters of the algorithm and not symbols for a component.

and

$$\dot{\boldsymbol{d}}_{n+1} = \dot{\boldsymbol{d}}_n + \left[\gamma \ddot{\boldsymbol{d}}_{n+1} + (1-\gamma)\ddot{\boldsymbol{d}}_n\right]\Delta t\,, \tag{7.5.3}$$

where Δt is the time step, i.e. $\Delta t = t_{n+1} - t_n$.

Due to its nonlinearity, (7.5.1) must be solved through an iteration procedure, e.g. the Newton's methods. In the following, the Newton-Raphson method will be used. Let $\boldsymbol{e}$ be the error vector, and we can write

$$\boldsymbol{e}(\ddot{\boldsymbol{d}}_{n+1}) = \boldsymbol{z}\ddot{\boldsymbol{d}}_{n+1} + (\alpha+1)\boldsymbol{c}\dot{\boldsymbol{d}}_{n+1} - \alpha\boldsymbol{c}\dot{\boldsymbol{d}}_n + \boldsymbol{F}^{\text{int}}(\boldsymbol{d}_{n+1+\alpha}) - \boldsymbol{F}^{\text{ext}}(t_{n+1+\alpha})\,, \tag{7.5.4}$$

where, with introduction of (7.5.2) and (7.5.3), $\boldsymbol{e}$ can be expressed as a function of $\ddot{\boldsymbol{d}}_{n+1}$. Suppose that the non-convergent solution at the end of ith iteration step is $\boldsymbol{d}^i_{n+1}$. Next, we search a new solution expressed as

$$\ddot{\boldsymbol{d}}^{i+1}_{n+1} = \ddot{\boldsymbol{d}}^i_{n+1} + \Delta\ddot{\boldsymbol{d}}^{i+1}\,. \tag{7.5.5}$$

such that $\boldsymbol{e}(\ddot{\boldsymbol{d}}^{i+1}_{n+1})$ meets the specified convergence criteria with respect to certain norms. Linearizing (7.5.1) about $\ddot{\boldsymbol{d}}^i_{n+1}$ yields

$$Lin[\boldsymbol{e}(\ddot{\boldsymbol{d}}^{i+1}_{n+1})] = \boldsymbol{e}(\ddot{\boldsymbol{d}}^i_{n+1}) + \frac{d}{d\varepsilon}[\boldsymbol{e}(\ddot{\boldsymbol{d}}^i_{n+1} + \varepsilon\Delta\ddot{\boldsymbol{d}}^{i+1})]\Big|_{\varepsilon=0} = \boldsymbol{e}(\boldsymbol{d}^i_{n+1}) + \boldsymbol{\Sigma}(\boldsymbol{d}^i_{n+1})\cdot\Delta\ddot{\boldsymbol{d}}^{i+1}\,, \tag{7.5.6}$$

where $\boldsymbol{\Sigma}$ is the tangent modulus given by

$$\boldsymbol{\Sigma}(\boldsymbol{d}^i_{n+1}) = \boldsymbol{z} + (1+\alpha)\gamma\Delta t\boldsymbol{c} + (1+\alpha)\beta(\Delta t)^2\boldsymbol{\kappa}\,. \tag{7.5.7}$$

and

$$\boldsymbol{\kappa} = \frac{\partial}{\partial \boldsymbol{d}_{n+1}}[\boldsymbol{F}^{\text{int}}(\boldsymbol{d}^i_{n+1})] \tag{7.5.8}$$

An explicit form of κ will be given later. Naturally, we expect that $Lin[e(\ddot{d}^{i+1}_{n+1})] = 0$.

This leads to

$$\Delta\ddot{d}^{i+1} = -\Sigma^{-1} \cdot e(d^{i}_{n+1}) \tag{7.5.9}$$

Table 7.1 Flow chart of the solution procedure for dynamic analysis

---

1. Set iteration counter $i = 0$
2. The *predictor* phase

$$\ddot{d}^{i}_{n+1} = 0$$
$$\dot{d}^{i}_{n+1} = \tilde{\dot{d}}_{n+1} = \dot{d}_n + (1-\gamma)\Delta t\ddot{d}_n$$
$$d^{i}_{n+1} = \tilde{d}_{n+1} = d_n + \dot{d}_n\Delta t + (\frac{1}{2} - \beta)(\Delta t)^2\ddot{d}_n$$

3. Evaluate $e(\ddot{d}^{i}_{n+1})$ with (7.5.4)
4. Solve (7.5.9) for $\Delta\ddot{d}^{i+1}$
5. The *multi-corrector* phase

$$\ddot{d}^{i+1}_{n+1} = \ddot{d}^{i}_{n+1} + \Delta\ddot{d}^{i+1}$$
$$\dot{d}^{i+1}_{n+1} = \tilde{\dot{d}}_{n+1} + \Delta t\gamma\Delta\ddot{d}^{i+1}$$
$$d^{i+1}_{n+1} = \tilde{d}_{n+1} + (\Delta t)^2\beta\Delta\ddot{d}^{i+1}$$

6. Calculate $e(\ddot{d}^{i+1}_{n+1})$ with (7.5.4)
7. Check convergence

If $\left\|e(\ddot{d}^{i+1}_{n+1})\right\| / \left\|e(\ddot{d}^{0}_{n+1})\right\| \le \varepsilon_1$: and $\left\|\Delta\ddot{d}^{i+1}\right\| / \left\|\Delta\ddot{d}^{1}\right\| \le \varepsilon_2$.

Then go to next time step.

Otherwise, set $i \leftarrow i+1$ and go to 4

The iteration procedure now is simplified as follows: solve (7.5.9) for $\Delta\ddot{d}^{i}$: update $\ddot{d}$, $\dot{d}$, and d by (7.5.5), (7.5.3), and (7.5.2), respectively; check convergence; go to the

next iteration step unless the convergence criteria are satisfied. The solution scheme with a predictor/multi-corrector algorithm now is summarized in the Table 7.1.

Note that, if $\alpha = 0$, the procedure presented above reduces to the Newmark method. When parameters $\{\alpha, \beta, \gamma\}$ are chosen such that $\alpha \in [-1/3.0]$, $\beta = (1-\alpha)^2/4$, and $\gamma = (1-2\alpha)/2$, the α-method is second-order accurate and unconditionally stable (in the sense of linearization) (Hughe, 1987: Ch. 9). Decrease in α increases the amount of numerical dissipation. For a linear problem, if α is chosen as –0.3, the maximum numerical dissipation can be achieved in using the above algorithm. Such a feature of the algorithm is desirable for a dynamic analysis, since the high-frequency modes stemming from numerical discretization may induce spurious behaviors and must be damped out.

The tangent modulus defined by (7.5.8) is evaluated in the following. Similar to the other global matrices, $\boldsymbol{K}$ is obtained by assembling its element counterparts, i.e.

$$\boldsymbol{K} = \mathop{\mathbf{A}}_{e=1}^{nel} ({}^{e}\boldsymbol{K}) \tag{7.5.10}$$

For the second form of the problem, i.e. (7.3.17), $\boldsymbol{F}^{int}$ is given by (7.3.18). By definition (7.5.8), we obtain

$${}^{e}\boldsymbol{K} = \begin{bmatrix} {}^{e}\boldsymbol{K}^{11}, & {}^{e}\boldsymbol{K}^{12}, & {}^{e}\boldsymbol{K}^{13} \\ \boldsymbol{0}, & {}^{e}\boldsymbol{K}^{22}, & \boldsymbol{0} \\ \boldsymbol{0}, & \boldsymbol{0}, & {}^{e}\boldsymbol{K}^{33} \end{bmatrix} \tag{7.5.11}$$

where the components of ${}^{e}\boldsymbol{K}^{22}$ and ${}^{e}\boldsymbol{K}^{33}$ have been given in (FE2-4) and (FE2-5), respectively; and the components of ${}^{e}\boldsymbol{K}^{11}$, ${}^{e}\boldsymbol{K}^{12}$, and ${}^{e}\boldsymbol{K}^{13}$ are given as

$$ {}^{e}\kappa^{11}_{ikAB} = \int_{\Omega^e} N^S_{A,j} C^S_{ijkl} N^S_{B,l} dV = \int_{\Omega^e} N^S_{A,j} \frac{\partial(\sigma_{ij})_{n+1}}{\partial(\varepsilon_{kl})_{n+1}} N^S_{B,l} dV , \tag{7.5.12} $$

$$ {}^{e}\kappa^{12}_{iAB} = \int_{\Omega^e} N^S_{A,j} c^W_{ij} N^W_B dV = \int_{\Omega^e} N^S_{A,j} \frac{\partial(\sigma_{ij})_{n+1}}{\partial p^W_{n+1}} N^W_B dV , \tag{7.5.13} $$

and

$$ {}^{e}\kappa^{13}_{iAB} = \int_{\Omega^e} N^S_{A,j} c^N_{ij} N^N_B dV = \int_{\Omega^e} N^S_{A,j} \frac{\partial(\sigma_{ij})_{n+1}}{\partial p^N_{n+1}} N^N_B dV \tag{7.5.14} $$

where C^S_{ijkl}, c^W_{ij}, and c^N_{ij} are the tangent moduli consistent with the stress-point algorithm used to integrated the stress-strain relationship. Hence, they are usually called the consistent (or algorithmic) tangent moduli. It is noted that, although C^S_{ijkl} possesses minor symmetry, i.e. $C^S_{ijkl} = C^S_{jikl}$ and $C^S_{ijkl} = C^S_{ijlk}$, in general, $C^S_{ijkl} \neq C^S_{klij}$.

For the first form of the problem, i.e. (7.2.11), $\boldsymbol{F}^{\text{int}}$ is given by (7.2.13), and we write

$$ {}^{e}\boldsymbol{K} = \begin{bmatrix} {}^{e}\boldsymbol{K}^{11}, {}^{e}\boldsymbol{K}^{12}, {}^{e}\boldsymbol{K}^{13} \\ {}^{e}\boldsymbol{K}^{21}, {}^{e}\boldsymbol{K}^{22}, {}^{e}\boldsymbol{K}^{23} \\ {}^{e}\boldsymbol{K}^{31}, {}^{e}\boldsymbol{K}^{32}, {}^{e}\boldsymbol{K}^{33} \end{bmatrix} \tag{7.5.15} $$

Similarly, the components of ${}^{e}\boldsymbol{K}^{mn}(m,n = 1,2,3)$ can be obtained by (7.5.8) with incorporation of (7.2.4) and (7.2.5). It is noted that, for the hyperelestoplastic model, (7.5.15) is symmetric to the extent if ${}^{e}\boldsymbol{K}^{11}$ possesses major symmetry, i.e. $C^S_{ijkl} = C^S_{klij}$.

In a computational procedure, the consistent tangent moduli can be replaced by the continuous moduli (e.g. the elastoplastic modulus) without deteriorating the accuracy of the results. As shown by Simo and Taylor (1985), however, use of the continuous moduli sometimes may drastically deteriorate the rate of the convergence.

7.6 Solution Procedures: Quasi-Static Analysis

For the quasi-static problems, e.g. the fluid diffusion or consolidation of the porous media, the inertial terms can be dropped, and (7.2.11) or (7.3.17) becomes

$$\boldsymbol{c}\dot{\boldsymbol{d}} + \boldsymbol{F}^{\text{int}}(\boldsymbol{d}) = \boldsymbol{F}^{\text{ext}}(t) \tag{7.6.1}$$

(7.6.1) can be solved by using the one-step generalized trapezoidal family of methods (Hughes, 1983), which consists of the following equations:

$$\boldsymbol{c}\dot{\boldsymbol{d}}_{n+1} + \boldsymbol{F}^{\text{int}}(\boldsymbol{d}_{n+1}) = \boldsymbol{F}^{\text{ext}}_{n+1}, \tag{7.6.2}$$

$$\boldsymbol{d}_{n+1} = \boldsymbol{d}_n + \Delta t\dot{\boldsymbol{d}}_{n+\theta}, \tag{7.6.3}$$

and

$$\dot{\boldsymbol{d}}_{n+\theta} = (1-\theta)\dot{\boldsymbol{d}}_n + \theta\dot{\boldsymbol{d}}_{n+1}, \tag{7.6.4}$$

where $\boldsymbol{F}^{\text{ext}}_{n+1} \approx \boldsymbol{F}^{\text{ext}}(t_{n+1})$ and $\theta \in [0,1]$. Notably, if $\theta \geq 0.5$, the generalized trapezoidal methods are unconditionally stable (for linear problems). Some of the well-known methods belonging to this family include the forward Euler method ($\theta = 0$), backward Euler method ($\theta = 1$), and Crank-Nicolson method ($\theta = 0.5$). If $\theta \geq 0.5$, this family of methods is unconditionally stable; otherwise, it is conditionally stable.

The Newton-Raphson method will be used to solve the nonlinear equation (7.6.2). Linearizing (7.6.2) about $\boldsymbol{d}^i_{n+1}$ and using (7.6.3) and (7.6.4), we derive

$$\boldsymbol{e}(\boldsymbol{d}^{i+1}_{n+1}) = \boldsymbol{e}(\boldsymbol{d}^i_{n+1}) + \boldsymbol{\Sigma}(\boldsymbol{d}^i_{n+1})\Delta\boldsymbol{d}^{i+1}, \tag{7.6.5}$$

where

$$\boldsymbol{\Sigma}(\boldsymbol{d}^i_{n+1}) = \boldsymbol{c} + \Delta t\theta\boldsymbol{\kappa} \tag{7.6.6}$$

and

$$\boldsymbol{e}(\boldsymbol{d}^{t}_{n+1}) = [\theta\Delta t\boldsymbol{F}^{ext}_{n+1} + (1-\theta)\Delta t\boldsymbol{c}\dot{\boldsymbol{d}}_{n} + \boldsymbol{c}\boldsymbol{d}_{n}] - \theta\Delta t\boldsymbol{F}^{int}(\boldsymbol{d}^{t}_{n+1}) - \boldsymbol{c}\boldsymbol{d}^{t}_{n+1}, \quad (7.6.7)$$

Forcing the right-hand side of (7.6.5) to be zero leads to

$$\Delta\boldsymbol{d}^{i+1} = -\boldsymbol{\Sigma}^{-1}\cdot\boldsymbol{e}(\boldsymbol{d}^{i}_{n+1}) \quad (7.6.8)$$

The solution procedure is implemented as described in Table 7.2.

Table 7.2 Flow chart of the solution procedure for quasi-static analysis

---

1. Set iteration counter $i = 0$
2. Calculate $\boldsymbol{e}(\boldsymbol{d}^{i}_{n+1})$ through (7.6.7).
3. Solve (7.6.8) for $\Delta\boldsymbol{d}^{i}$.
4. Update solution, $\boldsymbol{d}^{i+1}_{n+1} = \boldsymbol{d}^{i}_{n+1} + \Delta\boldsymbol{d}^{i}$.
5. Calculate $\boldsymbol{e}(\boldsymbol{d}^{i+1}_{n+1})$ through (7.6.7).
6. Check convergence:

   If $\|\boldsymbol{e}(\boldsymbol{d}^{i+1}_{n+1})\| / \|\boldsymbol{e}(\boldsymbol{d}^{0}_{n+1})\| \le \varepsilon$, go to next time step;

   Otherwise, set $i = i + 1$, and go to Step 3.

7.7 Some Remarks on Implementation

The second form of IBVP, i.e. (7.3.17), and its solution procedures have been implemented into a FORTRAN code, where $\boldsymbol{u}^{S}$, p^{W}, and p^{N} are used as nodal variables. In this semi-discrete finite element equation, coefficients $\mathcal{G}^{\beta}_{I}$, $\mathcal{G}^{\beta}_{\dot{I}}$, and $\mathcal{G}^{\beta}_{J}$ ($\beta = W, N$) remain to be evaluated (see (7.3.13)-(7.3.15)). They can be determined by integrating the constitutive relationships for the volume fractions of fluids. In a simpler

way, these coefficients may be obtained as follows. For geomaterials the bulk modulus of the solid component is very large so that the density of solid phase remains approximately constant. From the mass balance equation of the solid component, i.e. $m^{s} = (\det \boldsymbol{F}) n^{s} \rho^{s} = const$, one may derive

$$\dot{n} = \dot{n}^{s} \approx -n^{s} \boldsymbol{I} : \dot{\boldsymbol{u}}^{s} = -(1-n) \boldsymbol{I} : \dot{\boldsymbol{u}}^{s} \tag{7.7.1}$$

where n is the porosity, and use of $\dot{\rho}^{s} \approx 0$ has been made. In addition, $n^{w} = nS_{r}$ and $n^{a} = n(1-S_{r})$, where S_{r} is the degree of saturation. Hence, if a relationship between the degree of saturation and matric suction (sometimes called the moisture retention curve) is given, one may evaluate ϑ_{1}^{β}, ϑ_{2}^{β}, and ϑ_{3}^{β} through (7.3.13)-(7.3.15).

With ϑ_{1}^{β}, ϑ_{2}^{β}, and ϑ_{3}^{β} being evaluated in this way, (7.3.17) has a desirable feature that when the porous media becomes saturated (7.3.17) will change *smoothly* into its saturated counterpart. If the degree of saturation S_{r} tends to 100%, i.e. $p^{a} - p^{w} \to 0$, it follows that $\vartheta_{1}^{a} \to 0$, $\vartheta_{2}^{a} \to 0$, and $\vartheta_{3}^{a} \to 0$, and element matrix (7.3.22) becomes

$$^{e}\boldsymbol{C} = \begin{bmatrix} \boldsymbol{0}, & \boldsymbol{0}, & \boldsymbol{0} \\ {}^{e}\boldsymbol{C}^{21}, {}^{e}\boldsymbol{C}^{22} + {}^{e}\boldsymbol{C}^{23}, & \boldsymbol{0} \\ \boldsymbol{0}, & \boldsymbol{0}, & \boldsymbol{0} \end{bmatrix}. \tag{7.7.2}$$

Therefore, (7.3.17) collapses into the finite element formulation of saturated soils developed by Zienkiewicz and Shiomi (1984). In the computer code, switching an element from an unsaturated state into a saturated state (or *vice versa*) now is very simple. In fact, if one element becomes saturated (i.e. the matric suction is less than the

air entry value), it only needs to set the relative permeability of the nonwetting fluid in this element to a small value, and nothing else needs to be changed in the code. Based on numerical tests, this small quantity may be chosen as $k_r^N = 0.0001$. The above procedure allows the computer code to have capability of simultaneously handling both saturated and unsaturated conditions. It is shown from the numerical examples in the next chapter that the above procedure works very well.

Chapter 8 NUMERICAL EXAMPLES

The finite element discretization and numerical time integration procedures developed in Chapter 7 have been implemented into a FORTRAN finite element code called U_DYSAC2. U_DYSAC2 was created by modifying a saturated soil code DYSAC2 (Muraleetharan et al. 1988; 1997). In the new code, displacement ($\boldsymbol{u}$) and fluid pressures (p^{w} and p^{a}) are used as nodal variables. Four-node quadrilateral elements are employed for both displacement and pressures. Discussions on the merits and drawbacks of this kind of elements are abundant the literature (e.g., Belytschko et al., 2000: pp.451-461). It is believed that this kind of elements is more efficient than the higher-order elements for hyperbolic problems whose solutions are generally not smooth. The elastic models presented in Chapter 5 and the elastoplastic model developed by Muraleetharan and Nedunuri (1998) have been implemented into a constitutive driver that can be readily modified to include other constitutive models. The new code allows for static and dynamic 2-D (or 1-D) analysis of saturated and unsaturated porous media.

This chapter presents the numerical simulations of different kinds of problems. To validate the finite element code and the corresponding procedures, numerical results will be compared with analytical solutions or experimental data whenever it is possible.

8.1 Elastic Response of a Saturated Soil Column Subjected to Loading

The problem is defined in Figure 8.1a. A one-dimensional infinite soil column is separated from a half space consisting of a soil deposit saturated by an *incompressible* fluid. On the surface, the soil column is subjected to a load (traction) $f(t)$. It is assumed that the surface is a drained boundary (free boundary). Analytical solution of the problem has been presented by de Boer et al.(1993). This example is introduced to demonstrate the capability of the code in capturing the incompressibility conditions and to check the efficiency of the procedure introduced at the end of Chapter 7 to switch to the saturated conditions.

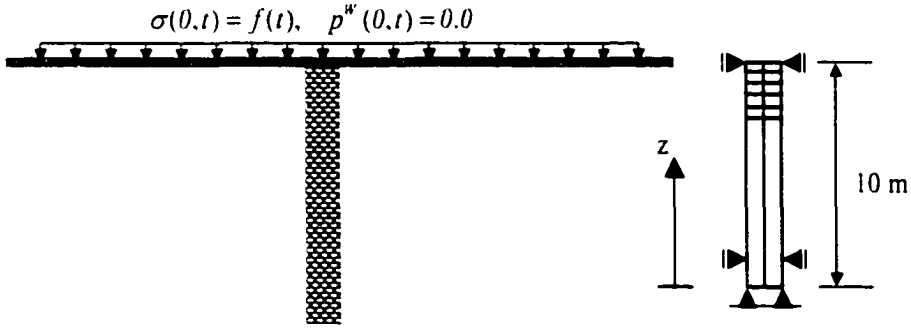

a) Geometry of the problem b) Finite element mesh: 20×2 elements

Figure 8.1 A soil column subjected to a load

In order to model the infinite soil column by using the finite element method, a soil column with a length of 10 m is considered. The solution will be reported for a very short time period so that no reflection wave from the *rigid* bottom boundary could influence

the solution. The finite element mesh used is schematically given in Fig. 8.1b. Two different kinds of loading are considered as given below:

Sinusoidal loading: $f(t) = 3.0[1 - \cos(\omega t)]$ [kPa], $\omega = 75\ s^{-1}$

Step loading: $f(t) = 3.0H(t)$ [kPa].

where $H(t)$ is the Heaviside function. The material parameters are

$$\rho^s = 2000\ kg/m^3, \quad \rho^w = 1000\ kg/m^3,$$
$$n^s = 0.67, \quad K_w = 1.0 \times 10^{10}\ kPa, \quad k = 0.01\ m/s$$
$$\lambda = 5583\ kPa, \quad \mu = 8375\ kPa$$

It is noted that K_w assumes a very large value due to the incompressibility of the fluid.

The numerical displacements and pore water pressures at various depths are reported and compared with the analytical solutions in Fig. 8.2 and 8.3, respectively. Fig. 8.4 presents the vertical displacements with depth at different times. In all the comparisons, the numerical results agree favorably with the analytical solutions. Fig. 8.2a shows some numerical oscillation at the early phase. This problem is induced by a sudden application of the step loading. As can be seen from Fig. 8.2b, however, no difference can be observed between the analytical and numerical displacements under the sinusoidal loading. Similar trends are observed in comparing the numerical and analytical pore water pressures (Fig. 8.3). Under the step loading, although the numerical oscillation in the pore water pressures is more prominent than that in the displacement, agreement between the numerical and analytical pore water pressures is reasonably good.

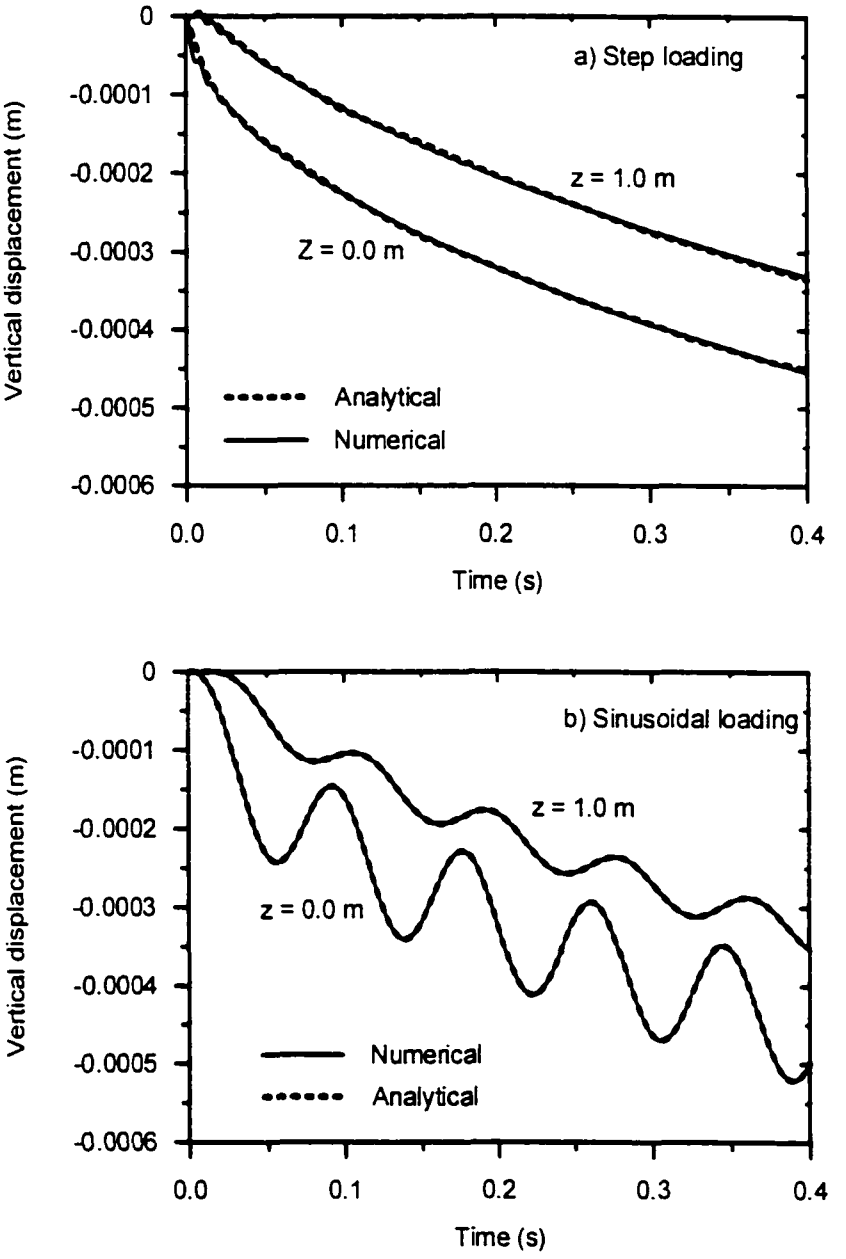

Figure 8.2 Comparisons of numerical and analytical solutions for vertical displacements at depth *0.0 m* and *1.0 m*

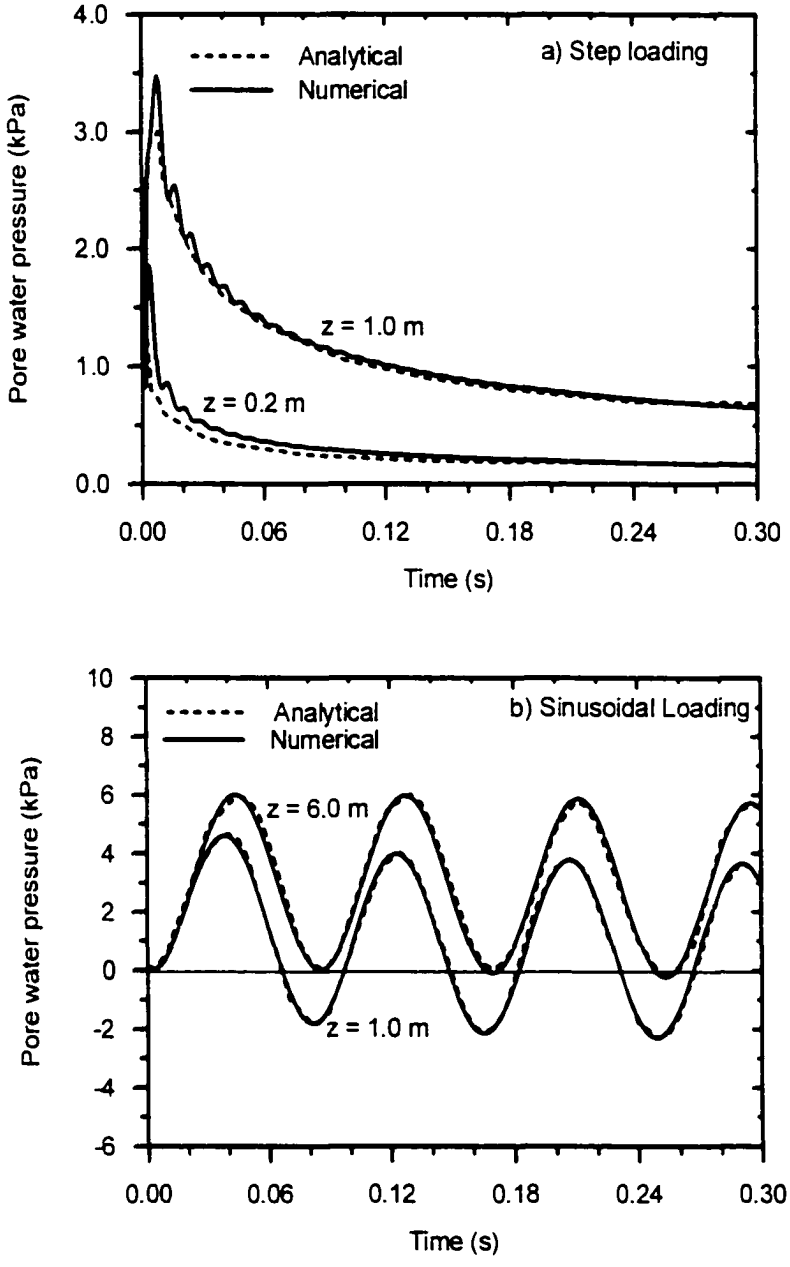

Figure 8.3 Comparisons of numerical and analytical solutions for pore water pressures at various locations

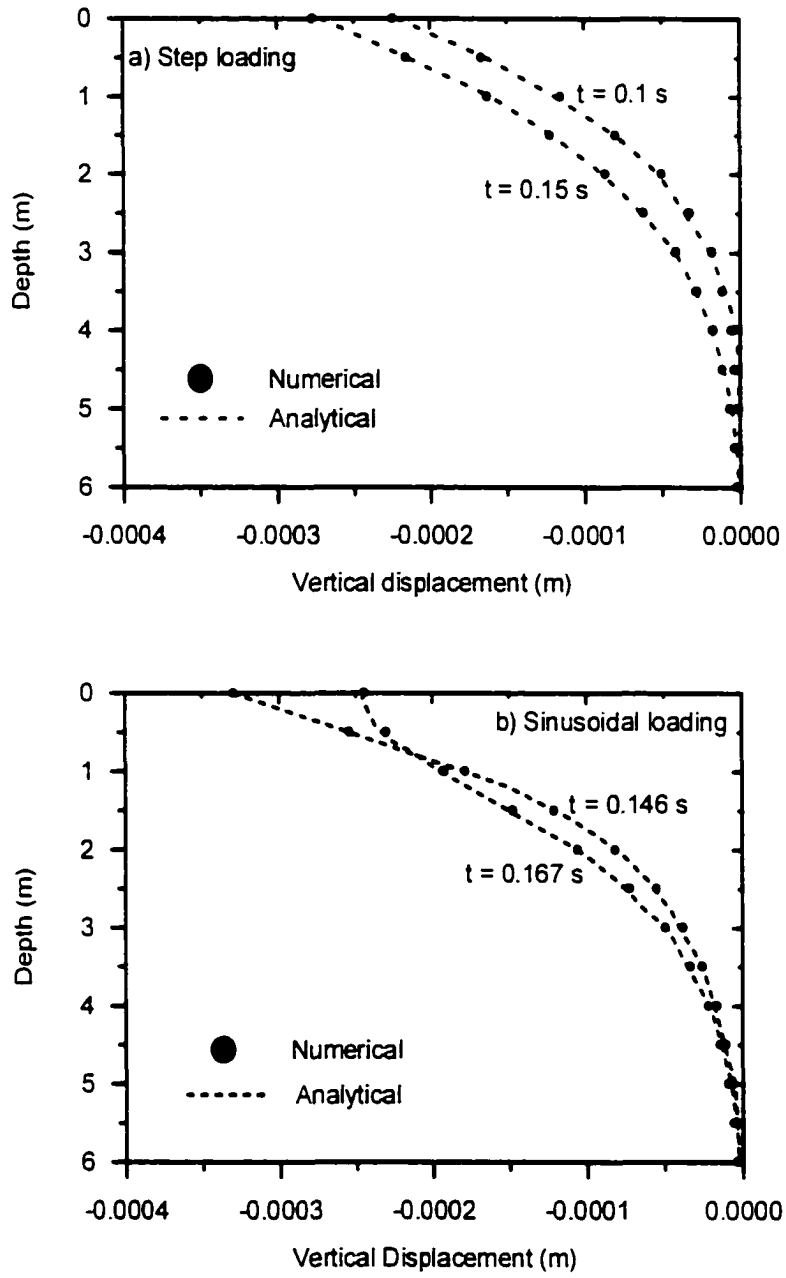

Figure 8.4 Comparisons of the numerical and analytical solutions for the vertical displacements along the column

It is noted that in this analysis the porous medium is considered as a three-phase material. The numerical results show that the procedure introduced in the last chapter to switch the saturation condition works very well. In fact, under both loading conditions (i.e., step and sinusoidal), the *virtual* air pressures (not shown) are found to be equal to the water pressures in all elements. That is, the matric suctions in all elements are always zero.

8.2 Propagation of a Step Displacement through an Unsaturated Soil Column

The geometry of this problem is the same as Fig. 8.1a. At the top boundary, instead of a specified load, a step displacement with amplitude of $1.0 \times 10^{-5} m$ is applied. The soil column used in numerical simulation has a height of 4.0 cm. The finite element mesh consists of four hundred elements with a dimension of 0.01cm. The element size and time step values have been selected such that there is enough time for the fastest wave to travel from one node to another. This can be done by first estimating the wave velocity based on the given material constants, and the wave velocities are used to estimate the element and time step sizes. The soil column is partially saturated with a degree of saturation equal to 70%. The material parameters are given as below.

$$\rho^{S} = 2700\ kg/m^{3},\ \rho^{W} = 1000\ kg/m^{3},\ \rho^{N} = 12.3\ kg/m^{3},$$
$$\lambda = 6.923 \times 10^{4}\ kPa,\ \mu = 4.615 \times 10^{4}\ kPa,$$
$$K_{w} = 2.177 \times 10^{6}\ kPa,\ n^{S} = 0.4,\ k = 1.0 \times 10^{-4}\ m/s$$

In addition, the relationship between suction and degree of saturation is described by the Brooks and Corey formulation, in which $S_{res} = 0.4$, $\lambda = 0.5$, and $p_{b} = 10$ kPa.

Numerical displacement and pore pressures are, respectively, given in Fig. 8.5 and 8.6 for two locations along the depth, i.e. *0.5 cm* and *2.0 cm*. Fig. 8.5 shows that the fronts of the three compressional waves merge into a single wave front. This is an expected result, since in the finite element code, the fluid pressures are used as nodal variables and the relative accelerations of the fluids are omitted. As discussed in Chapter 6, omitting the relative accelerations results in additional constraints over the wave propagation. In this case, all the three components coexisting in the porous media move together. It can be seen from Fig. 8.5 that numerical oscillation occurs at the moment when the wave front arrives. It is also noted that the sharp wave front is smeared out to some extent. This is the typical behavior resulting from using the so-called $u-p$ formulation to simulate the wave propagation problems (Simon et al., 1986; Gajo et al., 1994).

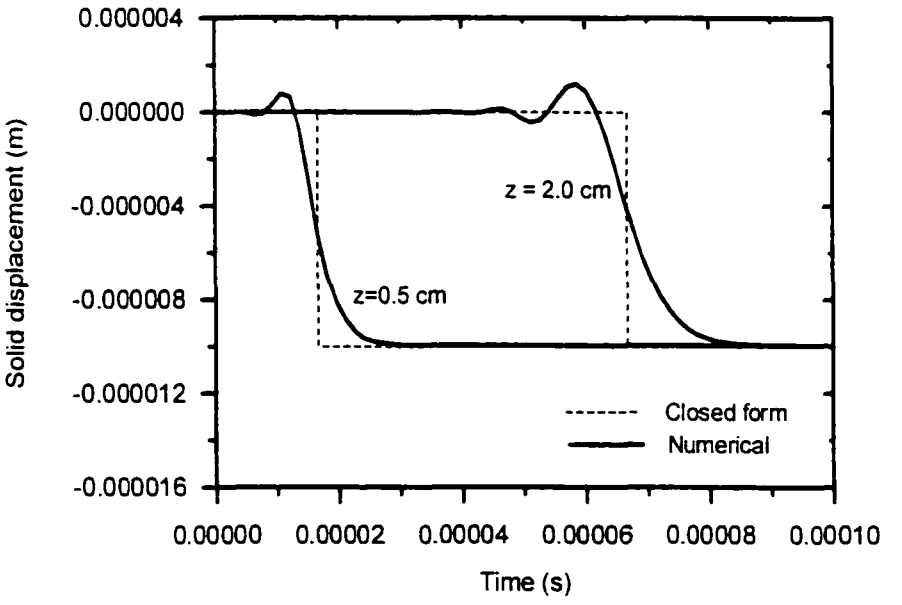

Figure 8.5 Time history of the vertical displacements at depth of 0.5 cm and 2.0 cm

The responses of air and water pressures are presented in Fig. 8.6. Both water and air pressures increase rapidly when the wave front arrived. After the wave front left, they reduced to the original values. At the same time, the suction experienced a decrease followed by an increase. This result may be explained as follows. From the finite element formulations (FE2-2) and (FE2-3), it is noted that if the inertial effects is neglected the changes in fluid pressures are determined by the changes in $\dot{m}^w$ and $\dot{m}^s$. It can be seen from (7.3.10) that $\dot{m}^\beta$ is determined by the volumetric strain rate ($\dot{u}_{i,i}$), the rate of volume fraction ($\dot{n}^\beta$), and the rate of mass density ($\dot{\rho}^\beta$). Before the wave front arrives or after the wave front leaves, the change in $\dot{m}^\beta$ is insignificant, since $\dot{\varepsilon}_v (= \dot{u}_{i,i})$, $\dot{n}^\beta$ and $\dot{\rho}^\beta$ remains approximately zero. Hence, the fluid pressures will take their original values. At the arrival of the wave front, however, $\dot{\varepsilon}_v$ will be changed drastically, leading to sudden changes in water and air pressures as shown in Fig. 8.6.

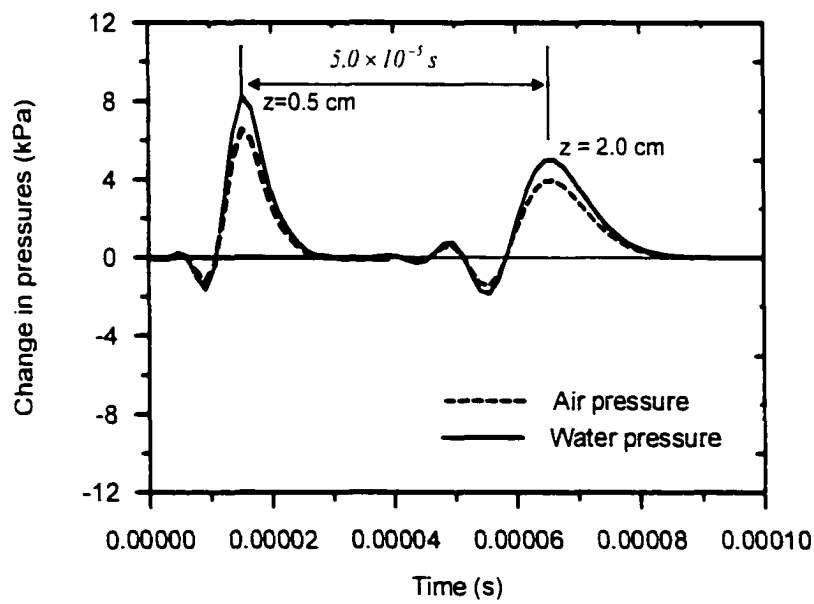

Figure 8.6 Pore water and air pressure responses at depth *0.5 cm* and *2.0 cm*.

Fig. 8.6 clearly shows that the value of wave velocity is about $(1.5\times10^{-2})\div(5.0\times10^{-5})\approx 300\ m/s$. This value can also be obtained by using equation (6.2.12). Since the relative accelerations of fluids have been omitted in the $u-p^{w}-p^{a}$ finite element formulation, (6.2.12) can be used to evaluate the wave velocity as discussed in Chapter 6. Here, due to its incompressibility, the solid phase have a very large bulk modulus, say, $K_s = 1.0\times10^{10}\ kPa$, and $\lambda_{,e}^{s} = 0.0\ kPa$. From (5.4.6) and (6.3.7), one may obtain $\lambda_s = 1.161\times10^{5}\ kPa$ and $\mu_s = 0.774\times10^{5}\ kPa$. Finally, assuming $\lambda_{,m}^{w} = \lambda_{,m}^{a} = 0.0$, one evaluates (6.2.12) and get $v_{,m}\approx 299\ m/s$. This result confirms the consistency between the linear models derived in Chapter 5 and the general model that has been developed in Chapter 4 and implemented into the finite element procedure in Chapter 7.

8.3 A Two-Phase Flow Problem

The problem is based on an experiment performed by Liakopoulos (1965) on a column of Del Monte sand (see Fig. 8.7). The sand column was instrumented to measure the matric suction at several points along the column during its desaturation. Before the start of the experiment, water was continuously injected from the top until a uniform flow condition was achieved solely under gravitational force. The water was allowed to drain freely at the bottom through a porous stone. Once the experiment started, the water supply on the top ceased and the tensiometor reading was activated. During the experiment, the air could flow freely through top boundary. The Del Monte sand had a porosity of 0.3, and its hydraulic properties were measured in an independent set of

experiments (Liakopoulos, 1965). The relationships between the degree of saturation and matric suction and relative permeability of water are given below,

$$S_r = 1.0 - 0.10152 \times \left(\frac{S_M}{9.81} \right)^{2.427} , \tag{8.3.1}$$

and

$$k_r^w = 1.0 - 2.207 \times (1.0 - S_r)^{1.0121} \tag{8.3.2}$$

where S_M is the matric suction with a unit kPa. Since in Liakopoulos's work no formulation was given for the relative permeability of the air, the Brook and Corey's relative permeability function of air (Brooks and Corey, 1964) will be used, i.e.

$$k_r^a = (1.0 - S_e)^2 \times (1.0 - S_e)^{5/3}, \; S_e = \frac{S_r - S_{rw}}{1.0 - S_{rw}} \tag{8.3.3}$$

The mechanical parameters of Del Monte sand are not available either. Hence, typical values of the material parameters for sand are selected and they are listed in Table 8.1.

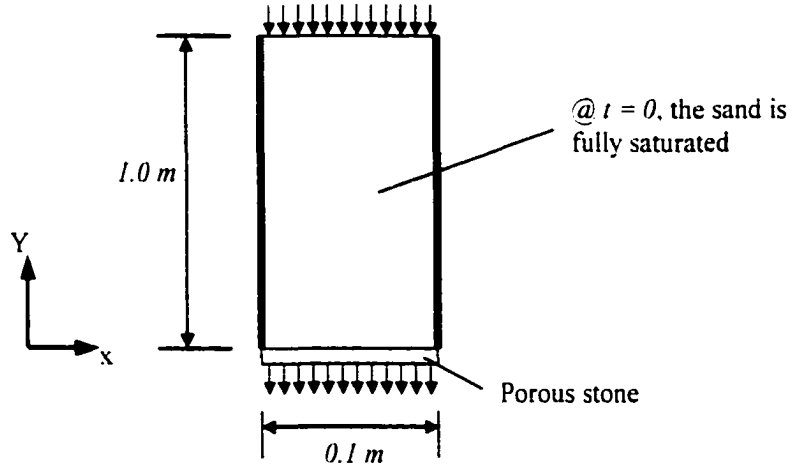

Figure 8.7 Schematic of Liakopoulos' experiment (Liakopoulos, 1965)

Table 8.1 Material parameters of Del Monte sand

Material parameters	Symbols	Values
Young's modulus	E	$1.5\times10^{4}\ kPa$
Poisson ratio	ν	0.2
Solid grain density	ρ^{S}	$2.0\times10^{3}\ kg/m^{3}$
Water density	ρ^{W}	$1.0\times10^{3}\ kg/m^{3}$
Air density	ρ^{N}	$1.2\ kg/m^{3}$
Bulk modulus of water	K_{w}	$2.2\times10^{6}\ kPa$
Water viscosity	η_{w}	$1.0\times10^{-3}\ Pa\cdot s$
Air viscosity	η_{N}	$1.8\times10^{-5}\ Pa\cdot s$
Intrinsic permeability	k	$4.5\times10^{-13}\ m^{2}$

For the numerical simulation, the above experiment was viewed as a 1-D problem, and 20 elements with a size of $0.05m\times0.1m$ was used. The boundary conditions are defined as follows:

@ the lateral sides: $u_{x}=0.0\ w_{n}^{W}=0.0;\ w_{n}^{N}=0.0$

@ the top: $w_{n}^{W}=0.0;\ p^{N}=0.0\ kPa$

@ the bottom: $u_{x}=u_{y}=0.0;\ p^{W}=p^{N}=0.0\ kPa$

where $p^{\beta}(\beta=W,N)$ represents the part of fluid pressure in excess of the atmospheric pressure; w_{n}^{β} is relative velocity of a fluid in the direction normal to the boundary. At $t=0.0$, the sand column is fully saturated and at a *mechanical* equilibrium state. Hence, $u_{x}=u_{y}=0.0$, $S_{r}=1.0$, and $p^{N}=0.0\ kPa$. Since the water is *initially* in a uniform flow

condition under gravitational force, the vertical gradient of potential equals to gravitational acceleration, i.e.

$$\frac{\partial}{\partial y}\left(\frac{p^{w}}{\rho^{w}} + gy\right) = g \qquad (8.3.3)$$

It follows from (8.3.3) that $p^{w} = 0.0\ kPa$ at $t = 0.0$. The initial stress states can now be obtained by solving the steady state equation with constraints $p^{w} = p^{a} = 0.0\ kPa$. Once the initial conditions are obtained, we can proceed to the numerical simulation of the experiment. Note that at $t = 0.0$ the fluid (water) is not in *static* equilibrium. Hence, in the numerical simulation, the initial condition (8.3.3) must be considered. This is done through activating the gravitational forces of the fluids at the moment the simulation process commences.

The numerical results are presented in Fig. 8.8 through Fig. 8.13. Experimental data are available only for the pore water pressures along the column at 5, 10, 20, 30, 60, and 120 minutes. No air pressure, degree of saturation, and displacement were recorded in Liakopoulos' experiment. It can be seen from Fig. 8.8 and 8.9 that the agreement between the numerical prediction and measured results is very good for the times after 30 minutes. Before 30 minutes, however, the pore water pressures decrease faster than the measured results in the numerical predictions. The values of pore water pressures in the early stages are very sensitive to the air entry value of the porous material. Unfortunately, the air entry value of Del Monte sand is not available (it was chosen as $7\ kPa$ in this example). Both analytical and experimental results in Fig. 8.9 shows that once the water supply at the top ceased, the pore pressures decrease rapidly and then tends to a stable value until the whole system attains a static equilibrium state.

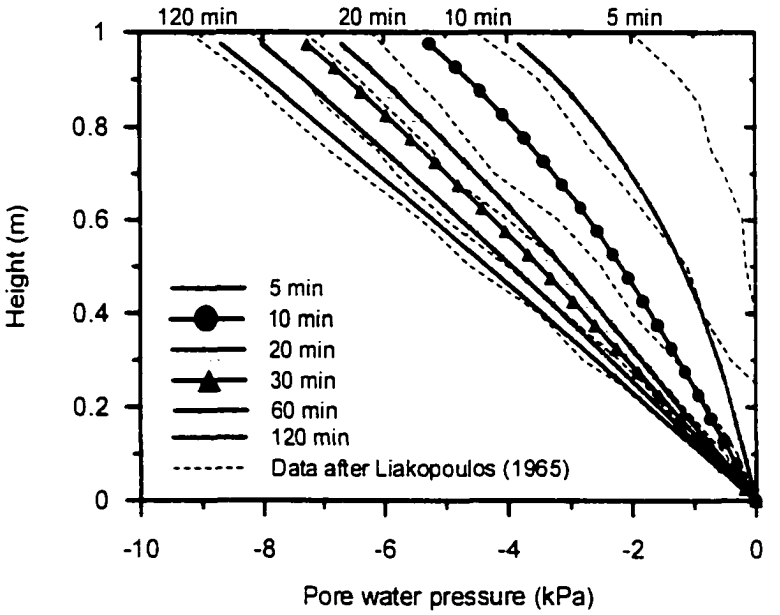

Figure 8.8 Comparisons of numerical predictions and experimental results for the pore water pressures along the sand column

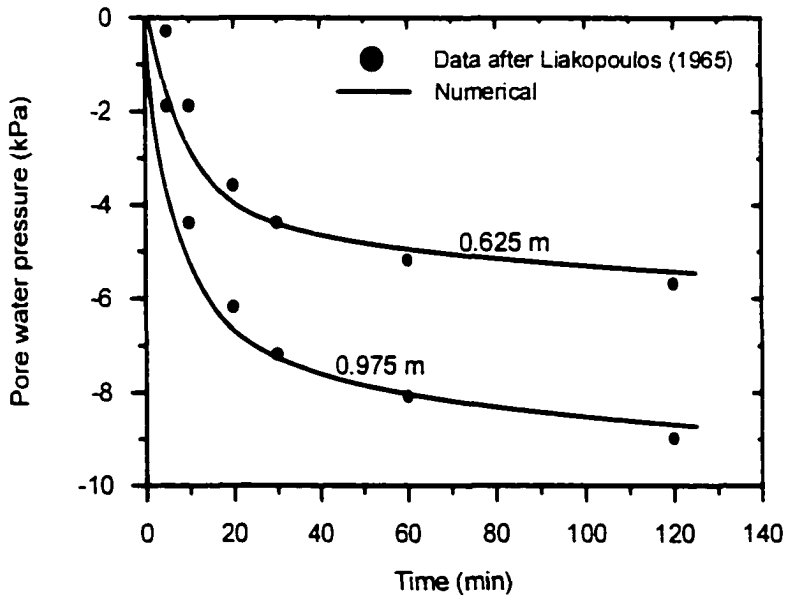

Figure 8.9 Comparison of numerical predictions and experimental results for the pore water pressures at height *0.975 m* and *0.625 m*

The pore air pressures along the soil column are presented in Fig. 8.10. At a certain depth, air pressure first decreases to a minimal value and then increases again. This dissipation process can be seen in Fig. 8.11. From these results, it is noted that air pressure may become significant in a multiphase flow process so that the so-called passive air phase assumption usually made in the analysis of two-phase flow is not acceptable. Evolutions of the degree of saturation at various depths are depicted in Fig. 8.12. The sand column became unsaturated in the upper part (from *0.4-1.0 m*). Fig. 8.13 describes evolution of the vertical displacement along the sand column. It can be seen that the deformation of the solid skeleton and the fluid flow are coupled.

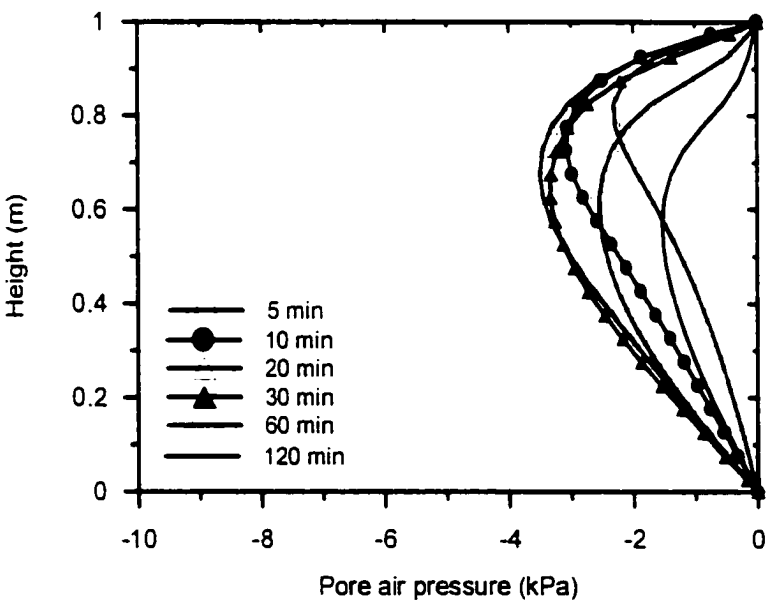

Figure 8.10 Evolution of the pore air pressure profile based on the numerical predictions

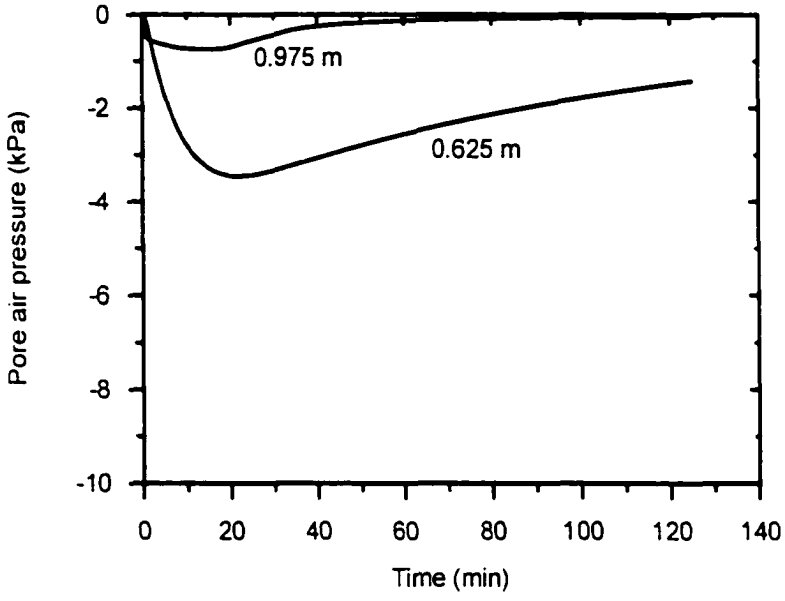

Figure 8.11 Time history of the pore air pressures at height *0.975 m* and *0.625 m* based on the numerical predictions

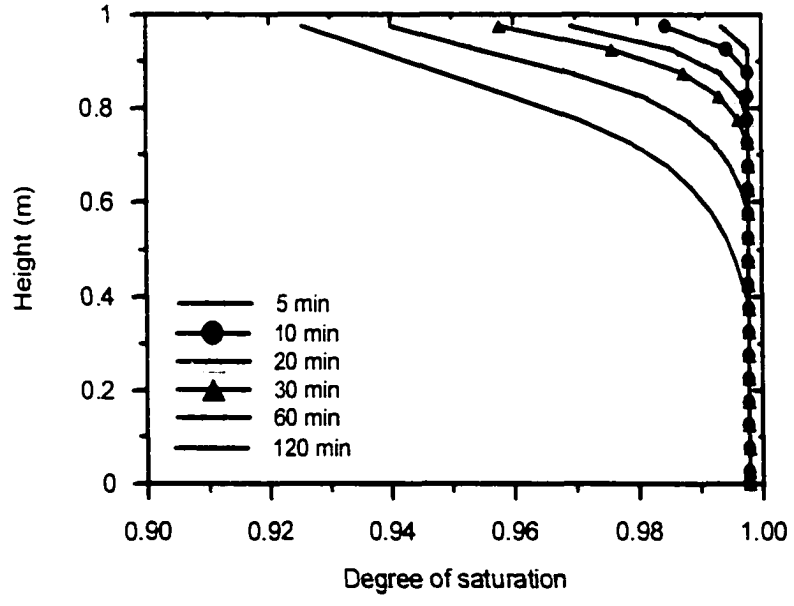

Figure 8.12 Evolution of the degree of saturation profile based on the numerical predictions

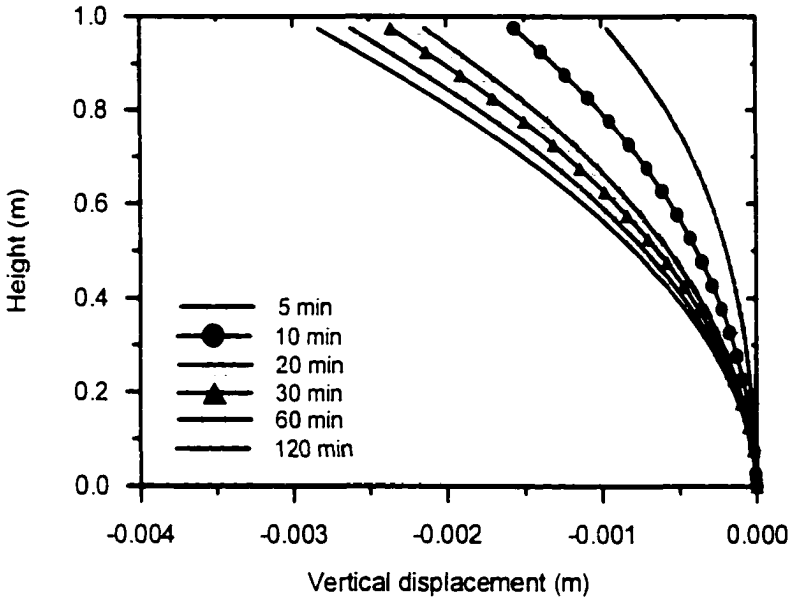

Figure 8.13 Evolution of the vertical displacement profile based on the numerical predictions

8.4 Flooding of a Centrifuge Model Embankment

This example is based on the centrifuge model test of a compacted Minco silt embankment that was originally performed to examine the settlement associated with flooding. A detailed analysis of the centrifuge test has been presented by Miller et al.(2000). Since for the time being we are unable to calibrate an elastoplastic constitutive model based on the swelling/collapse behavior of the Minco silt*, a comprehensive numerical analysis of the experimental results is impossible. In the following, however, this example is introduced to demonstrate how the numerical procedure developed in this

* A laboratory test program to obtain the stress-strain behavior of Minco silt is ongoing at the University of Oklahoma.

dissertation can be used to simulate some important behaviors of an unsaturated soil embankment subjected to flooding.

The centrifuge testing procedure is briefly given below. Well-prepared moist soil was compacted into three equal layers in the centrifuge box to the target dry unit weight. It was then carefully shaped into the chosen geometry. The miniature pore water pressure transducers and LVDTs are placed into various locations to measure the matric suction and displacement. At the first stage, the centrifuge was gradually brought up to an acceleration of 165g and then water was introduced through the bottom of the embankment. The geometry of the embankment and the instrumentation are schematically shown in Fig. 8.14. The time histories of the acceleration and water level are given in Fig 8.15.

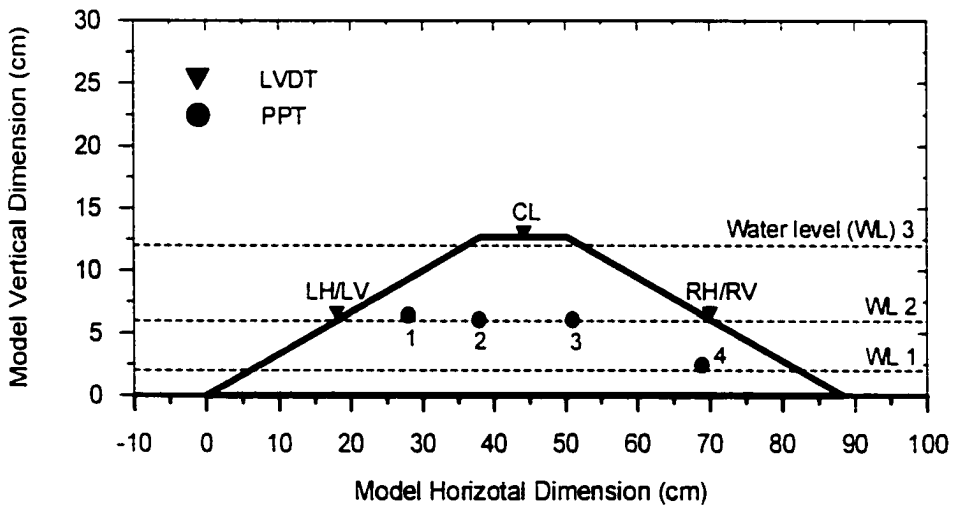

Figure 8.14 Model dimension and instrumentation for centrifuge model #3 (after Miller et al. (2000))

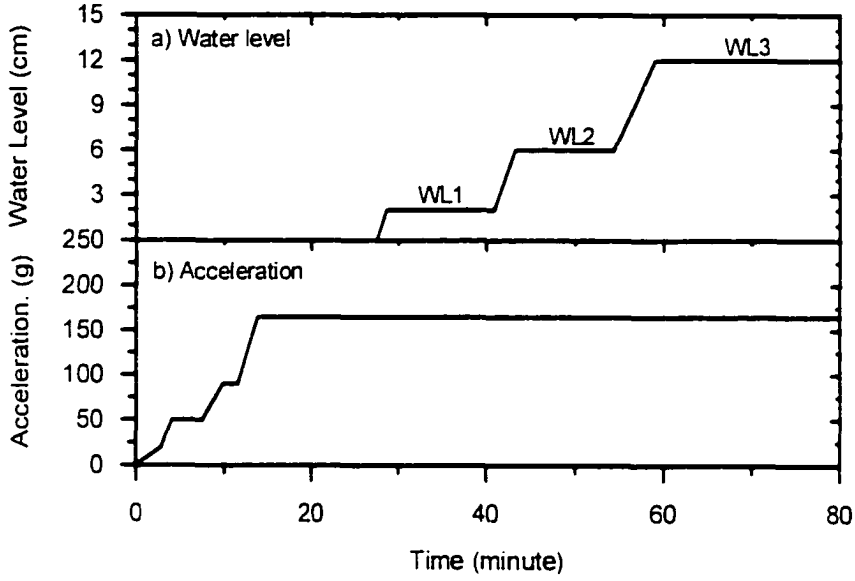

Figure 8.15 Time histories of water level and spin acceleration

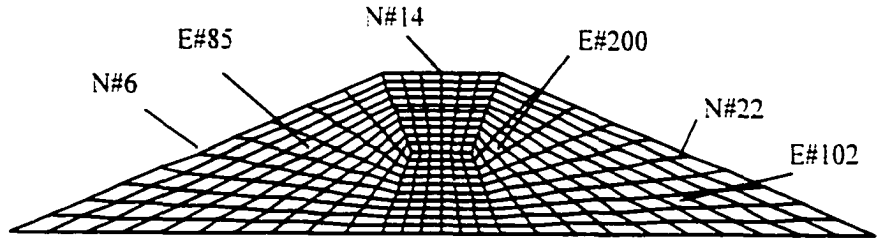

Figure 8.16 Finite element mesh of the centrifuge model embankment

Table 8.2 Material parameters of Minco silt

Material parameters	Symbols	Values
Young's modulus	E	$1.2\times10^{4}\ kPa$
Poisson ratio	ν	0.3
Solid grain density	ρ^{s}	$2.69\times10^{3}\ kg/m^{3}$
Water density	ρ^{w}	$1.0\times10^{3}\ kg/m^{3}$
Air density	ρ^{a}	$1.2\ kg/m^{3}$
Bulk modulus of water	K_w	$2.2\times10^{6}\ kPa$
Water viscosity	η_w	$1.0\times10^{-3}\ Pa\cdot s$
Air viscosity	η_a	$2.0\times10^{-5}\ Pa\cdot s$
Intrinsic permeability	k	$6.03\times10^{-12}\ m^{2}$

The finite element mesh used in the analysis is shown in Fig. 8.16. The material properties of Minco silt are summarized in Table 8.2. The relationship between matric suction and specific moisture content for Minco silt has been obtained by Muraleetharan and Granger (1999). This relationship can be represented by the Brooks and Corey formulation, in which $S_{rw}=0.25$, $\lambda=0.95$ and $p_b=3.0\ kPa$.

All the results are reported in the prototype scale obtained by multiplying the model scale by the acceleration scaling factor (i.e. 165). The predicted horizontal displacement of Node #22 is given in Fig. 8.17, and the predicted vertical displacements of Node #6, #22, and #14 are presented in Fig. 8.18a), b), and c), respectively. It is noted that the displacements during the ponding period do not agree well with the measured values.

This result is expected, since the embankment is collapsible when it is wetting. On the other hand, a calibrated constitutive model capable of describing the collapse of the unsaturated soils is not included in the current version of the finite element code, and only an elastic model is used here. Except for the flooding time period, the predicted displacements in the early spin-up period (< 35 hrs) are still acceptable when compared to the measured results. This may be explained as follows. During the early stage of spinning, the centrifuge acceleration was low and the embankment deformed elastically, and that was captured by the code. When the acceleration increased, the embankment behaved plastically. In this case, an elastoplastic constitutive model should be introduced to describe the material behavior. This example shows that a constitutive model capable of realistically describing the material behavior is crucial for a numerical analysis.

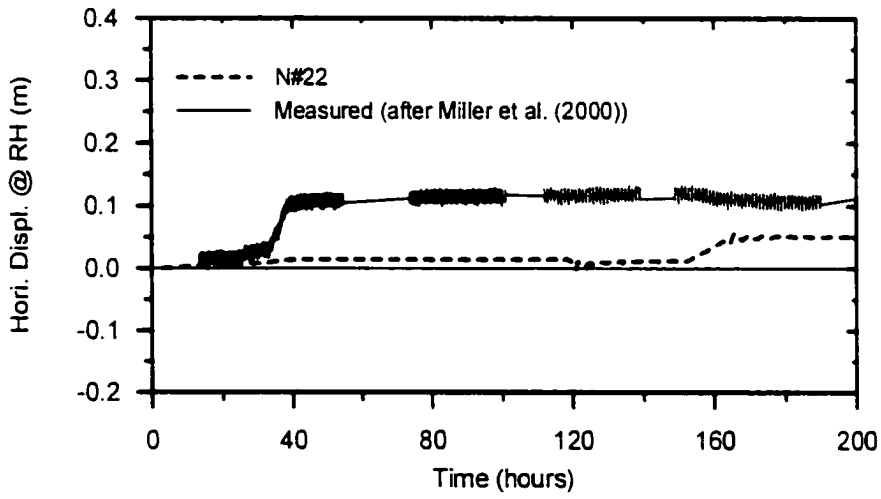

Figure 8.17 Comparison of the predicted horizontal displacement at Node # 22 with the measured results

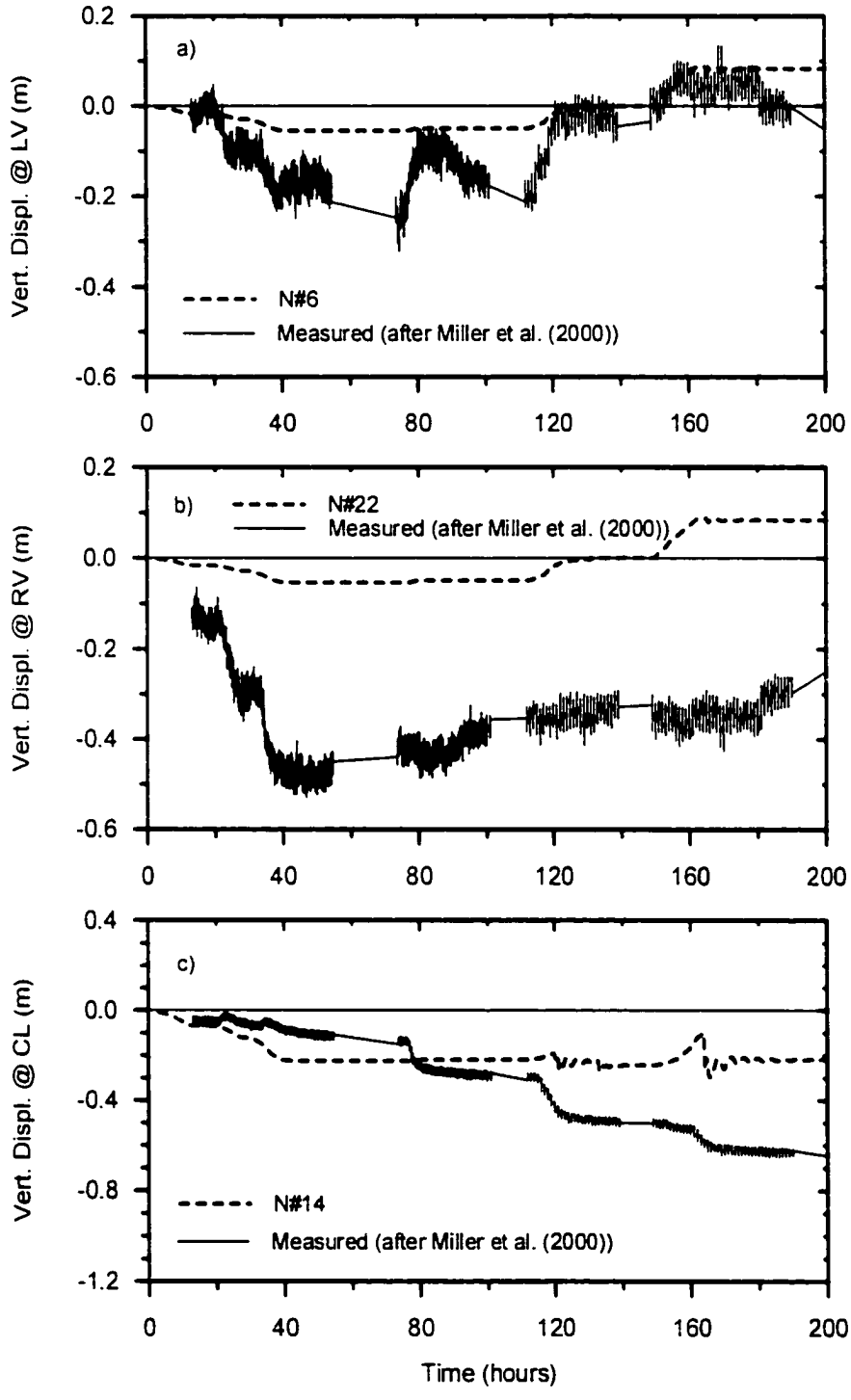

Figure 8.18 Comparison of predicted vertical displacements with the measurements

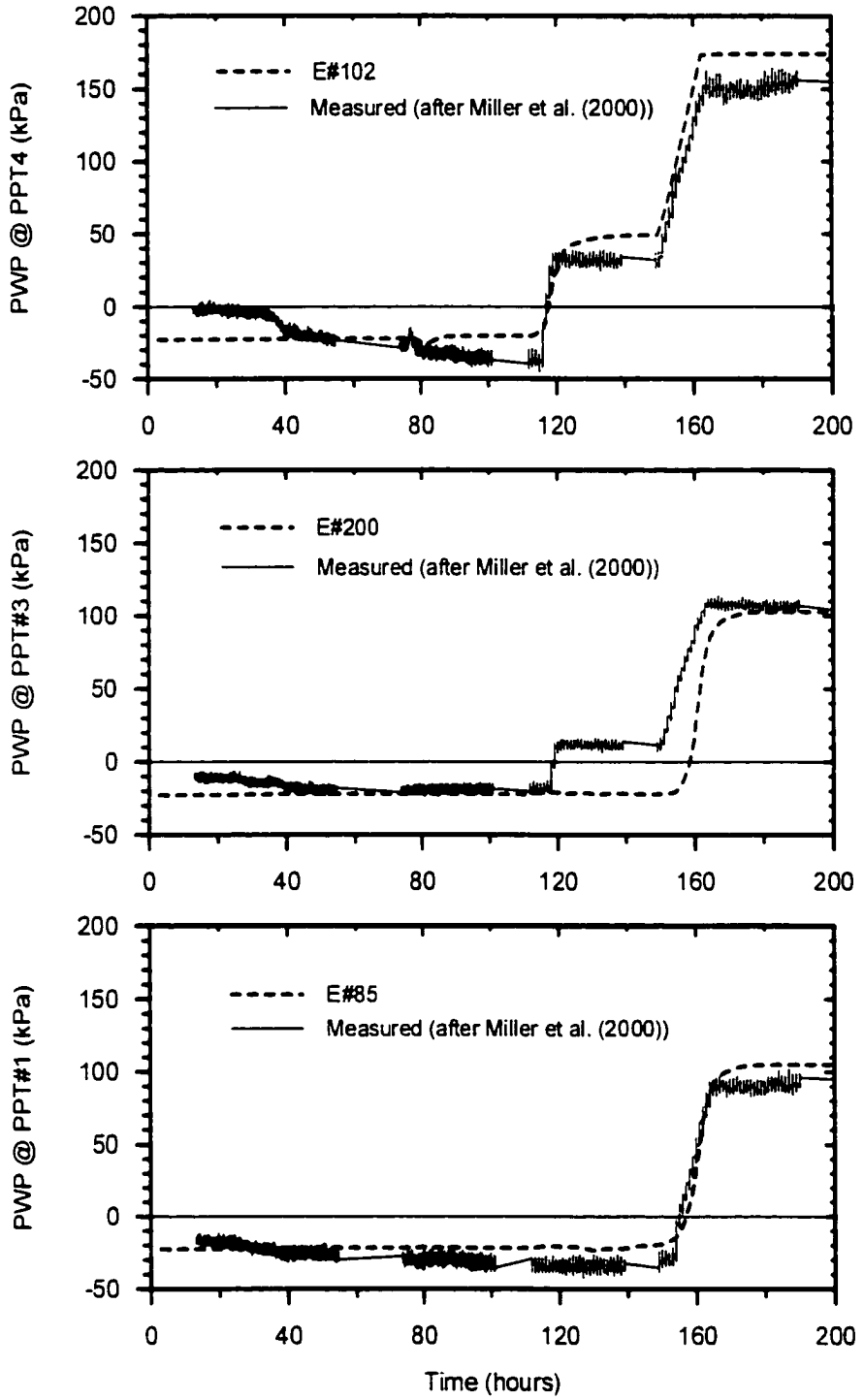

Figure 8.19 Comparisons of the predicted pore water pressures with the measurements

As compared to the predicted displacements, the predicted pore water pressure agrees well with measured results in general. This can be seen from Fig. 8.19. The numerical simulation properly depicts the evolving trends and the magnitudes of the pore water pressures around the locations of PPT1 and PPT4. At PPT3, the numerical pore water pressure is lower than the measured result during the time that the second water level (WL2) was increased, although both have similar values at the final stage. It needs to be pointed out that the deformation of soil matrix and the flow of fluid are coupled. If other constitutive models are alternately used in the analysis, numerical results may be somewhat different from those given in Fig. 8.19. However, inclusion of a more realistic constitutive model into the analysis procedure may improve the above numerical results.

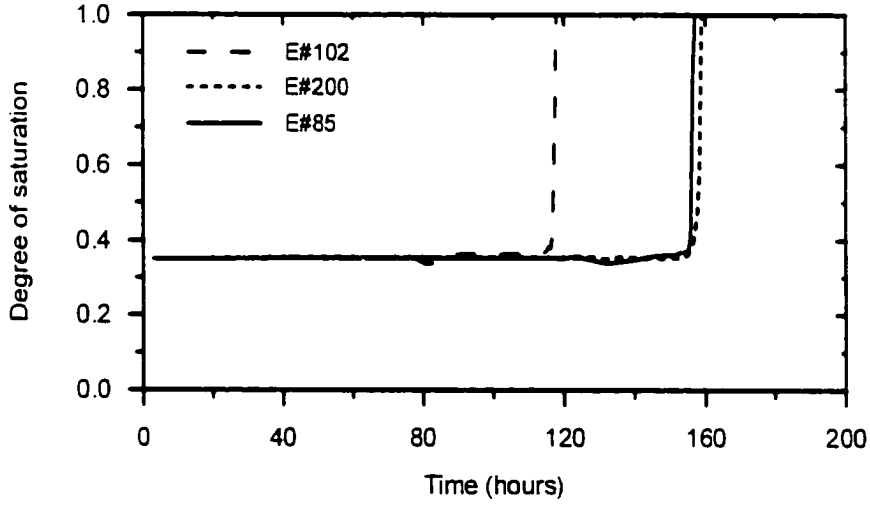

Figure 8.20 Changes in the degree of saturation of Element #85, #102, and #200.

The predicted changes in the degree of saturation of Element #85, 102 and 200 are described in Fig. 20. During the first increase in the water level, the moisture contents of

these elements change very slightly. All the three elements become fully saturated after the third water level increase. It is noted that the elements become saturated in a very short time. This is the typical behavior of silts and sands, since they generally have larger pores than clayey soils and hence their intrinsic permeability is relatively large.

8.5 An Embankment Subjected to Earthquake Loading

The finite element discretization of the embankment considered in the analysis is shown in Fig. 8.21. The embankment represents a speswhite kaolin centrifuge model tested by Kutter (1982). Kutter's (1982) models were constructed using saturated kaolin and subjected to base shaking. Additional details of the centrifuge model tests and the dynamic analysis of the *saturated* embankment using the computer code DYSAC2 (Muraleetharan et al. 1988, 1997) are presented by Muraleetharan et al. (1994).

Here, the numerical analysis is performed for the same embankment but it is assumed that the upper part of the embankment is unsaturated (Fig. 8.21). The initial degree of saturation of the unsaturated zone is 88%. For the unsaturated kaolin, the stress-strain behavior was modeled using a bounding surface elastoplastic model (Muraleetharan and Nedunuri 1998). Necessary unsaturated model parameters were obtained from suction controlled triaxial tests on kaolin (Wheeler 1996). All the model parameters pertaining to unsaturated kaolin are summarized in Table 8.3. Other bounding surface model parameters common to both the saturated and unsaturated soil can be found in Muraleetharan et al. (1994). The relationship between the matric suction and the degree of saturation is described by the Brooks-Corey relationship (1964). Permeability

coefficients of air and water were also varied according to the Brooks-Corey relationship (1964) starting with the values given in Table 8.3.

Table 8.3. Hydraulic and Mechanical Properties of Kaolin Used in the Analysis

Properties	Symbol	Value
Density of solid grains	ρ^s	$2620\ kg/m^3$
Density of water	ρ^w	$1000\ kg/m^3$
Density of air	ρ^a	$1.22\ kg/m^3$
Bulk modulus of water	K_w	$2.2 \times 10^6\ kPa$
Initial Bulk modulus of air	K_a	$100\ kPa$
Porosity	n	0.596
Intrinsic permeability	k	$1.7 \times 10^{-16}\ m^2$
Viscosity of water	η_w	$1.0 \times 10^{-6}\ kPa\ s$
Viscosity of air	η_a	$1.7 \times 10^{-10}\ kPa\ s$
Brooks-Corey (1964) Parameters:		
Residual volumetric water content	θ_r	0.1
Pore size distribution index	λ	0.5
Bubbling pressure	p_b	$75\ kPa$
Slope of the isotropic compression line on void ratio-mean net stress plot (Wheeler 1996)	$\lambda(S_{sf})$	0.128
Parameters describing the change of λ with suction (Alonso et al. 1990)	r	1.570
	β	0.013
Value of specific volume on the isotropic compression line when net mean stress is one atmospheric pressure (Wheeler 1996)	$N(S_{sf})$	2.122
Slope of the rebound line on void ratio-mean net stress and void ratio-suction plots (Wheeler 1996)	κ	0.02

Slope of the critical state line on deviatoric stress-net mean stress plot on the compression side (Wheeler 1996)	$M_c(S_M)$	*0.933*
Intersection of the critical state line on the deviatoric stress axis (Wheeler 1996)	$\mu(S_M)$	*54.2 kPa*

Note: S_r = degree of saturation, S_M = matric suction and the parameters dependent on suction are indicted with a S_M in the parenthesis.

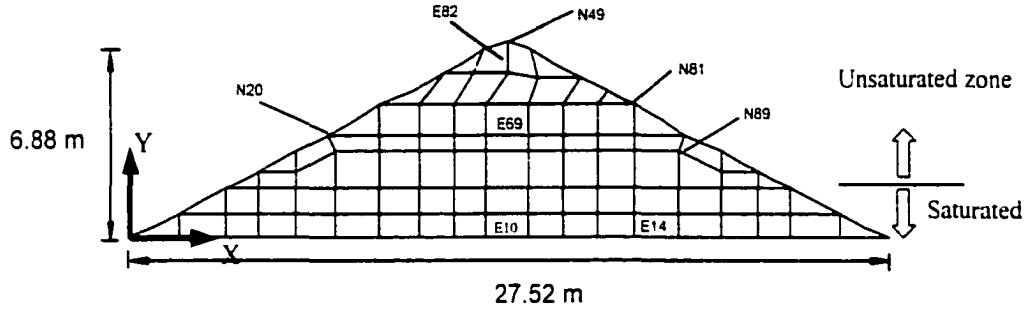

Figure 8.21 Finite element discretization of the kaolin embankment

The stress states before shaking (i.e. the initial stress states) are obtained by solving the steady state equation in Chapter 7 and depicted in the stress contours (Fig. 8.22). The embankment was subjected to the base motion shown in Fig. 8.25c. Numerical results are summarized in figures from 8.23 to 8.26. For comparison purposes, the behavior of the saturated embankment predicted by the previous analysis (Muraleetharan et al. 1994) are also shown. Although the analyses were conducted at the model (centrifuge) scale, all the results are presented in the prototype scale.



a) Contours of $\sigma_{xx} + p^{w}$ (kPa)



b) Contours of $\sigma_{yy} + p^{w}$ (kPa)



c) Contours of τ_{xy} (kPa)

Figure 8.22 Initial net stress contours of the embankment

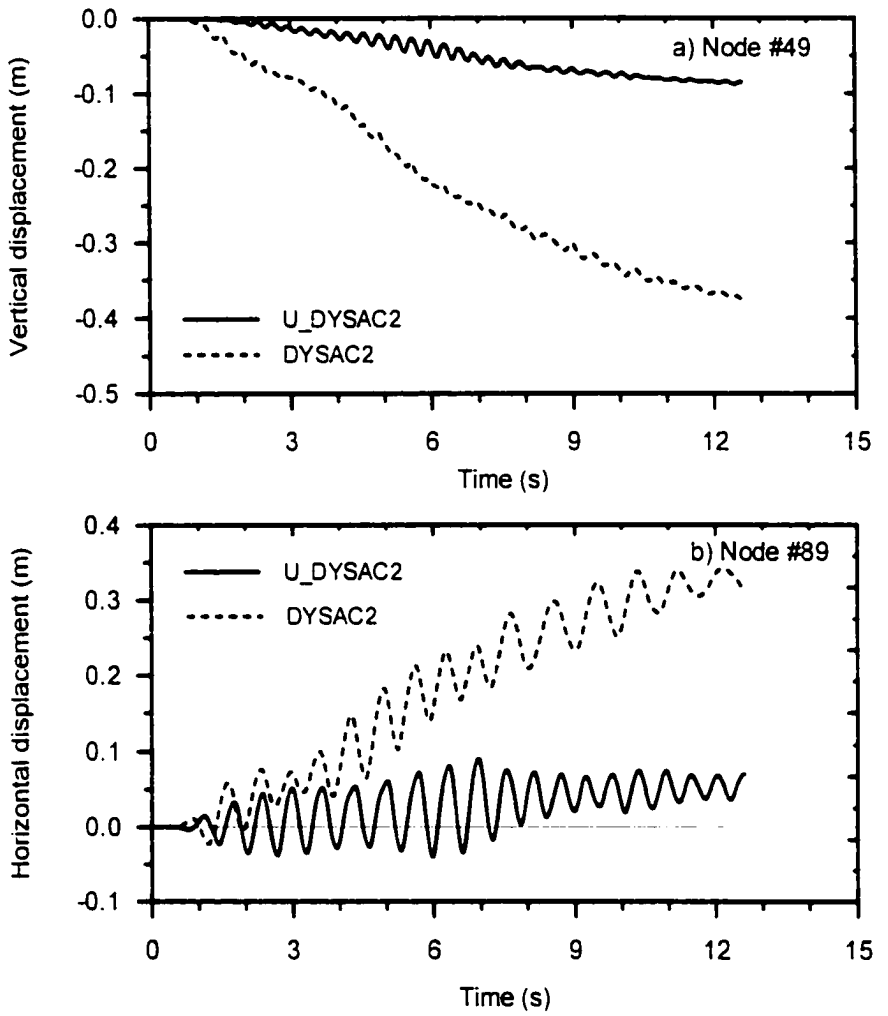

Figure 8.23 Time histories of the displacements at node #49 and #89

Fig. 8.23 presents the predicted time histories of the displacements at Node #49 and #89. The displacements of the *saturated* embankment obtained by DYSAC2 are also given. It can be seen that the *unsaturated* embankment experiences much less displacement than its saturated counterpart. This is of course expected, since the

desaturation always leads the embankment to become more rigid. Therefore, analyzing an embankment as an unsaturated soil embankment is economical for design purpose. Of course, one has to know the moisture history of the embankment throughout its lifetime before such analysis can be performed.

Fig. 8.24 gives the pore water pressure evolutions of Element #10, #14, and #69. The pore air pressure of Element #69 where the soil is unsaturated is also given. Fig. 8.24a) shows that both air and water pressures increase slightly during the shaking. It can also be seen that change in the matric suction ($p^{a} - p^{w}$) is very small. This can be explained as follows. The permeability of the kaolin is very small so that no significant change in degree of saturation may occur during the shaking. In this case, the change in matric suction is basically controlled by the volumetric strain (for Element #69, $\varepsilon_{vol} = 1.3\%$). Hence, the suction of element #69 would not experience significant change.

Element #10 and #14 are saturated, where positive excessive pore water pressure is accumulated (see Fig.8.24b and c). It is noted that in Element #14 the water pressure experiences significant oscillation. In Element #10, however, the water pressure shows more monotonic increase. This represents the effects of shear stress. It will be shown later that the shear stress field in Element#14 experienced significant change. The acceleration time histories of Element #82 are shown in Fig. 8.25. For both horizontal and vertical accelerations, the predicted values by U_DYSAC2 are larger than those predicted by DYSAC2. This again implies that the partially saturated embankment is more rigid than its fully saturated counterpart.

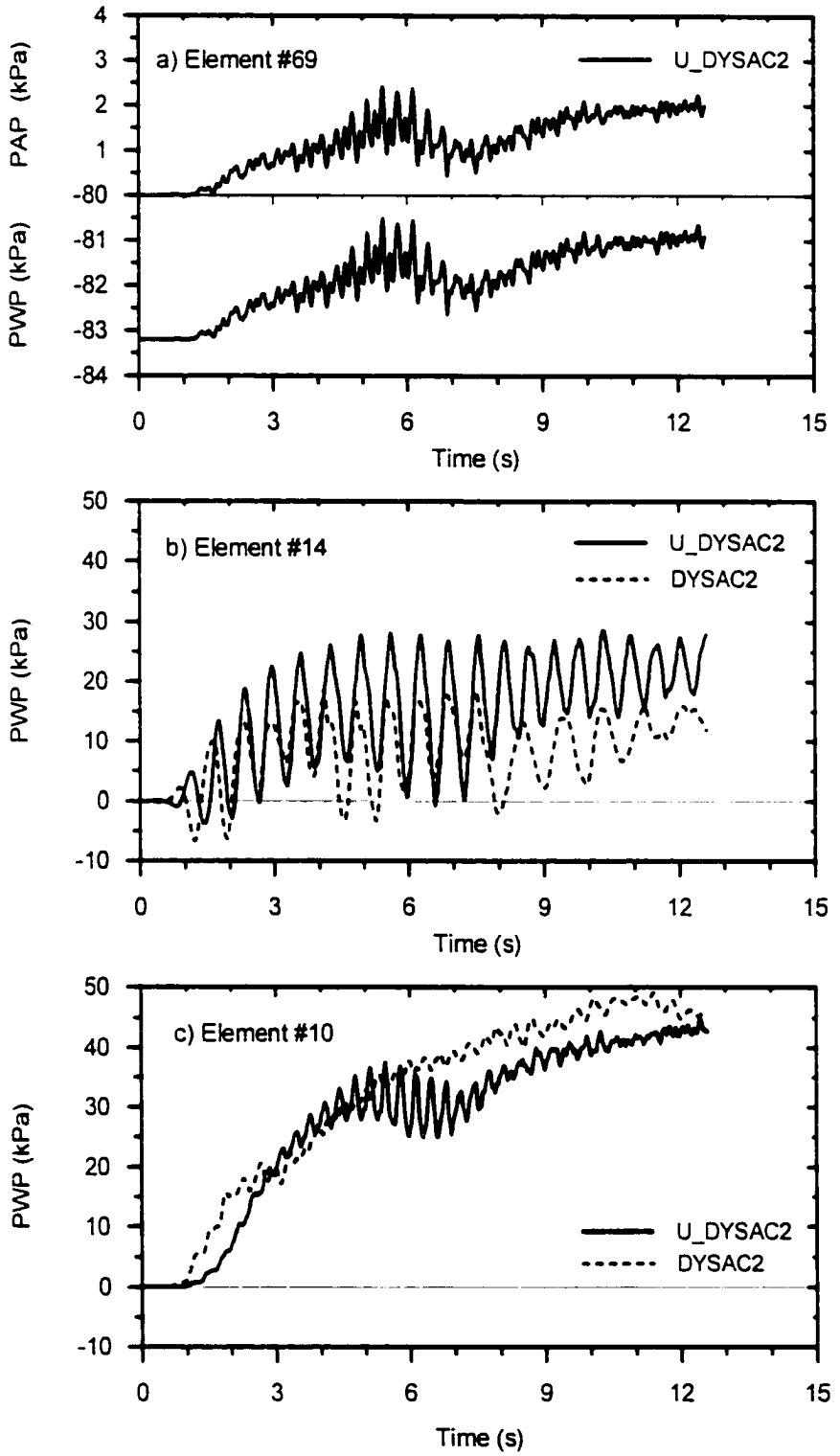

Figure 8.24 Time histories of the pore pressure in Element #10, #14, and #69

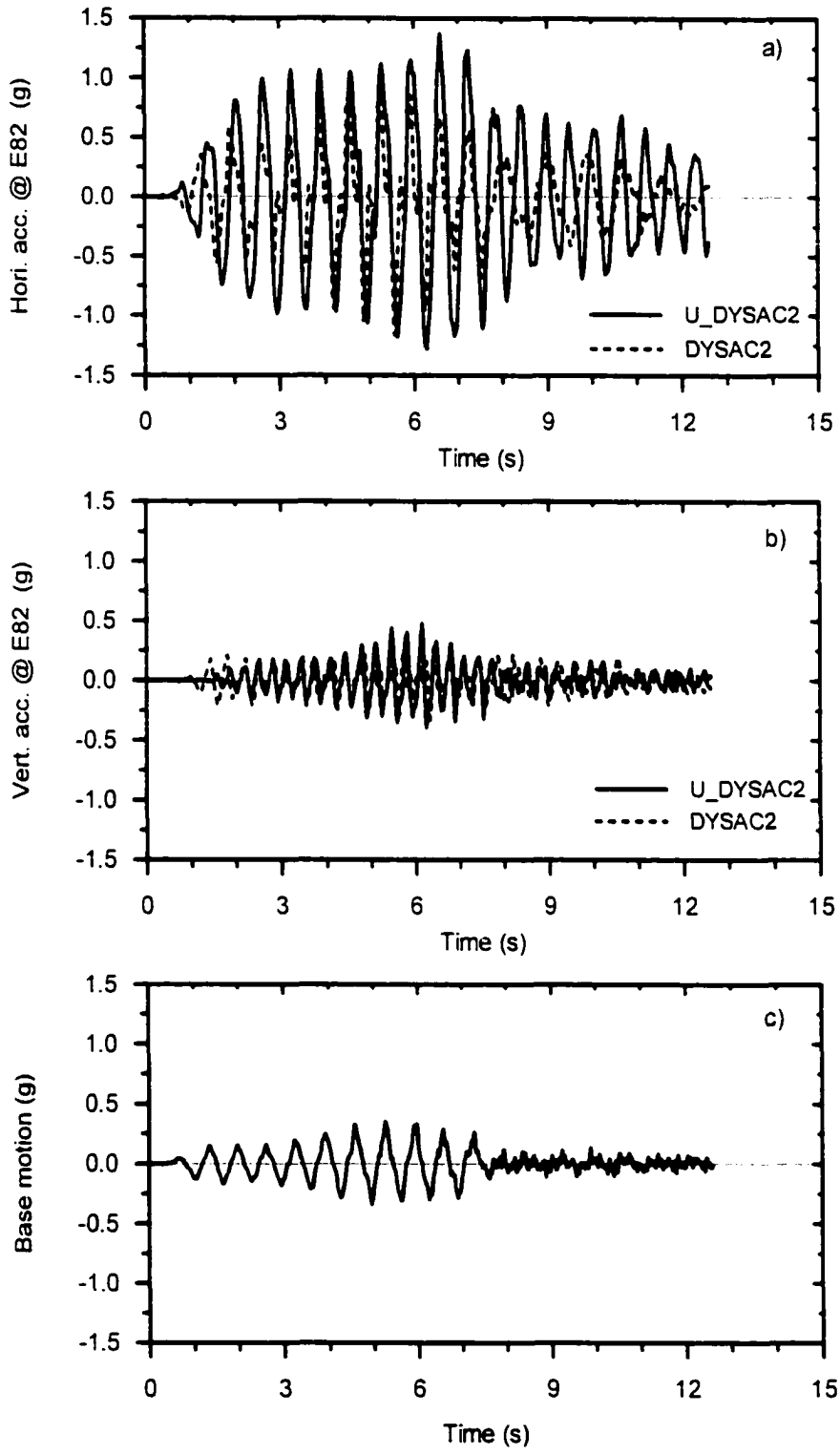

Figure 8.25 Time histories of the accelerations of Element # 82 and the base motion



a) Contours of $\sigma_{xx} + p^{w}$ (kPa)



a) Contours of $\sigma_{yy} + p^{w}$ (kPa)



a) Contours of τ_{xy} (kPa)

Figure 8.26 Stress contours at 15.5 seconds

The stress contours at 15.5 seconds are presented in Fig. 8.26. Compared with Fig. 8.22, it can be seen that all the stress fields have experienced significant change during the shaking event. Keeping in mind that in the saturated zone $p^{a} = p^{w}$ and the net stresses equals to the effective stresses, it can be noted from Fig. 8.26a that significant amounts of pore air (water) pressure has built up in the unsaturated (saturated) zone. This can also be seen in Fig. 8.26b. In the area near the toes, where σ_{yy} is small, the net stress ($\sigma_{yy} + p^{a}$) or effective stress ($\sigma_{yy} + p^{w}$) is very small due to the built-up of the fluid pressures, and the stresses are concentrated around the core of the embankment. Comparing Fig. 8.26c and Fig. 8.22c shows that the shear stress concentration has moved toward the toes on both sides. This is the typical mode of shear failure for an embankment. Also, it is noted that the shear stress in the central area did not have significant change. Since the soil in the central area was subjected to less initial shear stress than the other zones of the embankment, its stress state is further from the critical state line. This may explain the cause that a relatively smooth response of pressures is usually observed in this area as noted above (see, also, Muraleetharan et al., 1994).

8.6 Consolidation of the Soils below a Foundation

When a building is placed on the ground, pore water pressure will immediately increase and then gradually decrease. As a consequence, the settlement will vary with time. This is the classic consolidation problem of soils that is of great interest in geotechnical engineering (e.g., Zaman et al., 1991). The problem is schematically shown in Fig. 27. Because of symmetry, it is sufficient to model only one half of the problem.

The finite element mesh is shown in Fig. 8.27. The material parameters of the foundation soil are summarized in Table 8.4. It is assumed that the underground water table is at a depth of 3.0 m.

Table 8.4 Material parameters of the foundation soil

Material parameters	Symbols	Values
Young's modulus	E	$1.0\times10^{4}\ kPa$
Poisson ratio	ν	0.3
Solid grain density	ρ^{s}	$2.67\times10^{3}\ kg/m^{3}$
Water density	ρ^{w}	$1.0\times10^{3}\ kg/m^{3}$
Air density	ρ^{a}	$1.2\ kg/m^{3}$
Bulk modulus of water	K_{w}	$2.2\times10^{6}\ kPa$
Permeability	k	$1.0\times10^{-3}\ m/day$

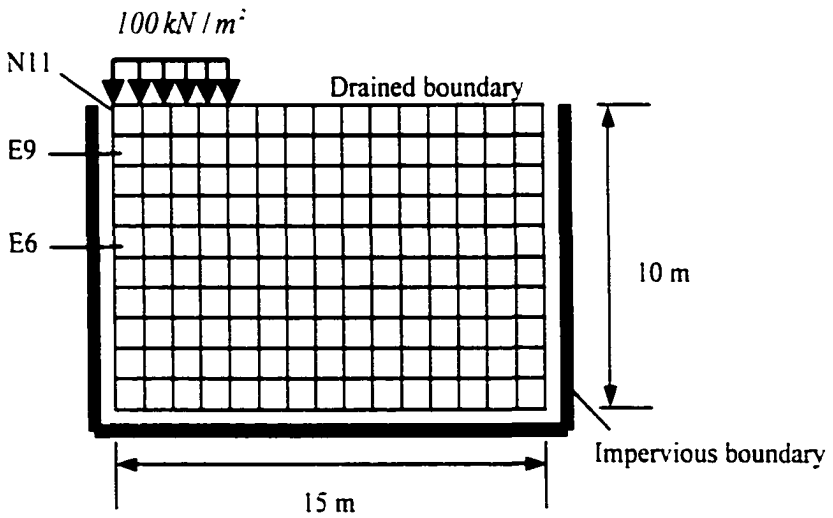

Figure 8.27 Definition of the consolidation problem

Numerical results are summarized in Fig. 8.28 to Fig. 8.30. Fig. 8.28 depicts the dissipation of pore water pressures in Element #6 and #9. It can be seen that in Element #6 the pore water pressure decays rapidly early after the loading is applied (the loading is applied in one day) and then the rate of decay becomes slower. Element #9 is in the unsaturated zone, and the pore water pressure increase slightly in the beginning. This is due to the increase in the air pressure under the compression. Then, when the air pressure dissipate, the water pressure decreases. Fig. 8.29 gives the evolution of the displacement at Node #11. Since the soil is unsaturated in the upper layer, the displacement developed rapidly due to the applied loading. Relatively small amount of settlement can be attributed to the pore water pressure dissipation. This behavior is sharply different from the fully saturated soils.

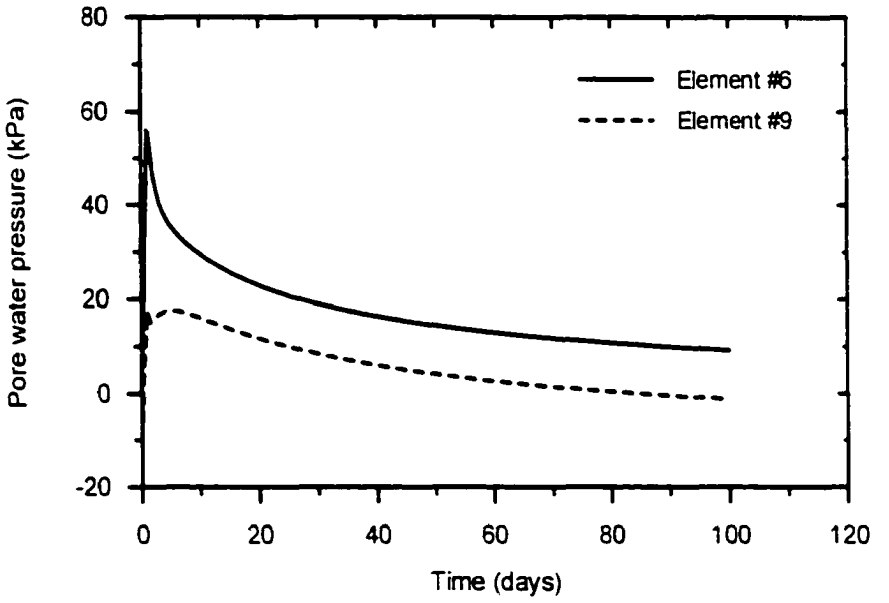

Figure 8.28 Pore water pressure dissipation in Element #6 and #9

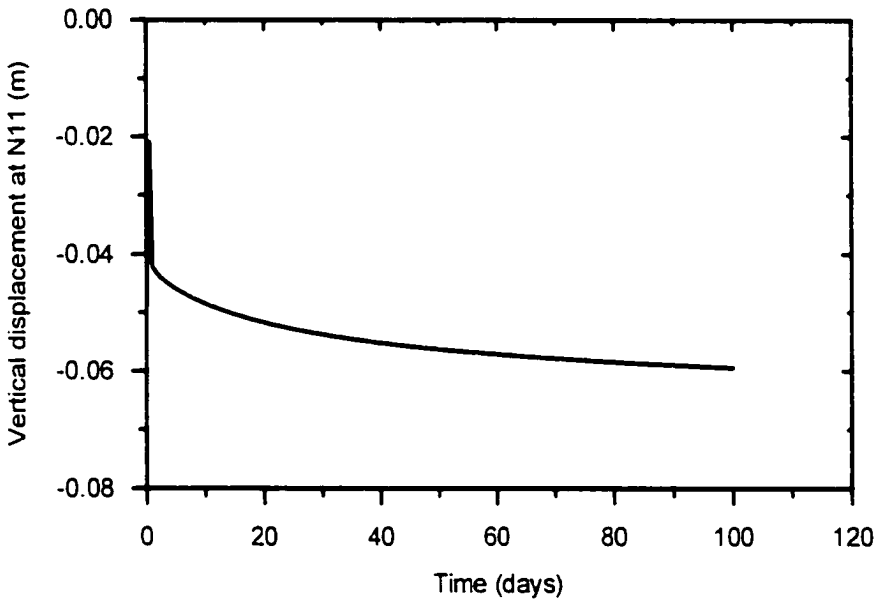

Figure 8.29 Change of the displacement at Node #11

The pressure dissipation process is described in Fig. 8.30, where several snapshots of the pressure contour at 1, 5, 10, 20, 40, and 100 days are presented. These contours clearly show the direction in which flow occurs. In the beginning, the pore water pressure is accumulated under the foundation. The water pressure in the area near the unsaturated zone dissipates faster than the deeper zone. As a consequence, the center of the highest pore water pressure keeps moving down with time until the consolidation process is completed.

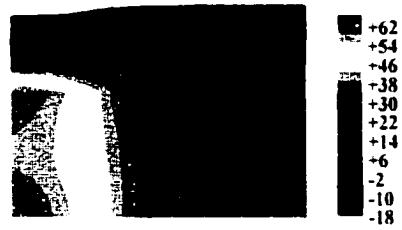

a) t = 1 day



b) t = 5 days



c) t = 10 days

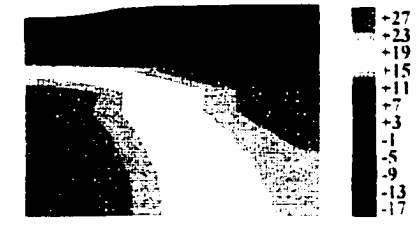

d) t = 20 days



e) t = 40 days

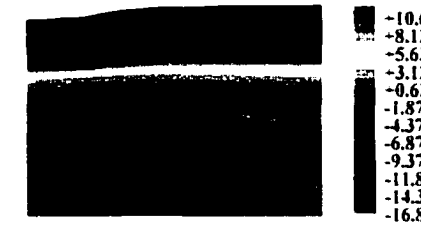

f) t = 100 days

Figure 8.30 Pore water pressure contours (in kPa)

Chapter 9 CONCLUDING REMARKS AND RECOMMENDATIONS

9.1 Summary

In this dissertation, an attempt is made to develop a continuum theory of porous media saturated by two immiscible fluids. The main focus is on how to characterize the *dynamic compatibility conditions on interfaces*. The dynamic compatibility condition represents the interaction on the interface between two bulk components in porous media. This concept is discussed in Chapter 1 based on microscopic considerations. The current state of relevant knowledge is discussed in Chapter 2. Thermodynamic arguments for the dynamic compatibility conditions on interfaces are given in Chapter 3, where general constitutive relationships of porous media are developed. In Chapter 4, a nonlinear continuum model of porous media is presented that is capable of handling the dynamic compatibility conditions on interfaces. Linearization of the general theory developed in Chapter 3 and Chapter 4 is given in Chapter 5, where a linear model of porous media is developed. In Chapter 6, the developed linear model is applied to the analysis of the propagation of acoustical waves in porous media. Initial/boundary value problems and finite element solution procedures are given in Chapter 7. Numerical examples are

presented in Chapter 8, showing the capability of the proposed model in modeling the behavior of multiphase porous media.

9.2 Conclusions

The following conclusions can be made based on the results obtained so far:

1. At microscopic level, the dynamic compatibility conditions on interfaces are the constraints on the pressure difference between two coexisting bulk components. It is shown (in Chapter 3) that these compatibility conditions are restricted under the second law of thermodynamics. The thermodynamic restriction yields the closure equations that is indispensable in a continuum model of porous media.

2. Behavior associated with capillary pressure and Terzaghi's effective stress can be characterized within a common framework. In this context, a theoretical framework of poroelastoplasticity is developed. This framework has a hierarchical structure, and describes the hysteresis in capillary pressure and plastic deformation of skeleton in a unified way.

3. It is found that the mixture theory-based models of porous media can be linked with Biot's poroelasticity theory. To that end, the principle of virtual dissipation (Biot, 1977) is introduced, with incorporation of a properly defined total free energy function of the porous media. Such a free energy function can be assumed as a mass-weighted average of all the free energies of bulk components.

4. A continuum model of porous media capable of accounting for the dynamic compatibility conditions on interfaces has been developed. It is shown that for a hyperelastic material, the dynamic compatibility conditions on interfaces represent the constraints on the material model. This result provides a way to incorporate the dynamic compatibility conditions into a constitutive model of porous media.

5. A linear model of porous media is developed. By using this model, the restrictive character of the principle of Terzaghi's effective stress can be released. It is shown that many classic models of porous media in geomechanics can be deduced from the proposed theory.

6. The linear model developed is used to analyze the propagation of acoustic waves in porous media. Theoretical results are compared with experimental data, and favorable comparisons are observed. The proposed model predicts existence of three compressional waves in the porous media saturated by two immscible fluids. The third (slowest) compressional wave is associated with the capillary phenomena.

7. The nonlinear model developed is used to represent the initial/boundary value problems associated with porous media. Finite element solution procedures have been developed and implemented into a computer code (U_DYSAC2). This code can be used in static and dynamic analysis of saturated and unsaturated porous media.

8. Numerical examples including wave propagation, two-phase flow, consolidation, and seismic response of an embankment are presented, showing the capability of the developed procedure in modeling the behavior of porous media.

9.3 Recommendations for Future Research

The following avenues of research may be followed to enhance the research performed in this dissertation:

1. To verify the procedure developed in this dissertation, further experiments and more numerical analyses should be performed.

2. An elastoplastic constitutive model may be developed within the theoretical framework developed in Chapter 3 and Chapter 4. The proposed constitutive model must be calibrated, implemented, and validated in applications.

3. Following the procedure discussed in Chapter 5, experiments may be performed to evaluate the material parameters in the linear model developed. This will help to further verify the procedure presented here.

4. Other robust algorithms should be introduced into the finite element code. The initial/boundary value problems (IBVP) associated with unsaturated porous media are different from those related to the saturated materials in that the IBVPs concerning the behavior of unsaturated porous media are highly nonlinear even when an elastic stress-strain model is used.

5. Other schemes for finite element discretization should be included. For instance, higher-order elements should be implemented into the computer code, and the efficiency of these elements must be examined through numerical analyses.

6. A numerical procedure based on the nonlinear model presented remains to be developed that can be used to analyze the behavior of porous media at finite strain.

7. The theory presented above may be further generalized to take into account some other important phenomena associated with porous media such as swelling, viscosity and molecular diffusion.

REFERENCES

1. E. C. Aifantis (1980), "On the problem of diffusion in solids." Acta Mechanica **37**, 265-296.

2. G. D. Aitchison, and I. B. Donald (1956), "Some preliminary studies of unsaturated soils. (b) Effective stress in unsaturated soils." Proc. 2nd Austr.-N. Zealand Conf. Soil Mech. Found. Eng., Christchurch, 192-199.

3. E. E. Alonso, A. Gens, and A. Josa (1990), "A constitutive model for partially saturated soils." *Geotechnique*, **40** (3), 405-430.

4. E. E. Alonso, A. Lloret, C. H. Delahaye, J.Vaunat, A. Gens and G. Volckaert (1998), "Coupled analysis of a backfill hydration test." *Int. J. Numer. Anal. Meth. Geomech.* **22**, 1-27.

5. P. Arduino, *Multiphase description of deforming porous media by the finite element method*, PhD thesis, Georgia Institute of Technology, 1996.

6. F. Armero (1999), "Formulation and finite element implementation of a multiplicative model of coupled poro-plasticity at finite strains under fully saturated conditions." *Comp. Meth. Appl. Mech. Eng.*, **171**, 205-241.

7. J. Bear, *Dynamics of Fluids in Porous Media*, American Elsevier, New York, 1972.

8. L. S. Bennethum, M. A. Murad, and J. H. Cushman (1997), "Modified Darcy's law, Tersaghi's effective stress principle and Fick's law for swelling clay soils." *Computers and Geotechnics* **20**(3/4), 245-266.

9. A. Bedford and Drumheller (1983), "Theories of immiscible and structured mixtures." *Int. J. Eng. Sci.* **21**, 863-960.

10. T. Belytschko, W. K. Liu, and B. Moran, *Nonlinear Finite Element for Continua and Structures*, John Wiley & Sons, New York, USA, 2000.

11. I. A. Beresnev, and P. A. Johnson (1994), "Elastic-wave stimulation of oil production: A review of methods and results." *Geophysics*, **59**(6), 1000-1017.

12. J. G. Berryman (1980), " Confirmation of Biot's theory," *Appl. Phy. Lett.* **37**, 382-384.

13. A. W. Bishop (1959), "The principle of effective stress," *Tek. Ukebl.* **106**(39), 113-143.

14. A. W. Bishop and I. B. Donald (1961), "The experimental study of partly saturated soils in triaxial apparatus," *Proc. 5th Int. Conf. Soil Mech. Found. Eng.* **1**, 13-21.

15. A. W. Bishop and G. E. Blight (1963), "Some aspects of effective stress in saturated and partly saturated soils," *Geotechnique* **13**(3), 177-197.

16. M. A. Biot (1941), "General theory of three-dimensional consolidation," *J. Applied Physics* **12**, 155-164.

17. M. A. Biot (1956a), "Theory of propagation of elastic waves in a fluid-saturated porous solid. I. Low-frequency range," *J. Acoust. Soc. Amer.*, **28**(2), 168-178.

18. M. A. Biot (1956b), "Theory of propagation of elastic waves in a fluid-saturated porous solid. II. Higher frequency range," *J. Appl. Phys.* **28**(2), 179-191.

19. M. A. Biot, and D. G. Willis (1957), " The elastic coefficients of the theory of consolidation," *J. Appl. Mech.* ASME 24, 594-601.

20. M. A. Biot (1962), "Mechanics of deformation and acoustic propagation in porous media," *J. Appl. Phys.* **33**(4), 1482-1498.

21. M. A. Biot (1972), "Theory of finite deformation of porous solid," *Ind. Univ. Math. J.* **21**(7), 597-620

22. M. A. Biot (1977), "Variational Lagrangian-thermodynamics of nonisothermal finite strain mechanics of porous solids and thermomolecular diffusion," *Int. J. Solids Structures* **13**, 579-597.

23. G. E. Blight (1965), "A study of effective stress for volume change," in *Moisture Equilibrium and Moisture Changes in Soils beneath Covered Areas*, 259-269, Sydney: Butterworths, Australia.

24. J. Bluhm and R. de Boer (1996), "Effective stresses---a clarification," *Arch. Appl. Mech.* **66**, 479-492.

25. G. Bolzon, B. A. Schrefler and O. C. Zienkewicz (1996), "Elasto-plastic constitutive laws generalized to partially saturated states," *Geotechnique* **46**(2), 279-289.

26. R. I. Borja, C. Tamagnini, and A. Amorosi (1997), "Coupling plasticity and energy-conserving elasticity models for clays," *J. Geotech. Geoenviron. Engrg.* **123**(10), ASCE, 948-957.

27. T. Bourbie, O. Coussy and B. Zinszner, *Accoustics of Porous Media*, Gulf Publ. Com., Book Division, Houston, Texa, 1987.

28. R. M. Bowen, "Theory of Mixtures," in Continuum Physics Volume III, Mixtures and EM Field Theories, edited by A. C. Eringen, New York: Academic Press, 1976.

29. R. M. Bowen (1980), "Incompressible porous media models by use of the theory of mixtures," *Int. J. Eng. Sci.* **18**, 1129-1148.

30. R. M. Bowen (1982), "Compressible porous media models by use of the theory of mixtures," *Int. J. Eng. Sci.* **20**(6), 253-268.

31. H. Brooks and A. T. Corey, *Hydraulic properties of porous media*, Colorado State Univ. Hydrol. Paper, No. 3, March 1964.

32. W. Brutsaert (1964), "The propagation of elastic waves in unconsolidated unsaturated granular mediums," *J. Geophys. Res.* **69**, 643-652, 1964.

33. W. Brutsaert and J. N. Luthin (1964), "The velocity of sound in soils near the surface as a function of moisture content," *J. Geophys. Res.* **69**(4), 643-652.

34. Y. A. Buyevich (1995), "Towards a theory of nonequilibrium multiphase filtration flow," *Transport in Porous Media* **21**, 145-162.

35. S. P. Clark, Jr. (Ed.), *Handbook of Physical Constants*: GSA Mem. 97, 1966.

36. M. A. Celia, and P. C. Reeves, H. K. Dahle, "On the use of pore-scale computational models for two-phase porous media flows," in *Computational Methods in Contamination and Remediation of Water resources*, (ed.) V. N. Burganos et al., Comput. Mech. Publ., Boston, USA, 1998, 397-404.

37. C. S. Chang and J. M. Duncan (1983), "Consolidation analysis of partially saturated clay by using a effective stress-strain model," *Int. J. Numer. Anal. Meth. Geomech.* **7**, 39-55.

38. J. D. Coleman (1962), "Stress strain relationship for partly saturated soils," *Geotechnique* **12**(4), 348-350.

39. O. Coussy (1989a), "Thermodynamics of saturated porous solid in finite deformation," *European J. Mech.*, A/Solid **8**, 1-14

40. O. Coussy (1989b), "A general theory of thermoporoelastoplasticity for saturated porous materials," *Transport in Porous Media* **4**, 281-293

41. O. Coussy, *Mechanics of Porous Continua*, Wiley, New York, 1995.

42. Y. J. Cui and P. Delage (1996), "Yielding and plastic behavior of an unsaturated compacted silt," *Geotechnique* **46**(2), 291-311.

43. Y. F. Dafalias, and L. R. Herrmann (1986), "Bounding surface plasticity II: application to isotropic cohesive soils," *J. Eng. Mech. Div.* ASCE, **112**, 1263-1291.

44. C. S. Desai, and H. J. Siriwardane, *Constitutive Laws for Engineering Materials with Emphasis on Geological Materials*, Prentice-Hall, Inc., New Jersy, 1984

45. R. de Boer (1996), "Highlights in the historical development of the porous media theory: Toward a consistent macroscopic model," *Appl. Mech. Rev.* **49** (4), 201-262.

46. R. de Boer, W. Ehlers and Z. Liu (1993), "One-dimensional transient wave propagation in fluid-saturated impressible porous media," *Arch. Appl. Mech.* **63** 59-72.

47. R. de Boer, and J. Bluhm (1999), "The influence of compressibility on the stresses of elastic porous solid---semimicroscopic investigations," *Int. J. Solid and Struct.* **36**, 4805-4819.

48. W. Ehlers (1989), "On the thermodynamics of elasto-plastic porous media," *Arch. Mech.* **41**(1), 73-93.

49. W. Ehlers (1993), "Constitutive equations for granular maerials in geomechanical context," *Continuum Mechanics in Environmental Sciences and Geophysics*, CISM Courses and Lecture Notes No.337:313-402, Wien: Springer Verlag.

50. V. Escario, and J. Sáez (1986), "Shear strength of partly saturated soils," *Geotechnique* **36** (13), 453-456.

51. G. Fichera, Existence theorems in elasticity, *Handbuch der Physik*, Bd. V1a/2, 347-389, Berlin: Spring-Verlag, 1972.

52. D. G. Fredlund (1979), "Appropriate concepts and technology for unsaturated soils," *Can. Geotech. J.* **16**, 121-139.

53. D. G. Fredlund and H. Rahardjo, *Soil Mechanics for Unsaturated Soils*, John Wiley and Sons, Inc., New York, 1993.

54. D. G. Fredlund and N. R. Morgenstern (1977), "Stress state variables for unsaturated soils," *J. Geotech. Eng.*, ASCE, **103**(GT5), 447-466.

55. D. G. Fredlund, H. Rahardjo, J. K. M. Gan (1987), " Nonlinearity of strength envelope for unsaturated soils," *Proc. 6th Int. Conf. Expansive Soils*, New Delhi, 48-54.

56. A. Gajo, and L. Mongiovi (1994), "The effects of measure accuracy in the interpretation of dynamic tests on saturated soils," *Proc., Int. Symp. on Pre-Failure Deformation Characteristics of Geomaterials*, Balkema, Japan, 163-168.

57. A. Gajo and L. Mongiovi (1995), "An analytical solution for the transient response of saturated linear elastic porous media," *Int. J. Numer. Anal. Meth. Geomech.* **19**, 399-

58. S. K. Garg, A. H. Nayfeh and A. J. Good (1976), "Compressional waves in fluid-saturated porous media," *J. Appl. Phy.*, **45**(5), 1968-1974.

59. S. K. Garg, and A. H. Nayfeh (1986), "Compressional wave propagation in liquid and/or gas saturated elastic porous media," *J. Appl. Phys.*, **60**(9), 3045-3056.

60. J. Geertsma, and D. C. Smit (1961), "Some aspects of elastic wave propagation in fluid-saturated porous solids," *Geophysics* XXVI (2), 169-181.

61. J. Ghaboussi and K. J. Kim, "Qusistatic and dynamic behavior of saturated and partially saturated soils," in *Mechanics of Engineering Materials*, C. S. Desai and Gallagher (eds), John Wiley and Sons, 1984.

62. M. A. Goodman and S. C. Gowin (1972), "Compressible porous media models by use of the theory of mixtures," *Arch. Rat. Mech. Anal.* **48**, 249-266.

63. W. G. Gray, and S. M. Hassanizadeh (1989), "Averaging theorems and averaged equations for transport of interface properties in multiphase systems," *Int. J. Multiphase Flow*, **15**(1), 81-95.

64. W. G. Gray, and S. M. Hassanizadeh (1991), "Unsaturated flow theory including interfacial phenomena," *Water Resources. Res.* **27**(8), 1855-1853.

65. S. M. Hassanizadeh, and W. G. Gray (1979), "General conservation equations for multiphase systems: a & b," *Adv. Water Resources.* **2**, 131-203.

66. S. M. Hassanizadeh, and W. G. Gray (1993), "Thermodynamic basis of capillary pressure in porous media," *Water Resources Res.* **29**(10), 3389-3405.

67. S. M. Hassanizadeh, and W. G. Gray (1990), "Mechanics and thermodynamics of multiphase flow in porous media including interphase boundaries," *Adv. Water Resources*, **13**(4), 169-186.

68. H. M. Hilber, T. J. R. Hughes, and R. L. Taylor (1977). "Improved numerical dissipation for time integration algorithms in structural dynamics," *Earthq. Eng. Struct. Dyn.* **5**, 283-292.

69. D. J. Hornbaker, R. Albert, I. Albert, A.-L. Barabási, and P. Schiffer (1997). "What keeps sandcastles standing?" *Nature* **387**(19), pp.765.

70. T. J. R. Hughes, "Analysis of transient algorithms with particular reference to stability," in *Computational Methods for Transient analysis*, T. J. R. Hughes and T. Belyschko (eds.), North-Holland, Amsterdam, 1983: Ch. 8&9.

71. T. J. R. Hughes, *The Finite Element Method---Linear Static and Dynamic Finite Element Analysis*, Englewood Cliffs, N. J.: Prentice_Hall, 1987.

72. R. J. Knops and L. E. Payne, *Uniqueness Theorems in Linear Elasticity*, Springer Tracts in Natural Philosophy 19, New York: Springer-Verlag, 1971

73. H. -J. Kumpel (1991), "Poroelasticity: parameter reviewed," *Geophys. J. Int.* 105, 783-799.

74. B. L. Kutter, *Centrifuge modeling of the response of clay embankments to earthquakes*, PhD thesis, University of California, Davis, California, 1982.

75. P. V. Lade and R. de Boer (1997), "The concept of effective stress for soils, concrete, and rock," *Geotechnique* **47**(1), 61-78.

76. P. V. Lade and R. B. Nelson (1987), "Modeling the elastic behavior of granular materials," *Int. J. Numer. Anal. Methods Geomech.* **11**, 521-542.

77. R. W. Lewis, and B. A. Schrefler, *The Finite Element Method in the Static and Dynamic Deformation and Consolidation of Porous Media*, John Wiley and Sons, New York, USA, 1998.

78. X. Li and O. C. Zienkiewicz (1992), "Multiphase flow in deforming porous media and finite element solutions," *Comput. Struct.* **45**(2), 211-227.

79. X. Li., H. R. Thomas, and Y. Fan (1999), "Finite element method and constitutive modelling and computation for unsaturated soils," *Comput. Methods Appl. Mech. Engrg.* **169**, 135-159.

80. A. C. Liakopoulos, *Transient flow through unsaturated porous media*, PhD thesis, University of California, Berkeley, 1965.

81. A. Lloret and E. E. Alonso (1980), "Consolidation of unsaturated soil including swelling and collapse behavior," *Geotechnique* **30**(4) 449-477.

82. A. Lloret and E. E. Alonso (1985). "State surface for partially saturated soils." *Proc. 11th Int. Conf. Soil Mech. Found. Eng.*, San Francisco, **2**, 557-562.

83. B. Loret, and N. Khalili (2000), "A three-phase model for unsaturated soils," *Int. J. Numer. Anal. Meth. Geomech.* **24**, 893-927.

84. B. Loret (1985), "On the choice of elastic parameters for sand," *Int. J. Numer. Anal. Methods Geomech.* **9**(3), 285-292.

85. J. Lubliner, *Plasticity Theory*, Macmillan Publishing Co., New York, 1990.

86. D. G. Luenberger, *Linear and Nonlinear Programming*, Addison-Wesley Publishing Company, Reading, Mass., 1984.

87. E. L. Matyas and H. S. Radhakrishna (1968), "Volume change characteristics of partly saturated soils," *Geotechnique* **18**(4), 432-448.

88. E. A. Meroi, B. A. Schrefler and O. C. Zienkiewicz (1995), "Large strain static and dynamic semi-saturated soil behavior," *Int. J. Numer. Anal. Meth. Geomech.* **19**, 81-106.

89. G. A. Miller, K. K. Muraleetharan, and Y. Y. Lim, *Wetting-induced settlement of compacted fill embankments*, internal report, University of Oklahoma, 2000.

90. F. Molenkamp (1988), "A simple model for isotropic npnlinear elasticity of frictional materials," *Int. J. Numer. Anal. Methods Geomech.* **12**(5), 467-475.

91. L. M. Morland (1972), "A simple constitutive theory for a fluid-saturated porous media," *J. Geophy. Res.* **77**(5), 890-900.

92. J. C. Muccino, W. G. Gray, and L. A. Ferrand (1998), "Toward an improved understanding of multiphase flow in porous media," *Advances of Geophysics*, **36**(3), 401-422.

93. M. A. Murad and J. H. Cushman (1997), " A multiscale theory of swelling porous media: II. Dual porosity models for consolidation of clays incorporating physical effects," *Transport in Porous Media* **28**, 69-108.

94. M. A. Murad (1999), "Thermomechanical model of hydration swelling in smectitic clays: I. Two-scale mixture-theory approach," *Int. J. Numer. Anal. Mech. Geomech.* **23**, 673-696.

95. K. K. Muraleetharan, K. D. Mish, C. Yogachandran, K. Arulannandan (1988), "DYSAC2 (Version 1.0): Dynamic Soil Analysis Code for 2-dimensional problems," *Computer code*, Department of Civil Engineering, University of California, Davis, California.

96. K. K. Muraleetharan, K. D. Mish and K. Arulanandan (1994), "A fully coupled analysis procedure and its verification using centrifuge test results," *Int. J. Numer. Anal. Meth. Geomech.*, **18**, 305-325.

97. K. K. Muraleetharan, K. D. Mish, C. Yogachandran, K. Arulannandan (1997), "DYSAC2 (Version 7.0): Dynamic Soil Analysis Code for 2-dimensional problems," *Technical Report*, School of Civil Engineering and Environmental Science, University of Oklahoma, Norman, Oklahoma.

98. K. K. Muraleetharan and C. F. Wei (1999), "Dynamic behavior of unsaturated porous media: governing equations using the theory of mixtures with interfaces (TMI)," *Int. J. Numer. Anal. Meth. Geomech.*, **23**, 1579-1608.

99. K.K. Muraleetharan, and P.R. Nedunuri (1998), "A bounding surface elastoplastic constitutive model for monotonic and cyclic behavior of unsaturated soils," *Proc., 12th Eng. Mech. Conf.*, ASCE, La Jolla, CA, 1331-1334.

100. K. K. Muraleetharan, and K. K. Granger (1999), "The use of miniature pore pressure transducers in measuring matric suction in unsaturated soils," *Geotechnical Testing Journal* **22**(3), ASTM, 226-234.

101. W. F. Murphy (1982), "Effects of partial water saturation on attenuation in Massilon sandstone and Vycor porous glass," *J. Acoust. Soc. Am.* **71**, 1458-1468.

102. W. F. Murphy (1984), "Acoustic measures of partial gas saturation in tight sandstones," *J. Geophys. Res.* **89** (B13), 11549-11559.

103. R. W. Ogden, *Non-linear Elastic Deformation*, Ellis Harwood Ltd., Chichester: E. Horwood; New York, 1984.

104. K. C. Park (1975), "An improved stiffly stable method for direct integration of nonlinear structural dynamic equations," *Trans.* ASME, 464-470.

105. S. L. Passman (1977), "Mixtures of granular materials," *Int. J. Eng. Sci.* **15**, 117-129.

106. T. Plona (1980), "Observation of a second bulk compressible wave in a porous medium at ultrasonic frequencies," *Appl. Phy. Lett.* **36**, 259-261.

107. J. H. Prevost (1980), "Mechanics of continuous porous media," *Int. J. Eng. Sci.*, **18**, 787-800.

108. P. C. Reeves, and M. A. Celia (1996), "A functional relationship between capillary pressure, saturation, and interfacial area," *Water Resources Res.* **32**(8), 2345-2358.

109. J. R. Rice (1975), "On the stability of dilatant hardening for saturated rock masses," *J. Geophys. Res.* **80**, 1531-1536.

110. M. B. Rubin, D. Elata, and A. V. Attia (1996), "Modeling added compressibility of porosity and the thermomechanical response of wet porous rock with application to M. T. Helen Tuff," *Int. J. Solids and Structures* **33** (6), 761-793.

111. J. E. Santos (1986 I), "Elastic wave propagation in fluid-saturated porous media. I. The existence and uniqueness theorems," *Math. Modeling and Numer. Anal.* **20**(1), 113-128.

112. J. E. Santos (1986 II), "Elastic wave propagation in fluid-saturated porous media. I. The Garlerkin procedures," *Math. Modeling and Numer. Anal.* **20**(1), 129-139.

113. A. Schofield and P. Wroth, *Critical State Soil Mechanics*, McGraw Hill, New York, 1968.

114. B. A. Schrefler and X. Zhan (1993), "A fully coupled model for water flow and airflow in deformable porous media," *Water Resources Res.* **29**, 155-167.

115. B. A. Schrefler (1990), "Mechanics of partially saturated porous media," in *Numerical Methods and Constitutive Modeling in Geomechanics*, CISM lecture notes, edited by. Desai, C. S. and Gioda G., 169-209, Springer-Verlag, Wien.

116. B. A. Schrefler, and R. Scotta (2001), "A fully coupled dynamic model for two-phase fluid flow in deformable porous media," *Comput. Methods Appl. Mech. Engrg.* **3223**, 3223-3246.

117. J. C. Simo, and R. L. Taylor (1985), "Consistent tangent operators for rate-independent elasto-plasticity," *Comput. Methods Appl. Mech. Engrg.* **48**, 101-118.

118. B. R. Simon, O. C. Zienkiewicz and D. K. Paul (1984), "An analytical solution for the transient response of saturated porous elastic solids," *Int. J. Numer. Anal. Meth. Geomech.* **8**, 381-398.

119. S. Soo, *Fluid Dynamics of Multiphase Systems*, Waltham, Massachusetts: Blaisdell, 1967.

120. B. Svendsen and K. Hutter (1995), "On the thermodynamics of a mixture of isotropic materials with constraints," *Int. J. Eng. Sci.* **33**(14), 2021-2054.

121. K. Terzaghi (1936), "The shear resistance of saturated soils," in *Pro. 1st Int. Conf. Soil Mech. Found. Eng.*, Vol. 1, Cambridge, MA, 54-56.

122. H. R. Thomas and Y. He (1998), "Modeling the behavior of unsaturated soil using an elasto-plastic constitutive model," *Geotechnique* **48**(5), 589-603.

123. K. Tuncay and M. Y. Corapcioglu (1997), "Wave propagation in poroelastic media saturated by two fluids," *J. Appl. Mech.* **64**, 313-320.

124. K. Tuncay and M. Y. Corapcioglu (1996), "Body waves in poroelastic media saturated by two imissible fluids," *J. Geophy. Res.* **101** (b11), 25149-25159.

125. M. T. Van Genuchten (1980), "A closed form equation for predicting the hydraulic conductivity of unsaturated soils," *Soil Sci. Soc. Am. J.* **44**, 892-898.

126. I. Vardoulakis, and D. E. Beskos (1983), "On the dynamic behavior of nearly saturated granular media," in *Geomechanics*, (ed.) S. Nemat-Nasser, AMD, Vol. 57, ASME, New York, 65-73.

127. I. Vardoulakis, and D. E. Beskos (1986), "Dynamic behavior of nearly saturated porous media," *Mech. Mater.* **5**, 87-108.

128. J. Vaunat, J. C. Cante, A. Ledesma, and A. Gens (2000), "A stress point algorithm for an elastoplastic model in unsaturated soils," *Int. J. Plasticity* **16**, 121-141.

129. P. A. Vermeer (1978), "A double hardening for sand," *Geotechnique* **28**(4), 413-433.

130. S. J. Wheeler and V. Sivakumar (1995), "An elasto-plastic critical state framework for unsaturated soils," *Geotechnique*, **45**(1), 35-53.

131. S. J. Wheeler (1996), "Inclusion of specific water volume within an elasto-plastic model for unsaturated soils," *Can. Geotech. J.* **33**, 42-57.

132. S. Whitaker (1969), "Advances in theory of fluid motion in porous media," *Industrial and Engineering Chemistry* **61**(12), 14-28.

133. K. Wilmanski (1995), "Lagrangean model of two-phase porous material," *J. Nonequilib. Thermodyn.* **20**, 50-77.

134. K. Wilmanski (1996), "Porous media at finite strains: the new model with the balance equation for porosity," *Arch. Mech.* **48**(4), 591-628.

135. K. Wilmanski, *Thermomechanics of Continua*, Springer-Verlag, Berlin, Germany, 1998

136. C. -S. Yin, M. L. Batzle, and B. J. Smith (1992), "Effects of partial liquid/gas saturation on extensional wave attenuation in Berea sandstone," *Geophysical Research Letters* **19** (13), 1399-1402.

137. C. -S. Yin, *Pulsating gas pockets and their effects on wave propagation in partially saturated porous solids*, Ph.D thesis, Columbia University, 1992, pp.1-35.

138. M. Zaman, A. Gopalasingam, and J. G. Laguros (1991), "Consolidation settlement of bridge approach foundation," *J. Geotech. Engrg.*, 117 (2), ASCE, 219-240.

139. O. C. Zienkiewicz, C. Humpheson, and R. W. Lewis, "A unified approach to soil mechanics problems (including plasticity and viscoplasticity)," Ch. 4, pp.151-178 G. Gudehus, (Ed.) in *Finite Element in Geomechanics*, Wiley, 1977.

140. O. C. Zienkiewicz (1982), "Basic formulation of static and dynamic behavior of soil and other porous media," in *Numerical Methods in Geomechanics*, J. B. Martin (ed.), D. Reidl.

141. O. C. Zienkiewicz and T. Shiomi (1984), "Dynamic behavior of saturated porous media: the generalized Biot's formulation and its finite element solution," *Int. J. Numer. Anal. Meth. Geomech.*, **8**, 71-96.

142. O. C. Zienkiewicz, Y. M. Xie, B. A. Schrefler, A. Ledesma, and N. Bicanic (1990a), "Static and dynamic behavior of soils: a rational approach to quantitative solutions. I fully saturated problems," *Proc. R. Sco. Lond. A*, **429**, 285-310.

143. O. C. Zienkiewicz, Y. M. Xie, B. A. Schrefler, A. Ledesma, and N. Bicanic (1990b), "Static and dynamic behavior of soils: a rational approach to quantitative solutions. II semi-saturated problems," *Proc. R. Sco. Lond. A*, **429**, 311-321.

APPENDICES

I. DISSIPATIVE FORCES AS FUNCTIONS OF FLUID MASS FLUXES

In (3.5.17) and (3.5.18), except for $\hat{\omega}^{\beta}$, all the other material coefficients do not transform in the usual sense. To make this point clear, we introduce two new variables: $\dot{M}^{\beta} = m_t^{\beta} W_t^{\beta}$ and $\dot{m}^{\beta} = n^{\beta}\rho^{\beta} w^{\beta}$, which represent the mass fluxes with respect to the reference and current configurations, respectively. $\dot{M}^{\beta}$ and $\dot{m}^{\beta}$ can be related to each other through the Piola transformation, i.e.

$$\dot{M}^{\beta} = J\dot{m}^{\beta} F^{-T} \tag{I.1}$$

In the following, $\dot{M}^{\beta}$ and $\dot{m}^{\beta}$ will be used to derive the dissipative forces instead of W_t^{β} and w^{β}. Uncoupling the fluid diffusion and heat conduction from the total residual dissipation, one obtains

$$\mathcal{D}_{diff} = -\sum_{\beta=1}^{N-1} \dot{M}^{\beta} \cdot \dot{\hat{R}}^{\beta} + GRAD\theta \cdot \dot{Q} \geq 0, \tag{I.2}$$

or equivalently,

$$\theta \Lambda_{diff} = -\sum_{\beta=1}^{N-1} \dot{m}^{\beta} \cdot \dot{\hat{r}}^{\beta} + \nabla\theta \cdot \dot{q} \geq 0, \tag{I.3}$$

where $\dot{\hat{R}}^{\beta} = (m_t^{\beta})^{-1} \dot{R}^{\beta}$, $\dot{\hat{r}}^{\beta} = (n^{\beta}\rho^{\beta})^{-1} \dot{r}^{\beta}$, and $\dot{q}^{\beta}$ is the dissipative part of q^{β}/θ. Now, using dissipation inequality (I.2) and following the same procedures in deriving (3.5.12) and (3.5.13), one obtains

$$\dot{\hat{R}}^{\gamma} = -\sum_{\beta=1}^{N-1} B_a^{\gamma} \cdot \dot{M}^{\beta} - B_a^{\gamma} \cdot GRAD\,\theta, \tag{I.4}$$

and

$$\dot{Q} = -\sum_{\beta=1}^{N} \boldsymbol{B}_{\beta}^{\alpha} \cdot \dot{\boldsymbol{M}}^{\beta} - \boldsymbol{B}_{\alpha}^{\alpha} \cdot GRAD\,\theta\,. \tag{I.5}$$

By using (3.5.4), (I.1), $\mathcal{O}_{\Delta\Pi} = J\theta\Lambda_{\Delta\Pi}$, and $GRAD\,\theta = \boldsymbol{F}^{T}\nabla\theta$, it can be proved that the spatial counterparts of (I.4) and (I.5) are,

$$\dot{\hat{\boldsymbol{r}}}^{\alpha} = -\sum_{\beta=1}^{N} \boldsymbol{b}_{\beta}^{\alpha} \cdot \dot{\boldsymbol{m}}^{\beta} - \boldsymbol{b}_{\alpha}^{\alpha} \cdot \nabla\theta\,, \tag{I.6}$$

and

$$\hat{\boldsymbol{q}} = -\sum_{\beta=1}^{N} \boldsymbol{b}_{\beta}^{\alpha} \cdot \dot{\boldsymbol{m}}^{\beta} - \boldsymbol{b}_{\alpha}^{\alpha} \cdot \nabla\theta\,. \tag{I.7}$$

The coefficients in (I.6) and (I.7) are related to those in (I.4) and (I.5) through the following transformations,

$$\boldsymbol{b}_{\beta}^{\alpha} = J\boldsymbol{F}^{-T}(\boldsymbol{B}_{\beta}^{\alpha})\boldsymbol{F}^{-1}, \qquad \boldsymbol{b}_{\alpha}^{\alpha} = \boldsymbol{F}^{-T}(\boldsymbol{B}_{\alpha}^{\alpha})\boldsymbol{F}^{T}. \tag{I.8}$$

and

$$\boldsymbol{b}_{\beta}^{\alpha} = \boldsymbol{F}(\boldsymbol{B}_{\beta}^{\alpha})\boldsymbol{F}^{-1}, \quad \boldsymbol{b}_{\alpha}^{\alpha} = J^{-1}\boldsymbol{F}(\boldsymbol{B}_{\alpha}^{\alpha})\boldsymbol{F}^{T}. \tag{I.9}$$

Comparing (I.8) and (I.9) with (3.5.17) and (3.5.18), one may notice that unlike the latter (I.8) and (I.9) are those usually applied to the contravariant and covariant tensors defined on various deforming configurations.

II. COEFFICIENTS IN FIELD EQUATIONS (5.2.10)-(5.2.13)

$$M_{11} = n_1^1(\lambda_1 + K_1 - 2\lambda_{11}^1) - \frac{n_1^1(K_1 - \lambda_{11}^1)^2(D_{11} + D_1 - 2D_{11}D_1)}{K_1(1 - D_1D_1)}. \tag{II.1}$$

$$M_{11} = \frac{n_1^1(\lambda_{11}^1 - K_1)(n_1^{11}\lambda_{11}^{11} - K_{11})(1 - D_1)D_{11}}{K_1(1 - D_1D_{11})}. \tag{II.2}$$

$$M_{11} = \frac{n_1^1(\lambda_{11}^1 - K_1)(n_1^1\lambda_{11}^1 - K_1)(1 - D_{11})D_1}{K_1(1 - D_1D_1)}. \tag{II.3}$$

$$M_{111} = n_1^{11}K_{11} - \frac{n_1^1(n_1^{11}\lambda_{11}^{11} - K_{11})^2 D_{11}}{K_1(1 - D_1D_1)}. \tag{II.4}$$

$$M_{11} = \frac{n_1^1(n_1^{11}\lambda_{11}^{11} - K_{11})(n_1^1\lambda_{11}^1 - K_1)D_{11}D_1}{K_1(1 - D_1D_1)}. \tag{II.5}$$

$$M_{11} = n_1^1K_1 - \frac{n_1^1(n_1^1\lambda_{11}^1 - K_1)^2 D_1}{K_1(1 - D_1D_1)}. \tag{II.6}$$

$$H_{12} = n_1^1(\lambda_{12}^1 - \lambda_{11}^1) - \frac{n_1^1(K_1 - \lambda_{11}^1)[E_{11}D_{11} + E_1D_1 - (E_{11} + E_1)D_{11}D_1]}{K_1(1 - D_{11}D_1)}. \tag{II.7}$$

$$H_{112} = n_1^{11}\lambda_{11\theta}^{11} + \frac{n_1^1(K_{11} - n_1^{11}\lambda_{11}^{11})(E_{11} - E_1D_1)D_{11}}{K_1(1 - D_1D_1)}. \tag{II.8}$$

$$H_{12} = n_1^1\lambda_{11\theta}^1 + \frac{n_1^1(K_1 - n_1^1\lambda_{11}^1)(E_1 - E_{11}D_{11})D_1}{K_1(1 - D_{11}D_1)}. \tag{II.9}$$

where

$$D_{11} = \frac{n_1^{11}K_1}{n_1^1K_{11} + n_1^{11}K_1 + n_1^1n_1^{11}(n_1^{11}\Theta_1^{11} - 2\lambda_{11}^{11})}. \tag{II.10}$$

$$D_1 = \frac{n_1^1K_1}{n_1^1K_1 + n_1^1K_1 + n_1^1n_1^1(n_1^1\Theta_1^1 - 2\lambda_{11}^1)}. \tag{II.11}$$

$$E_{11} = \lambda_{11\theta}^1 + n_1^{11}\lambda_{11\theta}^{11} - \lambda_{11\theta}^{11}. \tag{II.12}$$

$$E_1 = \lambda_{11\theta}^1 + n_1^1\lambda_{11\theta}^1 - \lambda_{11\theta}^1. \tag{II.13}$$

III. DERIVATIONS OF DYNAMIC COMPATIBILITY CONDITIONS (6.1.5)-(6.1.7)

Let $\mathcal{P}$ be a subdomain of $\mathcal{B}$, $\mathcal{P} \subset \mathcal{B}$. Consider a field $\varphi(\boldsymbol{X},t)$, $\boldsymbol{X} \in \mathcal{P}$. Its *global* balance equation in Lagrangian description can be expressed as

$$\frac{d}{dt}\int_{\mathcal{P}} \varphi(\boldsymbol{X},t)dV = \oint_{\partial\mathcal{P}} \psi(\boldsymbol{X},t)\boldsymbol{N}dS + \int_{\mathcal{P}} \psi_{\mathrm{r}}(\boldsymbol{X},t)dV + \int_{\mathcal{P}} \varphi^{*}(\boldsymbol{X},t)dV. \qquad \text{(III.1)}$$

where $\psi(\boldsymbol{X},t)$, $\psi_{\mathrm{r}}(\boldsymbol{X},t)$, and $\varphi^{*}(\boldsymbol{X},t)$ denotes the flux density, supply, and production of $\varphi(\boldsymbol{X},t)$, respectively; $\boldsymbol{N}$ is the unit normal vector to the boundary $\partial\mathcal{P}$ of the subbody $\mathcal{P} \subset \mathcal{B}$. If φ, ψ, ψ_{r}, and φ^{*} are continuous over $\mathcal{P} \subset \mathcal{B}$, one obtains the following *local* form of the balance equation,

$$\frac{\partial\varphi}{\partial t} = DIV\psi + \psi_{\mathrm{r}} + \varphi^{*}. \qquad \text{(III.2)}$$

where *DIV* denotes the divergence operator with respect to $\boldsymbol{X}$.

Now, our attention is turned to the subbody $\mathcal{P} \subset \mathcal{B}$ containing points of discontinuity of the field φ. It is assumed that these discontinuity points form an orientable two-dimensional differentiable manifold $\varsigma_{\sigma}(t)$. The unit normal of $\varsigma_{\sigma}(t)$ is represented also by $\boldsymbol{N}$. If any effects connected with the gliding of $\varsigma_{\sigma}(t)$ in the tangential direction are exluded, the only nontrivial component of the surface velocity is U in $\boldsymbol{N}$ direction and given by (6.1.3). Let $[\![\varphi]\!]$ and $[\![\psi]\!]$ be the jump values of φ and ψ through $\varsigma_{\sigma}(t)$, respectively. Assuming the continuity of U, $[\![\varphi]\!]$ and $[\![\psi]\!]$ *on* the surface $\varsigma_{\sigma}(t)$, one may prove that

$$[\![\varphi]\!]U + [\![\psi]\!]\boldsymbol{N} = 0. \qquad \text{(III.3)}$$

This is the so-called Kotchine's condition (Wilmanski, 1998: pp.53-56).

Note that

$$\frac{\partial}{\partial t}\left(GRAD\, v^{\alpha}\right) = GRAD\left(\frac{\partial v^{\alpha}}{\partial t}\right) = DIV\left(\frac{\partial v^{\alpha}}{\partial t}\otimes \boldsymbol{I}\right), \tag{III.4}$$

where $GRAD$ is the gradient operator with respect to $\boldsymbol{X}$; $\boldsymbol{I}$ is the second-order unit tensor with components δ_{ij} (i.e. Kronecker's delta); χ^{α} and v^{α} are the motion and velocity of α-phase, respectively. By using (3.1.1) and (3.1.2), χ^{α} and v^{α} can be cast into functions of coordinate $\boldsymbol{X}\,(\in \mathcal{B} = \mathcal{B}^{\alpha})$ and t. (III.4) implies that $(\partial v^{\alpha}/\partial t \otimes \boldsymbol{I})$ plays the role of the flux of $GRAD\, v^{\alpha}$. Integrating (III.4) over the subdomain $\mathcal{P} \subset \mathcal{B}$, one obtains

$$\frac{d}{dt}\int_{\mathcal{P}} (GRAD\, v^{\alpha})dV = \oint_{\partial \mathcal{P}} \frac{\partial v^{\alpha}}{\partial t}\otimes \boldsymbol{N}dS. \tag{III.5}$$

Hence, it follows from (III.3) that

$$[\![GRAD\, v^{\alpha}]\!]U + \left[\!\left[\frac{\partial v^{\alpha}}{\partial t}\right]\!\right]\otimes \boldsymbol{N} = 0. \tag{III.6}$$

The spatial form of (III.6) is

$$[\![\nabla v^{\alpha}]\!]U + \left[\!\left[\frac{\partial v^{\alpha}}{\partial t}\right]\!\right]\otimes \boldsymbol{n} = 0. \tag{III.7}$$

where $\boldsymbol{n}$ is the unit normal to $\varsigma_{\alpha}(t)$ with respect to the current configuration. Let $\boldsymbol{a}^{\alpha}$ be the jump amplitude of ∇v^{α} through $\varsigma_{\alpha}(t)$; then,

$$[\![\nabla v^{\alpha}]\!] = \boldsymbol{a}^{\alpha}\otimes \boldsymbol{n}. \tag{III.8}$$

Inserting (III.8) into (III.7), one obtains

$$\left[\!\left[\frac{\partial v^{\alpha}}{\partial t}\right]\!\right] = -\boldsymbol{a}^{\alpha}U. \tag{III.9}$$

Equations (III.7)-(III.9) are usually called the Hadamard's relationships (Coussy, 1995: pp.252).

Similarly, using

$$\frac{\partial}{\partial t}\left[GRAD(GRAD\,\boldsymbol{\chi}^{\alpha})\right] = DIV\left[(GRAD\,\boldsymbol{v}^{\alpha})\otimes \boldsymbol{I}\right], \tag{III.10}$$

one may prove that

$$[\![GRAD(GRAD\,\boldsymbol{\chi}^{\alpha})]\!]U + [\![GRAD\,\boldsymbol{v}^{\alpha}]\!]\otimes \boldsymbol{N} = 0, \tag{III.11}$$

or equivalently,

$$[\![\nabla\nabla\,\boldsymbol{\chi}^{\alpha}]\!]U + [\![\nabla\boldsymbol{v}^{\alpha}]\!]\otimes \boldsymbol{n} = 0. \tag{III.12}$$

Finally, inserting (III.8) into (III.12) and employing (3.1.5), one obtains

$$[\![\nabla\nabla\,\boldsymbol{u}^{\alpha}]\!] = -U^{-1}\boldsymbol{a}^{\alpha}\otimes\boldsymbol{n}\otimes\boldsymbol{n}. \tag{III.13}$$

IV. NOMENCLATURE

Latin symbols

$\boldsymbol{a}^{\alpha}$	acceleration of α-phase, $[LT^{-2}]$
A^{α}	Helmholtz free energy of α-phase, $[L^2T^{-2}]$
$a^{\alpha\beta}$	area density of αβ-interface, $[L^{-1}]$
$\boldsymbol{b}^{\alpha}$	macroscopic external supply of linear momentum of α-phase, $[L^2T^{-2}\theta^{-1}]$
C_{α}	compressibility of α-phase, $[M^{-1}LT^2]$
c	coefficient matrix of generalized velocity
$\hat{D}$	dissipation function
$\boldsymbol{d}^{\alpha}$	the symmetric part of velocity gradient of α-phase, $[T^{-1}]$
E^{α}	macroscopic internal energy per unit mass of α-phase, $[L^2T^{-2}]$
E	total internal energy of the mixture, $[L^2T^{-2}]$
$\mathbf{E}'$	Lagrangian stain tensor
$\hat{e}^{\alpha}_{\alpha\beta}$	mass exchange rate from αβ-interface to α-phase, $[ML^{-3}T^{-1}]$
$\boldsymbol{F}$	deformation gradient of the solid skeleton
G	shear modulus of the mixture, $[ML^{-1}T^{-2}]$
$\mathbf{g}$	gravitational acceleration, $[LT^{-2}]$
h^{α}	external supply of energy to α-phase, $[L^2T^{-3}]$
$h^{\alpha\beta}$	external supply of energy to αβ-interface, $[L^2T^{-3}]$
$\boldsymbol{I}$	isotropic second order tensor with component δ_{ij}
J	jacobi of $\boldsymbol{F}$, i.e. $J = \det \boldsymbol{F}$
$\boldsymbol{k}$	global matrix of tangent modulus
k	intrinsic permeability, $[L^2]$
k_r^{β}	relative permeability of β-fluid
K	bulk modulus of the mixture, $[ML^{-1}T^{-2}]$
K_{α}	bulk modulus of α-phase, $[ML^{-1}T^{-2}]$
K_U	undrained bulk modulus of the mixture, $[ML^{-1}T^{-2}]$
K_D	drained bulk modulus of the mixture, $[ML^{-1}T^{-2}]$
m_r^{α}	current mass of α-phase in a volume of porous medium that is unit before deformation, $[ML^{-3}]$

m^{β} change in m_r^{β}, [ML^{-3}]

M^{β} total mass flowed across a surface that before the deformation is a unit area, [ML^{-4}]

m^{β} total mass flowed across a surface that after the deformation is a unit area, [ML^{-4}]

n porosity

n^{α} volume fraction of α-phase

$\boldsymbol{P}$ nominal stress, [$ML^{-1}T^{-2}$]

$\boldsymbol{P}^{I}$ the first Piola-Kirchhoff stress, [$ML^{-1}T^{-2}$]

P^{α} Kirchhoff pressure of α-phase, [$ML^{-1}T^{-2}$]

p^{α} thermodynamic pressure of α-phase, [$ML^{-1}T^{-2}$]

q^{α} heat flux vector of α-phase, [MT^{-3}]

$\hat{Q}^{\alpha}_{\alpha\beta}$ body supply of heat to α-phase from αβ-interface, [$ML^{-1}T^{-3}$]

$\hat{r}^{\alpha}$ non-equilibrium part of the linear momentum exchange of α-phase, [$ML^{-2}T^{-2}$]

r^{β}_{eq} equilibrium part of the linear momentum exchange of α-phase, [$ML^{-2}T^{-2}$]

$\boldsymbol{S}$ the second Piola-Kirchhoff stress tensor, [$ML^{-1}T^{-2}$]

S_r degree of saturation

S_{ul} matric suction (capillary pressure associated with contractile skin), [$ML^{-1}T^{-2}$]

$\hat{\boldsymbol{T}}^{\alpha}_{\alpha\beta}$ body supply of momentum to α-phase from αβ-interface, [$ML^{-2}T^{-2}$]

σ' effective stress tensor, [$ML^{-1}T^{-2}$]

$\mathbf{t}^{\alpha}$ macroscopic stress tensor of α-phase, [$ML^{-1}T^{-2}$]

$\mathbf{u}^{\beta}_r$ relative displacement of β-fluid with respect to skeleton, [LT^{-1}]

$\mathbf{u}^{\alpha}$ diplacement of α-phase, [L]

$\hat{V}$ specific energy function of the mixture, [$ML^{-1}T^{-2}$]

$\mathbf{v}^{\alpha}$ macroscopic velocity of α-phase, [LT^{-1}]

W total free energy function of mixture, [$ML^{-1}T^{-2}$]

$\boldsymbol{W}^{\beta}_r$ convected relative velocity of β-fluid, [LT^{-1}]

$\boldsymbol{w}^{\beta}$ relative velocity of β-fluid, [LT^{-1}]

$\boldsymbol{x}$ position vector of the solid phase in deformed configuration, [L]

$\boldsymbol{X}_{\alpha}$ position vector of a material point of α-phase in undeformed configuration, [L]

z global mass matrix

Greek symbols

σ	total Cauchy stress tensor, $[ML^{-1}T^{-2}]$
Π^{β}	capillary potential of β-fluid with respect to the skeleton, $[ML^{-1}T^{-2}]$
Π^{nw}	capillary potential of nonwetting fluid with respect to wetting fluid, $[ML^{-1}T^{-2}]$
η^{α}	macroscopic internal entropy per unit mass of α-phase, $[L^{2}T^{-2}\theta^{-1}]$
η	total macroscopic internal entropy per unit mass of the mixture, $[L^{2}T^{-2}\theta^{-1}]$
$\eta^{\alpha\beta}$	macroscopic internal entropy per unit mass of αβ-interface, $[L^{2}T^{-2}\theta^{-1}]$
θ	temperature, [θ]
Λ	entropy,
ρ	overall (volumetric) mass density of the mixture, $[ML^{-3}]$
ρ^{α}	intrinsic (volumetric) mass density of α-phase, $[ML^{-3}]$
φ^{α}	macroscopic entropy flux vector of α-phase, $[MT^{-3}\theta^{-1}]$
Θ_{α}^{β}	material coefficients, $[ML^{-1}T^{-2}]$
χ_{β}	effective stress parameters
λ_{s}	elastic constant of the skeleton, $[ML^{-1}T^{-2}]$
μ_{s}	elastic constant of the skeleton, $[ML^{-1}T^{-2}]$
λ & μ	Lamé coefficients of the mixture, $[ML^{-1}T^{-2}]$
ν	Poisson ratio

Special notation

A	operator to assemble the element matrices into a global matrix
$\mathcal{B}^{\alpha}$	reference configuration of α-phase
$\mathcal{S}_{t}^{\alpha}$	current configuration of α-phase
$\mathcal{B}$	domain spanned by the solid skeleton before deformation, i.e. $\mathcal{B}^{S}$
Ω^{e}	finite element *e*
$\mathcal{C}$	space of configuration
$\mathcal{V}$	space of variation
∇	gradient operator with respect to the deformed configuration **x**, $[L^{-1}]$
det	determinant of a matrix

div	divergence operator with respect to the deformed configuration $\mathbf{x}$, $[L^{-1}]$
$\frac{D^{\alpha}}{Dt}$	material derivative following the motion of α-phase, $[T^{-1}]$
GRAD	gradient operator with respect to the reference frame $\mathbf{X}$, $[L^{-1}]$
DIV	divergence operator with respect to the reference frame $\mathbf{X}$, $[L^{-1}]$
sym()	symmetrical part of a second-order tensor